MIXING LAYERS

by

L.-K. Tseng, P.-K. Wu and G. M. Faeth

15 August 1992

College of Engineering

DEPARTMENT OF AEROSPACE ENGINEERING

The University of Michigan
Ann Arbor, Michigan 48109-2140

DISCLAIMER NOTICE

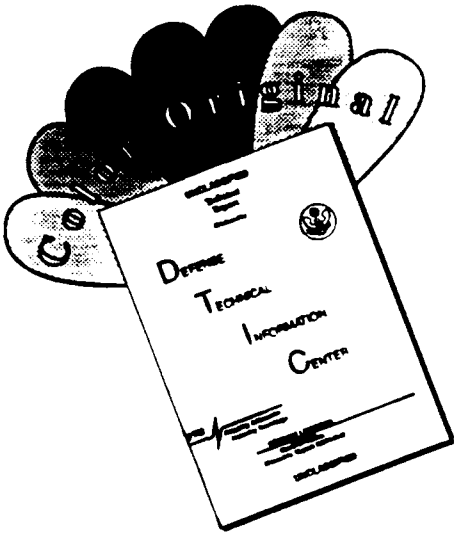

THIS DOCUMENT IS BEST QUALITY AVAILABLE. THE COPY FURNISHED TO DTIC CONTAINED A SIGNIFICANT NUMBER OF COLOR PAGES WHICH DO NOT REPRODUCE LEGIBLY ON BLACK AND WHITE MICROFICHE.

GDL/GMF-92-02

HIGH-SPEED MULTIPHASE MIXING LAYERS

by

L.-K. Tseng, P.-K. Wu and G. M. Faeth

15 August 1992

Prepared for:

Department of the Navy
Office of Naval Research
Mechanics Division, Code 1132P
800 N. Quincy Street
Arlington, Virginia 22217-5000

Grant No. N00014-89-J-1199
Gabriel D. Roy
Scientific Program Officer

UNCLASSIFIED

SECURITY CLASSIFICATION OF THIS PAGE (When Data Entered)

REPORT DOCUMENTATION PAGE		READ INSTRUCTIONS BEFORE COMPLETING FORM
1. REPORT NUMBER	2. GOVT ACCESSION NO.	3. RECIPIENT'S CATALOG NUMBER
4. TITLE (and Subtitle) High-Speed Multiphase Mixing Layers		5. TYPE OF REPORT & PERIOD COVERED Final Report 11/15/88 - 6/30/92
		6. PERFORMING ORG. REPORT NUMBER GDL/GMF-92-02
7. AUTHOR(s) L.-K. Tseng, P.-K. Wu and G. M. Faeth		8. CONTRACT OR GRANT NUMBER(s) N00014-89-J-1199
9. PERFORMING ORGANIZATION NAME AND ADDRESS Department of Aerospace Engineering The University of Michigan Ann Arbor, MI 48109-2140		10. PROGRAM ELEMENT, PROJECT, TASK AREA & WORK UNIT NUMBERS
11. CONTROLLING OFFICE NAME AND ADDRESS Office of Naval Research 800 North Quincy Street Arlington, VA 22217-5000		12. REPORT DATE August 1991 13. NUMBER OF PAGES
14. MONITORING AGENCY NAME & ADDRESS(if different from Controlling Office)		15. SECURITY CLASS. (of this report) Unclassified 15a. DECLASSIFICATION/DOWNGRADING SCHEDULE

16. DISTRIBUTION STATEMENT (of this Report)

Approved for public release; distribution unlimited

17. DISTRIBUTION STATEMENT (of the abstract entered in Block 20, if different from Report)

18. SUPPLEMENTARY NOTES

19. KEY WORDS (Continue on reverse side if necessary and identify by block number)

Multiphase flow, primary breakup, atomization

20. ABSTRACT (Continue on reverse side if necessary and identify by block number)

This is the final report of a research program whose objective was to study the structure and liquid breakup properties of high-speed multiphase mixing layers. The research is relevant to both gas injection into liquids, e.g., liquid metal combustion processes, and liquid injection into gases, e.g., pressure-atomized sprays. The investigation was divided into two phases, considering the structure of multiphase mixing layers and primary breakup at liquid surfaces, respectively.

DD FORM 1 JAN 73 1473 EDITION OF 1 NOV 65 IS OBSOLETE

S/N 0102-LF-014-6601

Unclassified

SECURITY CLASSIFICATION OF THIS PAGE (When Data Entered)

20. Abstract (continued)

The structure of multiphase mixing layers was studied using large round liquid jets (9.5 mm diameter) in still air at pressures of 1-8 atm; with both slug flow and fully-developed turbulent pipe flow at the jet exit. Measurements included mean liquid volume fractions using gamma-ray absorption and dispersed-phase properties using single-and double-pulsed holography. It was found that mixing was affected strongly by the liquid/gas density ratio and the degree of flow development at the jet exit, with the smallest gas/liquid density ratios and fully-developed turbulent pipe flow yielding the fastest mixing rates. Predictions of flow structure based on the locally-homogeneous flow approximation (where velocity differences between the phases are neglected) were reasonably good at large liquid volume fractions but progressively overestimated the rate of flow development as liquid volume fractions decreased and liquid/gas density ratios increased. Liquid volume fractions were low in the dispersed flow region so that primary and secondary breakup dominated flow properties rather than collisions. Separated flow effects were important in the dispersed flow region, but tended to decrease as liquid/gas density ratios decreased due to reduced drop sizes from secondary breakup.

Primary breakup was studied along the surface of large round liquid jets (3.6-9.5 mm diameter, with water, n-heptane and glycerol mixtures) in still gases (helium, air, Freon 12) at pressures of 1 and 2 atm, with both slug and fully-developed turbulent pipe flow at the jet exit. Measurements included flash photography, pulsed shadowgraphy and single- and double-pulsed holography. Drop sizes after primary breakup satisfied Simmons' universal root normal distribution and could be characterized by the Sauter mean diameter alone. The behavior of nonturbulent primary breakup could not be explained using existing unstable wave growth theories but could be correlated by a mechanism based on the vorticity within boundary layers along the passage walls; the drops formed were intrinsically unstable to secondary breakup which appears to be the main aerodynamic effect for these conditions. When liquid/gas density ratios were greater than 500, primary breakup of turbulent liquids was controlled by liquid turbulence properties alone, yielding successful correlations for both onset conditions and the subsequent evolution of drop sizes after primary breakup with distance along the mixing layer. Aerodynamic effects become important at lower liquid/gas density ratios and reduced the distance required for onset and drop sizes at onset by enhancing the growth of small scale surface distortions. Drops sizes after primary breakup downstream of the onset condition were reduced by aerodynamic effects as well, due to merging of primary and secondary breakup. Both these effects on turbulent primary breakup were correlated successfully using phenomenological theories.

ACKNOWLEDGMENTS

The authors wish to acknowledge the assistance of the staff of the Gas Dynamics Laboratories of the Department of Aerospace Engineering: D. R. Glass, W. C. Eaton, G. L. Gould, T. L. Griffin, D. Huddleson and T. M. Larrow for help with the experiments; Debbie Laird and S. C. Bauerle for help with publications and financial management.

TABLE OF CONTENTS

LIST OF TABLES

LIST OF FIGURES

LIST OF FIGURES (continued)

NOMENCLATURE

C_B	constant in nonturbulent primary breakup correlation
C_s	empirical constant for SMD after secondary breakup
C_{sa}	empirical constant for enhanced breakup
C_{si}	empirical constant for SMD at onset of breakup
C_{sx}	empirical constant for SMD variation with distance
C_{xi}	empirical constant for x at onset of breakup
d	injector diameter
d_p	drop or liquid element effective diameter
e_p	drop or liquid element effective ellipticity
ℓ	drop diameter length scale
L_c	liquid core length
L, L_p	injector passage length
MMD	spray mass median diameter
Oh_i	Ohnesorge number based on length i, $\mu_f/(\rho_f i\sigma)^{1/2}$
r	radial distance
Re_{ij}	Reynolds number based on conditions of phase i and length j, $\rho_i j u/\mu_f$
SMD	spray Sauter mean diameter
u	jet streamwise velocity
u_p	drop streamwise velocity
v	crosstream velocity
v_p	drop crosstream velocity
We_{ij}	Weber number based on density of phase i and length j, $\rho_i j\, u^2/\sigma$
x	streamwise distance

Greek

α	volume fraction
μ	molecular viscosity
Λ	turbulent crosstream integral length scale, d/8 for fully-developed turbulent pipe flow
ρ	density
σ	surface tension
τ_b	aerodynamic secondary breakup time
τ_R	Rayleigh breakup time

Subscripts

f	liquid phase property
FD	fully-developed nonturbulent primary breakup regime
g	gas-phase property
i	property at onset of breakup
o	jet exit condition

Superscripts

$(\bar{})$	time-average quantity
(~)	Favre-averaged quantity
$(\bar{})'$	root-mean-squared time-averaged fluctuation

1. INTRODUCTION

This investigation considered the properties of high-speed multiphase mixing layers involving gases and liquids. Such flows are encountered in a number of applications of interest to the Navy and can involve injection of either gases into liquids or liquids into gases. Typical applications of gas injection into liquids include liquid metal combustion for underwater propulsion systems, direct contact condensers, metal processing systems, gas dissolution systems, reservoir destratification systems and nuclear reactor pressure suppression systems, among others. Typical applications of liquid injection into gases primarily involve numerous liquid atomization processes.

The present investigation seeks a better understanding of both gas and liquid injection processes, however, it is a direct outgrowth of an earlier ONR-sponsored study of gas injection into liquids (Chuech et al. 1989, Loth and Faeth 1988, 1989, 1990). This earlier investigation was motivated by interest in developing the stored Chemical Energy Propulsion System (SCEPS) for underwater propulsion (Bush and Merrill 1981; Hughes et al. 1981). This process involves injection of gaseous sulfur hexafluoride into a high-temperature molten bath containing molten lithium and the liquid combustion products of the reaction between sulfur hexafluoride and lithium. Unsteady injector flow at low gas flow rates causes clogging of injector passages because the liquid combustion products solidify at relatively high temperatures, ca. 1050-1100K. Thus, the injectors usually operate as underexpanded jets which yields a steadier flow that eliminates the clogging problem. Pressures within the reaction vessel primarily are controlled by the vapor pressure of the liquid reactant/product mixture within the molten bath and usually are subatmospheric, however, they can vary over a relatively wide range depending on the power level and the extent of reaction.

The actual SCEPS combustion process is a difficult environment for detailed measurements; therefore, most studies of the process have involved analogous processes of noncondensing and condensing gas jets into liquids (Chan et al. 1987; Chen and Faeth 1982; Kerney et al. 1972; Loth and Faeth 1988, 1989, 1990; Weimer et al. 1973). The general picture that emerges from these studies is illustrated in Fig. 1, which specifically is based on air injection into water from Loth and Faeth (1988, 1989, 1992). Basic to the SCEPS process, the flow leaves the passage as a sonic gas jet. Expansion to the ambient pressure is initiated by an expansion fan at the periphery of the jet exit, which accelerates the bulk of the gas flow to supersonic velocities. The expansion waves reflect as compression waves from the sonic line region of the multiphase mixing layer at the flow periphery; these compression waves subsequently steepen to form shock waves. The shock waves cross the flow and then are reflected as expansion waves from the sonic line region of the mixing layer, tending to repeat this pattern in a succession of shock cells. The shock cells eventually disappear, ending the external expansion region, when the sonic line within the mixing layer reaches the axis. Clearly, the process is unusually complicated, involving patches of supersonic flow, multiphase flow, liquid breakup into drops, gas breakup into bubbles, and reactive phenomena that yield a number of intermediate solid and immiscible liquid phases (Avery and Faeth 1975; Chan et al. 1988; Chen and Faeth 1983; Loth and Faeth 1988, 1989, 1990).

Even though the SCEPS process, and other noncondensing and condensing gas injection processes like it, is very complex, some progress has been made toward modeling the flow for engineering purposes (Avery and Faeth 1975; Chan et al. 1987, 1988; Chen and Faeth 1982, 1983; Chuech et al. 1989; Faeth 1987, 1990; Loth and Faeth 1988, 1989, 1990). These methods generally simplify the treatment of multiphase flow and reaction effects by adopting the locally-homogeneous-flow (LHF) approximation, which implies local kinematic equilibrium (velocities of all the phases locally the same) and

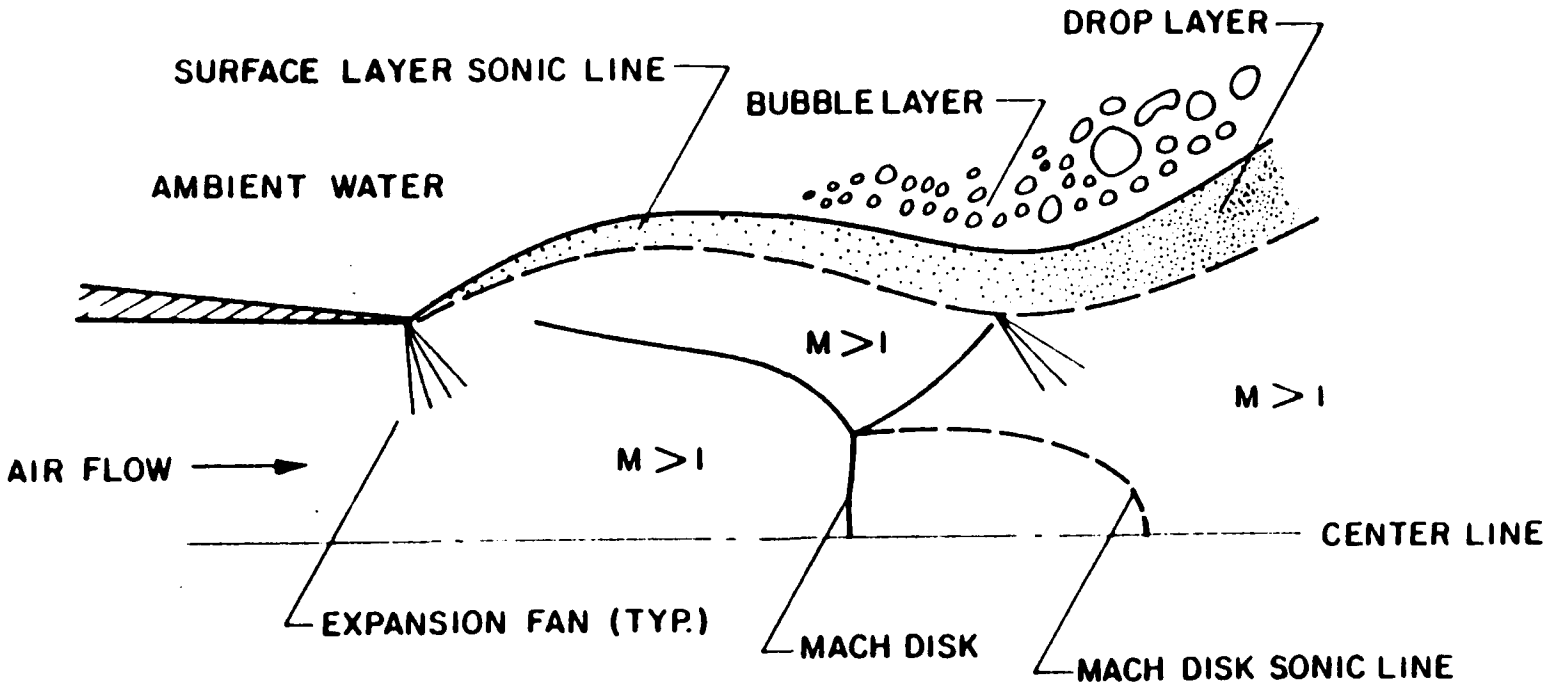

Figure 1 Sketch of gas injection into liquids

thermodynamic equilibrium (temperatures of all phases the same and the chemical potential of each species equal in all phases). Turbulent mixing generally is treated using a turbulence model, with recent approaches employing Favre-averaged k-ε-g models. Finally, the complexities of the external expansion region have either been treated by full gas-dynamic analyses or approximated as an equivalent adapted jet (if the gas or vapor containing region is large in comparison to the external expansion region). Models of this type have been reasonably successful for treating gross features like the length of the gas or vapor containing region, when evaluated using measurements (Chen and Faeth 1982, 1983; Loth and Faeth 1988, 1989, 1990). However, more detailed features of the flow, like the structure and liquid breakup properties of the multiphase mixing layer, that are crucial to the development of the flow, have not been predicted very satisfactorily using the LHF approach. This deficiency that has been attributed to effects of separated flow, e.g., lack of kinematic and thermodynamic equilibrium between the phases (Loth and Faeth 1988, 1989, 1990).

Even though the gas dynamic features of underexpanded gas jets in liquids are complicated, it is generally within the capabilities of current technology to treat these effects. In contrast, the properties of the multiphase mixing layer along the periphery of the flow are not well understood (Faeth 1987, 1990). In particular, the rate of generation of drops at the surface, which controls mixing rates between the phases, and the size and velocities of the drops after breakup, which control the importance of separated flow effects, are unknown. Thus, further progress to develop more effective models of gas injection processes primarily depends on a better understanding of the multiphase mixing layer; therefore, studying this portion of the flow was the primary objective of the present investigation.

Several features of multiphase mixing layers must be addressed for applications reverent to gas injection processes. First of all the liquid phase generally is turbulent so that effects of liquid turbulence on the structure of the mixing layer and primary breakup of liquid at the liquid surface must be known. Secondly, gas injection systems operate over a relatively wide range of liquid/gas densities ratios and effects of this important variable must be considered. Additionally, properties like liquid viscosity and surface tension vary widely as well, and their effects must be addressed. Finally, the velocity difference across the mixing layer is known to affect the structure of the mixing layer and this behavior must be understood. These features all were specifically addressed during the present investigation.

In view of the present limited understanding of multiphase mixing layers, however, it also was necessary to neglect some features of gas injection processes in order to keep the study tractable. First of all, the presence of gas dynamic features like shock and expansion waves in the mixing layer are substantial complications; therefore, such effects were not studied pending the development of background information on the simpler constant pressure multiphase mixing layer. One feature of the flow that helps to mitigate lack of consideration of strong gas dynamic features, like shock waves, is the fact that the sonic line is located at some distance of the surface, so that the most important part of the mixing layer near the liquid surface only involves subsonic flow with no direct interactions with shock waves. The next simplification was to reverse the process to consider a high-speed liquid flow in still gas, rather that a high-speed gas flow over a relatively still liquid. This was done to illuminate problems of overall flow instability (like those encountered at low flow rates for the SCEPS system) that would complicate study of mixing layer properties, and to provide well-defined liquid turbulence properties. This allowed provision of various relative velocities across the mixing layer but is only appropriate to the extent that flow properties are independent of the source of the momentum. Fortunately, for multiphase mixing layers, separated-flow effects are the dominant feature and the direction

of the velocity vector with respect to the liquid has little effect on primary breakup at the liquid surface. Due to the density difference, however, the overall structure of the multiphase mixing layer, is affected by the direction of the velocity vector; nevertheless, gaining understanding of conditions where the momentum is carried by the liquid still is a reasonable first step toward understanding gas injection processes. Naturally, the present experimental configuration yields information that is directly applicable to pressure atomization, particularly the near-injector region.

This is a final report of accomplishments during the investigation. The present report is brief, additional details can be found in other articles, papers and theses generated during the course of the study, see Table 1 for a summary of these publications. In addition, the articles by Faeth (1990), Ruff et al. (1992), Tseng et al. (1992a,b), Wu et al. (1991, 1992) and Wu and Faeth (1992) are appended to provide a convenient reference. Finally, Tseng (1991) and Wu (1992) provide detailed descriptions of the research as well as complete tabulations of data.

Table 1. Summary of Publications

Faeth, G. M. (1990) Structure and atomization properties of dense turbulent sprays. Twenty-Third Symposium (International) on Combustion, The Combustion Institute, Pittsburgh, 1345-1352.

Chuech, S. G., Lai, M.-C. and Faeth, G. M. (1989) Structure of turbulent sonic underexpanded free jets. AIAA J. 27, 549-559.

Loth, E. and Faeth, G. M. (1989) Structure of underexpanded round air jets submerged in water. Int. J. Multiphase Flow 15, 589-603.

Ruff, G. A., Wu, P.-K., Bernal, L. P. and Faeth, G. M. (1992) Continuous-and dispersed-phase structure of dense nonevaporating pressure-atomized sprays. J. Prop. Power 8, 280-289.

Tseng, L.-K., Ruff, G. A. and Faeth, G. M. (1992a) Effects of gas density on the structure of liquid jets in still gases. AIAA J. 30, 1537-1544.

Tseng, L.-K., Wu, P.-K. and Faeth, G. M. (1992b) Dispersed-phase structure of pressure atomized sprays at various gas densities, J. Prop. Power, in press.

Wu, P.-K. and Faeth, G. M. (1992) Aerodynamic effects on primary breakup of turbulent liquids. Atomization and Sprays, submitted.

Wu, P.-K., Ruff, G. A. and Faeth, G. M. (1991) Primary breakup in liquid/gas mixing layers. Atomization and Sprays 1, 421-440.

Wu, P.-K., Tseng, L.-K. and Faeth, G. M. (1992) Primary breakup in gas/liquid mixing layers for turbulent liquids. Atomization and Sprays, in press.

Papers:

Faeth, G. M., Tseng, L.-K. and Wu, P.-K. (1990) Structure and mixing properties of high-speed gas/liquid mixing layers. 27th JANNAF Combustion Meeting, Cheyenne, WY.

Faeth, G. M., Tseng, L.-K. and Wu, P.-K. (1991) Primary breakup of round pressure atomized sprays. 28th JANNAF Combustion Meeting, San Antonio, TX.

Ruff, G. A. and Faeth, G. M. (1990) continuous-and dispersed-phase structure of dense nonevaporating pressure-atomized sprays. AIAA 28th Aerospace Sciences Meeting, Reno, NV, AIAA Paper. No. 90-0464.

Tseng, L.-K. and Faeth, G. M. (1991) Dispersed-phase structure of pressure-atomized sprays at various gas densities. ICLASS-91, NIST, Gaithersburg, MD.

Tseng, L.-K., Ruff, G. A. and Faeth, G. M. (1991) Effects of ambient gas density on the structure of pressure-atomized sprays. AIAA 29th Aerospace Sciences Meeting, Reno, NV, AIAA Paper No. 91-0690.

Tseng, L.-K., Wu, P.-KJ. and Faeth, G. M. (1992) Dispersed-phase structure of pressure atomized sprays at various gas densities. AIAA 30th Aerospace Sciences Meeting, Reno, NV, AIAA Paper No. 92-0230.

Wu, P.-K. and Faeth, G. M. (1991) Primary breakup of round turbulent liquid jets in still air. ICLASS-91, NIST, Gaithersburg, MD.

Wu, P.-K. and Faeth, G. M. (1993) Aerodynamic effects on primary breakup of turbulent liquids. 31st AIAA Aerospace Sciences Meeting, Reno, NV, AIAA Paper No. 93-0903.

Wu, P.-K., Ruff, G. A. and Faeth, G. M. (1991a) Primary breakup in liquid/gas mixing layers. AIAA 29th Aerospace Sciences Meeting, Reno, NV, AIAA Paper No. 91-0285.

Wu, P.-K., Tseng, L.-K. and Faeth, G. M. (1991 Breakup of round pressure-atomized sprays. 28th JANNAF Combustion Meeting, San Antonio, TX.

Wu, P.-K., Tseng, L.-K. and Faeth, G. M. (1992) Primary breakup in gas/liquid mixing layers for turbulent liquids. AIAA 30th Aerospace Sciences Meeting, Reno, NV, AIAA Paper No. 92-0462.

Wu, P.-K., Hsiang, L.-P. and Faeth, G. M. (1993) Aerodynamic effects on primary and secondary spray breakup. First International Symposium on Liquid Rocket Combustion Instability, The Pennsylvania State University, University Park, PA.

Theses:

Tseng, L.-K. (1991) Near-injector structure of nonevaporating pressure-atomized sprays at various ambient densities. Ph.D.. thesis, The University of Michigan, Ann Arbor, MI.

Wu, P.-K. (1992) Liquid surface breakup for nonturbulent and turbulent liquids. Ph.D. thesis, The University of Michigan, Ann Arbor, MI.

The investigation was divided into two phases, one considering the overall structure of multiphase mixing layers, and the other specifically treating primary breakup processes at the liquid surface. Highlights of each of these phases of the research are discussed in the following, in turn.

2. STRUCTURE OF MULTIPHASE MIXING LAYERS

2.1 Introduction

This phase of the investigation involved study of multiphase mixing layers formed along the sides of nonevaporating liquid jets injected into still gases. Experiments were limited to the atomization breakup regime, where liquid breakup into drops and the development of a multiphase mixing layer, begins right at the jet exit because this regime is most important for practical applications such as gas injection into liquids and pressure-atomized sprays. Jet exit conditions included both fully-developed turbulent pipe flow and low turbulence intensity slug flow in order to examine the effect of liquid turbulence on flow structure. The measurements were made using large diameter (9.5 mm) round liquid jets in order to extend the region where the structure of the multiphase mixing layer could be observed; however, the complete breakup properties of these flows, as the entire liquid column disintegrates, was not considered. Effects of various liquid/gas density ratio were studied by injecting water into still air at pressures in the range 1-8 atm. The measurements were used to evaluate predictions of flow structure based on the LHF approximation.

Discussion of past work will be limited because reviews treating multiphase jets and dense sprays have appeared recently (Faeth 1987,1990). Past measurements have established the main features of the near injector region of liquid jets in still gases within the atomization breakup regime. The flow consists of a liquid core, much like the potential core of a single-phase jet, surrounded by a dispersed drop/gas mixing layer. The liquid core becomes shorter as liquid/gas density ratios decrease due to increased entrainment rates (Chehroudi et al. 1985). Other features of these flows, however, have only be studied for injection of water into air at atmospheric pressure using relatively large diameter (19.1 and 9.5 mm) round liquid jets (Rufi et al. 1988, 1991). These measurements included liquid volume fraction distributions using gamma-ray absorption, drop sizes and velocities using double-pulse holography and air entrainment rates using laser velocimetry. The measurements of mean liquid volume fraction distributions showed that the rate of development of the mixing layer increased with increased liquid turbulence levels. Predictions based on the LHF approximation were effective, including effects of liquid turbulence, for liquid volume fractions greater than 0.2, however, they progressively failed as the flow became dilute. This difficulty with the LHF approach was found to be due to significant separated flow effects in regions where liquid volume fractions were low. Additionally, because entrainment rates mainly are governed by processes within dilute portions of the flow, the LHF predictions generally overestimated entrainment rates due to separated flow phenomena. However, the predictions suggested improved performance of LHF methods as the We_{df} increased, with this limit approached more rapidly as the liquid/gas density ratio decreases.

The objective of the present investigation was to explore effects of liquid/gas density ratio on the mixing properties of liquid jets in still gases and the adequacy of predictions of flow properties based on the LHF approximation. Experiments involved measurements of liquid volume fraction distributions within large round water jets (9.5 mm initial diameter) in still air at pressures of 1-8 atm. The measurements were compared with predictions based on the LHF approach to determine whether this methodology could treat effects of varying liquid/gas density ratios.

The discussion of the study begins with a brief description of experimental and theoretical methods. Results then are considered, treating liquid volume fractions and dispersed-phase properties in turn. The present description is brief, see Tseng (1991), Ruff et al. (1992) and Tseng et al. (1992a,b) for more details. For convenience, the latter three papers can be found in Appendices B, C and D.

2.2 Experimental Methods

Apparatus. Experimental methods were similar to Ruff et al. (1988, 1991) except that the flow was contained in a large pressure vessel so that the pressure of the ambient air could be changed. A sketch of the apparatus appears in Fig. 2. The arrangement involves a steady water jet injected vertically downward within a 1.5m diameter × 4.5 m high pressure vessel. Instrumentation was mounted rigidly so that flow structure was measured by traversing the injector. Water collected at the bottom of the chamber and was drained continuously. Two injectors were used, identical to those of Ruff et al. (1988, 1991); one yielding nonturbulent slug flow, the other yielding fully-developed turbulent pipe flow.

Instrumentation. Distributions of liquid volume fractions were measured using gamma-ray absorption similar to Ruff et al. (1988). This was based on an iodine-125 isotope source within a lead casket having a small (1.6 mm diameter) outlet aperture. The gamma rays passing through the flow were detected through a second lead aperture using a Bicron x-ray probe and an EG&G Ortec single-channel analyzer and counter timer. Absorption measurements (20,000-25,000 counts) were made for 30-60 parallel paths through the flow; these results then were deconvoluted to find the radial variation of time-averaged liquid volume fraction.

The appearance of the liquid surface and the properties of drops in the dispersed-flow region were observed using single-and double-pulsed holography. A sketch of the holocamera appears in Fig. 3. It was based on an off-axis arrangement using a ruby laser with a pulse duration of 20 ns (and pulse separations as small as 1 μs) to stop the flow. This arrangement allowed objects as small as 2 μm to be observed and drops having diameters as small as 5 μm to be measured, while double pulsing allows drop velocities to be measured. Measurements were obtained over $6 \times 6 \times 4$ mm^3 volume, using at least three holograms per position. The holograms were reconstructed and analyzed using a high magnification video system in conjunction with a Gould FD 5000 Image Processor.

Test Conditions. Mean flow conditions were the same for slug and fully-developed flows. This involved a water flow rate of 3.47 kg/s, an average jet exit velocity of 49.1 m/s, Re_{fd} = 462,000, Oh_d = 0.00121, We_{fd} = 312,000 and We_{gd} = 380,760, 1520 and 3040 at pressures of 1, 2, 4 and 8 atm.

2.3 Theoretical Methods.

Flow properties were predicted using the LHF model of Ruff et al. (1988, 1991). In addition to the LHF approximation, the major assumptions of the model were as follows: steady (in the mean) axisymmetric flow with no swirl, boundary-layer approximations apply, negligible kinetic energy and viscous dissipation of the mean flow, buoyancy only affects the mean flow, equal exchange coefficients of all species and phases, and negligible mass transport between the phases (no evaporation). These assumptions are either conditions of the experiments or are justified by past practice except for the LHF approximation which will be evaluated.

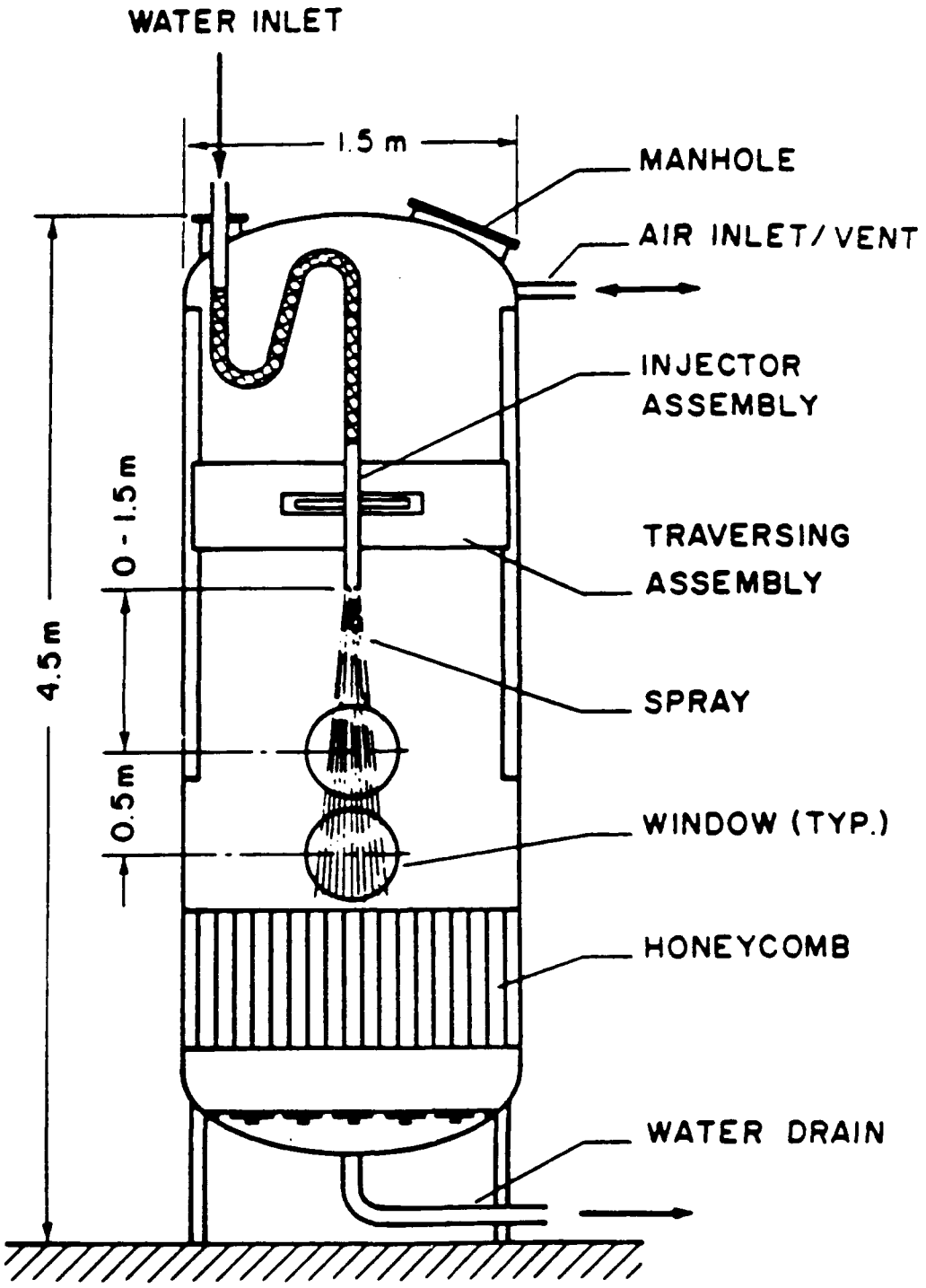

Figure 2 Sketch of test apparatus

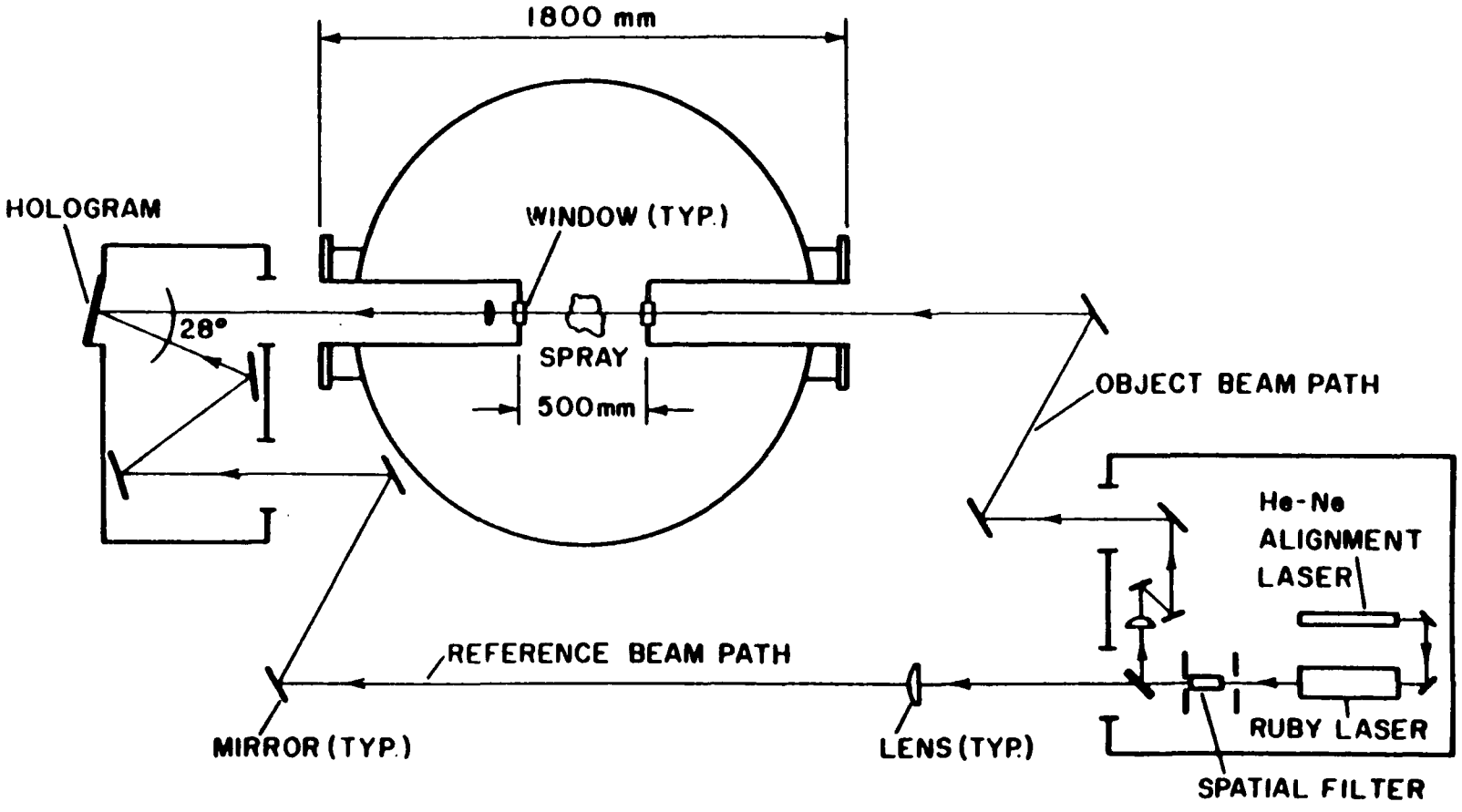

Figure 3 Sketch of holocamera

Under these approximations the flow field can be found from a simplified version of the conserved-scalar formulation. This involved solving Favre-averaged governing equations for conservation of mass, stream wise mean momentum, mean mixture fraction, turbulence kinetic energy, and the rate of dissipation of turbulence kinetic energy. The specific formulation, all empirical constants, calibration of the approach for variable-density single-phase jets, the specification of initial and boundary conditions, and the details of the numerical computations, can be found in Ruff et al. (1988, 1991).

2.4 Results and Discussion

Mean Liquid Volume Fractions. Measured and predicted time-averaged mean liquid volume fractions along the jet axis are plotted in Figs. 4 and 5 for fully-developed and slug flow jet exit conditions, respectively. Predictions for slug flow are shown for passage length to diameter ratios, L/d = 0 and 5, which bounds the potential degree of flow development within the injector passage. Measurements of Ruff et al. (1988) for similar test conditions at 1 atm also are shown on the plot: they agree very well with present measurements. The substantial effect of jet exit turbulence levels on mixing rates is clearly evident, with fully-developed flow yielding the fastest mixing rates. The faster mixing rates as liquid/gas density ratios decrease (or pressure increases) also is indicated by the measurements.

The LHF predictions are in reasonably good agreement with the measurements for fully-developed flow (Fig. 4) and provide the correct trend of effects of ambient pressure. However, the conditions of Fig. 4 represent relatively low levels of mixing. For example, although mean liquid volume fractions as small as 0.03 are reached, the entire range considered still represents Favre-averaged mixture fractions greater than 0.85 due to the relatively large liquid/gas density ratios of the flow (Tseng et al. 1992a). There are significant differences between predictions for pure slug flow (L/d = 0) and allowance for boundary layer growth within the injector passage (L/d = 5), see Fig. 5. These conditions bound the range of possibilities for present tests, and it is encouraging that the two predictions tend to bound the measurements. Nevertheless, there are significant discrepancies between predictions and measurements at x/d = 100 and 4 and 8 atm. This region involves rapid streamwise variation of flow properties and dilute flows where both predictions overestimate the rate of development of the flow — behavior that can be attributed to effects of separated flow based on subsequent results.

Predicted and measured radial profiles of mean liquid volume fractions at 1 atm are illustrated for fully developed and slug flow in Figs. 6 and 7 (results at other pressures are qualitatively similar). The results of Ruff et al. (1988) also a plotted on the figures: they generally agree with present measurements within experimental uncertainties. The comparison between predicted and measured mean liquid volume fractions is reasonably good, however, the measurements generally involve large mixture fractions as noted earlier. In particular, as mixture fractions become small at large x/d, predictions clearly overestimate rate of flow development, indicating significant effects of separated flow as the flow becomes dilute.

Drop Properties. The failure of the LHF approximation within the dispersed flow region can be proven directly based on measurements of drop properties. An important simplification was observed with respect to drop size properties that is illustrated in Fig. 8. This is a plot of drop size distributions according to Simmons' (1977) universal root normal distribution for various positions along the liquid surface and across the multiphase mixing layer considering both fully-developed and slug slow conditions. Remarkably, the data generally satisfies this distribution function with the ratio MMD/SMD = 1.2: a few

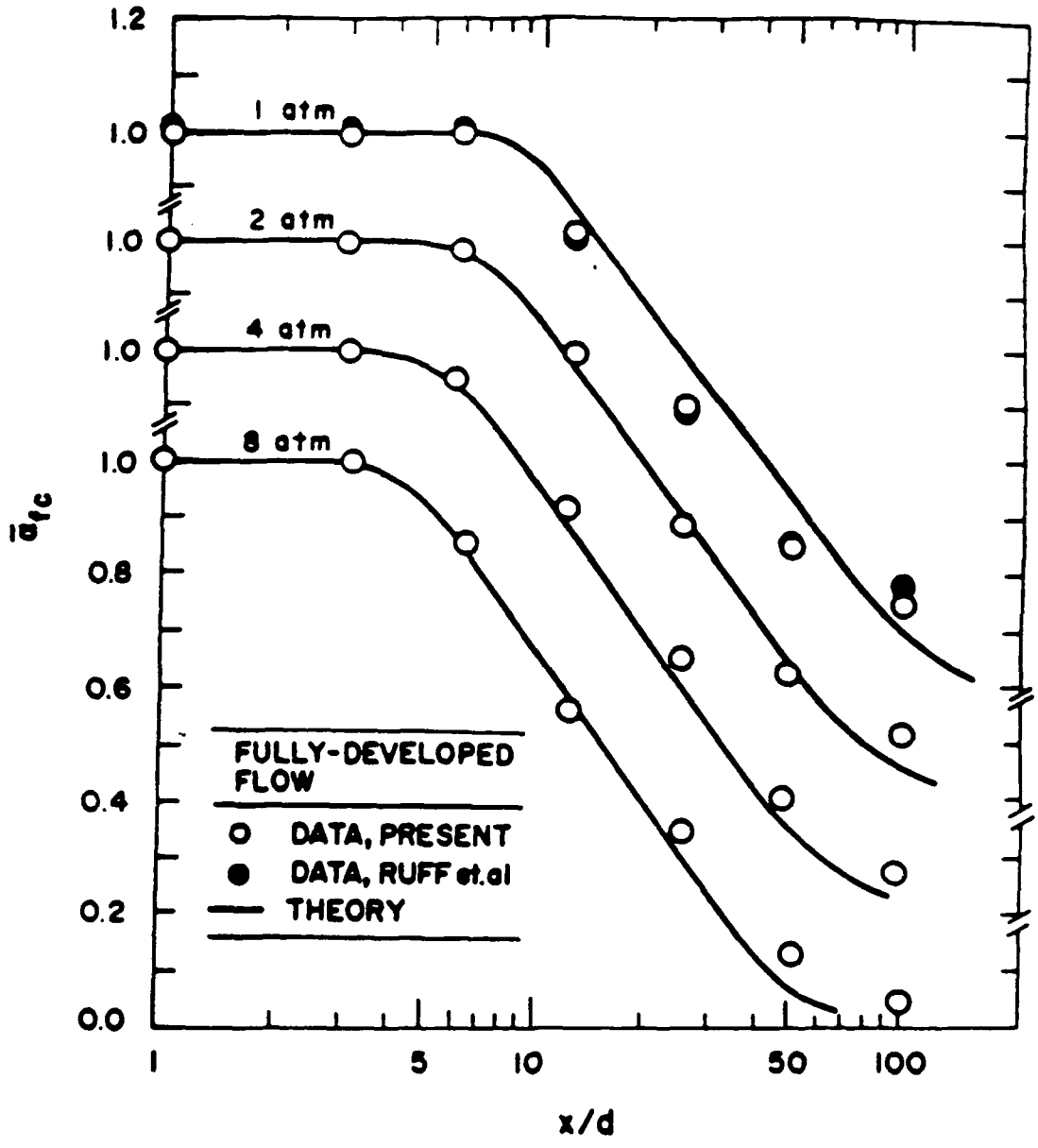

Figure 4 Liquid volume fractions along axis for fully-developed flow

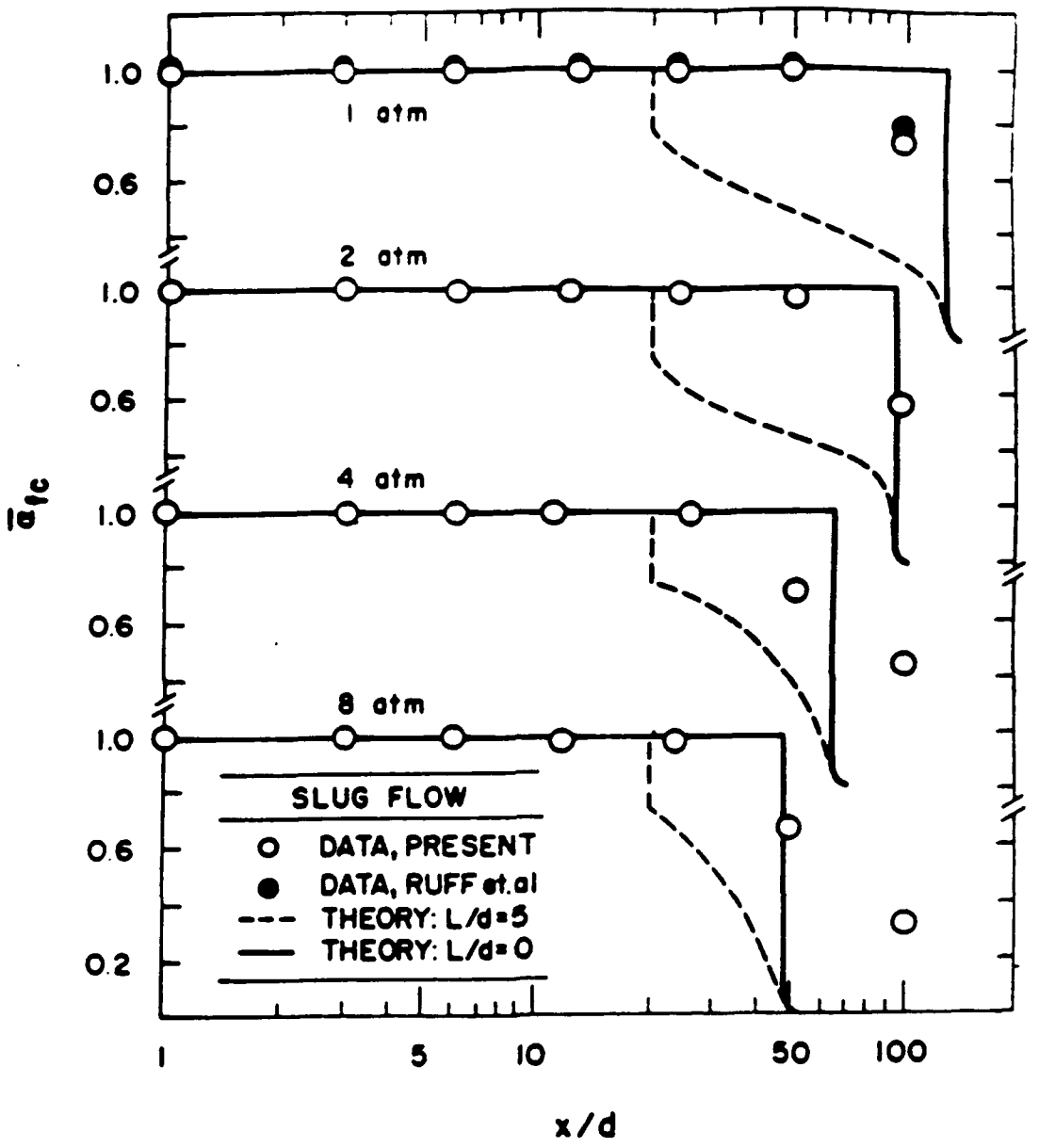

Figure 5 Liquid volume fractions along axis for slug flow

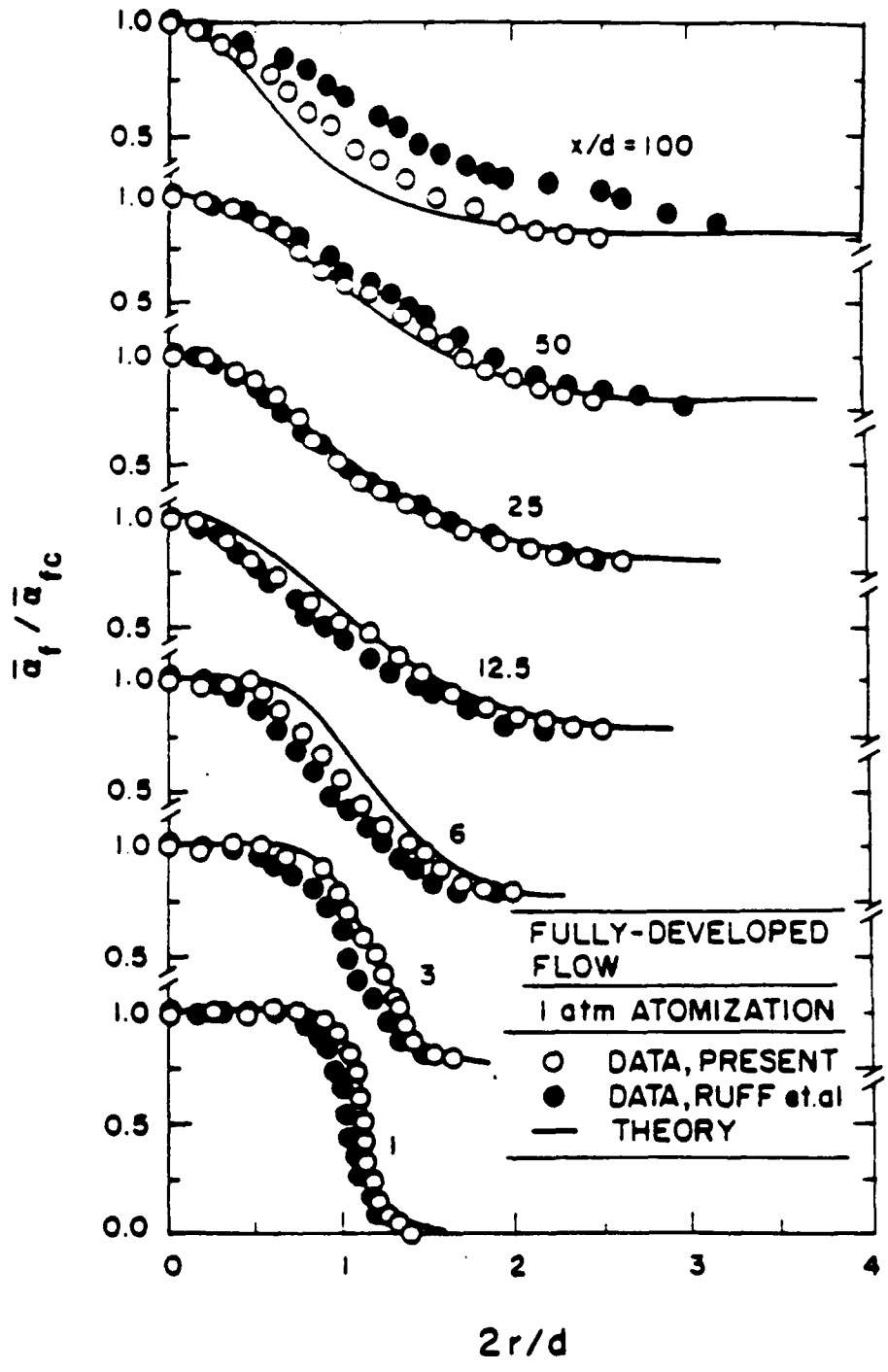

Figure 6 Radial profiles of liquid volume fractions for fully-developed flow

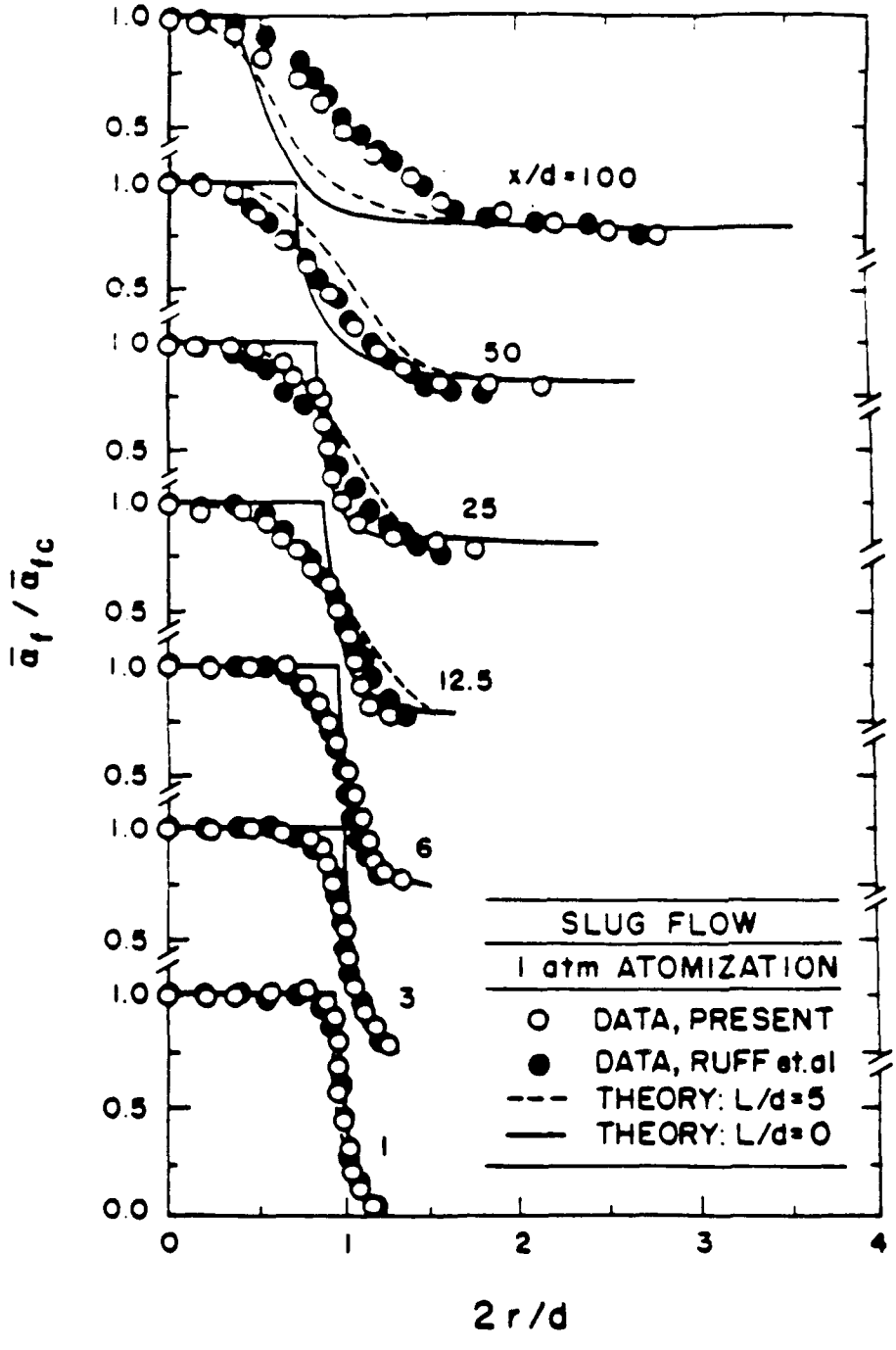

Figure 7 Radial profiles of liquid volume fractions for slug flow

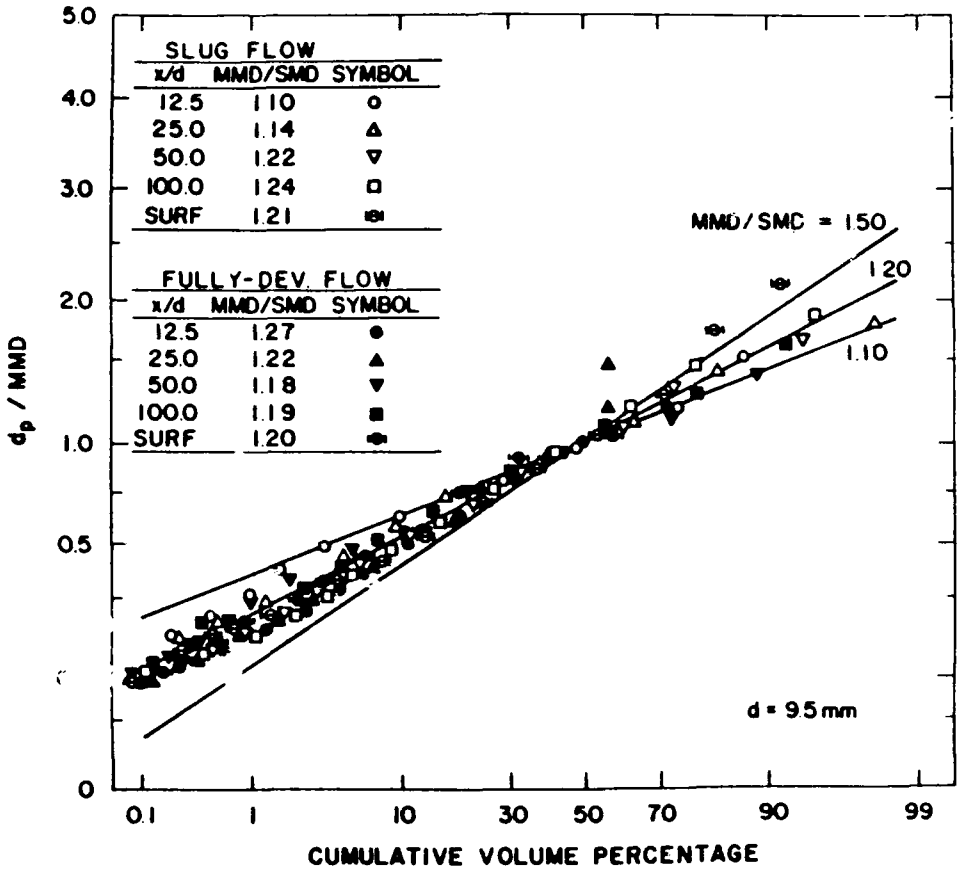

Figure 8 Drop size distributions

exceptions at large cumulative volume percentages are felt to be due to sampling limitations for large drops. This is a two-parameter distribution; therefore, taking the best estimate value, MMD/SMD = 1.2, implies that the entire distribution can be represented by the SMD alone. Thus, drop size results will be reported in terms of SMD in the following.

Typical distributions of drop properties across the mixing layer for fully-developed flow, illustrating flow properties for turbulent primary breakup, appear in Figs. 9 and 10 (see Tseng (1991) and Tseng et al. (1992b) for results at other test conditions). These measurements are for x/d = 25 at pressures of 1 and 4 atm. Properties illustrated include the variation of ellipticity (mass averaged ratio of maximum to minimum drop dimensions), SMD and drop velocities across the dispersed flow region. Predictions of flow velocities using the LHF approach also are shown on the plots.

Many of the features observed in Figs. 9 and 10 are similar to the earlier observations of Ruff et al. (1991) at atmospheric pressure, however, significant effects of reducing the liquid/gas density ratio are observed as well. Thus, at atmospheric pressure, the largest values of e_p and SMD are in the region of the liquid surface, supporting the presence of primary breakup yielding large drops which subsequently undergo secondary breakup. At the higher pressure, however, e_p approaches unity and drop sizes are smaller near the surface, with smaller variations of these properties across the width of the flow: this suggests merging of primary and secondary breakup processes near the liquid surface as the liquid/gas density ratio decreases. In general, there are substantial differences among the velocities of drops of different size, which is direct proof of the deficiency of the LHF approximation in this region (the LHF predictions also clearly are not very good for any drop size). Increasing pressures tend to reduce drop velocities but the velocities of small drops are surprising low and suggest small gas velocities. This implies that momentum exchange between the liquid and gas is not very effective. This occurs due to the large relaxation time of the large drops that carry most of the liquid momentum, aided by the fact that liquid volume fractions in the dispersed flow region are very low (less than 0.1%). Thus, this region intrinsically is subject to separated flow effects, with relatively large drops moving a large velocities in a dilute multiphase flow.

The structure of the dispersed phase and the effect of varying liquid/gas density ratio is quite different for slug flow. Some typical results for x/d = 25 and pressures of 1 and 4 atm are illustrated in Figs. 11 and 12. First of all, drop sizes are clearly much smaller for slug then for fully developed flow (cf. Figs. 9 and 10, and 11 and 12) even though fully-developed flow mixes more rapidly as a whole. Values of e_p and SMD are largest near the surface, suggesting effects of secondary breakup as before, however, drop ellipticity and SMD across the mixing layer are far more uniform for slug flow than for fully-developed flow. Decreasing the liquid/gas density ratio also has much less effect on drop properties for slug than for fully-developed flow. However, drop velocities vary significantly with drop size, suggesting significant effects of separated flow as before.

Taken together, these results demonstrated rather different primary breakup properties for turbulent and nonturbulent liquids but important effects of separated flow in a dilute dispersed flow region for both. Reduced liquid/gas density ratios for water/air flows at pressures of 1-8 atm also yield evidence of aerodynamic breakup effects with drop sizes after primary breakup particularly reduced for turbulent liquids. The key to treating separated-flow phenomena is an understanding of the outcome of primary breakup (drop size and velocity distributions); therefore, this issue was addressed in some detail during the second phase of the investigation, which will be considered next.

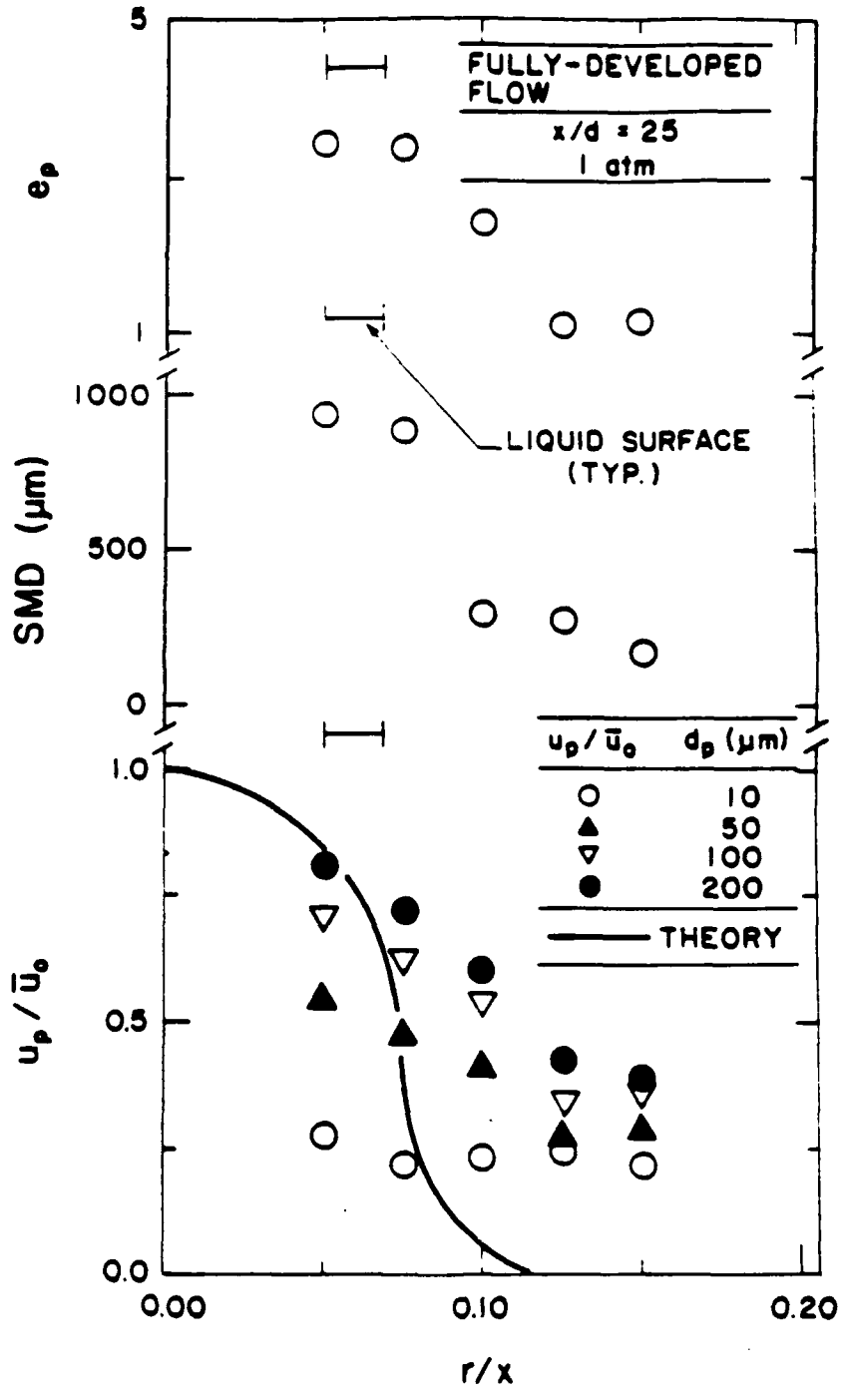

Figure 9 Drop properties for fully-developed flow at x/d = 25 and 1 atm

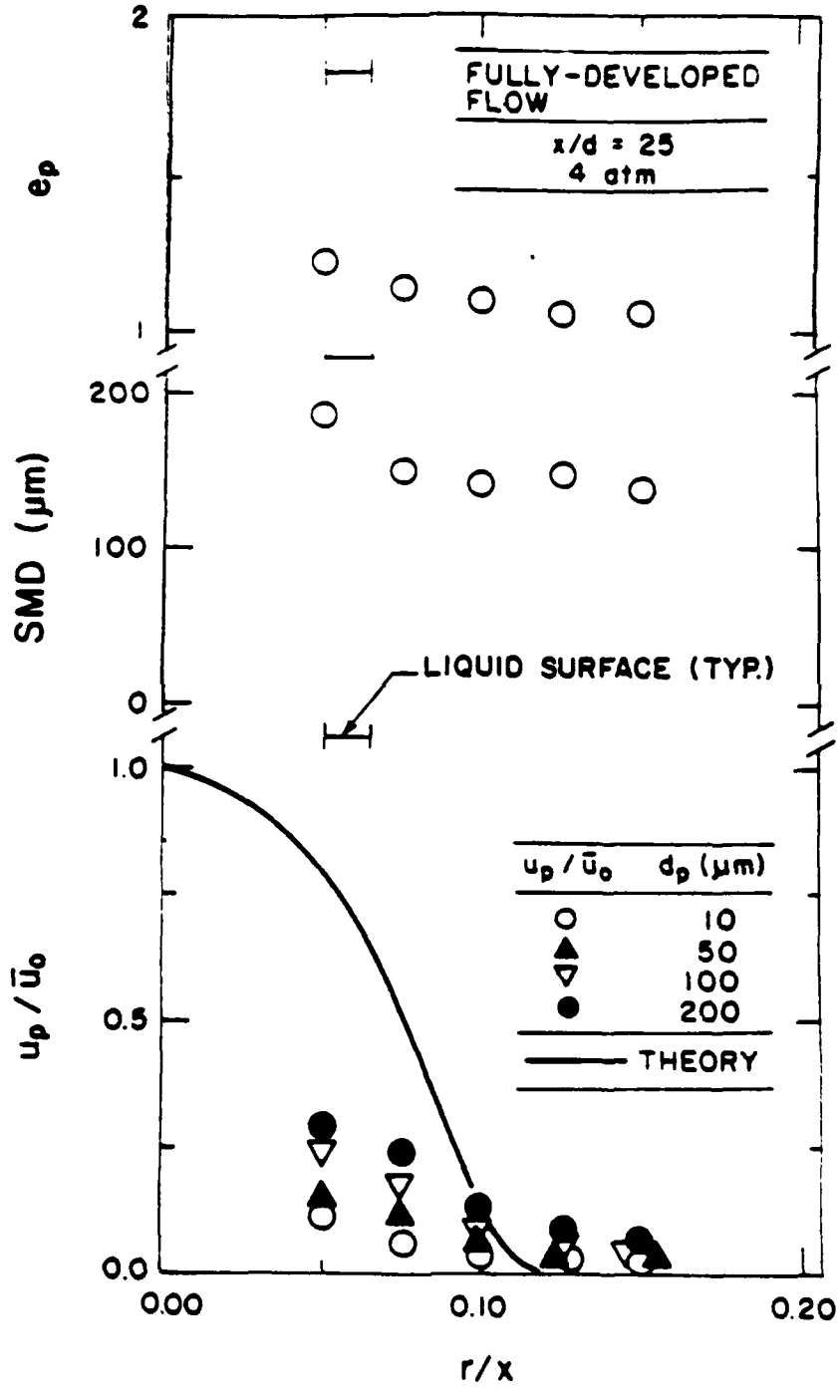

Figure 10 Drop properties for fully-developed flow at x/d = 25 and 4 atm

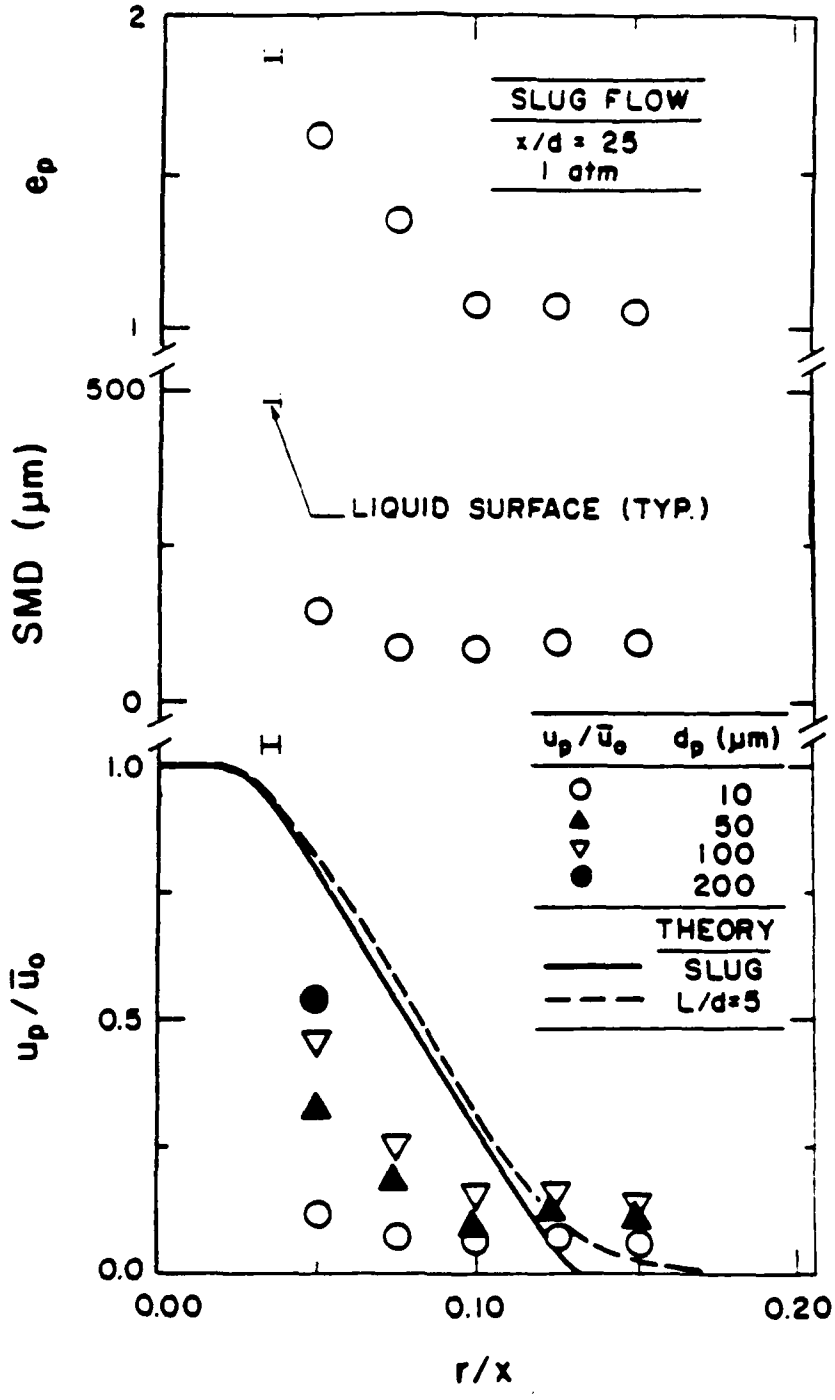

Figure 11 Drop properties for slug flow at x/d = 25 and 1 atm

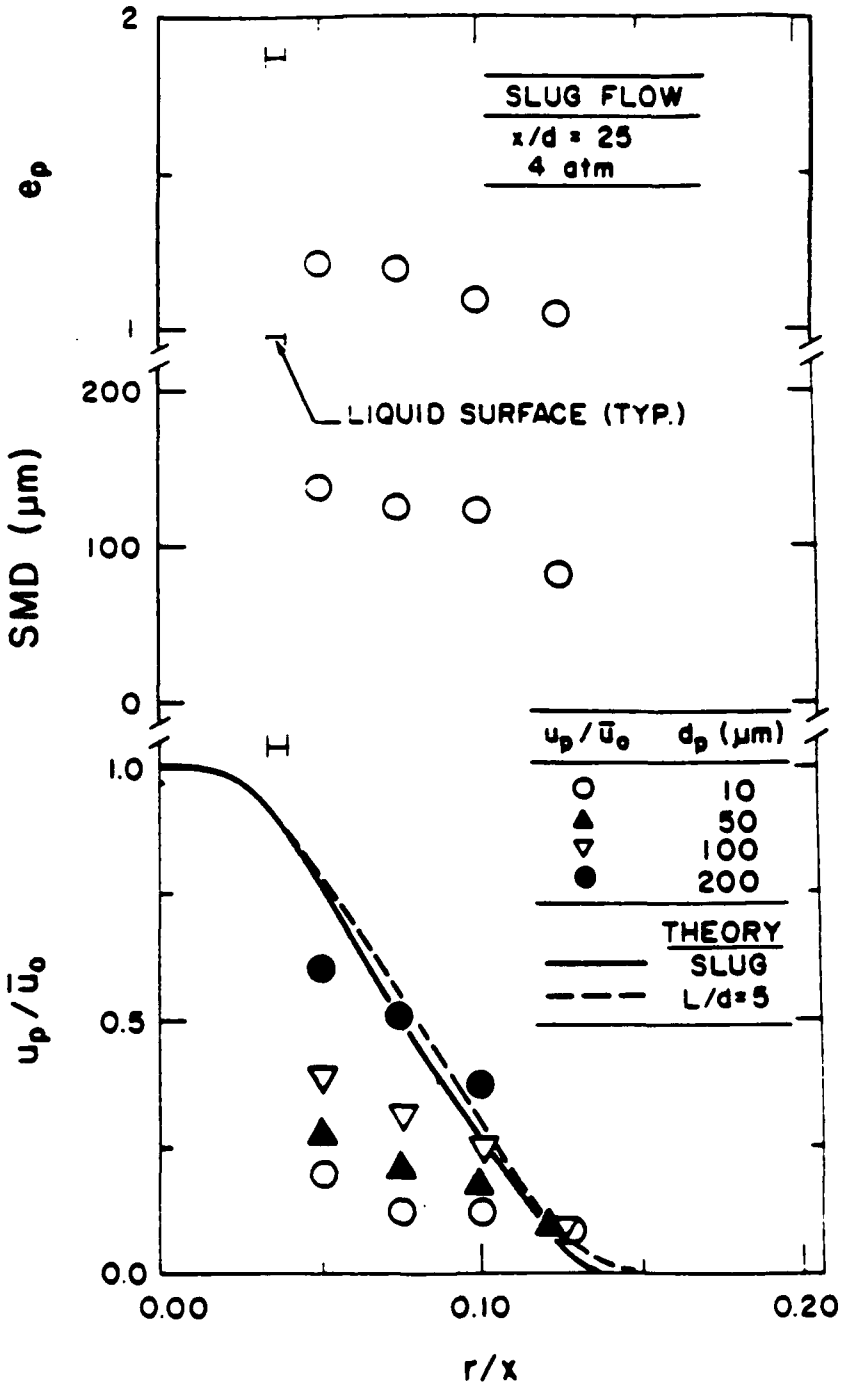

Figure 12 Drop properties for slug flow at x/d = 25 and 4 atm

2.5 Conclusions

The structure and mixing properties of nonevaporating multiphase mixing layers along the sides of liquid jets in still gases were studied for various liquid/gas density ratios. The major conclusions of the study are as follows:

1. Decreasing liquid/gas density ratios increases the rate of mixing and the flow width, analogous to the behavior of single-phase mixing layers.

2. Increasing turbulence levels in the liquid increase the mixing rates and flow width as well.

3. Use of the LHF approximation yielded good results for mean liquid volume fractions greater than 0.1 including predictions of effects of liquid turbulence. However, these conditions correspond to relatively low levels of mixing (mixture fractions greater than 0.85) due to the large liquid/gas density ratios of the present flows.

4. Effects of separated flow were observed for mean liquid mass fractions less than 0.85, causing poor performance of predictions based on the LHF approximation in this region.

5. Local drop size distributions throughout the dispersed flow region satisfied Simmons' (1977) universal root normal distribution function with MMD/SMD = 1.2, and can be characterized completely by the SMD alone.

6. Drop sizes after primary breakup were larger for turbulent than laminar liquids even though the rate of mixing is more rapid for turbulent liquids.

7. Effects of decreasing the liquid/gas density ratio on drop sizes after primary breakup were relatively small for nonturbulent liquids but caused drop sizes to progressively decrease for turbulent liquids.

8. Drops sizes were largest at the liquid surface while mean liquid volume fractions within the dispersed phase were less than 0.1%; this implies that secondary breakup is a dominant feature of the mixing layer, rather than collisions.

Thus, pending resolution of existing uncertainties about primary and secondary breakup, the LHF approach offers a useful treatment of high-speed multiphase mixing layers. It should be recognized, however, that the LHF approach will over-estimate the rate of development of the flow by a degree that can not be quantified until uncertainties about breakup are quantified. This process will be treated next.

3. PRIMARY BREAKUP AT LIQUID SURFACES

3.1 Introduction

The objective of this phase of the investigation was to study primary breakup along the liquid surface in multiphase mixing layers. Based on the results discussed in Section 2, the investigation was divided into two parts, considering primary breakup of nonturbulent and turbulent liquids. However, aerodynamic effects were considered in both cases. Experimental methods were similar to the study of multiphase mixing layers, mainly

involving observations of primary breakup along the surfaces of liquid jets in still gases using single-and double-pulsed holography.

A number of reviews of liquid atomization processes have appeared (Clift et al. 1978; Faeth 1987, 1990; Harrje and Reardon 1972; Lefebvre 1980; Levich 1962; McCarthy and Malloy 1974; Reitz and Bracco 1982); therefore, only the main features of past work will be considered. Beginning with nonturbulent primary breakup, past work has sought to explain mean drop sizes after primary breakup. Two major approaches have been proposed: (1) aerodynamic breakup based on linear wave growth theory, which was proposed initially by Taylor (1940), with subsequent development by Ranz (1959) and Levich (1962) and later application by Reitz and Bracco (1982), among others; and (2) sheltered wave growth theory due to Mayer (1961) and Adelberg (1968) which is based on the surface wave growth model of Jeffreys (1926). Intrinsic to both approaches is that primary breakup is induced by instabilities growing on the liquid surface due to aerodynamic effects in spite of extensive evidence of strong effects of vorticity in the liquid at the passage exit on primary breakup properties (Faeth 1990, Wu et al. 1991). Thus, these methods have not been very successful and have only been evaluated using data that was probably affected by secondary breakup, yielding a long history of continued use due to the absence of alternatives and limited acceptable ranges of application (Harrje and Reardon 1972). Strong effects of liquid vorticity on spray breakup have been reported for some time. First of all, the early studies of pressure atomization of DeJuhasz et al. (1932) and Lee and Spencer (1933) showed that atomization quality differed for nonturbulent and turbulent liquids. Next, Grant and Middleman (1966) and Phinney (1966) observed that jet stability and the onset of breakup were affected by the presence of turbulence. Additionally, Chehroudi et al. (1985) observed effects of jet exit turbulence on the length of the liquid core for pressure atomization. Finally, Hoyt and Taylor (185) found virtually no effect of breakup properties when gas velocities were varied at atmospheric pressure for fixed liquid flow conditions: clear proof that most of the existing data base at atmospheric pressure was not affected by aerodynamic phenomena in spite of continued use of aerodynamic theories to correlate measurements over limited data ranges.

The present investigation seeks to clarify some of the difficulties of current understanding of primary breakup. The approach was to make measurements of primary breakup properties, exploiting recent progress in the use of holography for measurements of this type (Ruff et al. 1991). This was accompanied by the use of phenomenological theories in an attempt to explain and correlate the measurements, in order to capture the physics of the process with a tractable investment in analysis and computations.

The discussion begins with a brief description of experimental methods. Results are then considered, treating the findings of measurements and phenomenological analysis for the primary breakup of nonturbulent and turbulent liquids in turn. The present description is brief, see Wu (1992), Wu and Faeth (1992) and Wu et al. (1991, 1992) for more details. For convenience, the latter three papers may be found in Appendices E, F and G.

3.2 Experimental Methods

Apparatus. The apparatus consisted of a pneumatically-driven piston/cylinder arrangement as illustrated in Fig. 13. For nonturbulent breakup experiments the cylinder outflow was through a smooth convergent passage with injection into room air. For turbulent breakup experiments, the convergent passage was followed by a constant area passage (41 diameters long) to provide fully-developed turbulent pipe flow at the exit; in this case, injection was either into room air or into a windowed chamber filled with helium, air or Freon 12 at pressures of 1 and 2 atm. Liquid sample sizes within the cylinder were

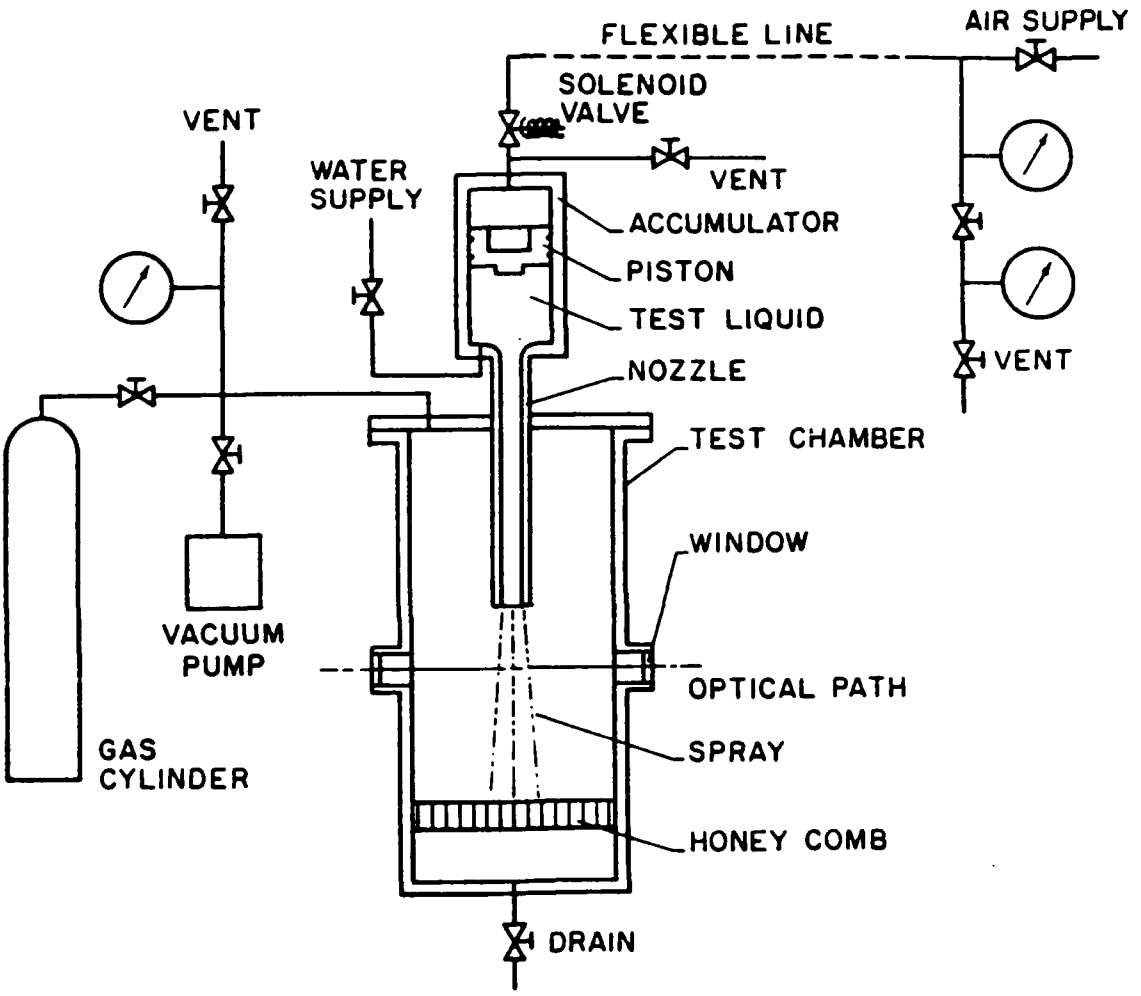

Figure 13 Sketch of test apparatus

roughly 500 ml with passage diameters in the range 3.6-6.4 mm. Instrumentation was mounted rigidly so that various positions were studied by traversing the entire injector/chamber assembly.

The piston/cylinder arrangement was filled while venting gas trapped below the piston face. Operation was initiated by admitting high-pressure air to the upper side of the piston through a solenoid value which forced the liquid through the jet passage. Total times of injection were 180-1400 ms due to the finite liquid sample size; however, this was not problematical because flow development times were generally less than 1% of the flow time for conditions of interest. Jet exit velocities were calibrated using an impact plate.

Instrumentation. The measurements consisted of pulsed shadowgraphy and single- and double-pulse holography. The arrangement of the holocamera was the same as Ruff et al. (1991) as illustrated in Fig. 14. An off-axis arrangement was used based on a ruby laser with a 20 ns pulse duration that could be double-pulsed with separation times as small as 1 μs. The optics allowed measurements of drop diameters as small as 5 μm, while double pulsing allowed drop velocities to be measured. The holograms were reconstructed and analyzed using a Gould FD 5000 Image Processor. The shadowgraphs were made by blocking the reference beam, with other aspects of these measurements the same as holography.

Test Conditions. Test conditions for nonturbulent primary breakup involved water, n-heptane and glycerol mixtures (21, 42 and 63% by mass) in still air at atmospheric pressure. Present work used a 5 mm injector diameter with liquid velocities in the range 16.5-133.8 m/s. This was supplemented by measurements using a 9.5 mm diameter injector, with velocities of 49-60 m/s and ambient air at pressures of 1-4 atm from Ruff et al. (1991, 1992) and Tseng et al. (1992a,b).

Test conditions for turbulent primary breakup involved water, n-heptane and glycerol (42% dry mass) in still helium, air and Freon 12 at pressures of 1 and 2 atm. Injector diameters were 3.6 and 6.4 mm with liquid velocities in the range 16-109 m/s. These results also were supplemented by measurements from Ruff et al. (1991, 1992) and Tseng et al. (1992a,b) for a 9.5 mm diameter injector.

3.3 Nonturbulent Liquid Breakup

Similar to the results discussed in Section 2, drop sizes after primary breakup satisfied Simmons' (1977) universal root normal distribution with MMD/SMD = 1.2. Thus, drop size information will be presented solely in terms of the SMD in the following.

It was found that drop characteristics varied with distance along the mixing layer at first but eventually approached a regime where the rate of variation was relatively slow. This latter regime will be termed the fully-developed primary breakup regime in the following. Approach to fully developed conditions was slower for more viscous liquids and tended to correlate as a function of Re_{fx} as illustrated for SMD in Fig. 15. The data are relatively limited, however, the fully-developed primary breakup regime seems to be reached for Re_{fx} on the order of 10^6. The values of e_p for nonturbulent primary breakup generally were in the range 1.2-1.5 for the fully-developed regime after reaching maximum values in the range 1.5-2.0 for Re_{fx} near 10^6 (Wu et al. 1991).

A correlation of the SMD after nonturbulent primary breakup in the fully-developed regime was attempted based on the existing theoretical correlations of Taylor (1940),

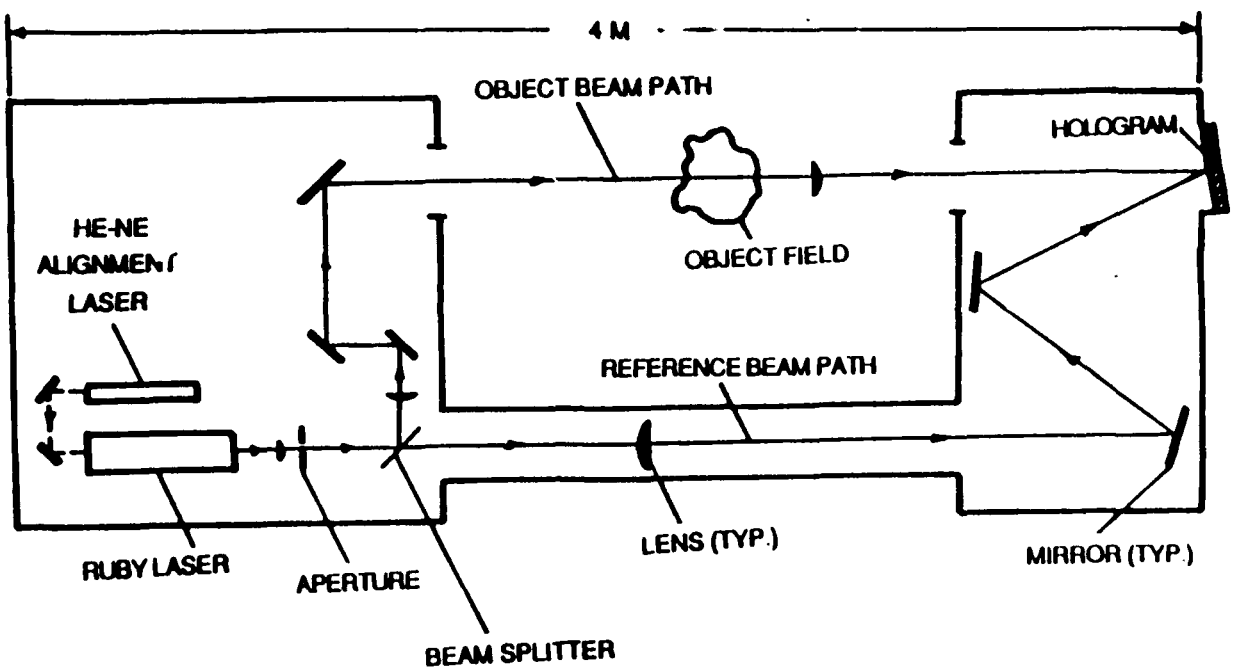

Figure 14 Sketch of holocamera

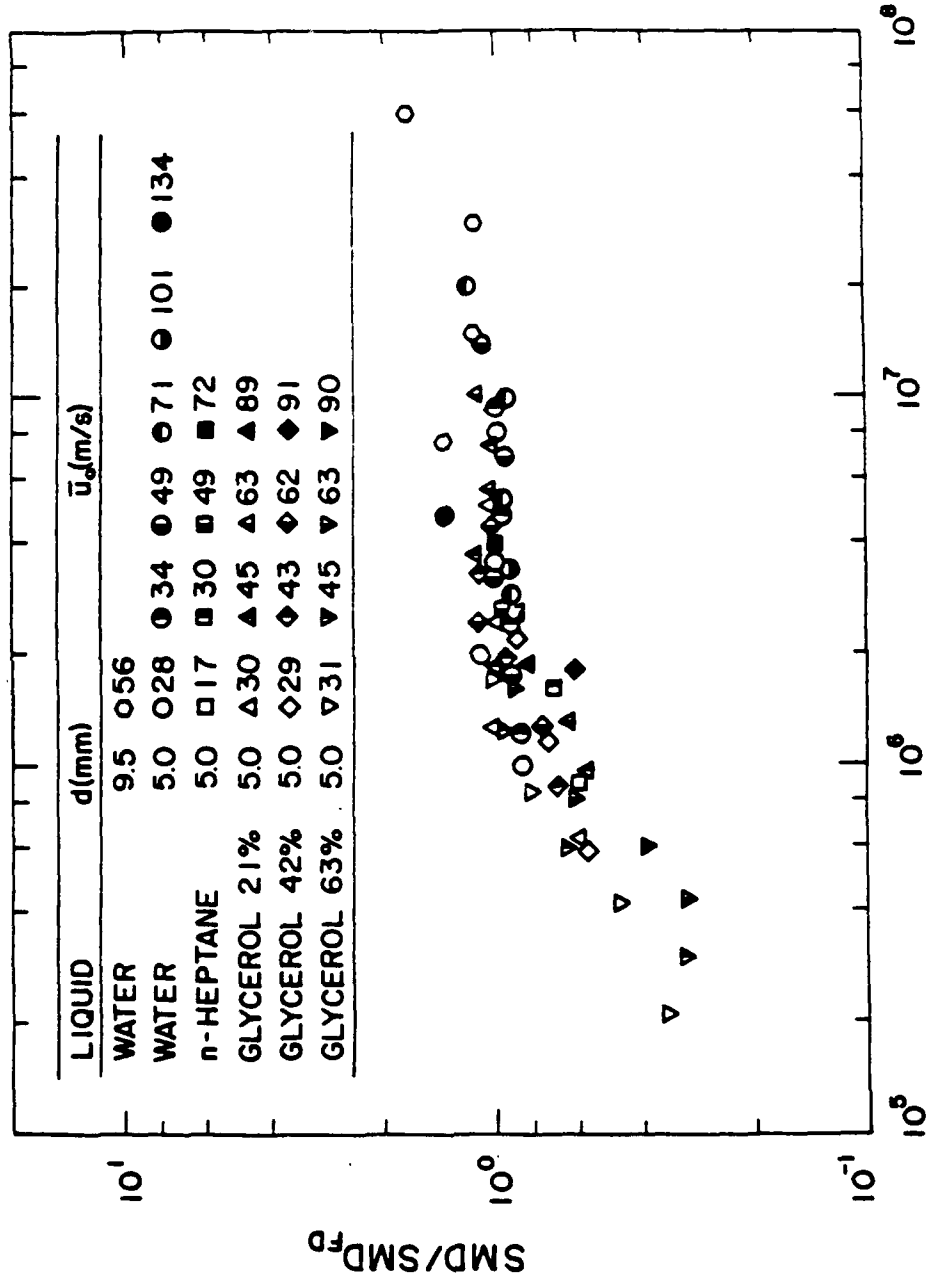

Figure 15 Streamwise variation of SMD for nonturbulent breakup

Levich (1962), Mayer (1961) and Adelberg (1968). All these correlations can be expressed in terms of the same variables as shown in Fig. 16. The Taylor (1940) and Levich (1962) correlations are identical at small values of the independent variable (the Taylor number) and have been fitted to the measurements of Ruff et al. (1991) for illustrative purposes. The limit of primary breakup proposed by Levich (1962) at a Taylor number on the order of unity also is shown on the plot. The correlations of Mayer (1961) and Adelberg (1968) are plotted using recommended empirical coefficients although these are known to vary widely for particular injector designs (Harrje and Reardon 1972).

Clearly, none of the theoretical expressions illustrated in Fig. 16 provide a successful correlation of present measurements. In particular, results for a given liquid do not yield the correct velocity dependence, while changes of liquids yield shifts of behavior that are not anticipated by any of the theories. The correlations of Mayer (1961) and Adelberg (1968) provide the best approximation of velocity effects, which probably accounts for their continued use for liquid rocket engine applications (Harrje and Reardon 1972).

Initially, an alternative approach was developed based on the development of surface boundary layers on the windward side of waves along the liquid surface (Wu et al. 1991). This was successful for treating data from a given injector but was problematical due to unexplained shifts in measurements resulting from changes in the length of the injector passage. Coupled with the observations of small aerodynamic effects from Hoyt and Taylor (1985), this led to a modified approach based on vorticity developed by the injector passage boundary layers (Wu et al. 1992). Thus, present considerations will be limited to this mechanism.

A sketch of the injector passage vorticity mechanism appears in Fig. 17. In this case, it is assumed that drop generation is due to vorticity produced by the wall boundary layer formed when liquid passes through the injector passage. This is plausible because the surface only can be distorted and ligaments ejected when vorticity exists near the liquid surface. Thus, once the liquid leaves the injector passage, boundary layer vorticity starts to distort the liquid surface and causes ligaments to be shed. After a certain distance, liquid surface disturbances have fully developed and the resulting drop sizes remain almost constant in the fully-developed regime. It then is assumed that drop sizes in the fully-developed primary breakup regime are proportional to the wall boundary layer thickness at the jet exit. Due to the large contraction ratio, it is further assumed that the wall boundary layer remains laminar. Then, applying predictions for a laminar flat plate boundary having a nozzle contraction curve length, L_p, there results:

$$We_{gSMD} = C_B(L_p/d)^{1/2}We_{gd}/Re_{f\,d}^{1/2} \qquad (1)$$

Measurements for the fully-developed nonturbulent primary breakup regime are plotted in terms of the variables of Eq. (1) in Fig. 18. Experimental results include present measurements and those of Ruff et al. (1991) and Tseng et al. (1992b). The best fit of the measurements also is shown on the plot; it has a slightly different power than Eq. (1) as follows:

$$We_{gSMD} = 6.81[(L_p/d)^{1/2}We_{gd}/Re_{f\,d}^{1/2}]^{0.85} \qquad (2)$$

The reduction of the power on the right hand side of Eq. (2) from unity to 0.85 is statistically significant but is not large in view of the qualitative nature of the development of the correlation. The correlation coefficient of the fit is 0.98, which is excellent.

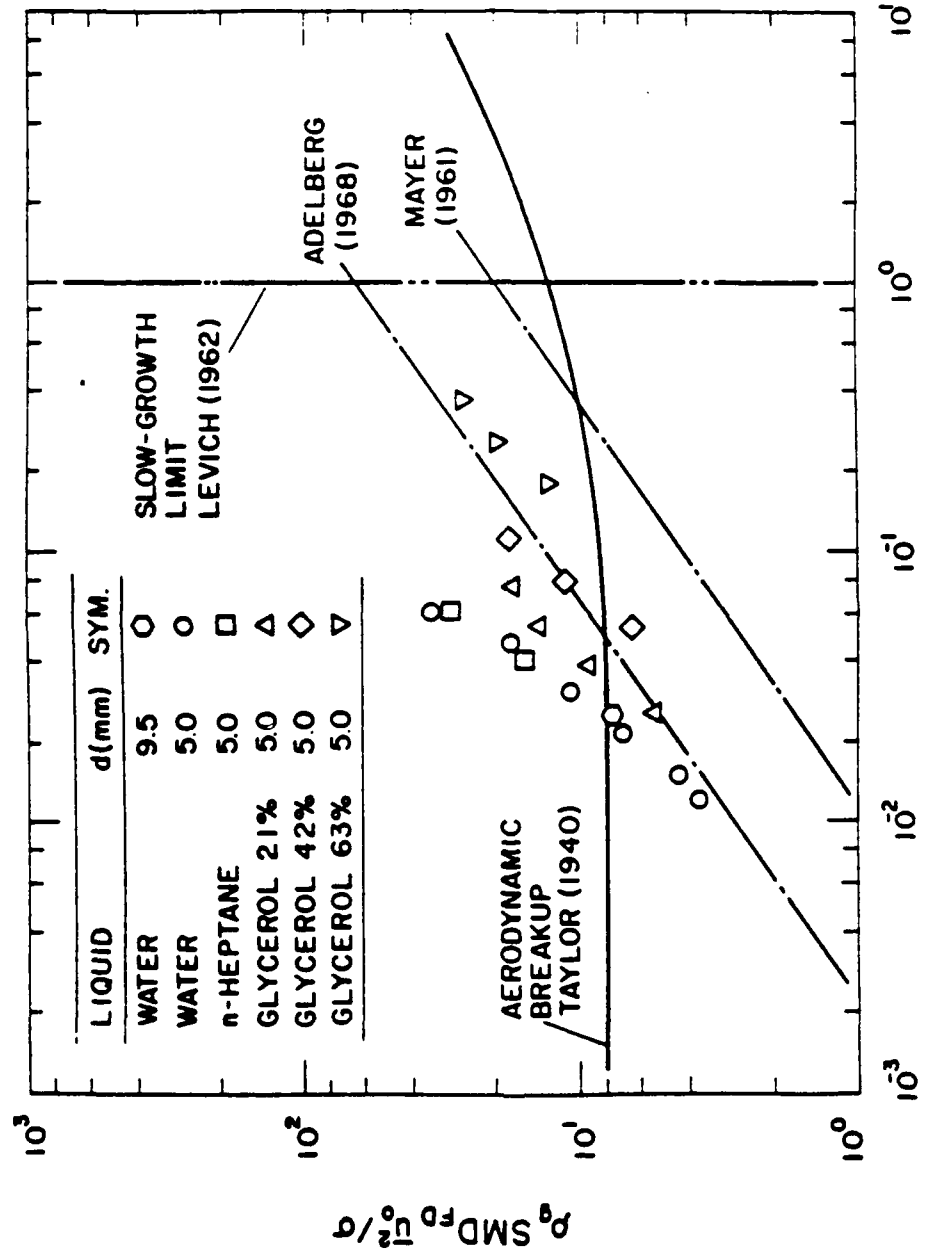

Figure 16 Correlation of SMD for fully-developed nonturbulent primary breakup using existing theories

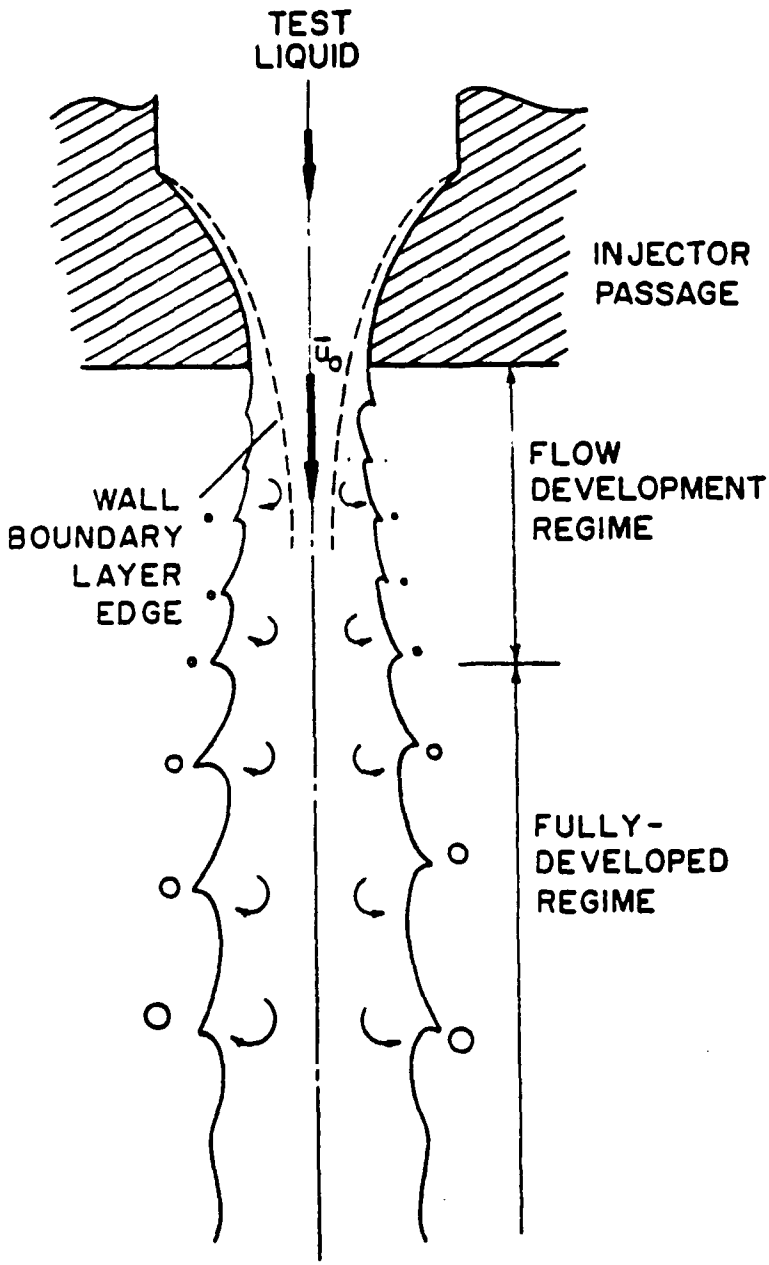

Figure 17 Sketch of injector passage boundary layer vorticity mechanism

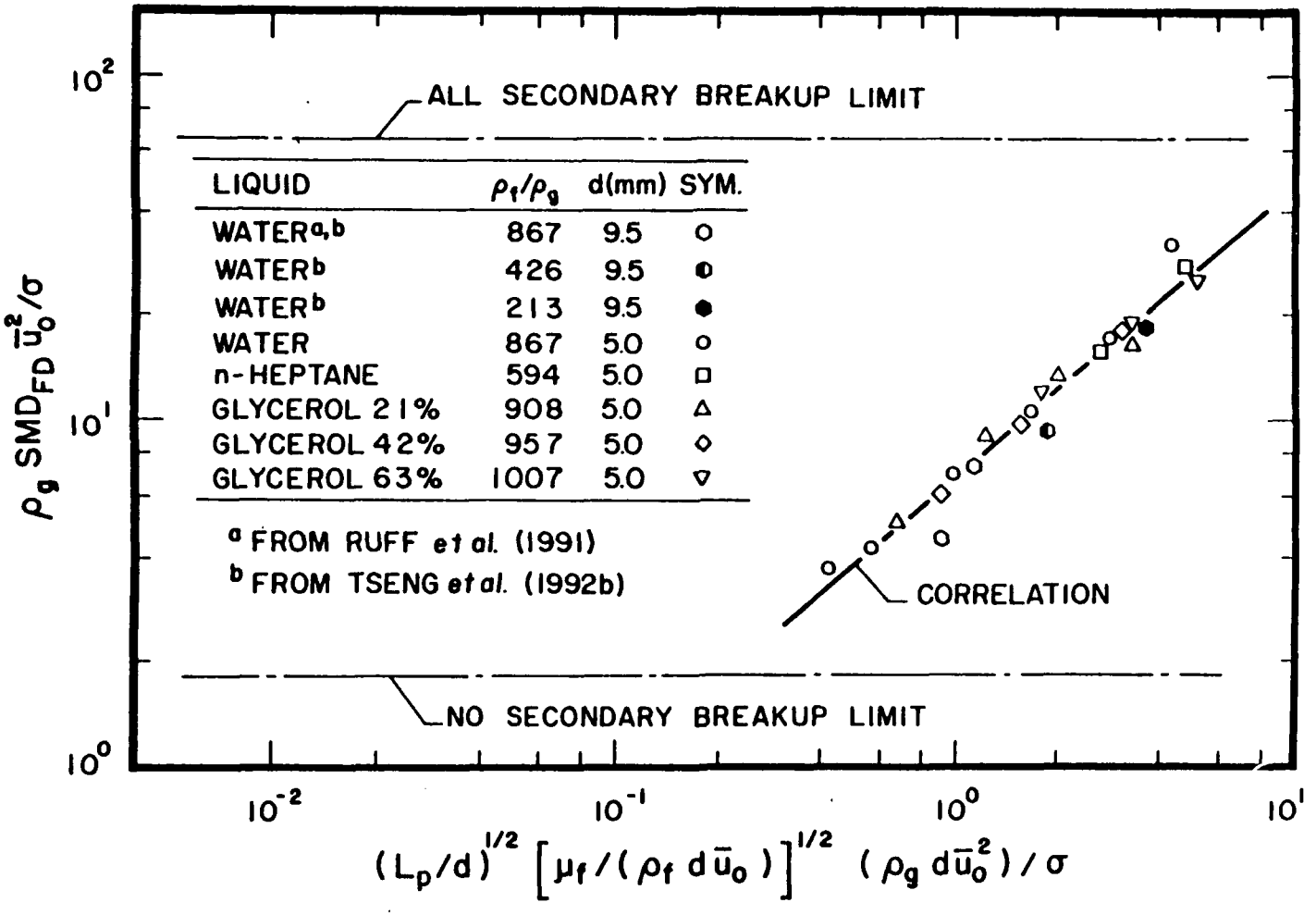

Figure 18 Correlation of SMD for fully-developed nonturbulent primary breakup based on the boundary layer vorticity mechanism

The excellent performance of Eq. (2) suggests that boundary layer growth inside the injector passage determines drop dimensions in the fully-developed breakup regime. This implies that the surrounding gas plays no role in the breakup process through aerodynamic effects even though relative velocities are large for present test conditions, with the possible exception being a contribution to the reduction of the power. This agrees with the observations of Hoyt and Taylor (1985) that there is no significant change of liquid surface structures in either co-flowing or counter-flowing air streams flowing at a variety of relative velocities at atmospheric pressure. Additionally, the results of Tseng et al. (1992) for gas density variations over the range 1-4 atm showed modest effects of gas density on drop sizes after primary breakup. These results also are seen to be effectively correlated by Eq. (2) in Fig. 18. Thus, it appears that liquid vorticity dominates low levels of vorticity due to aerodynamic drag for present test conditions, which accounts for the failure of the aerodynamic drag theories seen in Fig. 16. This also highlights a limitation of present work; namely, that only two injectors of similar general passage design were considered (Wu 1991). Based on past experience (Harrje and Reardon 1972) variations of C_B with different passage designs can be anticipated. Finally, the connection between these results and gas injection processes for nonturbulent liquids is not clear. However, this is not a major limitation because most practical gas injection processes involve turbulent liquids.

Another interesting feature of the results of Fig. 18 is the potential for secondary breakup. First, of all, it generally is agreed that drops are unstable to secondary breakup when their Weber number exceeds a critical value, as follows (Lefebvre 1980, Ruff et al. 1992):

$$We_{gp} = \rho_g d_p \bar{u}_o^2/\sigma > 6.5 \qquad (3)$$

Equation (3) has been written assuming that the relative velocity of large drops subject to secondary breakup is equal to the relative velocity of the mixing layer, which is reasonable based on existing measurements (Ruff et al. 1991, 1992). Now the universal root normal drop size distribution implies that 99.7% of the spray mass is in the diameter range $0.098 \leq d_p/SMD \leq 3.5$. This information and Eq. (3) implies that $We_{gSMD} = 1.8$ and 66 define limiting conditions where virtually no drops and all drops undergo secondary breakup.

The limits of secondary breakup are shown in Fig. 18 along with the primary breakup correlation. Noting that it is difficult to achieve primary breakup for values of the independent variable much lower than the present test range, it is evident that drops formed by nonturbulent primary breakup generally are unstable to secondary breakup. This helps explain the durability of primary breakup correlations like those of Taylor (1940) and Levich (1962): any contamination of measurements by secondary breakup causes reductions in the range of We_{gSMD}, tending to support the trends of these relationships, since past measurements of drop sizes were carried out after the sprays were dilute, providing time for completion of secondary breakup processes. Additionally, the results of secondary breakup do not depend on jet diameter, which helps to explain the weak, or absent, jet diameter effects seen in early correlations of primary breakup (Faeth 1990).

Finally, it was argued that effects of ambient gas density on present observations of nonturbulent primary breakup were small. However, parameters controlling secondary breakup (see Eq. (3)) respond rapidly to gas density changes. Thus, higher gas densities than those considered by Tseng et al. (1992b) could involve merging of primary and secondary breakup similar to observations of turbulent primary breakup to be discussed next: this should be explored.

3.4 Turbulent Liquid Breakup

Drop Size Distribution. Similar to the other conditions, drop sizes after turbulent primary breakup satisfied Simmons' (1977) universal root normal distribution with MMD/SMD = 1.2. Thus, drop sizes will be represented by SMD alone in the following.

Drop Velocities. Drop velocities after turbulent primary breakup were measured over the full range of test conditions. The measurements of volume (mass) averaged streamwise and crosstream drop velocities are plotted as a function of distance along the mixing layer in Fig. 19. Results for $\rho_f/\rho_g < 500$ are shown as darkened and half-darkened symbols, while results for $\rho_f/\rho_g > 500$ are shown as open symbols, in order to highlight properties at the low liquid/gas density ratio regime where aerodynamic effects are important. This practice will be followed on subsequent plots of data as well.

The normalized drop velocities shown in Fig. 19 provide crude correlations in terms of x/d but other factors are involved. Near the jet exit, $\tilde{u}_p/\bar{u}_o$ is roughly 0.6, which increases to roughly 0.9 for x/d > 20. This behavior is consistent with streamwise drop velocities after turbulent primary breakup being roughly the same as streamwise liquid velocities, with lower velocities near the jet exit due to the retarding effect of the passage wall. Superimposed on this behavior, however, is a clear trend that measurements for $\rho_f/\rho_g < 500$ have significantly lower streamwise velocities than the rest. This behavior can be attributed to effects of aerodynamic drag.

Similar trends with respect to density variations are much less clear for $\tilde{v}_p/\bar{u}_o$ in Fig. 19. In general, crosstream drop velocities are comparable to crosstream velocity fluctuations in the liquid, e.g., $\bar{v}_o'/\bar{u}_o = 0.058$ for fully-developed turbulent pipe flow (Hinze 1975; Tennekes and Lumley 1972). The absence of an effect of aerodynamic drag in this case can be explained due to a compensating aerodynamic acceleration effect over the tips of liquid protuberances that will be discussed next in connection with the onset of breakup.

Onset. Phenomenological analysis to find drop properties at the onset of breakup is based on the concept illustrated in Fig. 20. It is assumed that onset involves the formation of a drop from a turbulent eddy of characteristic size ℓ and a characteristic crosstream velocity relative to the surrounding liquid, v_ℓ. The smallest drops that can be formed either are comparable to the Kolmogorov scale of the turbulence or the smallest eddy that has sufficient mechanical energy needed to form a drop, whichever is larger. For present conditions, drop energy was the limiting factor and only this limit was pursued. The mechanical energy available consists of the kinetic energy of the eddy relative to its surroundings, plus the added mechanical energy due to the pressure drop caused by acceleration of the surrounding gas over the tip of the protuberance. Then equating these energies, assuming that the eddy is in the inertial range of the turbulence spectrum, to the surface tension energy of the resulting drop, there results:

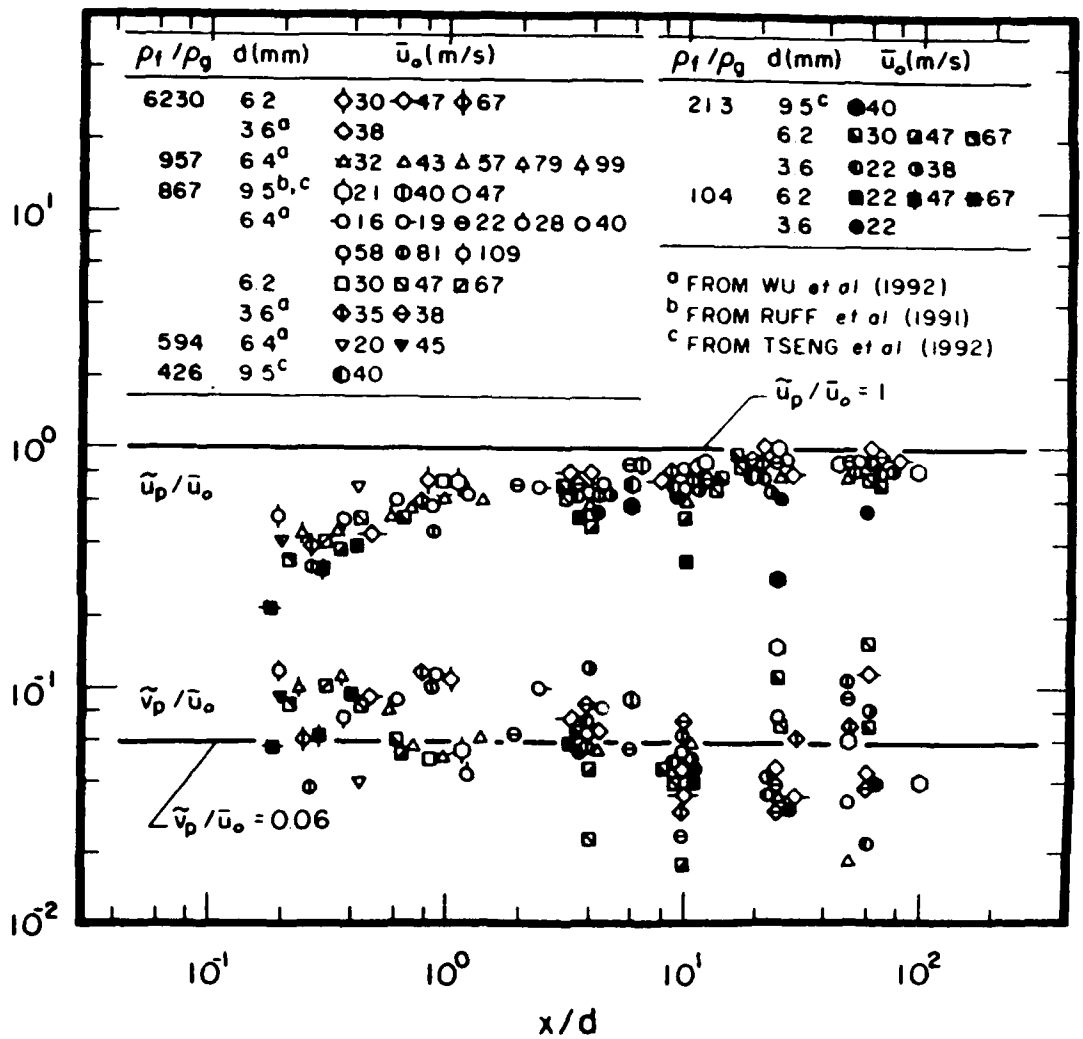

Figure 19 Mass-averaged drop velocities after turbulent primary breakup

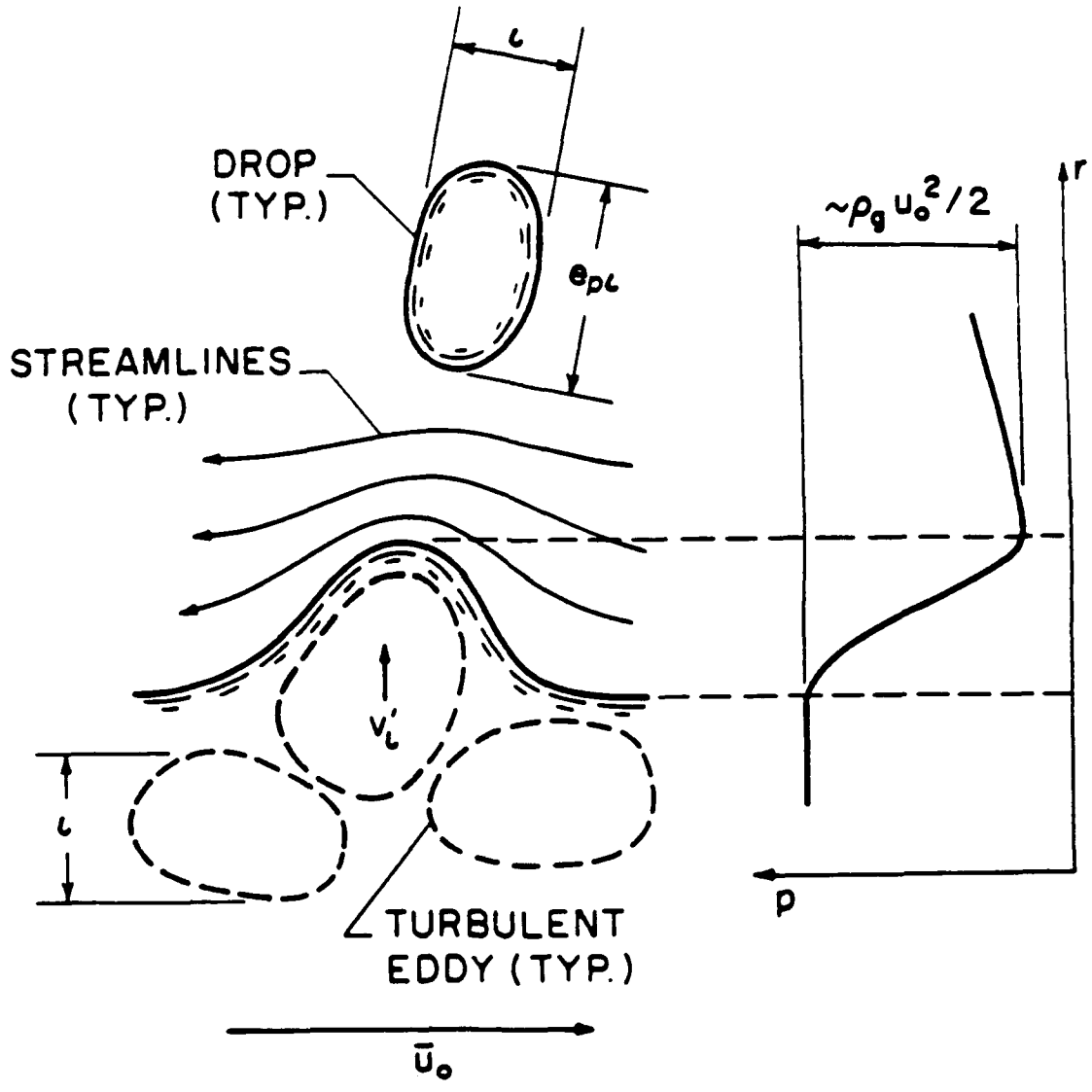

Figure 20 Sketch of aerodynamically-enhanced turbulent primary breakup at the liquid surface

$$(SMD_i/\Lambda)(1 + C_{sa}(\rho_g/\rho_f)(\bar{u}_o/\bar{v}_o')^2(\Lambda/SMD_i)^{2/3})^{3/5}$$

$$= C_{si}(\bar{u}_o/\bar{v}_o')^{6/5}We_{f\Lambda}^{-3/5} \quad (4)$$

where turbulence properties in the liquid are assumed to be the same as at jet exit conditions, C_{sa} and C_{si} are empirical constants and Λ is the radial integral scale (which is taken to be equal to d/8 for fully-developed turbulent pipe flow, see Hinze (1975)).

Present measurements of SMD_i are plotted in terms of Eq. (4) in Fig. 21. In doing this, C_{sa} was optimized to a value of 0.04, based on taking $\bar{v}_o'/\bar{u}_o = 0.058$ for fully-developed turbulent pipe flow (Hinze 1975). The correlation of the data all conditions generally is within anticipated experimental uncertainties. The power of $We_{f\Lambda}$ is not -3/5 as suggested by Eq. (4), however, and the results can be correlated best by the following empirical fit that is shown on the plot:

$$(SMD_i/\Lambda)(1 + 0.04(\rho_g/\rho_f)(\bar{u}_o/\bar{v}_o')^2(\Lambda/SMD_i)^{2/3})^{3/5}$$

$$= 2.5(\bar{u}_o/\bar{v}_o')^{6/5}We_{f\Lambda}^{-0.69} \quad (5)$$

The reduction in the power of $We_{f\Lambda}$ from Eq. (4) to Eq. (5) is not statistically significant while the correlation coefficient of the fit 0.97, which is excellent. Aerodynamic effects are carried by the term multiplied by $C_{sa} = 0.04$ which largely depends on the liquid/gas density ratio and is small for $\rho_f/\rho_g > 500$.

Given SMD_i, it was assumed that the drop-forming eddy convects along the surface with a velocity $\bar{u}_o$ for the distance x_i required to form a drop. The time of convection was taken to be the Rayleigh breakup time of the protruding ligament found from Weber (1931), after ignoring a liquid viscosity term that is small for present test conditions. Then using Eq. (4) to specify SMD_i, the following expression for x_i is obtained:

$$(x_i/\Lambda)(1 + C_{sa}(\rho_g/\rho_f)(\bar{u}_o/\bar{v}_o')^2(\Lambda/SMD_i)^{2/3})^{9/10}$$

$$= C_{xi}(\bar{u}_o/\bar{v}_o')^{9/5}We_{f\Lambda}^{-4/10} \quad (6)$$

where C_{xi} is a constant of proportionality. Similar to Eqs. (4) and (5), aerodynamic effects in Eq. (6) largely are controlled by the liquid/gas density ratio.

Adopting $C_{sa} = 0.04$ as before, the measurements of x_i are plotted in terms of the variables of Eq. (6) in Fig. 22. The correlation of the measurements is reasonably good in view of the relatively large experimental uncertainties of x_i. The best fit of the measurements can be expressed as follows:

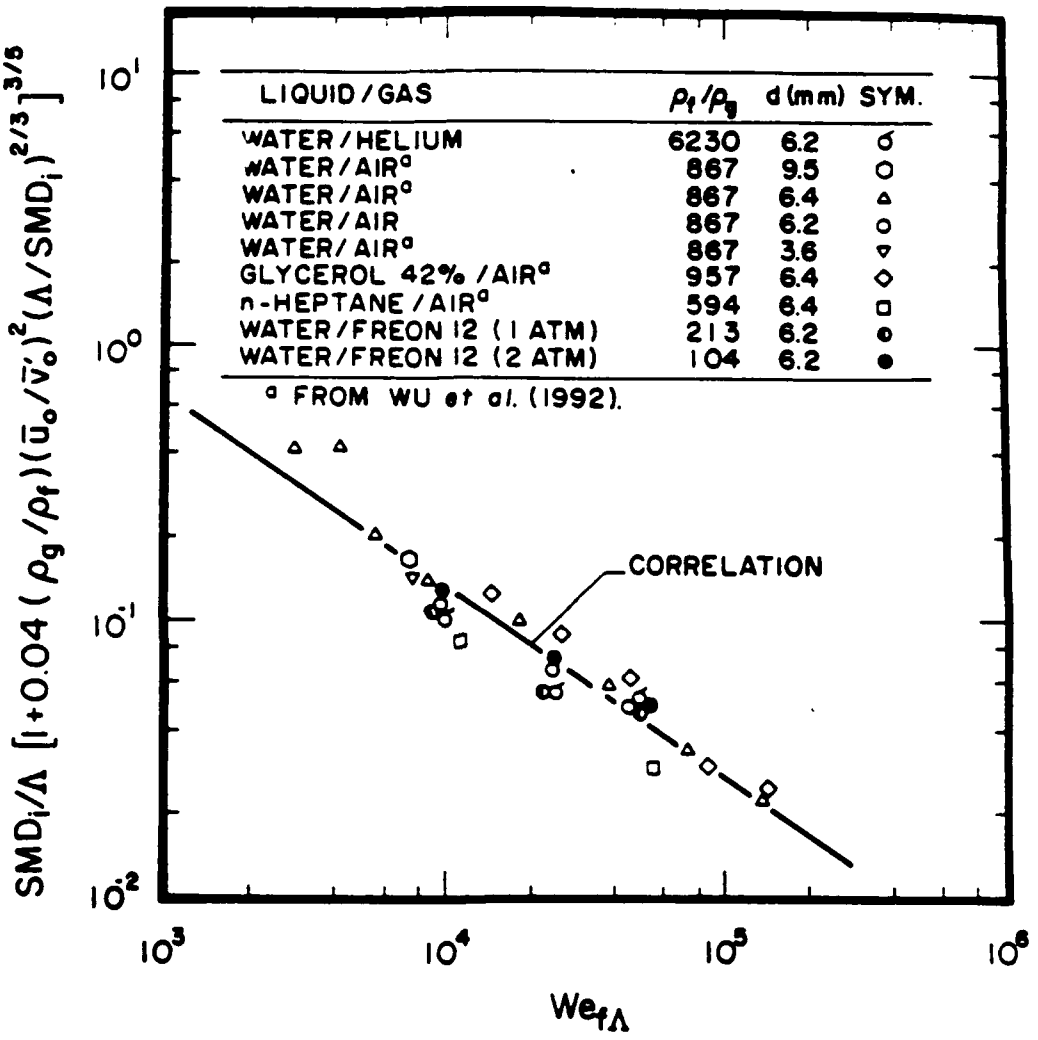

Figure 21 SMD at the onset of turbulent primary breakup

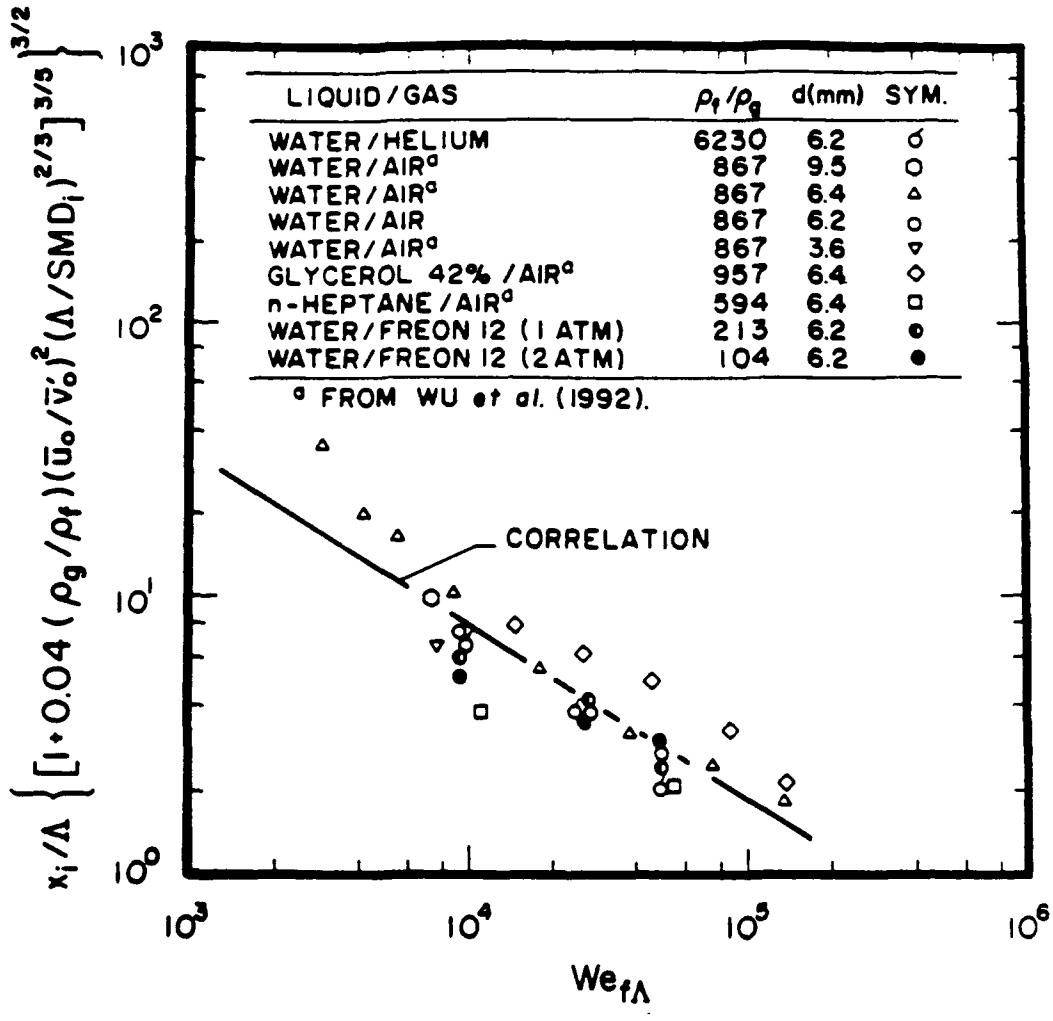

Figure 22 Length to initiate turbulent primary breakup

$$(x_i/\Lambda)(1 + 0.04(\rho_g/\rho_f)(\bar{u}_o/\bar{v}_o')^2(\Lambda/SMD_i)^{2/3})^{9/10}$$

$$= 12(\bar{u}_o/\bar{v}_o')^{9/5}\, We_{f\Lambda}^{-0.63} \qquad (7)$$

with the correlation coefficient of the fit being 0.89. Thus, the difference between the powers of $We_{f\Lambda}$ in Eqs. (6) and (7) is statistically significant but is not large in view of the approximations used to develop the correlating expression.

Drop Sizes after Onset. Aerodynamic secondary breakup times scale like $\ell(\rho_f/\rho_g)^{1/2}\bar{u}_o$ for an object of size ℓ and relative velocity $\bar{u}_o$ (Ranger and Nicholls 1969; Hsiang and Faeth 1992, 1993). Thus, for conditions where aerodynamic effects are important, the Rayleigh breakup times of ligaments increase more rapidly than secondary breakup times as ℓ increases. This yields two possible turbulent primary breakup mechanisms after the onset conditions: (1) nonaerodynamic primary breakup, and (2) merged primary and secondary breakup when aerodynamic effects are important. The configuration of the two mechanisms is illustrated in Fig. 23.

When aerodynamic effects are not important, it is assumed that the SMD is proportional to the largest drop that can be formed at a particular position because the SMD is dominated by the largest drops. Then adopting the Rayleigh breakup mechanism to relate drop size and position, similar to the treatment of onset conditions, the following expression is obtained:

$$SMD/\Lambda = C_{sx}(x/(\Lambda\, We_{f\Lambda}^{1/2}))^{2/3} \qquad (8)$$

where C_{sx} is an empirical constant.

Under the present assumptions, principles relating SMD to x are the same for both the onset of breakup and at larger distances, which suggests that SMD/Λ should be correlated as a function of $x/(\Lambda\, We_{f\Lambda}^{-0.54})$ from Eqs. (5) and (7). Present measurements and those of Ruff et al.(1991) for $\rho_f/\rho_g > 500$, where aerodynamic effects are not important, are correlated in terms of these variables in Fig. 24. Two correlations are shown on the plot as well: (1) the best fit of all the data, and (2) the correlation based on onset conditions alone. The best fit correlation of all the data is:

$$SMD/\Lambda = 0.69[\, x/(\Lambda\, We_{f\Lambda}^{-0.54}\,]^{0.57} \qquad (9)$$

which yields a correlation coefficient of 0.98, which is excellent. Notably, results for injection into still air and helium at atmospheric pressure are essentially the same, in spite of the substantial difference of ρ_f/ρ_g, proving that aerodynamic effects are small for these conditions.

Differences between the two correlations illustrated in Fig. 24 are small so that drop formation both at the onset of breakup and at distances farther along the multiphase mixing layer appear to be similar when aerodynamic effects are weak. The SMD of the smallest drops, formed at the onset of breakup, are in the range 10-20 μm which is roughly ten

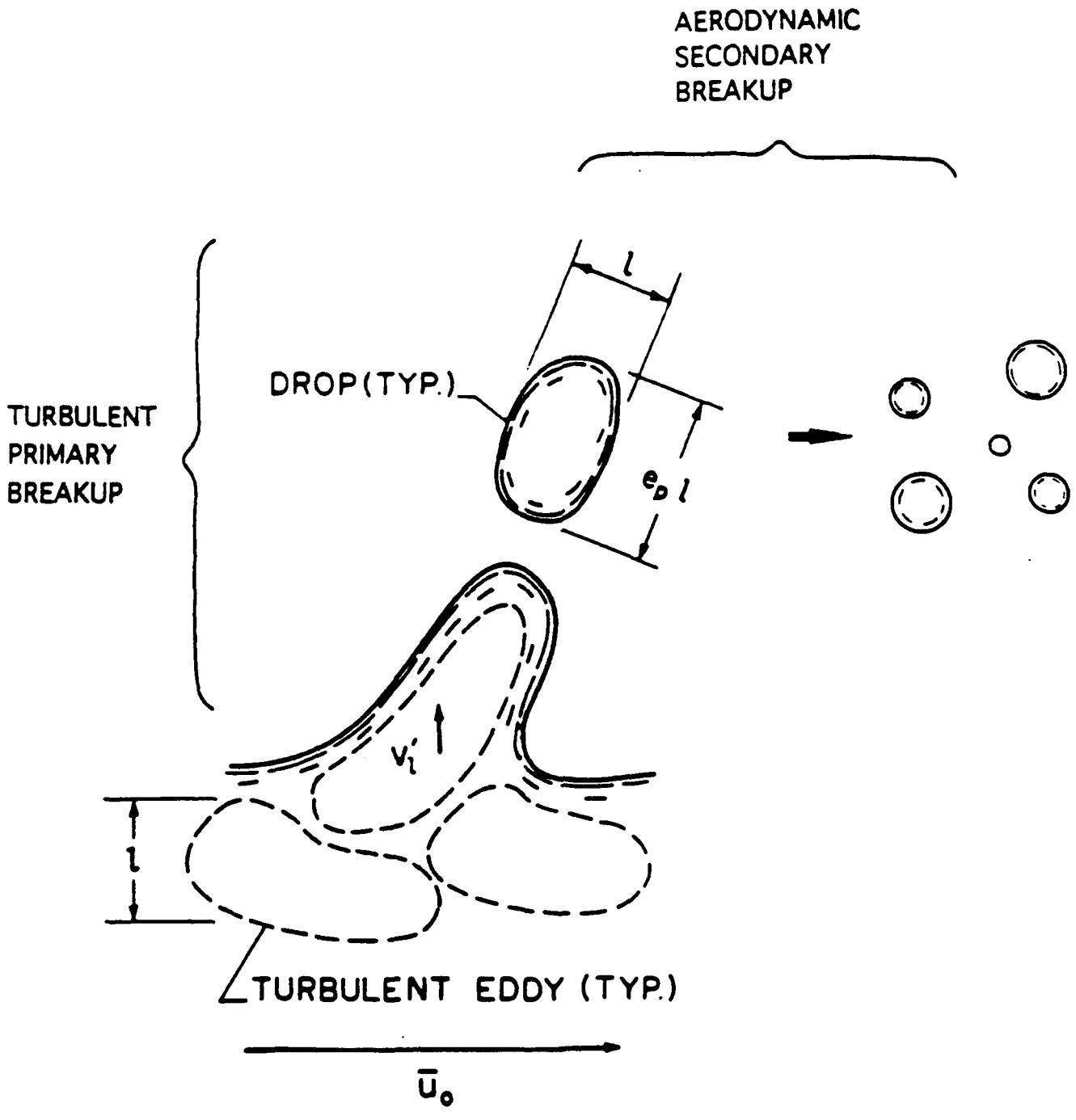

Figure 23 Sketch of turbulent breakup processes

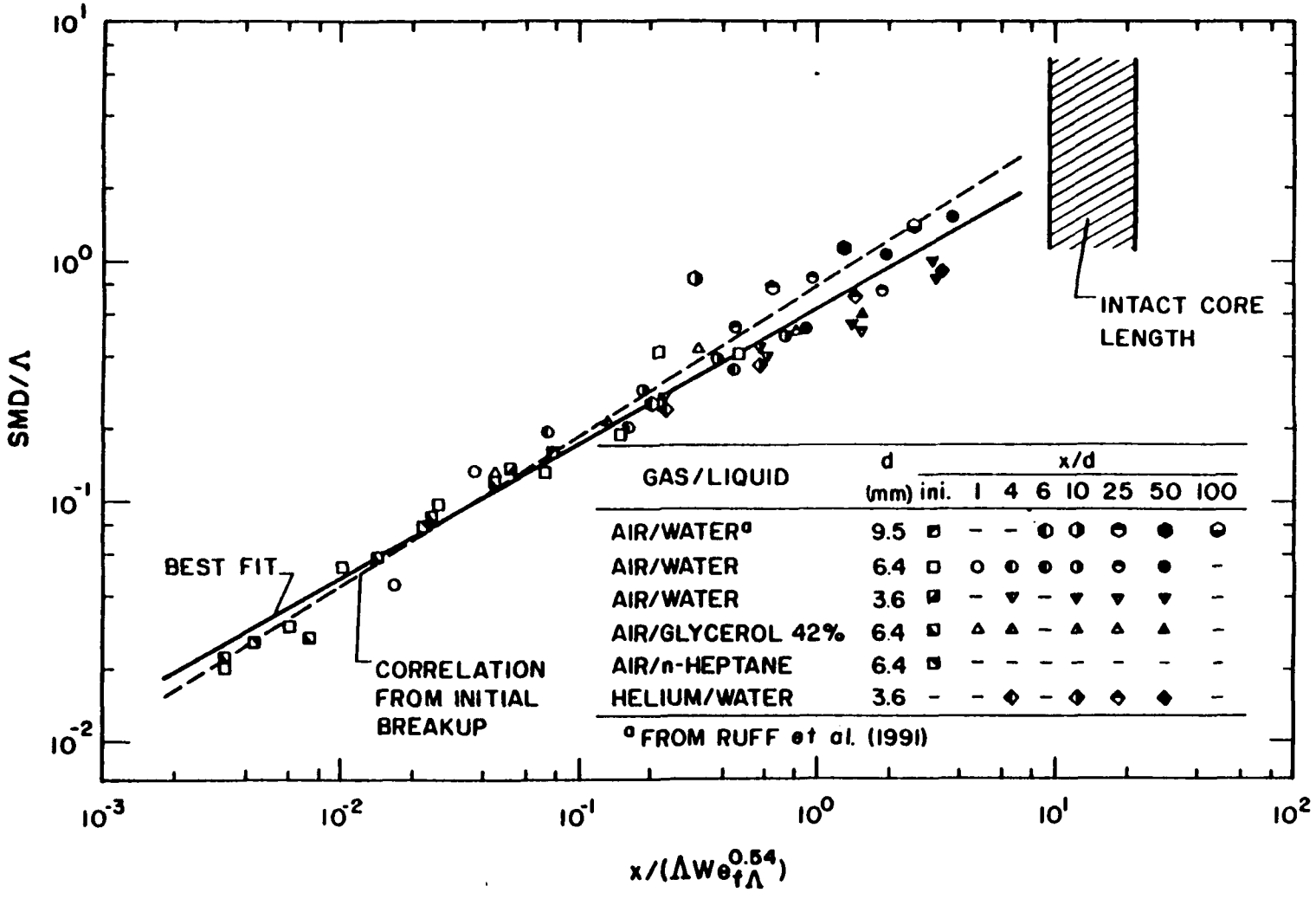

Figure 24 SMD after turbulent primary breakup when aerodynamic effects are small

times larger than Kolmogorov length scales for these test conditions. The characteristics of turbulent breakup should change when Kolmogorov scales are involved which is an interesting issue for future study. The largest SMD seen in Fig. 24 approach the radial integral scales of the turbulence; much larger values are unlikely for round liquid jets due to the finite length of the liquid core. This is shown on the figure by indicating the core length from Grant and Middleman (1966):

$$L_c/d = 8.5\, We_{fd}^{0.32} \tag{10}$$

where the range of L_c/d shown in the figure is due to the variation of We_{fd} over the present test range. A more recent correlation of Chehroudi et al. (1985) yields similar values of L_c but a somewhat broader range. That the SMD approaches Λ when x approaches L_c, and thus is comparable to the diameter of the liquid core itself in this region, is consistent with the liquid column breaking up as a whole.

When aerodynamic effects are important, it is assumed that turbulent primary and secondary breakup merge as illustrated in Fig. 23. In this regime, Eq. (8) is used to estimate the drop size after primary breakup with properties after secondary breakup found from the recent results of Hsiang and Faeth (1992, 1993). Assuming that the appropriate relative velocity is $\bar{u}_o$, the expression for the SMD after secondary breakup of a drop having a diameter d_p is as follows (Hsiang and Faeth 1992):

$$SMD/d_p = C_s(\rho_f/\rho_g)^{1/2}(\mu_f/(\rho_f d_p \bar{u}_o))^{1/2} \tag{11}$$

Then assuming that d_p is proportional to the SMD after primary breakup, Eqs. (8) and (11) can be combined to yield the SMD after merged primary and secondary breakup as follows:

$$\rho_g SMD\bar{u}_o^2/\sigma = C_s C_{sx}^{1/2}(x/\Lambda)^{1/3}(\rho_g/\rho_f)^{3/4} We_{f\Lambda}^{5/6} Re_{f\Lambda}^{-1/2} \tag{12}$$

where C_s in Eq. (12) is modified from Eq. (11) to account for a range of initial drop sizes rather than a single drop.

Present measurements of aerodynamic turbulent primary breakup, along with some results from Tseng et al. (1992b), are plotted according to the variables of Eq. (12) in Fig. 25. The following best fit correlation of the measurements also is shown on the plot:

$$\rho_g SMD\bar{u}_o^2/\sigma = 12[(x/\Lambda)^{1/3}(\rho_g/\rho_f)^{3/4} We_{f\Lambda}^{5/6} Re_{f\Lambda}^{-1/2}]^{1.17} \tag{13}$$

which yields an overall correlation coefficient of the fit of 0.92. Additionally, adopting the best fit values of C_s and C_{sx} in Eq. (12) yields the following theoretical prediction for the SMD:

$$\rho_g SMD\bar{u}_o^2/\sigma = 12.9(x/\Lambda)^{1/3}(\rho_g/\rho_f)^{3/2} We_{f\Lambda}^{5/6} Re_{f\Lambda}^{-1/2} \tag{14}$$

which also is shown on the plot. The standard deviation of the constant in Eq. (14) is 21%; thus, the differences between Eqs. (13) and (14) are not statistically significant. All

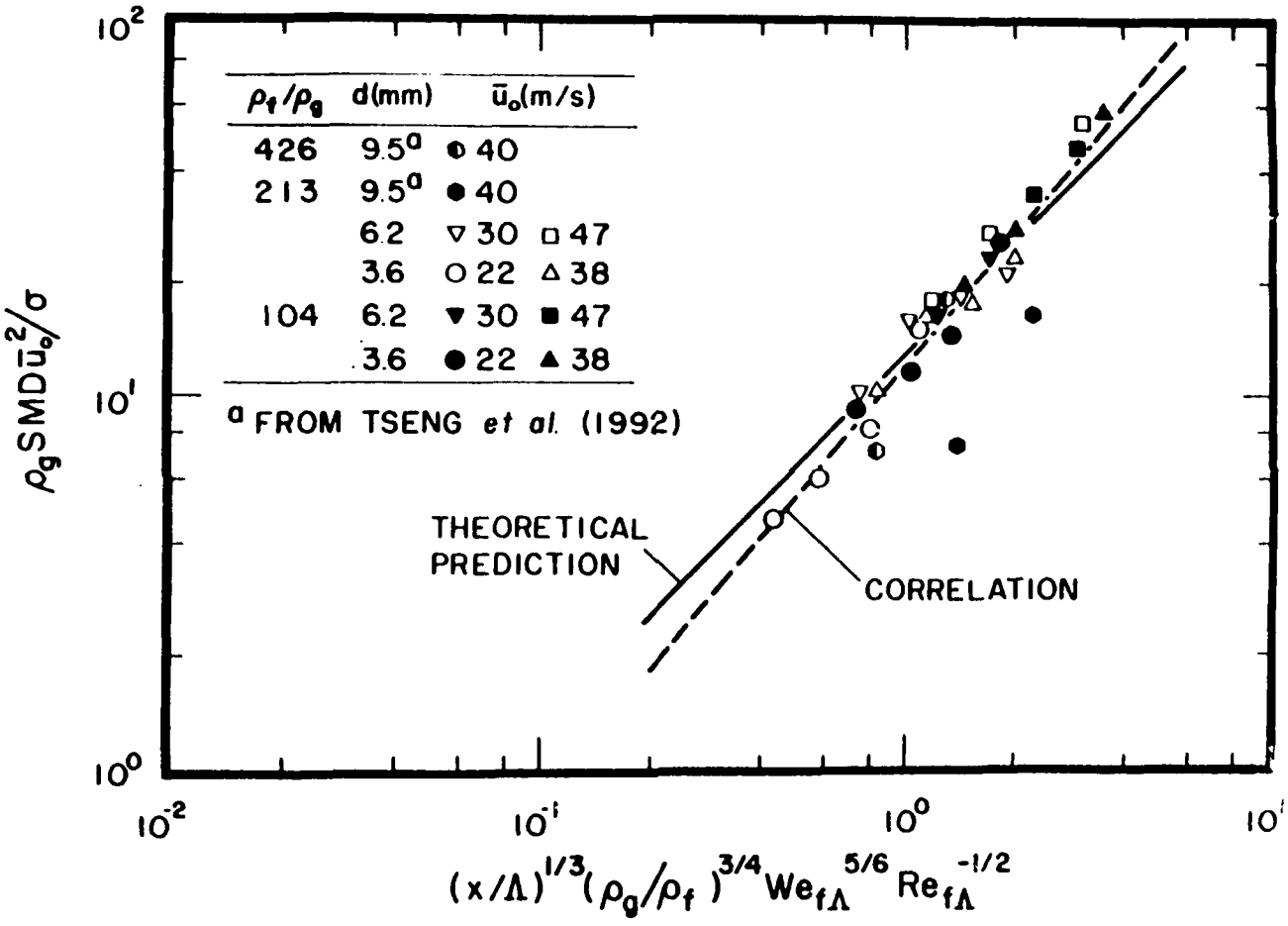

Figure 25 SMD after aerodynamically-enhanced turbulent primary breakup

the measurements are in reasonably good agreement with Eqs. (13) and (14) except for the highest pressure results of Tseng et al. (1992b) which yield significantly smaller drops near the liquid surface. An explanation of this behavior is that these flows involved the largest drop concentrations of all the measurements so that drop properties near the surface could be influenced by small drops migrating from other parts of the multiphase mixing layer due to turbulent dispersion.

Breakup Regimes. The present measurements suggest three regimes of turbulent primary breakup: (1) non-aerodynamic turbulent primary breakup; (2) aerodynamically-enhanced turbulent primary breakup, observed at onset conditions; and (3) aerodynamic turbulent primary breakup, involving merged turbulent primary and secondary breakup. The results also indicated that the liquid/gas density ratio and the relative characteristic Rayleigh breakup times of ligaments and secondary breakup times of liquid objects fixed the boundaries of these regimes. The ratio of the characteristic times can be expressed as follows (Wu and Faeth 1992):

$$\tau_R/\tau_b = (\rho_g/\rho_f)^{1/2}(x\, We_{f\Lambda}/\Lambda)^{1/3} \tag{15}$$

The resulting primary breakup regimes, based on present measurements and those of Ruff et al. (1991) and Tseng et al. (1992b), are illustrated in terms of ρ_f/ρ_g and τ_R/τ_b in Fig. 26. The results yield the following criteria for transitions between regimes

$$\rho_f/\rho_g = 500, \text{ non-aerodynamic/aerodynamic transition} \tag{16}$$

$$\tau_R/\tau_b = 4, \text{ enhanced/merged-aerodynamic transition} \tag{17}$$

Thus, Eqs. (4) and (5) always provide onset conditions — whether aerodynamic effects are important or not. Equation (9) provides the SMD subsequently, when aerodynamic effects are not important. Finally, Eq. (12) provides the SMD after onset, when aerodynamic effects are important in the merged primary and secondary breakup regime.

3.5 Conclusions

The mechanisms of primary breakup of nonturbulent and turbulent liquids were studied within multiphase mixing layers. Various liquids and ambient gas conditions were studied to highlight effects of both liquid properties and liquid/gas density ratio — the latter controlling the importance of aerodynamic phenomena. Confirming earlier observations, all breakup processes yielded drop size distributions that satisfied Simmons' (1977) universal root normal distribution with MMD/SMD = 1.2. Additionally, drops formed by primary breakup are intrinsically unstable to secondary breakup, which is a dominate process in the multiphase mixing layer. Other conclusions differ for nonturbulent and turbulent primary breakup as discussed in the following.

Major conclusions concerning nonturbulent primary breakup are as follows:

1. Drop properties after primary breakup varied with distance along the mixing layer but became relatively uniform in a fully-developed primary breakup regime for Re_{fx} greater than 10^6, see Fig. 15.

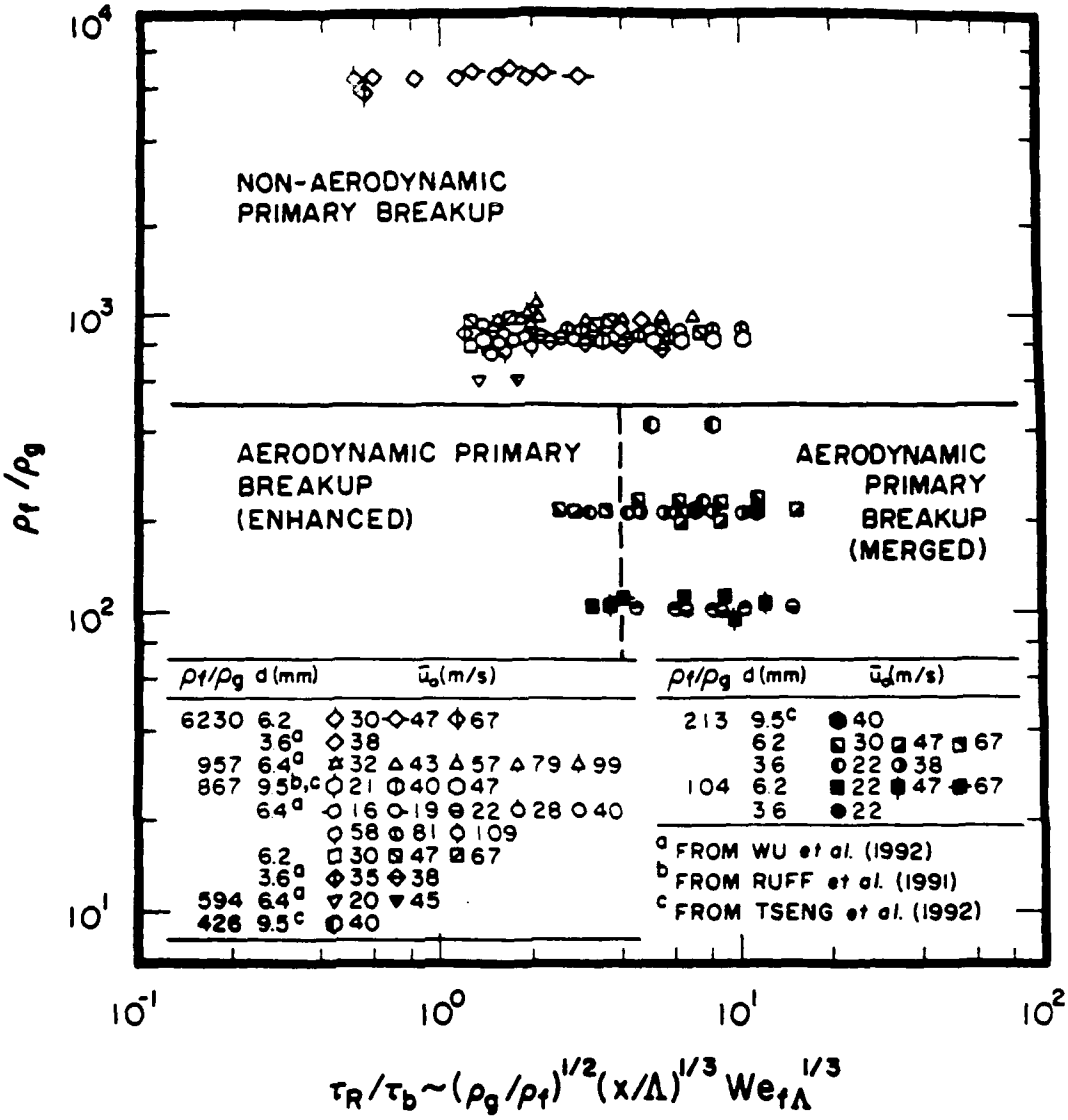

Figure 26 Turbulent primary breakup regime map

2. Existing correlations of SMD after primary breakup based on aerodynamic wave growth, due to Taylor (1940), Levich (1962), Mayer (1961) and Adelberg (1968), were ineffective for present measurements because aerodynamic effects were small and were dominated by low levels of liquid vorticity at the start of the multiphase mixing layer, see Fig. 16.

3. A reasonably good correlation of SMD after fully-developed primary breakup — for various liquids, injector diameters, relative velocities and liquid/gas density ratios—was achieved using Eq. (2), see Fig. 18. This expression was based on drop sizes being proportional to the thicknesses of boundary layers in the injector passage, with the best empirical fit fortuitously accounting for aerodynamic effects as well as over the present test range.

Major conclusions concerning turbulent primary breakup are as follows:

1. The presence of aerodynamic phenomena for primary breakup is largely controlled by the liquid/gas density ratio, and appear when this ratio is less than 500, see Fig. 26.

2. Drop sizes at the onset of turbulent primary breakup could be explained by equating the surface tension energy required to form a drop to both the kinetic energy of a corresponding liquid eddy relative to its surroundings, assisted by the pressure reduction over the tips of liquid protrusions when aerodynamic effects are important. Phenomenological analysis based on these ideas yielded a good correlation of drop sizes at the onset of breakup, see Fig. 21, as well as the distance along the mixing layer required for breakup to begin, see Fig. 22.

3. Drop sizes from primary breakup progressively increased with distance along the mixing layer, which could be explained by associating the SMD with the largest drops that had sufficient residence time to form by Rayleigh breakup of protruding liquid elements when aerodynamic effects were small, see Fig. 24.

4. For conditions where secondary breakup times become small in comparison to the Rayleigh breakup time of ligaments, processes of primary and secondary breakup merge to reduce drop sizes. The reduction of drop sizes could be explained by combining the turbulent primary breakup mechanism with secondary breakup results of Hsiang and Faeth (1992, 1993), see Fig. 25.

5. Mass-averaged drop velocities after primary breakup approximate mean and rms velocity fluctuations in the liquid in the streamwise and crosstream directions, respectively. However, there was a tendency for streamwise velocities to be reduced somewhat when aerodynamic effects were important, see Fig. 19.

REFERENCES

Adelberg, M. (1968) Mean drop size resulting from the injection of a liquid jet into a high-speed gas stream. AIAA J. 6, 1143-1147.

Avery, J.F. and Faeth, G.M. (1975) Combustion of submerged gaseous oxidizer jet in a liquid metal. *Fifteenth Symposium (International) on Combustion*, The Combustion Institute, Pittsburgh, 419-428.

Bush, K.L. and Merrill, G.L. (1981) SCEPS — an advanced thermal power plant for torpedos. AIAA Paper No. 81-1602.

Chan, S.H., Janke, P.J., Shen, T.R., Amano, R.S. and Shin, H.D. (1987) Reaction zone structure of a gaseous hydrogen chloride jet submerged in an aqueous ammonia solution. ASME Paper No. 87-HT-38.

Chan, S.H., Janke, P.J. and Shen, T.R. (1988) Equilibrium computations of multiphase nonideal electrolytic systems and structure of turbulent reacting dissolving jets. *Twenty-Second Symposium (International) on Combustion*, The Combustion Institute, Pittsburgh, 721-729.

Chehroudi, B., Onuma, Y., Chen, S.-H. and Bracco, F. V. (1985) On the intact core of full cone sprays. SAE Paper No. 850126.

Chen, L.-D. and Faeth (1982) Condensation of submerged vapor jets in subcooled liquids. J. Heat Transfer 104, 774-780.

Chen, L.-D. and Faeth (1983) Structure of turbulent reacting gas jets submerged in liquid metals. Combust. Sci. Tech. 31, 277-296.

Chuech, S.G., Lai, M.-C. and Faeth, G.M. (1989) Structure of turbulent sonic underexpanded free jets. AIAA J. 27, 549-559.

Clift, R., Grace, J.R. and Weber, M.E. (1978) *Bubbles, Drops and Particles*, Academic Press, New York, 346 ff.

De Juhasz, K.J., Zahm, O.F., Jr. and Schweitzer, P.H. (1932) On the formation and dispersion of oil sprays. Bulletin No. 40, Engineering Experimental Station, Pennsylvania State University, University Park, PA, 1932, 63-68.

Faeth, G.M. (1987) Mixing, transport and combustion in sprays. Prog. Energy Combust. Sci. 13, 293-345.

Faeth, G.M. (1990) Structure and atomization properties of dense turbulent sprays. *Twenty-Third Symposium (International) on Combustion*, The Combustion Institute, Pittsburgh, 1345-1352.

Grant, R.P. and Middleman, S. (1966) Newtonian jet stability. AIChE J. 12, 669-678.

Harrje, D.T. and Reardon, F.H. (1972) *Liquid Rocket Combustion Instability*, NASA SP-194, 49-55.

Hinze, J.O. (1975) *Turbulence*, 2nd ed., McGraw-Hill, New York, 427 and 724-734.

Hoyt, J.W. and Taylor, J.J. (1985) Effect of nozzle boundary layer on water jets discharging in air. *Jets and Cavities* (J.H. Kim, O. Furuya and B.R. Parkin, ed.) ASME-FED-31, ASME, New York, 93-100.

Hsiang, L.-P. and Faeth, G.M. (1992) Near-limit drop deformation and secondary breakup. Int. J. Multiphase Flow, 18, 635-652.

Hsiang, L.-P. and Faeth, G.M. (1993) Deformation and secondary breakup of drops. AIAA Paper No. 93-0814.

Hughes, T.G., Smith, R.B. and Kiely, D.H. (1981) A stored chemical energy propulsion system (SCEPS) for underwater applications: its development and future. AIAA Paper No. 81-1601.

Jeffries, H. (1926) On the formation of water waves by wind. Proc. Roy. Soc. London A110, 241-247.

Kerney, P.J., Faeth, G.M. and Olson, D.R. (1972) Penetration characteristics of a submerged steam jet. AIChE J. 18, 548-553.

Lee, D.W. and Spencer, R.C. (1933) Photomicrographic studies of fuel sprays. NACA Report No. 454.

Lefebvre, A.W. (1980) Airblast atomization. Prog. Energy Combust. Sci. 6, 223-246.

Levich, V.G. (1962) *Physicochemical Hydrodynamics*, Prentice-Hall, Inc., Englewood Cliffs, NJ, 639-646.

Loth, E. and Faeth, G.M. (1988) Underexpanded noncondensing turbulent gas jets in liquids. Final report — ONR Contract No. N00014-85-K-0604, The University of Michigan, Ann Arbor, MI.

Loth, E. and Faeth, G.M. (1989) Structure of underexpanded round air jets submerged in water. Int. J. Multiphase Flow 15, 589-603.

Loth, E. and Faeth, G.M. (1990) Study of plane underexpanded air jets in water AIChE J. 36, 818-826.

Mayer, E. (1961) Theory of liquid atomization in high velocity gas streams. ARS J. 31, 1783-1785.

McCarthy, M.J. and Malloy, N.A. (1974) Review of stability of liquid jets and the influence of nozzle design. Chem. Engr. J. 7, 1-20.

Phinney, R.E. (1973) The breakup of a turbulent liquid jet in a gaseous atmosphere. J. Fluid Mech. 60, 689-701.

Ranger, A.A. and Nicholls, J.A. (1969) Aerodynamic shattering of liquid drops. AIAA J. 7, 285-290.

Ranz, W.E. (1958) Some experiments on orifice sprays. Can. J. Chem. Engr. 36, 175-181.

Reitz, R.D. and Bracco, F.V. (1982) Mechanism of atomization of a liquid jet. Phys. Fluids 25, 1730-1742.

Ruff, G.A., Sagar, A.D. and Faeth, G.M.(1988) Structure and mixing properties of pressure-atomized sprays. AIAA J. 27, 901-908.

Ruff, G.A., Bernal, L.P. and Faeth, G.M. (1991) Structure of the near-injector region of non-evaporating pressure-atomized sprays. J. Prop. Power, 7, 221-230.

Ruff, G.A., Wu, P.-K., Bernal, L. P. & Faeth, G.M. (1992) Continuous- and dispersed-phase structure of dense nonevaporating pressure-atomized sprays. J. Prop. Power, 8, 280-289.

Simmons, H.C. (1977) The correlation of drop-size distributions in fuel nozzle sprays. J. Engr. for Power 99, 309-319.

Taylor, G.I. (1940) Generation of ripples by wind blowing over a viscous liquid. *The Scientific Papers of Sir Geoffrey Ingram Taylor.* 3, Cambridge Univ. Press, Cambridge, England, 1963, 244-254.

Tennekes, H. and Lumley, J.L. (1972) *A First Course in Turbulence,* M.I.T. Press, Cambridge, MA, 22, 248-286.

Tseng, L.-K., (1991) Near-injector structure of non-evaporating pressure-atomized sprays at various ambient densities. Ph.D. thesis, The University of Michigan, Ann Arbor, MI.

Tseng, L.-K., Ruff, G.A. and Faeth, G.M., (1992a) Effects of gas density on the structure of liquid jets in still gases. AIAA Journal, 30, 1537-1544.

Tseng, L.-K., Wu, P.-K. and Faeth, G.M. (1992b) Dispersed-phase structure of pressure atomized sprays at various gas densities. J. Prop. Power, in press.

Weber, C. (1931) Zum zerfall eines Flussigkeitsstrahles. Z. Angew. Math. Mech. 2, 136-141

Weimer, J.C., Faeth, G.M. and Olson, D.R. (1973) Penetration of vapor jets submerged in subcooled liquids. AIChE J. 19, 552-558.

Wu, P.-K. (1992) Liquid surface breakup for nonturbulent and turbulent liquids. Ph.D. thesis, The University of Michigan, Ann Arbor, MI.

Wu, P.-K. and Faeth, G.M. (1992) Aerodynamic effects in primary breakup of turbulent liquids. Atomization and Sprays, submitted.

Wu, P.-K., Ruff, G.A. and Faeth, G.M (1991) Primary breakup in liquid/gas mixing layers. Atomization and Sprays 1, 421-440.

Wu, P.-K., Tseng, L.-K. and Faeth, G.M. (1992) Primary breakup in gas/liquid mixing layers for turbulent liquids. Atomization and Sprays, in press.

APPENDIX A: FAETH (1990)

Twenty-Third Symposium (International) on Combustion/The Combustion Institute 1990/pp. 1345–1352

STRUCTURE AND ATOMIZATION PROPERTIES OF DENSE TURBULENT SPRAYS

G. M. FAETH

Department of Aerospace Engineering
The University of Michigan
Ann Arbor, MI 48109-2140, U.S.A.

Aspects of the structure and atomization properties of the near-injector (dense-spray) region of turbulent sprays are reviewed, considering: spray breakup regimes, dense-spray structure, and liquid breakup processes. The discussion is limited to nonevaporating round pressure-atomized sprays—a fundamental configuration that is representative of dense sprays since they normally occupy the cool portions of combusting sprays where vaporization rates are modest.

Due to the complexity of spray breakup, criteria for breakup regime transitions are still not well developed. More information is particularly needed concerning effects of flow properties at the injector exit, ambient turbulence levels, and high Ohnesorge numbers where viscous effects become important.

Existing measurements of dense-spray structure are limited to atomization breakup, since most practical applications involve this regime. The dense-spray region for atomization breakup consists of a liquid core (like the potential core of a single-phase jet) surrounded by a multiphase mixing layer that begins right at the injector exit. Recent measurements within the multiphase mixing layer show that the flow is surprisingly dilute and support the classical view of atomization, i.e., primary breakup at the liquid surface followed by secondary breakup of ligaments and large drops with only minor effects of collisions. In contrast, some recent computational studies suggest significant effects of collisions in dense sprays—clearly, this controversy must be resolved. Accepting the classical view, characteristic secondary-breakup and residence times are comparable in dense sprays; therefore, breakup dominates dense sprays much like drop vaporization dominates dilute sprays. Continued primary breakup along the liquid core implies significant separated-flow effects within the multiphase mixing layer, with locally-homogeneous flow only approached at large Weber numbers for sufficiently low Ohnesorge numbers. Thus, many unresolved problems of separated flow in dilute sprays are relevant to dense sprays, while breakup and modification of turbulence by dispersed phases are particularly important for dense sprays.

Primary and secondary breakup have been widely studied but the dense-spray environment highlights new problems. In particular, more information is needed concerning breakup regime transitions, the temporal evolution and outcome of breakup processes, breakup mechanisms when the liquid core is turbulent, and effects of gas-phase turbulence on breakup.

Introduction

A wide variety of physical phenomena and practical applications have motivated numerous studies of noncombusting and combusting turbulent sprays. Much of this work, however, is limited to the dilute-spray region, located at some distance from the injector exit, where both observations and analysis are relatively tractable due to small liquid volume fractions. As a result, many features of dilute sprays are reasonably well understood, see several recent review articles and references cited therein.[1–3] Thus, attention is turning to the less accessible dense-spray region near the injector exit, in an effort to better understand how the characteristics of injectors, injected liquids, and the ambient enivronment affect the flow properties entering the dilute-spray region. The objective of this paper is to briefly review current understanding of the structure and atomization properties of turbulent dense sprays, and to highlight areas where additional research is needed.

Present considerations will be limited to nonevaporating round pressure-atomized sprays in still gases. Ignoring evaporation is reasonable, since the dense-spray region of combusting sprays generally involves relatively cool portions of the flow. For example, at the locally-homogeneous-flow (LHF) limit, where interphase transport rates are infinitely fast so that both phases have the same velocity and are in thermodynamic equilibrium, mixture fractions where liquid volume fractions become small are roughly an order-of-magnitude larger than those where combustion is complete; therefore, well-atomized sprays have dense-spray regions that are somewhat remote from high-temperature regions where vaporization is significant.[3] Additionally, jet flows are attractive for studying dense sprays, since they can be described by relatively few parameters. Information on other spray processes and injection systems can be found in Refs. 1-6 and references cited therein.

The following aspects of dense sprays will be addressed: spray breakup regimes; dense-spray structure and its effect on collisions, breakup and separated flow; primary breakup at the liquid-surface; and secondary breakup of drops. Generalizations based on available limited information for dense sprays are risky; therefore, the paper concludes with characteristic-time considerations to help infer behavior for the many situations that have not been studied.

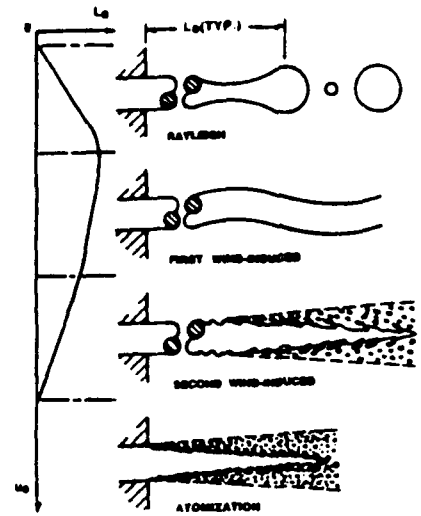

FIG. 1. Spray breakup lengths and regimes for nonturbulent round liquid jets in still gases.

Spray Breakup Regimes

Description:

The first issue concerning dense sprays is to define the topography or spray breakup regime of the flow. Several spray breakup regimes have been identified for nonturbulent liquids in still gases, as follows: nonjetting or drip, stable liquid jet, Rayleigh breakup, first and second wind-induced breakup, and atomization breakup.[7–18] The drip regime involves low flow rates with $We_f < 3$-4, ending when the jet momentum is large enough to overcome surface tension forces at the passage exit.[7] Stable liquid jets occur for $Oh > 2$-4, where viscous forces are large enough to damp all disturbances that would lead to breakup.[8] Naturally, neither of these regimes produce dense sprays.

The remaining spray breakup regimes for nonturbulent liquids are illustrated in Fig. 1. With increased flow rates, breakup regimes occur in the following order: Rayleigh, first wind-induced, second wind-induced, and atomization breakup. Rayleigh breakup involves interactions between liquid inertia and surface tension, yielding drop diameters somewhat larger than the injector diameter with jet lengths to breakup increasing with increasing flow rates. The remaining breakup regimes involve gas-phase aerodynamic effects with breakup lengths decreasing with increasing flow rates. First wind-induced breakup is caused by twisting or helical instability of the liquid column as a whole, yielding drops having diameters comparable to the injector diameter. Second wind-induced breakup involves both helical and surface instabilities of the liquid column yielding a wide range of drop sizes extending to the injector diameter. Atomization breakup is reached when breakup at the surface begins right at the injector exit, yielding drops that are generally small in comparison to the injector diameter. The dense-spray region during atomization breakup consists of a liquid core, like the potential core of a single-phase jet, surrounded by a developing multiphase mixing layer (see Fig. 1). Since practical sprays require small drops for adequate mixing, the topography of atomization breakup is most important for dense-sprays.

Breakup Regime Transitions:

Spray breakup regimes have been plotted in a variety of ways.[9–11] Figure 2 is a convenient form since the important transitions to wind-induced and atomization breakup involve nearly constant Oh and We_g. In contrast, transition from the drip regime is a function of density ratio, since $We_f = (\rho_f/\rho_g)$ $We_g = 4$ at transition. This implies a progressively narrower Rayleigh breakup regime as ρ_f/ρ_g decreases. Ranz[9] suggests transition to wind-induced breakup at $We_g = 0.4$ for low Oh, while Sterling and Sleicher[12] observe transition at $We_g = 1.2 + 3.41\,Oh^{0.9}$ for $Oh \leq 0.4$.[11] Transition between first and second wind-induced breakup is gradual and a transition criterion has not yet been found.[11] Tran-

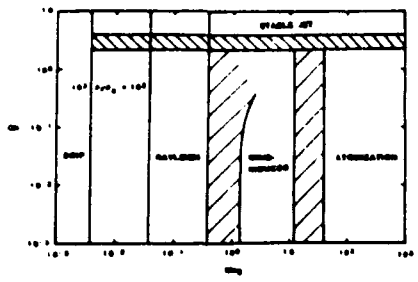

FIG. 2. Spray breakup regime transitions for nonturbulent round liquid jets in still gases. Ranges of transition uncertainties are indicated by crosshatching.

sition to atomization breakup is also relatively broad with Ranz[9] and Miesse[10] suggesting $We_g \approx 13$ and 40.

Transitions to the stable jet regime have received little attention, but, all transitions at large Oh probably behave like the Sterling and Sleicher[12] result for wind-induced breakup. Uncertainties in transitions at high Oh are not very important for many liquids at low pressures, e.g., water and kerosene at 30° C have Oh ca. 5×10^{-3} for a 1 mm diameter injector. However, heavy fuels have higher Oh while Oh becomes large for all liquids at high ambient pressures as the thermodynamic critical point of the liquid surface is approached;[3] therefore, more study of high Oh transitions is needed. Additionally, both liquid- and gas-phase turbulence affect breakup,[13,14] and their influence on breakup regime transitions should be quantified.

Dense-Spray Structure

Available Measurements:

Few measurements of the structure of dense sprays are available. In the following, recent measurements of dense-spray structure by Ruff and coworkers[14–16] will be considered in order to provide some background about the nature of the flow. These experiments involved large-scale (d = 9.5 and 19.1 mm) water jets in still air with effects of liquid turbulence evaluated by considering nonturbulent slug flow and fully-developed turbulent pipe flow at the jet exit. Effects of separated flow were also studied by comparing measurements with predictions based on the LHF approximation (see Refs. 3, 14 and 15 for computational details).

Liquid Volume Fractions:

Effects of spray breakup regime and jet-exit turbulence levels on dense sprays can be seen from the distributions of time-averaged liquid volume fractions along the axis of the water sprays illustrated in Fig. 3.[14] Predictably, mixing is fastest for atomization breakup and turbulent jet exit conditions, and is slowest for first-wind-induced breakup and nonturbulent slug flow at the jet exit. For the high jet Reynolds numbers of these tests ($Re \geq 52000$), the LHF predictions are independent of flow rate so that a single prediction represents each jet exit turbulence level. Within the second wind-induced and atomization breakup regimes, the LHF predictions are marginally successful for $\bar{\alpha}_{fc} > 0.2$ and accurately represent the striking effect of jet exit turbulence on mixing. However, the LHF predictions fail to represent the much slower mixing levels in the first wind-induced breakup regime and overestimate rates of mixing for all test conditions when $\bar{\alpha}_{fc} < 0.2$, where the spray becomes more dilute.

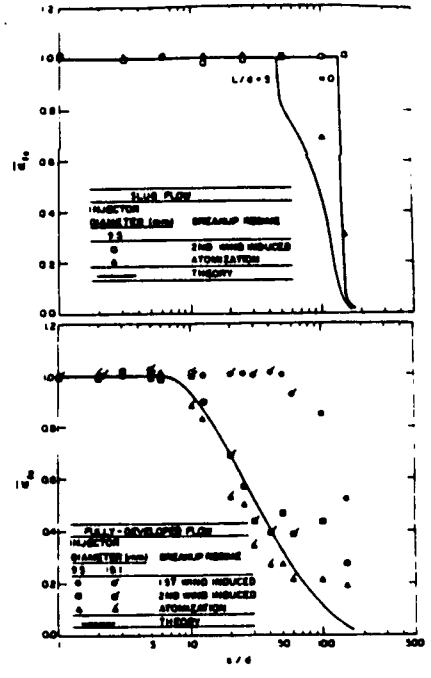

FIG. 3. Time-averaged liquid volume fractions along the axis for slug and fully-developed jet exit conditions. From Ruff et. al.[14]

Liquid volume fractions near the jet exit are unity in Fig. 3, indicating the presence of the liquid core. Reduced liquid volume fractions for fully-developed flow suggest a relatively short liquid core, however, this is not the case: flow visualization showed liquid cores extending well beyond x/d = 100 for these measurements.[15] The reason for this behavior is that liquid volume fractions in the range 0.1–1.0 actually correspond to mixture fractions in the range 0.99–1.0 due to the large density ratio of the flow. This highlights the fact that the region where the LHF predictions were successful involved disappointingly low levels of mixing.

Mixing Layer Properties:

Double-flash holograms of the water sprays provided details concerning the structure of the multiphase mixing layer.[15,16] Results for atomization breakup and nonturbulent jet exit conditions at x/d = 25 are illustrated in Fig. 4; findings at other locations were similar.[15] The region near the liquid surface consists of large, irregular, ligament-like elements (large SMD and e_p) while the dilute spray region near the edge of the flow involves smaller round drops. This is direct evidence of important effects of secondary breakup near the surface. Additionally, the multiphase mixing layer is surprisingly dilute ($\bar{\alpha}_f < 1\%$), implying that collisions between liquid elements are improbable.[3] These findings, as well as consideration of secondary breakup to be discussed later, support the conventional picture of atomization within dense sprays: breakup of the liquid surface into ligaments and large drops followed by secondary breakup into smaller round drops. This conflicts with recent hypotheses, based on computational studies, that small drops are formed at the liquid surface and then collide and coalesce to create larger drops within the multiphase mixing layer.[17] Additional measurements are needed to resolve this controversy.

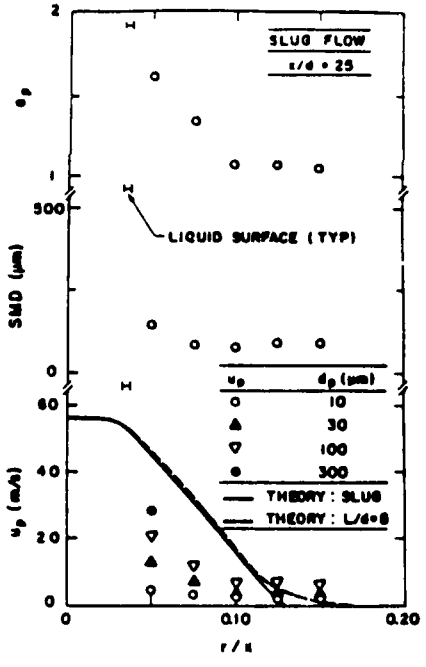

FIG. 4. Dispersed-phase properties for slug flow and atomization breakup at x/d = 25. From Ruff et al.[15]

Drop sizes along the liquid surface were larger for turbulent than laminar liquids.[15] Yet in spite of effects of secondary breakup and liquid turbulence, the MMD/SMD ratio was roughly 1.2 everywhere, which agrees with Simmons'[18] observations for a wide variety of nonevaporating dilute sprays. Furthermore, drop-size distributions for all conditions also satisfied Simmons'[18] universal root-normal distribution for this MMD/SMD ratio.[16] This is helpful since the entire drop size distribution can be related in a simple manner to the SMD. However, an explanation of this behavior and more evidence concerning its generality for dense sprays is needed.

The distributions of drop velocities illustrated in Fig. 4 show that they vary substantially with drop diameter at each point in the flow. Near the liquid core, the largest drops have velocities comparable to liquid injection velocities (ca. 56 m/s); however, velocities decrease with drop size and radial distance. A surprising feature is that gas velocities (which approximate the velocities of the smallest drops)[16] are low and nearly constant across the mixing layer. This implies relatively ineffective momentum exchange between the phases since large drops contain most of the momentum and respond slowly to drag forces. The velocity variation with drop size provides direct evidence that the LHF approximation is not suitable, so it is not surprising that the LHF predictions in Fig. 4 are poor. Thus, the success of the LHF approach at large $\bar{\alpha}_{fc}$ in Fig. 3 occurs because the momentum of the gas and small drops has little influence on flow dynamics at large mixture fractions, not because the LHF approximation is correct.

Primary Breakup

Aerodynamic Breakup:

Atomization breakup of nonturbulent liquids involves a stripping mechanism at the liquid surface.

Current estimates of drop sizes from primary breakup are based on theories of aerodynamically-induced wave growth on liquid surfaces, assuming that the mean drop size is proportional to the size of the fastest growing waves, and either ignoring (low Oh limit),[8,19,20] or considering,[21,22] effects of liquid viscosity on wave growth. Using SMD to represent mean drop diameter for these limits yields.[19,21]

$$\rho_g \, SMD \, \dot{u}_{rel}^2/\sigma = 2\pi \, C_B, \qquad = 9\pi(16)^{1/3} \, C_v((\rho_g/\rho_f)^{1/2} \, \mu_f \, \dot{u}_{rel}/\sigma)^{2/3} \quad (1)$$

where the larger of the two estimates should be used. Limited measurements in this laboratory suggest $C_B \approx 0.4$ and $C_v \approx 1.3$. Additionally, Levich[20] suggests the presence of a high Oh limit where aerodynamic breakup ends due to viscous damping when $(\rho_g/\rho_f)^{1/2} \, \mu_f \, \dot{u}_{rel}/\sigma \approx 1$.

More study is needed to evaluate Eqs. (1) as a means of estimating SMD from primary breakup within dense sprays. Additionally, there are also conceptual problems concerning the mechanism leading to Eqs. (1). Aerodynamic breakup theory considers roll waves which are assumed to separate from the liquid surface as crosstream ligaments and then divide by Rayleigh breakup into drops.[8,19] Yet, observations of the liquid surface during atomization breakup shows that the ligaments are more aligned with the streamwise direction, somewhat reminiscent of horseshoe vortices eminating from surfaces in single-phase boundary layers.[23] Clearly, these observations must be accommodated by any complete theory of primary breakup for nonturbulent liquids.

There are several other open issues with respect to primary breakup of nonturbulent liquids. First of all, the rate of removal of liquid at the surface is needed for any model of the flow. One approach that has been to use LHF analysis to estimate liquid mixing at high mixture fractions where LHF predictions are reasonably good. Combusting monopropellant sprays have been treated in this manner with some success but the evaluation of primary breakup was not definitive.[24] A second approach has been to use aerodynamic breakup theory to correlate the length of the liquid core, yielding:

$$L_c/d = C_c(\rho_f/\rho_g)^{1/2} \quad (2)$$

where Chehroudi *et al.*[25] find C_c in the range 7-16 for atomization breakup of pressure-atomized round jets in still gases. Geometrical approximations of the core geometry using this length are then used to estimate liquid removal rates. This is plausible for modeling purposes but quantitative evaluation of the method is needed, while effects of liquid turbulence on Eq. (2) have not been resolved. Finally, no information is available concerning drop velocities after primary breakup. Thus, critical aspects of primary breakup for nonturbulent liquids must be resolved before the dense-spray region can be addressed in a rational manner.

Turbulent Breakup:

The much larger drops from primary breakup for turbulent jet exit conditions are due to turbulent distortion of the liquid surface, stabilized by surface tension.[16] Lee and Spencer[26] provide early observations of this breakup mechanism at low ambient pressures. The properties of turbulent breakup can be estimated by considering the momentum required to overcome surface tension forces when forming a drop,[16] using the relationship between velocity fluctuations and eddy size within the inertial region of the turbulence spectrum.[27] This yields the following expression for the range of drop sizes that can be formed[16]

$$\rho_f \Lambda \, \dot{v}'^2_\Lambda \, (d_p/\Lambda)^{5/3}/\sigma \geq 6 \, C_t' \quad (3)$$

where C_t' is a constant of order unity. The maximum drop size and SMD are assumed to be on the order of the radial turbulent integral scale of the *liquid turbulence, thus:*

$$SMD/\Lambda = C_t' \quad (4)$$

where C_t' is of order unity and Eq. (4) is appropriate only when Eq. (3) is satisfied for $d_p = \Lambda$. Laufer[28] finds $\Lambda/d = 0.10$–0.15 for turbulent pipe flow while turbulence properties within the liquid [illegible] normally don't vary significantly from jet exit conditions.[15] This yields $C_t' = 0.9$–1.3 from the results of Ruff *et al.*[15] Thus, the turbulent breakup mechanism is consistent with the observations of Ruff *et al.*[14–16] and deserves additional study as a possible way of estimating other properties of this primary breakup mechanism.

Equations (3) and (4) help put observations of effects of liquid turbulence from large-scale sprays into perspective. In particular, small injector diameters imply relatively small maximum drop sizes from this mechanism so that aerodynamic breakup effects normally dominate primary breakup. Additionally, most practical injectors have small length-to-diameter ratios so that liquid turbulence is not highly developed even when jet Reynolds numbers are high. Thus, turbulent primary breakup is probably not a major feature of most practical dense sprays.

Secondary Breakup

The general importance and relevant mechanisms of secondary breakup will be considered in the following. Criteria for secondary breakup behind shock waves, and for slower accelerations in free fall, are as follows:[5,29]

$$We_{pg} \geq We_{pg}^* = 6.5; \; We_{pg} \geq We_{pg}^* = 8/C_D^* \quad (5)$$

Stable large drops in sprays have drag coefficients in the range 0.8–1.2,[3] therefore, the two equations yield similar breakup criteria.

Measurements in the water sprays were consistent with Eqs. (5) since only drops near the surface exceeded the criteria.[16] This is generally the case for nonturbulent liquids based on the primary breakup estimates of Eqs. (1). At low Oh, for example, Eqs. (1) imply that the SMD Weber number after primary breakup is $6\pi C_B \approx 8$; therefore, all drops having diameters greater than roughly the SMD, which involves most of the spray liquid, exceed criteria for secondary breakup. Naturally, effects of viscosity or turbulent breakup can yield even larger drops with a greater propensity for secondary breakup.

There have been numerous studies of drop breakup, see Refs. 4, 5 and 30–34. Viscous effects inhibit drop breakup for $Oh_p > 2$,[8] but three types of drop breakup have been identified for low Oh_p: deformation, stripping and drop-piercing breakup.[5,30–34] Deformation breakup involves distortion of the drop by gas pressure variations, causing simple division into a few large drops or bag-like breakup yielding some large drops accompanied by many very small drops. Stripping breakup is analagous to surface breakup of sprays with the bulk of the drop generating small drops. Drop-piercing breakup occurs at very high relative velocities due to Taylor instability of the windward side of the drop at high accelerations and yields small drops as well.

An illustration of the deformation and stripping regimes, due to Borisov et el.,[32] appears in Fig. 5. The transitions shown reflect regions that have been observed experimentally and the regimes are probably larger: breakup should occur for $We_{pg} > 6$–8, while transition between deformation and stripping correlates as $We_{pg}/Re_p^{1/2} > 1$.[32] Transition to drop-piercing breakup occurs for $We_{pg} > We_{pg}^* = 7000/C_D^*$, which is well beyond conditions shown in Fig. 5.[30,32]

Conditions pertinent to dense sprays are also indicated in Fig. 5. The experiments of Ruff et al.[14–16] involve a single trajectory on this plot for nonturbulent and turbulent liquids, with breakup in the deformation and weakly stripping regimes—which was observed. More general limits are shown for aerodynamics breakup of nonturbulent liquids. These ranges were found as follows: the low Oh SMD Weber number is roughly 8 from Eqs. (1), while the universal drop size distribution implies a maximum We_{pg} of 26, after primary breakup, and the

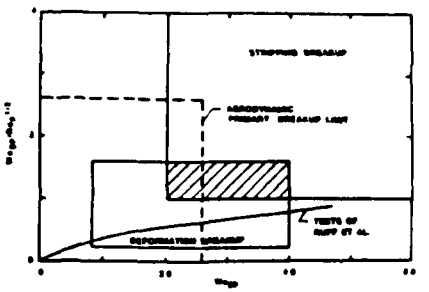

FIG. 5. Drop breakup regime transitions at low Oh_p.

Reynolds numbers of large drops in sprays are 10^2–10^3, yielding maximum values of $We_{pg}/Re_p^{1/2}$ of roughly 2.6 (with somewhat larger values possible when viscous effects are important). This indicates that secondary breakup in dense sprays is largely due to deformation and weak stripping. While information is available concerning breakup times in these regimes,[5,31–34] outcomes in terms of drop size and velocity distributions are largely unknown. Additionally, turbulent secondary breakup could be a *factor for these relatively weak breakup modes.* Recent measurements provide evidence for large turbulence intensities in dense sprays so this mechanism should be investigated as well.[15]

Characteristic Times

Characteristic times are discussed in the following in order to generalize findings concerning secondary breakup and effects of separated flow. Relevant characteristic times are as follows: flow-residence, liquid-core-residence, drop-response and drop-breakup times. The largest drops are of interest, having velocities of roughly u_0 and yielding flow-residence times to reach x of

$$\tau_f = x/u_0 \quad (6)$$

Based on the correlation for L_c from Eq. (2), the liquid-core residence time is

$$\tau_c = L_c/u_0 = C_c(d/u_0)(\rho_f/\rho_g)^{1/2} \quad (7)$$

Drop-response time is defined as $\tau_p = -1/(d \, u_p/dx) = -u_p/(d \, u_p/dt)$.[16] Using Eq. (5) to represent the largest stable drop (having relative velocity u_0) in the flow, then yields[16]

$$\tau_p = 4 \, We_{pg}^* \, \rho_f \sigma/(3 \, C_D^* \, \rho_g^2 \, u_0^3) \quad (8)$$

Finally, drop breakup times for deformation and

stripping can be correlated in a similar manner. Adopting the correlation of Ranger and Nichols[33] for stripping, and considering the maximum stable drop size as before, yields[16]

$$\tau_b = C_b\, We_{pg}^{*}\, \sigma\rho_f/\rho_g^{3/2}/(\rho_f\, u_0^3) \qquad (9)$$

where $C_b \approx 4$ is an empirical stripping factor.

A variety of response time ratios can be formed to highlight various properties of dense sprays. First of all, small values of the ratio

$$\tau_b/\tau_p = (3\, C_b\, C_D{}^{*}/4)(\rho_g/\rho_f)^{1/2} \qquad (10)$$

indicate that breakup times are small in comparison to the time required for drops to approach gas velocities. At atmospheric pressure, τ_b/τ_p is ca. 0.1 so that secondary breakup is relatively fast and its outcome has the greatest influence on spray properties. At high pressures, however, $\tau_b/\tau_p \approx 1$ and breakup extends over distances comparable to those required for large drops to approach gas velocities, then, drop breakup must be treated like a finite-rate process, analogous to effects of drag and vaporization on drop motion.

Another perspective on secondary breakup can be found from

$$\tau_b/\tau_c = C_b\, We_{pg}^{*}/(C_c\, We_g) \qquad (11)$$

which is the ratio of secondary-breakup to liquid-core-residence time. Near the atomization spray breakup limit (Fig. 2), τ_b/τ_c reaches values of 0.1–0.3 which implies that secondary breakup proceeds rather slowly in the multiphase mixing layer (particularly since new drops are formed all along the liquid core). Thus, for these conditions, secondary breakup tends to control processes in dense sprays, somewhat like drop drag and vaporization tends to control processes in dilute sprays.

Insight concerning separated flow can be obtained from

$$\tau_f/\tau_p = (3\, C_D{}^{*}/4)\, We_{pg}^{*}(\rho_g/\rho_f)^2(\rho_f x\, u_0^2/\sigma) \qquad (12)$$

which is the ratio of flow-residence time to drop-response time. Large values of τ_f/τ_p correspond to regions where separated flow effects are small. Interpreting x in Eq. (12) as the distance from breakup implies significant effects of separated flow near the liquid core. Drops near the edge of the flow, however, originate near the injector and exhibit smaller effects of separated flow. These trends correspond to existing observations at atmospheric pressure,[15,16] while sprays at higher pressure should exhibit smaller effects of separated flow—particularly at large injection velocities.

For a round-jet most of the liquid enters the flow near the jet exit and large values of the ratio

$$\tau_c/\tau_p = (3\, C_c\, C_D{}^{*}/4)\, We_{pg}^{*}(\rho_g/\rho_f)^{3/2}\, We_f \qquad (13)$$

implies that separated flow effects are small within the dense spray region. The effect of density ratio is smaller for τ_c/τ_p than τ_f/τ_p since the liquid core becomes shorter as ρ_g/ρ_f increases from Eq. (2). Equation (13) indicates that large diameter jets, like those of Refs. 14–16, have reduced effects of separated flow in comparison to practical sprays due to their large We_f. Thus, the LHF limit is approached at large We_f, with this limit approached more rapidly as ρ_g/ρ_f increases, as long as Oh is sufficiently small. However, experimental evidence for this behavior must still be obtained.

Nomenclature

C_i	empirical coefficient for process i
C_D	drop drag coefficient
d, d_p	injector exit and drop diameters
e_p	drop ellipicity
L, L_B, L_c	injector passage, liquid breakup and liquid core lengths
MMD	mass mean diameter
Oh, Oh_p	jet and drop Ohnesorge numbers: $\mu_f/(\rho_f d\sigma)^{1/2}$, $\mu_f/(\rho_f d_p\sigma)^{1/2}$
r	radial distance
Re, Re_p	jet and drop Reynolds numbers: $\rho_f\, u_0\, d/\mu_f$, $\rho_g\, u_r\, d_p/\mu_g$
SMD	Sauter mean diameter
t	time
u, u_r	streamwise absolute and relative velocities
v	radial velocity
We_i, We_{pi}	jet and drop Weber numbers based on phase i: $\rho_i\, u_0^2\, d/\sigma$, $\rho_i\, u_r^2\, d_p/\sigma$
x	streamwise distance
α_f	liquid volume fraction
Λ	radial integral scale
μ	molecular viscosity
ρ	density
σ	surface tension
τ_i	characteristic time i, Eqs. (6)–(9)

Subscripts

f	liquid-phase property
g	gas-phase property
p	drop property
s	liquid surface property
o	injector exit condition

Superscripts

$\bar{(\ )}$	time-averaged mean property
$(\ )^{*}$	critical condition

Acknowledgments

The author's research on sprays has been supported by the Air Force Office of Scientific Research, Grant No. AFOSR-89-0516; and the Office of Naval Research, Grant No. N00014-89-J-1199. The U.S. Government is authorized to reproduce and distribute copies for Governmental purposes notwithstanding any copyright notation thereon.

REFERENCES

1. Law, C. K., Prog. Energy Comb. Sci. 8, 169 (1982).
2. Sirignano, W. A., Prog. Energy Comb. Sci. 9, 291 (1983).
3. Faeth, G. M., Prog. Energy Comb. Sci. 13, 254 (1987), ibid 9, 1 (1983), ibid. 3, 191 (1977).
4. Giffen, E. and Muraszew, A., The Atomization of Liquid Fuels, John Wiley & Sons, 1953.
5. Clift, R., Grace, J. R. and Weber, M. E., Bubbles, Drops and Particles, Academic Press, 1978.
6. Lefebvre, A. H., Gas Turbine Combustion, p. 371, Hemisphere Publishing, 1983.
7. Scheele, G. F. and Meister, B. J., AIChE J. 14, 9 (1968).
8. Ranz, W. E., On Sprays and Spraying, Engineering Research Bulletin No. 65, The Pennsylvania State University, 1956; ibid., Can. J. Chem. Engr. 36, 175 (1958).
9. Ohnesorge, G., Z. Angew. Math. Mech. 16, 355 (1936).
10. Miesse, C. C., Ind. Eng. Chem. 47, 1690 (1955).
11. Reitz, R. D., Atomization and Other Breakup Regimes of a Liquid Jet, Ph. D. Dissertation No. 1375-T, Princeton University, 1978.
12. Sterling, A. M. and Sleicher, C. A., J. Fluid Mech. 68, 477 (1975).
13. Hinze, J. O., AIChE J. 1, 289 (1955).
14. Ruff, G. A., Sagar, A. and Faeth, G. M., AIAA J. 27, 549 (1989).
15. Ruff, G. A., Bernal, L. P. and Faeth, G. M., AIAA Paper No. 89-0050 (1989), ibid., J. Prop. Power, in press.
16. Ruff, G. A. and Faeth, G. M., AIAA Paper No. 90-0464 (1990).
17. Reitz, R. D. and Bracco, F. V., Encyclopedia of Fluid Mechanics (N. P. Cheremisinoff, Ed.), Vol. III, Chapt. 11, 1984.
18. Simmons, H. C., J. Eng. Power 99, 309 (1977), ibid., 315 (1977).
19. O'Rourke, P. J. and Bracco, F. V., Inst. Mech. Eng. Pub. ISBN 0852984693, 101 (1980).
20. Levich, V. G., Physiochemical Hydrodynamics, Prentice-Hall, pp. 639-646, 1962.
21. Mayer, E., ARS J. 31, 1783 (1961).
22. Adelberg, M., AIAA J. 6, 1143 (1968).
23. Hoyt, J. W. and Taylor, J. J., Phys. Fluids 20, S253 (1977).
24. Lee, T.-W. and Faeth, G. M., AIAA Paper No. 90-0463 (1990); ibid., J. Prop. Power, submitted.
25. Chehroudi, B., Onuma, Y., Chen, S.-H. and Bracco, F. V., SAE Paper No. 850126 (1985).
26. Lee, D. W. and Spencer, R. C., NACA Tech. Note No. 424, 1932, ibid., 454, 1933.
27. Hinze, J. O., Turbulence, Chap. 7, McGraw-Hill, 2nd ed., 1975.
28. Laufer, J., NACA Tech. Note 2123, 1950.
29. Pruppacker, H. R. and Klett, J. D., Microphysics of Clouds and Precipitation, p. 123, D. Reidel Publishing, 1978.
30. Harper, E. Y., Grube, G. W. and Chang, I.-D., J. Fluid Mech. 52, 565 (1972).
31. Gel'fand, B. E., Gubin, S. A. and Kogarko, S. M., Inzh-Fiz. Zh. 27, 120 (1974).
32. Borisov, A. A., Gel'fand, B. E., Natanzon, M. S. and Kossov, O. M., Inzh.-Fiz. Zh. 40, 64 (1981).
33. Ranger, A. A. and Nicholls, J. A., AIAA J. 7, 285 (1969).
34. Wierzba, A. and Takayama, A., Rept. Inst. High-Speed Mech. 53, p. 1, Tohoku University, 1987.
35. Parthesarathy, R. N. and Faeth, G. M., J. Fluid Mech., 220, 485 (1990).

APPENDIX B: RUFF ET AL. (1992)

JOURNAL OF PROPULSION AND POWER
Vol 8, No. 2, March–April 1992

Continuous- and Dispersed-Phase Structure of Dense Nonevaporating Pressure-Atomized Sprays

G. A. Ruff,* P.-K. Wu,† L. P. Bernal,‡ and G. M. Faeth§
University of Michigan, Ann Arbor, Michigan 48109

The structure and breakup properties of the dense-spray region of nonevaporating pressure-atomized sprays were studied. The multiphase mixing layer near the injector exit was emphasized, considering large-scale (9.5-mm injector diameter) water jets injected vertically downward in still room air. Phase-discriminating laser velocimetry and double-pulse holography were used to measure phase velocities and drop-size properties for both nonturbulent and turbulent jet exit conditions. Present test conditions involved two types of primary breakup: 1) aerodynamic breakup for nonturbulent jets where properties could be correlated using earlier aerodynamic breakup theories; and 2) turbulent breakup for turbulent jets where drop properties could be related to liquid turbulence properties. Both mechanisms yielded Weber numbers exceeding secondary drop breakup limits near the liquid surface. Significant effects of separated flow were observed for present test conditions; however, scaling analysis suggests reduced effects of separated flow at higher injector velocities and ambient pressures—largely due to finer atomization.

Nomenclature

C_B = aerodynamic breakup coefficient
C_b = drop breakup time coefficient
C_c = liquid core length coefficient
C_D = drop drag coefficient
C_t, C_t' = turbulent breakup coefficients
d = injector exit diameter
d_p = drop diameter
k = Favre-averaged turbulence kinetic energy
L = injector passage length
L_c = liquid core length
N = number of measurements
Oh = jet Ohnesorge number, $\mu_f/(\rho_f d\sigma)^{1/2}$
Re = jet Reynolds number, $\rho_f u_0 d/\mu_f$
r = radial distance
S = separated-flow factor, Eq. (9)
t = time
u = streamwise velocity
u_r = relative streamwise velocity
V = volume of sample
v = radial velocity
We_i = jet Weber number based on phase i, $\rho_i u_0^2 d/\sigma$
We_{pi} = drop Weber number number based on phase i, $\rho_i u_r^2 d_p/\sigma$
$\tilde{We}_g$ = Favre-averaged spray Weber number, Eq. (8)
x = streamwise distance
Λ = radial integral scale
μ = molecular viscosity
ρ = density
σ = surface tension
τ_b = drop breakup time, Eq. (18)
τ_c = liquid core residence time, Eq. (12)
τ_f = flow residence time, Eq. (10)
τ_p = drop response residence time, Eq. (16)

Subscripts
f = liquid-phase property
g = gas-phase property
p = drop property
s = liquid surface property
0 = injector exit condition

Superscripts
$\bar{(\ )}$, $(\ )'$ = time-averaged mean and root-mean-squared fluctuating quantities
$\tilde{(\ )}$, $(\ )''$ = Favre-averaged mean and root-mean-squared fluctuating quantities
$(\ )^*$ = critical breakup condition

Introduction

THERE have been numerous efforts to develop methods to analyze spray processes. The present investigation seeks to contribute to this methodology by studying the dense-spray region near the exit of the injector passage for pressure atomization. Experiments were limited to relatively large-scale (9.5-mm injector diameter) nonevaporating round water jets injected into still air at normal temperatures and pressures. Earlier measurements of liquid volume fractions, entrainment rates, and dispersed-phase properties in the dense-spray region of these flows[1,2] were extended to provide gas-phase and additional dispersed-phase properties. The new measurements, along with additional information obtained from the data of Ruff et al.,[1] were used to continue study of locally homogeneous-flow (LHF) analysis of the process, e.g., analysis based on the assumption of infinitely fast interphase transport rates so that both phases have the same velocity and are in thermodynamic equilibrium at each instant and point within the flow. Present measurements were limited to the atomization breakup regime where a multiphase mixing layer along the edge of the flow begins to develop right at the injector exit.[3,4] Jet exit conditions involved both slug and fully developed turbulent pipe flow because past work had shown sensitivity of dense-spray properties to liquid-phase turbulence levels.[1,2]

For atomization breakup, the flow near the injector exit involves a liquid core (much like the potential core of a single-

Presented as Paper 90-0464 at the AIAA 28th Aerospace Sciences Meeting, Reno, NV, Jan. 8–11, 1990; received April 20, 1990; revision received Feb. 20, 1991; accepted for publication Feb. 21, 1991.

*Graduate Assistant, Department of Aerospace Engineering; currently, Assistant Professor, Department of Mechanical Engineering, Drexel University, Philadelphia, PA 19104.
†Graduate Assistant, Department of Aerospace Engineering.
‡Associate Professor, Department of Aerospace Engineering. Member AIAA.
§Professor, Department of Aerospace Engineering. Fellow AIAA.

phase jet), surrounded by a multiphase mixing layer that begins to develop right at the injector exit.[3-5] The dense-spray region is normally considered to include both the liquid core and the multiphase mixing layer up to the point where the liquid core disappears. There have been several studies of the length of the liquid core, taken as the length of unbroken liquid extending from the passage exit.[6-8] Findings indicate that this length is influenced by the breakup regime, turbulence properties at the injector exit, and the gas/liquid density ratio. For atomization breakup of typical liquids in gases at atmospheric pressure, however, the dense-spray region extends quite far from the injector, ca. 200–400 injector diameters. Thus, dense sprays are an important feature of spray injection processes due both to their extent and their influence on drop properties at the start of the dilute-spray region.

The multiphase mixing layer is also affected by the breakup regime, jet exit turbulence properties, and the density ratio of the flow.[1,2,9-11] Ruff et al.[1] provide information on liquid-phase properties in the multiphase mixing layer for water jets in still air at atmospheric pressure, using double-pulse holography to find liquid element (drop) sizes and velocities. It was found that the multiphase mixing layer had liquid volume fractions less than 1% for their test conditions. The inner portion of the mixing layer contained large irregularly shaped liquid elements and drops while the proportion of spherical drops increased and drop sizes decreased with increasing radial distance, suggesting significant effects of secondary breakup in the flow. The velocities of large drops were generally much larger than small drops, implying that separated flow effects were important as well. Increased turbulence levels at the jet exit had a substantial effect on the structure of the flow, increasing the number and size of irregular liquid elements by promoting ejection of liquid from the liquid surface and increasing the width of the liquid-containing region of the multiphase mixing layer. Wu et al.[9] also observed significant effects of jet exit conditions on the rate of spread of the outer edge of the multiphase mixing layer.

The complexities of dense sprays—involving stripping of liquid from the all-liquid core, the presence of irregular liquid elements, secondary breakup, and turbulent dispersion of drops toward the edge of the flow—make the LHF approximation attractive as a means of circumventing detailed descriptions of these phenomena. Ruff et al.[2] found that LHF predictions were reasonably effective for estimating distributions of liquid volume fractions for atomization breakup in the region where mean liquid volume fractions were greater than 0.2. However, the multiphase mixing layer dominates flow properties at lower liquid volume fractions and exhibits significant effects of separated flow, which limits the effectiveness of the LHF approximation.[1] Other evaluations of the LHF approximation find varying degrees of success, at times yielding encouraging results and at other times overestimating the rate of development of the flow as the spray becomes dilute.[5,9-12] Unfortunately, methods for determining conditions when the LHF approximation is appropriate for dense sprays have not been developed. The main difficulty is that success of the LHF approximation depends on drops being small enough to respond quickly to changes in gas properties, while information on both drop sizes and gas properties in dense sprays is very limited.

The objective of the present investigation was to seek a better understanding of the properties of dense sprays by studying both gas- and dispersed-phase velocities in the multiphase mixing layer for the same test conditions as Ruff et al.[1,2] Coupled with the existing measurements of liquid-phase properties (drop sizes and velocities), this provides a relatively complete picture of the structure of these flows. Furthermore, knowledge of both drop size distributions and phase velocities allows direct evaluation of primary breakup properties, the propensity for secondary drop breakup, and quantitative estimates of effects of separated flow. Mean and fluctuating gas velocities near the edge of the multiphase mixing layer were measured using phase-discriminating laser velocimetry (LV), whereas double-pulse holography was used near the liquid surface where LV was no longer feasible. The measurements were compared with predictions based on the LHF approximation to help provide a measure of separated-flow effects. Scaling considerations of drop breakup and response were also used to interpret dense-spray properties and gain insight concerning use of the LHF approximation.

The paper begins with brief descriptions of experimental methods and the approach used for the LHF computations. Experimental results are then described, considering phase velocities, liquid breakup properties, and separated-flow parameters. The paper concludes by considering scaling of various processes in the flow. The present discussion is brief; additional details and a complete tabulation of data can be found in Ruff.[13]

Experimental Methods

Apparatus

The experimental apparatus was identical to past work,[1,2] and will be described only briefly. The arrangement involved large-scale (9.5-mm injector diameter) water jets injected vertically downward in still room air. City water was supplied to the injector by a centrifugal pump with the water flow rate measured using a paddle-wheel flow meter that was calibrated by collecting water for timed intervals.

The slug and fully developed flow injectors were also identical to Ruff et al.,[1,2] and are described by Ruff.[13] Measurements of mean and fluctuating velocities across the exit of the injectors[13] showed that the slug flow injector provided relatively uniform velocities, with a streamwise turbulence intensity of roughly 1%, at the jet exit, while the fully developed flow injector yielded jet exit properties that approximated fully developed turbulent pipe flow.[14,15] The tests involved a mean jet velocity of 56.3 m/s, yielding other jet exit parameters as follows: water flow rate, 3.99 kg/s; Reynolds number, 534,000; Weber numbers based on gas and liquid densities, 500 and 412,000, respectively; and Ohnesorge number, 0.00121. These conditions are well within the atomization breakup regime and properly yielded a multiphase mixing layer that began at the exit of the injector.[3,4]

Instrumentation

Laser Velocimetry

The ambient air was seeded with condensed oil particles having diameters less than 1 μm for LV measurements. The seeding particles had a flat frequency response to the gas motion up to about 30 kHz, which was adequate for present LV measurements. A large enclosure ($3 \times 3 \times 4$ m high) was constructed around the spray facility to avoid contaminating laboratory equipment with seeding particles. For an enclosure of this size, the induced counterflow velocity is less than 2% of the axial velocities in the region measured near the edge of the jets.

A phase-discriminating LV system, similar to that of Modarress et al.,[16] was used to avoid biasing gas-phase velocity signals with liquid velocity signals. The LV signal was obtained using the green line (514.5 nm) of an argon-ion laser (4W, Coherent, INNOVA 90-4) in the dual-beam forward-scatter mode. A 3.75:1 beam expander was used to minimize the dimensions of the measuring volume and to improve signal-to-noise ratios. The plane of the LV beams was rotated to measure both streamwise and crosstream velocities. The LV was frequency shifted (40 MHz Bragg cell, TSI model 9180-12) to eliminate effects of directional bias and ambiguity. The receiving optics observed the probe volume of the LV at an angle of 30 deg from the forward-scattering direction, yielding a measuring volume having a diameter of 60 μm and a length of 110 μm.

The phase-discrimination system involved surrounding the LV measuring volume with the beam from a 5-mW HeNe laser directed at an angle of 15 deg from the LV axis, with collection optics in the forward-scattering direction also at an angle of 15 deg from the LV axis. This yielded a region viewed by the discriminator that had a diameter of 0.6 mm and a length of 1.3 mm, surrounding the LV measuring volume. Thus, droplets that could graze or cross the LV measuring volume yielded a scattering signal on the discriminator output so their velocities could be eliminated from the velocity record.

The LV scattering signal was recorded using a photomultiplier (TSI model 9160) and processed using a burst counter (TSI model 1990 C). The measurements involved low burst densities (one seeding particle in the measuring volume) and high data densities (time between validated velocity signals small in comparison to integral time scales); therefore, the analog output of the processor was time averaged to yield unbiased time averages. This involved low-pass filtering (Ithaco model 4213) of the output signal before it was digitized (LeCroy models 8212A/8 and 8800A) and transferred to a microcomputer for processing and storage.

The performance of the phase-discriminator system was checked by measuring LV data rates with and without seeding particles present. It was required that the LV data rate at least double for the measurements to be considered valid. Additionally, no measurement was accepted if more than 40% of the LV signal was rejected due to signals from the phase discriminator system. Evaluation of this approach, using velocities of small particles measured by double-pulse holography as an upper bound for gas velocities, indicated significant upward bias of LV gas velocity measurements by particles if these limits were exceeded.

LV signals were averaged for 2 min (128,000 samples) to provide repeatable values of mean and fluctuating gas velocities. Experimental uncertainties (95% confidence) are estimated to be less than 8% for mean streamwise velocities, and less than 15% for streamwise and cross-stream velocity fluctuations, largely dominated by finite sampling times. Measurements were repeatable well within these limits.

Double-Pulse Holography

LV data rates from drops alone were too high near the liquid surface so that double-pulse holography was used in this region. This approach is tedious and less accurate, due to difficulties in accumulating sufficient velocity samples and reduced particle response because only particles having diameters of roughly 5 μm and greater could be measured. Nevertheless, holography provided access to portions of the multiphase mixing layer that were no longer feasible using LV.

Ruff et al.[1] describe the holocamera and reconstruction systems. Velocity data were obtained over 6 × 6 × 4 mm volumes, using at least three holograms per position. The data were spatially averaged over the width of the measuring volumes, or ± one-half the distance between adjacent radial positions, whichever was smaller. Velocity measurements were based on the motion of the centroid of the image and were correlated as a function of diameter using a linear least squares fit, considering drops having diameters less than 30 μm for present estimates of gas velocities. This typically involved correlation of 50–150 individual velocity determinations. The value given by the fit at a diameter of 5 μm, which is the lower end of the range that could be resolved, was used as the estimate of mean gas velocities. Unfortunately, sample sizes were too small to obtain reliable estimates of velocity fluctuations.

Gradient broadening and bias errors of mean gas velocities were not significant for present conditions, yielding experimental uncertainties (95% confidence) estimated to be less than 30%, largely governed by sampling limitations (except as noted later). Experimental uncertainties (95% confidence) for Sauter mean diameter (SMD) and mass median diameter (MMD) were both less than 10%, largely governed by sampling limitations, similar to past work.[2]

Theoretical Methods

Predictions of flow properties were based on the LHF approximation, neglecting evaporation of the liquid, similar to Ruff et al.[1] Other major assumptions of the analysis are as follows: steady (in the mean) axisymmetric flow with no swirl; negligible kinetic energy and viscous dissipation of the mean flow; buoyancy only affects the mean flow; and equal exchange coefficients of all species and phases. Under these assumptions, the flowfield can be found using a simplified version of the conserved-scalar formalism of Lockwood and Naguib[17] but based on mass-weighted (Favre) averages, following Bilger.[18] Initial conditions were based on the LV velocity measurements of jet properties at the injector exit,[13] supplemented by available information on the properties of fully developed turbulent pipe flows when appropriate.[14,15]

Justification of the assumptions and other details of the LHF predictions can be found in Ruff et al.[1] Notably, the formulation has been successfully calibrated for a variety of constant- and variable-density single-phase round jets.[19] Additionally, the same formation has been used successfully to estimate the structure of turbulent round air jets injected into water, which involves the same density ratio as the present flow.[20] Thus, the main issue of the present evaluation is the adequacy of the LHF approximation in the near-injector region for liquid injection into gases.

Results and Discussion

Phase Velocities

Mean Velocities

Measured mean velocities in the multiphase mixing layer for slug and fully developed flow jet exit conditions are illustrated in Figs. 1 and 2. Velocities are plotted as a function of r/x, the radial similarity variable for turbulent jets, to indicate the width of the flow; however, flow properties do not exhibit similarity in the r/x coordinate system. Three sets of velocity measurements are shown: continuous (gas)-phase mean velocities found using the phase-discriminating LV; dispersed (drop)-phase mean velocities for 5-μm-diameter particles, measured using double-flash holography (which are taken to be representative of mean gas-phase velocities in the region where LV was no longer feasible); and Favre-averaged velocities of the mixture as a whole for comparison with predictions. The Favre-averaged velocities were found by summing over the sample volume V containing N drops, as follows:

$$\tilde{u} = \frac{\sum_{i=1}^{N} (\pi/6)\rho_f d_{pi}^3 u_{pi} + (V - \sum_{i=1}^{N} (\pi/6) d_{pi}^3)\rho_g \bar{u}_g}{\sum_{i=1}^{N} (\pi/6)\rho_f d_{pi}^3 + (V - \sum_{i=1}^{N} (\pi/6) d_{pi}^3)\rho_g} \quad (1)$$

where drop size and velocity determinations included the full range of the data reported by Ruff et al.[1] Mean gas velocities in Eq. (1) were obtained from the LV measurements, if available, or from holography measurements (based on 5-μm-diameter drops), otherwise. The range of positions of the liquid surface, observed using holography, is indicated by the cross-hatched regions in the figures. Finally, LHF predictions of Favre-averaged velocities are also illustrated on the plots. Two predictions are shown for slug flow, ignoring and allowing for boundary-layer development along the walls of the injector passage, the latter using a flow development length of $L/d = 5$. These limits should bound the properties of the slug flow injector; however, differences between the two predictions are not very significant.

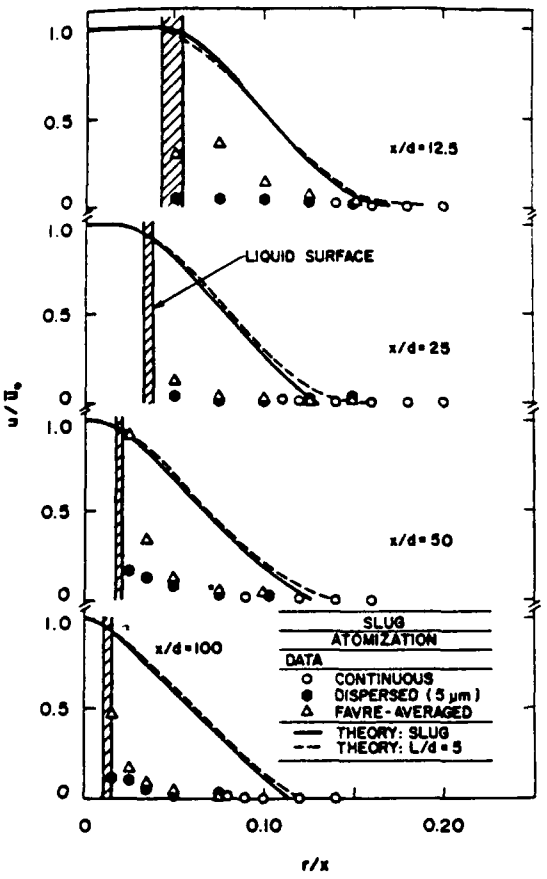

Fig. 1 Mean phase velocities for slug flow and atomization breakup.

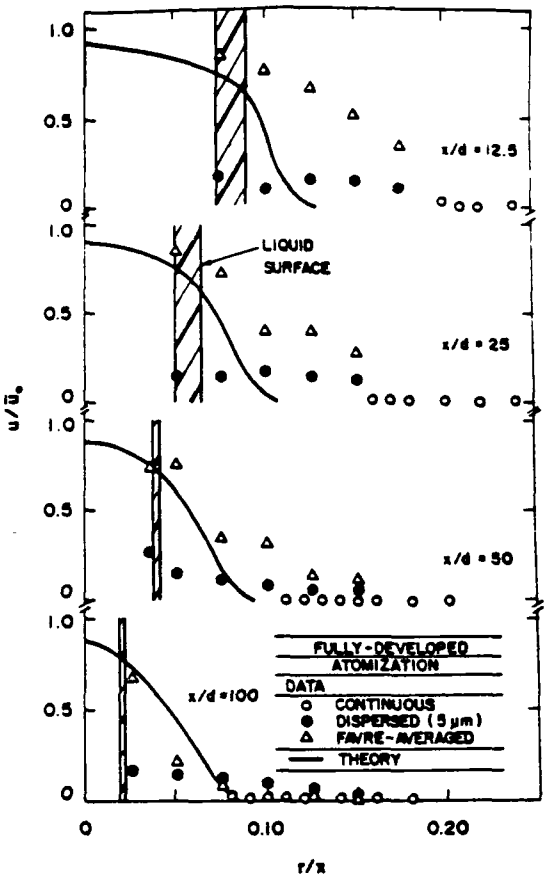

Fig. 2 Mean phase velocities for slug flow and atomization breakup.

The results for slug flow jet exit conditions (Fig. 1) exhibit reasonably good agreement between mean velocity measurements found by LV and particle tracking in the region where they overlap. Gas velocities remain quite low in the mixing layer, and only increase slightly near the liquid surface as distance from the injector exit increases. Near the injector exit, Favre-averaged velocities are significantly greater than gas velocities except near the outer edge of the mixing layer. Farther from the injector, however, differences between phase velocities are only significant near the liquid surface. Nevertheless, separated-flow effects are important throughout the mixing layer and LHF predictions of mean velocities are not satisfactory.

The results for the fully developed jet exit conditions (Fig. 2) exhibit greater differences between mean velocities found by LV and particle tracking than for slug flow jet exit conditions. In general, velocities measured by particle tracking are biased upward from the LV results. This is felt to be the result of the breakup of larger liquid elements that are more common for fully developed flow than for slug flow, generating small drops with relatively high initial velocities. Measurement of the velocity of these drops before they relax to the gas velocity would tend to bias present velocity measurements toward higher velocities. The extent of this effect is difficult to quantify; therefore, the particle velocities of Fig. 2 are at best representative of an upper bound on gas velocities. Similar to slug flow, gas velocities remain relatively low throughout the mixing layer, Favre-averaged velocities are generally significantly greater than gas velocities indicating significant effects of separated flow, and LHF predictions are not very satisfactory as a result.

Gas Velocity Fluctuations

Measured and predicted gas velocity fluctuations are illustrated in Figs. 3 and 4 for slug and fully developed flow jet exit conditions. The measurements are limited to streamwise and radial velocity fluctuations found by LV, which generally only covers the outer half of the mixing layer. Predictions are based on the isotropic approximation, $\tilde{u}''^2 = \tilde{v}''^2 = 2k/3$, and are Favre averages under the LHF assumption. Measured velocity fluctuations are nearly isotropic near the outer edge of the mixing layer, which is similar to the behavior of single-phase jets. Streamwise velocity fluctuations are substantially greater than radial velocity fluctuations, however, as the spray becomes dense (this is particularly evident for $x/d = 12.5$). Such behavior is typical of dense sprays in regions where relative velocities are significant.[5,21,22] Other than indicating that velocity fluctuations should increase in the dense portions of the mixing layer, in a qualitative way, the LHF predictions of velocity fluctuations are not very useful.

Liquid Breakup

Drop-Size Distributions

Table 1 is a summary of drop-size properties for nonturbulent and turbulent jet exit conditions. These properties were relatively independent of position along the liquid surface, and over the flow cross section if the region near the liquid surface was excluded. Thus, SMD and MMD/SMD ratio have been grouped accordingly in Table 1 with properties over the cross section represented by results at $x/d = 100$. Gas velocities along the liquid surface varied irregularly due to experimental uncertainties so that only the range of values is summarized in Table 1. Velocities in the liquid core remain close to jet exit velocities, ca. 56 m/s.[1]

For each jet exit turbulence level, SMD along the liquid surface is substantially greater than over the cross section, providing evidence for significant effects of secondary breakup. Additionally, liquid turbulence substantially increased drop

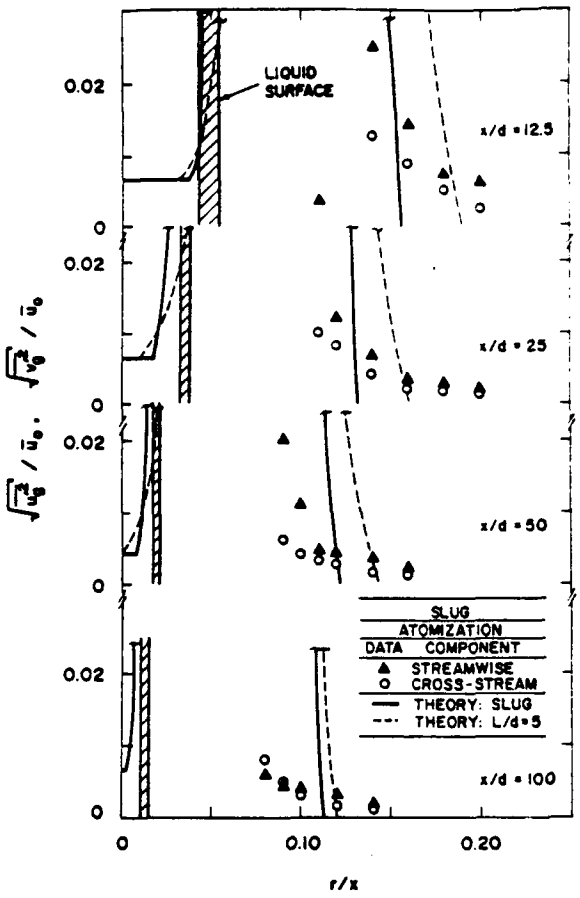

Fig. 3 Gas-phase velocity fluctuations for slug flow and atomization breakup.

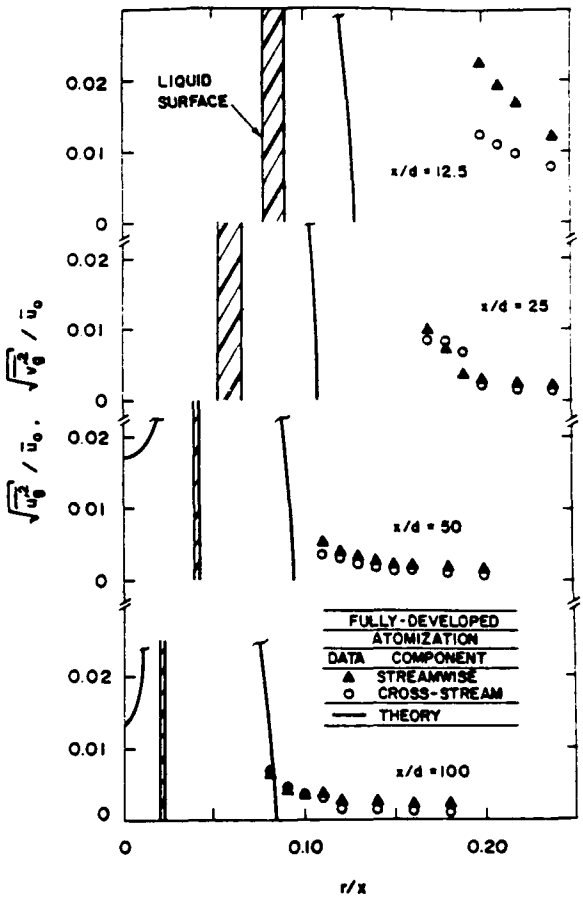

Fig. 4 Gas-phase velocity fluctuations for fully developed flow and atomization breakup.

sizes everywhere in comparison to nonturbulent conditions: roughly 7:1 after primary breakup at the surface, and roughly 2:1 over the cross section. In view of the larger drop sizes for a turbulent liquid, it is somewhat surprising that this flow mixes fastest (cf. Figs. 1 and 2). This behavior is due to faster primary breakup for the turbulent liquid,[1] perhaps with enhanced radial drop velocities due to radial velocity fluctuations in the liquid.

In spite of effects of turbulence on primary breakup, as well as secondary breakup, the MMD/SMD ratio is roughly 1.2 for all conditions in Table 1. This value agrees with observations for a wide variety of nonevaporating dilute sprays.[23] This motivated examination of whether the drop-size distributions in the dense sprays satisfy Simmons' universal root-normal drop-size distribution function.[23] These results are illustrated in Fig. 5, considering every position measured for both nonturbulent and turbulent jet exit conditions. It is evident that the root-normal distribution with MMD/SMD = 1.2 provides a reasonably good fit of all the measurements. Notably, except for $x/d = 12.5$, where effects of flow development are strongest, individual evaluations of the MMD/SMD ratio yield a value of roughly 1.2 as well. The correlation of Fig. 5 is very helpful because the entire drop-size distribution can be related in a simple manner to SMD.[23] However, an explanation of this behavior and more evidence that it is generally suitable for dense sprays is needed.

Nonturbulent Primary Breakup

Present results indicate different breakup mechanisms for nonturbulent and turbulent liquids at otherwise identical conditions in the atomization breakup regime with low *Oh*. It is generally agreed that atomization breakup at low *Oh* involves a stripping mechanism for nonturbulent liquids.[2,3,5] Among

Table 1 Drop-size properties[a]

Flow	Liquid surface, 12.5 ≤ x/d ≤ 100 $\bar{u}_{gs}$, m/s[b]	SMD, μm	MMD/SMD	Cross section, x/d = 100 SMD, μm	MMD/SMD
Slug	3–9	174	1.21	95	1.18
Fully developed	8–15	1330	1.20	220	1.22

[a]SMD and MMD are based on equivalent spherical drops as described in Ruff et al.[2]
[b]Gas velocity estimated from 5-μm-diam drops near surface.

others, Levich[24] has proposed a formula to estimate drop sizes due to primary breakup for these conditions based on Taylor's[25] theory of aerodynamically induced growth of surface waves, assuming that the average diameter of drops formed at the surface is proportional to the wavelength of the unstable surface waves having the highest growth rates. Using SMD to represent the average drop diameter then yields

$$\mathrm{SMD} = 6\pi C_B \sigma / [\rho_g (\bar{u}_{fs} - \bar{u}_{gs})^2] \qquad (2)$$

where C_B is a constant of proportionality near unity.

For present conditions, $\bar{u}_{fs}$ is roughly equal to $u_0 = 56.3$ m/s, based on LHF computations, as well as measurements of the velocity of protuberances from the liquid surface. Then, matching the primary breakup SMD in Table 1, using an average value of $\bar{u}_{gs}$, yields $C_B = 0.4$. Since C_B is expected to be on the order of unity, the aerodynamic primary breakup correlation of Eq. (2) appears to be reasonable for nonturbulent conditions within dense sprays. However, additional evaluation of the expression for other test conditions is clearly needed.

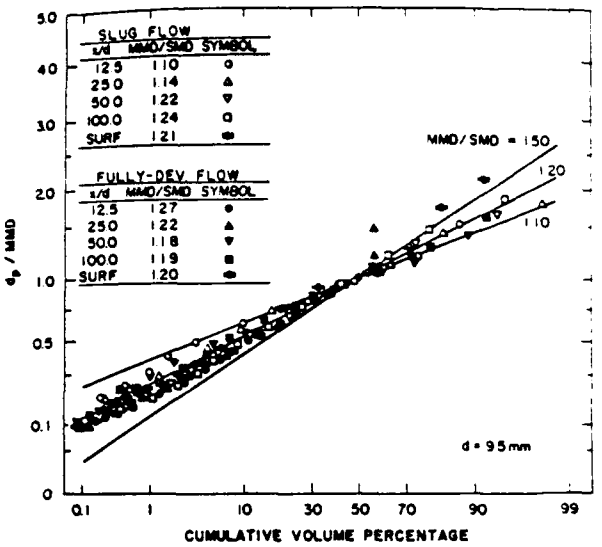

Fig. 5 Drop-size distributions at liquid surface and across mixing layer for slug and fully developed flow and atomization breakup.

Turbulent Primary Breakup

The much larger drop sizes after primary breakup for turbulent jet exit conditions are best explained by a turbulent breakup mechanism with relatively small aerodynamic effects. Lee and Spencer[26] report early observations of the turbulent breakup mechanism, based on tests at low ambient pressures where aerodynamic effects are negligible. Reitz[27] and Reitz and Bracco[28] also identify breakup induced by liquid-phase turbulence as one of the possible mechanisms contributing to the atomization process. This mechanism involves turbulent distortion of the liquid surface to form drops, with surface tension acting to stabilize the distortion, so that maximum drop sizes should be comparable to the radial integral scale of the liquid turbulence. Taking the SMD to be representative of maximum drop sizes, this implies

$$\mathrm{SMD}/\Lambda = C_1' \tag{3}$$

where C_1' is a constant on the order of unity. Laufer[14,29] finds $\Lambda/d = 0.10$–0.15 for turbulent pipe flow while properties within the liquid core do not vary significantly from jet exit conditions based on the LHF computations.[1] Then, based on the SMD measurements in Table 1 for turbulent jet exit conditions, Eq. (3) yields $C_1' = 0.9$–1.3, with the range resulting from Laufer's[29] range of Λ/d. Additionally, the ratio of streamwise to cross-stream integral scales for turbulent pipe flow is roughly 4:1,[29] which is comparable to the mass-averaged ellipticity (ratio of maximum to minimum liquid element dimensions) observed for turbulent breakup conditions near the liquid surface.[1] Thus, the turbulent breakup mechanism provides a plausible description of the large-scale features of the sprays after primary breakup.

Additional evidence supporting the turbulent breakup mechanism can be found by considering the criterion for this mechanism to be active. This can be estimated, similar to transition from the drip to the jetting regime of liquid jets in gases,[30] by equating the momentum available from turbulent fluctuations of scale d_p to the surface tension forces resisting the formation of a drop of similar size. Using the relationship between velocity fluctuations and eddy size within the inertial region of the turbulence spectrum,[29] the expression for the range of drop sizes that can be formed by the turbulent primary breakup mechanism is

$$\rho_f \Lambda \overline{v'^2_f} (d_p/\Lambda)^{5/3}/\sigma \geq 6C_1 \tag{4}$$

where C_1 is a constant on the order of unity. Taking $C_1 = 1$, Eq. (4) implies that the minimum drop diameter resulting from turbulent breakup for the conditions of Table 1 is ca. 250 μm, which is in good agreement with observations. In contrast, Eq. (4) is not satisfied even when $d_p = \Lambda$ for the first wind-induced test condition for the present sprays.[1,2] This also corresponds to observations because the liquid surface only was roughened by turbulent distortion for this test condition and no drop breakup occurred. Thus, the turbulent breakup mechanism is consistent with present observations and deserves additional study over a wider range of test conditions.

Equations (3) and (4) also help to put observations of effects of liquid turbulence on primary breakup for the present large-scale sprays into perspective. For example, small injector diameters imply relatively small maximum drop sizes from this mechanism, while the aerodynamic breakup correlation, Eq. (2), is essentially independent of injector diameter (as long as Oh is sufficiently low. Thus, aerodynamic breakup is likely to be more dominant for conventional sized injectors, because it yields larger drops than turbulent breakup, even when jet exit conditions are fully turbulent. Additionally, most practical injectors have small length-to-diameter ratios so that liquid turbulence is not highly developed even when jet Reynolds numbers are large. Based on these considerations, turbulent primary breakup is probably not a major feature of most practical sprays, as suggested by Reitz[27] and Reitz and Bracco.[28]

Secondary Breakup

Criteria for secondary breakup are frequently stated in terms of a drop Weber number, defined as follows:

$$We_{pg} = \rho_g d_p (u_p - u_g)^2/\sigma \tag{5}$$

One criterion, discussed by Clift et al.,[30] is based on water drops accelerated by shock waves, yielding:

$$We_{pg} > We_{pg}^* = 6.5 \tag{6}$$

Another criterion, discussed by Pruppacker and Klett,[31] was obtained for liquid drops falling in still air:

$$We_{pg} > We_{pg}^* = 8/C_D^* \tag{7}$$

For present test conditions, drop drag coefficients are in the range of 0.8–1.2 for the largest drops, based on the standard drag coefficient for spheres[5]; therefore, Eqs. (6) and (7) yield similar values of We_{pg}^*.

In order to quantify the potential for secondary drop breakup in the mixing layer, mass-weighted Weber numbers were computed as follows:

$$\bar{We}_g = \sum_{i=1}^{N} (\rho_g d_p (u_p - \bar{u}_g)^2/\sigma)_i d_{pi}^3 \Big/ \sum_{i=1}^{N} d_{pi}^3 \tag{8}$$

given N drop measurements at a point. The resulting distributions of $\bar{We}_g$ for the sprays having slug and fully developed jet exit conditions are plotted in Fig. 6. The values of $\bar{We}_g$ are greatest near the liquid surface and decrease monotonically with increasing distance from the surface. In general, values of $\bar{We}_g$ near the liquid surface exceed We_{pg}^* for breakup from Eqs. (6) and (7), supporting significant effects of secondary breakup in the mixing layer. The larger liquid elements ejected from the surface when the liquid is turbulent imply greater effects of secondary breakup for these conditions.

Primary followed by secondary breakup is likely to be a general mechanism for dense sprays. For example, the value of We_{pg} for a drop having a diameter equal to the SMD is roughly 8 for aerodynamic primary breakup from Eq. (2). Thus, drops having diameters of the order of the SMD and

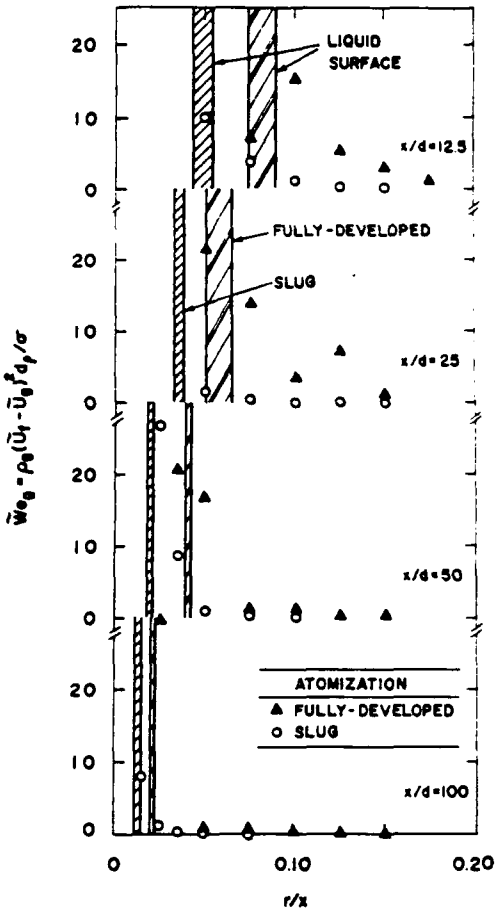

Fig. 6 Favre-averaged drop Weber numbers for slug and fully developed flow and atomization breakup.

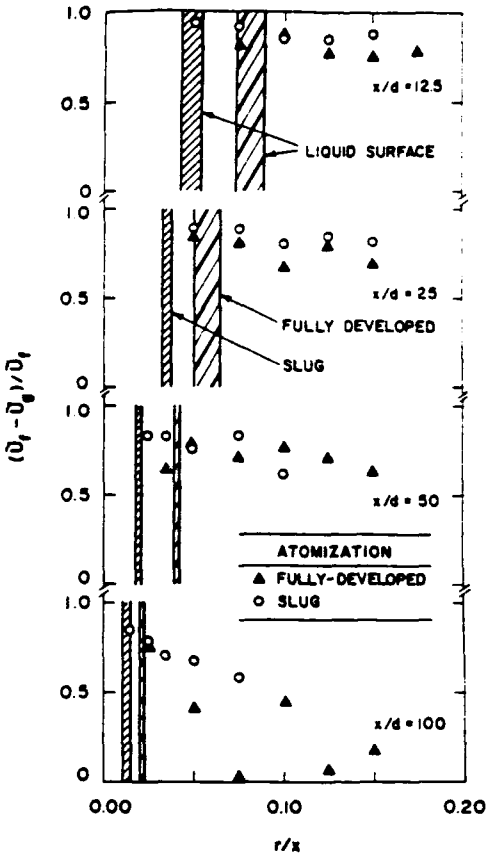

Fig. 7 Favre-averaged separated-flow factor for slug and fully developed flow and atomization breakup.

larger, which comprise more than half the mass of the liquid in the spray for MMD/SMD = 1.2, have Weber numbers that exceed We_{pg}^{*} from Eqs. (6) and (7). Naturally, the turbulent breakup mechanism, if active, yields even larger values of SMD and a greater propensity for secondary breakup. These observations, as well as the relatively small liquid volume fractions within the multiphase mixing layer,[1] suggest that secondary breakup rather than drop collisions is a dominant feature of dense sprays.

Separated Flow Effects

The results illustrated in Figs. 1 and 2 are somewhat misleading because small velocities give the impression that separated flow effects are small near the edge of the flow. This is not the case, which can be seen from the plots of Favre-averaged separated-flow factor, defined as follows:

$$S = (\tilde{u}_f - \tilde{u}_g)/\tilde{u}_f \tag{9}$$

Distributions of S are illustrated in Fig. 7 for both slug and fully developed jet exit conditions. Values of S approaching unity are observed throughout the mixing layer near the jet exit, and near the liquid surface for all streamwise positions. Values of S near the outer edge of the flow tend to decrease with increasing distance from the injector, however, approaching values in the range 0.1–0.2 for fully developed jet exit conditions at $x/d = 100$. In spite of the presence of larger drops near the liquid surface, values of S are generally lower for fully developed than slug flow jet exit conditions.

The trends seen in Fig. 7 result from both the generation of drops at the liquid surface and momentum exchange between the phases in the mixing layer. Velocities within the liquid core remain near liquid injection velocities so that newly formed drops near the injector exit and along the liquid surface generally have velocities that are significantly greater than gas velocities, yielding relatively large values of S. Drops near the outer edge of the flow, however, must have had significant residence times in the gas so that turbulent dispersion can transport them to this region. Therefore, drops near the edge of the flow tend to relax toward gas velocities, particularly when residence times are long (at large x/d). Additionally, fully developed jet exit conditions increase drop concentrations in the mixing layer in comparison to slug flow exit conditions, causing greater acceleration of the gas within the mixing layer. This compensates for the higher velocities associated with larger drops produced by fully developed exit conditions and tends to reduce S. Nevertheless, the values of S on the order of unity throughout most of the mixing layer, separated-flow effects are clearly important, which explains why predictions based on the LHF approximation are poor for present test conditions.

Scaling

Characteristic Times

Characteristic times are considered in the following to evaluate secondary breakup and effects of separated flow, and to help relate present observations for large sprays to practical pressure-atomized sprays. Characteristic times of interest are flow residence, liquid core residence, drop response, and drop breakup times. The largest drops are of interest, which have velocities of roughly u_0; therefore, an appropriate flow residence time is

$$\tau_f = x/u_0 \tag{10}$$

where x is to be interpreted as the distance from the position where the drop entered the mixing layer after primary breakup.

It is also of interest to assess response over the length of the liquid core as a measure of the length of the dense-spray region. Taylor's[25] aerodynamic breakup analysis yields the following expression for the length of the liquid core:

$$L_c/d = C_c(\rho_f/\rho_g)^{1/2} \tag{11}$$

Chehroudi et al.[8] find C_c in the range 7–16 for the contiguous length of liquid core for pressure atomized round jets in still gases within the atomization breakup regime. Taking the characteristic velocity of large drops to be u_0, the characteristic residence time of the liquid core becomes:

$$\tau_c = L_c/u_0 = C_c(d/u_0)(\rho_f/\rho_g)^{1/2} \tag{12}$$

The largest drops have the longest characteristic response times. The results illustrated in Fig. 6 suggest that the largest drops have Weber numbers comparable to $We^*_{\rho g}$ from Eq. (6) for both laminar and turbulent liquid conditions, and this condition will be used as a measure of maximum drop sizes. This yields a critical drop size of

$$d^*_p = \sigma We^*_{\rho g}/(\rho_g u_0^2) \tag{13}$$

assuming that relative velocities are comparable to u_0 based on present measurements for large drops.[1] A characteristic response time for drops can be defined in terms of their rate of deceleration, as follows:

$$\tau_p = -(du_p/dx)^{-1} = -u_p/(du_p/dt) \tag{14}$$

Virtual mass and Basset history forces generally can be ignored when computing drop motion in sprays because $\rho_f/\rho_g >> 1$, while pressures within the mixing layer are constant; therefore, conservation of momentum for a drop yields[5]:

$$du_p/dt = -3\rho_g C_D(u_p - u_g)^2/(4\rho_f d_p) \tag{15}$$

Streamwise velocities have been assumed to be large in comparison to cross-stream velocities to obtain Eq. (15), which is justified due to the boundary-layer character of the mixing layer. Substituting Eq. (15) into Eq. (14), assuming $u_g << u_p \approx u_0$ as before, and using Eq. (13) to identify the critical drop size, then yields:

$$\tau_p = 4We^*_{\rho g}\rho_f\sigma/(3C^*_D\rho_g^2u_0^3) \tag{16}$$

Because C_D does not vary appreciably for large drops in sprays,[5] Eq. (16) shows that increased gas densities and jet exit velocities reduce drop response times, both due to effects of breakup which reduces drop sizes and the relative increase of drag in comparison to inertia of the drops for a particular size [see Eq. (15)].

Finally, the characteristic time required for secondary breakup is an important feature of dense sprays. As noted earlier, drop Weber numbers are not much greater than the breakup limit, so that deformation and stripping breakup are the main mechanisms of secondary breakup.[32] Therefore, adopting the correlation of Ranger and Nicholls[33] for stripping breakup yields

$$\tau_b = C_b d_p(\rho_f/\rho_g)^{1/2}/(u_p - u_g) \tag{17}$$

where the empirical factor $C_b \approx 4$. Taking $d_p = d^*_p$ and $u_g << u_p \approx u_0$, as before, Eq. (17) becomes:

$$\tau_b = C_b We^*_{\rho g}\sigma(\rho_f/\rho_g)^{3/2}/(\rho_f u_0^3) \tag{18}$$

Characteristic Time Ratios

A variety of characteristic time ratios can be formed to highlight various properties of dense sprays. Forming the ratio τ_b/τ_p from Eqs. (16) and (18) yields:

$$\tau_b/\tau_p = (3C_bC^*_D/4)(\rho_g/\rho_f)^{1/2} \tag{19}$$

Small values of τ_b/τ_c imply that secondary breakup times are small in comparison to the time required for drops to relax to the local gas velocity. Taking $C^*_D = 1$, as before, implies that τ_b/τ_p is ca. 0.1 for present test conditions so that secondary breakup is relatively fast, which agrees with observations that the largest drops were close to the liquid surface. Under these conditions, the outcome of secondary breakup has the greatest effect on dense-spray properties. At high pressures, however, $\tau_b/\tau_p \approx 1$ and breakup extends over distances required for drops to approach gas velocities; then, drop breakup must be treated like a finite rate process, similar to effects of drag and vaporization on drop motion.

Another perspective on secondary breakup can be found from the ratio of Eqs. (12) and (18)

$$\tau_b/\tau_c = C_b We^*_{\rho g}/(C_c We_g) \tag{20}$$

which is the ratio of secondary breakup to liquid core residence time. For present test conditions, τ_b/τ_c ca. 0.005, so that breakup times are short in comparison to residence times in the mixing layer. This also agrees with observations that the large drops resulting from primary breakup were associated with the region near the liquid surface. However, this is not always the case. For example, transition from wind-induced to atomization breakup requires $We_g > We^*_g = 13$–40.[2,3] Near the transition limit, τ_b/τ_c is in the range 0.1–0.3, which implies that secondary breakup proceeds rather slowly within the mixing layer (particularly because new drops are formed all along the liquid core). Under these conditions, rates of secondary breakup should control processes in dense sprays, somewhat like drop drag and vaporization tends to control processes in dilute sprays.

Insight concerning effects of separated flow can be obtained from

$$\tau_f/\tau_p = (3C^*_D/4We^*_{\rho g})(\rho_g/\rho_f)^2(\rho_g x u_0^2/\sigma) \tag{21}$$

where large values of τ_f/τ_p correspond to regions of the flow where effects of separated flow are small. For present flows, drops continue to be formed at the liquid surface throughout the region where measurements were made. Therefore, characteristic distances, x, and the corresponding values of τ_f/τ_p remain small, which is consistent with the large values of $(\bar{u}_f - \bar{u}_g)/\bar{u}_f$ seen in Fig. 7 in this region. In contrast, drops near the edge of the flow originate near the jet exit. Then, estimating the empirical parameters in Eq. (21) as before, τ_f/τ_p varies in the range 0.5–4 as x/d varies in the range 12.5–100. This implies significant effects of separated flow near the jet exit, with separated-flow effects decreasing near the edge of the flow at larger streamwise distances, which is also consistent with the results illustrated in Fig. 7.

For a round jet, most of the liquid enters the mixing layer near the jet exit, and large values of the ratio

$$\tau_c/\tau_p = (3C_cC^*_D/4We^*_{\rho g})(\rho_g/\rho_f)^{3/2}We_f \tag{22}$$

implies that separated-flow effects are small within the dense spray region. The effect of the density ratio ρ_g/ρ_f is somewhat reduced for τ_c/τ_p in comparison to τ_f/τ_p, because the length of the liquid core is reduced as this density ratio increases through Eq. (11). For present test conditions, L_c/d is in the range 200–460 from Eq. (11) while τ_c/τ_p is in the range 11–25 from Eq. (22). Thus, the values of τ_c/τ_p imply modest effects of separated flow over the length of the liquid core, although separated-flow effects are still significant for the

relatively low range of x/d ($x/d \leq 100$) where present measurements were made. More generally, Eq. (22) implies that large-diameter jets, like those of the present experiments, have reduced effects of separated flow because of their large We_f in comparison to practical sprays having similar jet exit velocities. Thus, the LHF limit is approached at large We_f, with this limit approached more rapidly as ρ_g/ρ_f increases, as long as Oh is sufficiently small. Additional measurements, however, are needed to confirm the trends suggested by Eqs. (19–22).

Conclusions

The multiphase mixing layer in the near-injector region of large-scale pressure-atomized sprays was investigated, considering both nonturbulent slug and fully developed turbulent pipe flow at the jet exit. The major conclusions of the study are as follows:

1. Present measurements, combined with the earlier results of Ruff et al.[1] for the same flows, tend to support the classical view of atomization: a surprisingly dilute multiphase mixing layer (liquid volume fractions less than 1%) dominated by secondary breakup and separated-flow processes, while effects of collisions appear to be small.

2. Use of the LHF approximation was not effective for estimating the properties of the multiphase mixing layers for present test conditions, because large drops are continuously formed along the liquid surface and require significant times to relax to gas velocities. Characteristic time considerations suggest that locally homogenous flow is approached at large We_f, with this limit approached more rapidly as ρ_g/ρ_f increases.

3. For nonturbulent jet exit conditions, the SMD for primary breakup agreed with aerodynamic breakup theory,[24] with $C_t = 0.4$. For turbulent jet exit conditions, SMD for primary breakup was explainable by turbulent breakup theory with the SMD roughly equal to the radial integral scale of the liquid turbulence.

4. Drop-size distributions after aerodynamic primary breakup, turbulent primary breakup, and secondary breakup all exhibited MMD/SMD ratios of roughly 1.2 and agreed reasonably well with Simmons's root-normal drop-size distribution.[23] This is a useful simplification because the entire drop-size distribution is known if a single moment, like SMD, can be found.

5. An expression for the range of drop sizes that can be formed from the turbulent primary breakup mechanism was developed and indicated the dependence of drop size on the integral scale and intensity of liquid-phase turbulence. The expression was generally supported by present measurements. However, the importance of this breakup mechanism for practical injectors having small diameters is questionable.

6. Based on present measurements, more than half of the mass of the spray is contained in drops that are unstable to secondary breakup after aerodynamic breakup, while turbulent primary breakup yields larger drops that have a greater propensity for secondary breakup. Thus, secondary breakup appears to be an intrinsic process of dense sprays in the atomization spray breakup regime.

The conclusions are based on limited measurement for liquid jets having large diameters which have relatively slow flow development rates in comparison to practical injectors and are only provisional pending additional experimental evaluation.

Acknowledgments

This research was sponsored by the Air Force Office of Scientific Research Grants AFOSR 85-0244 and 89-0516, and by the Office of Naval Research, Grant N00014-89-J-1199. The U.S. Government is authorized to reproduce and distribute copies for governmental purposes notwithstanding any copyright notation thereon.

References

[1]Ruff, G. A., Bernal, L. P., and Faeth, G. M., "Structure of the Near-Injector Region of Non-Evaporating Pressure-Atomized Sprays," *Journal of Propulsion and Power*, Vol. 7, No. 2, 1991, pp. 221–230.

[2]Ruff, G. A., Sagar, A. D., and Faeth, G. M., "Structure and Mixing Properties of Pressure-Atomized Sprays," *AIAA Journal*, Vol. 27, No. 7, 1989, pp. 901–908.

[3]Ranz, W. E., "Some Experiments on Orifice Sprays," *Canadian Journal of Chemical Engineering*, Vol. 36, Aug. 1958, pp. 175–181.

[4]Miesse, C. C., "Correlation of Experimental Data on Disintegration of Liquid Jets," *Industrial and Engineering Chemistry*, Vol. 47, Sept. 1955, pp. 1690–1697.

[5]Faeth, G. M., "Mixing, Transport and Combustion in Sprays," *Progress in Energy Combustion Science*, Vol. 13, 1987, pp. 293–345.

[6]Phinney, R. E., "The Breakup of a Turbulent Liquid Jet in a Gaseous Atmosphere," *Journal of Fluid Mechanics*, Vol. 60, Oct. 1973, pp. 689–701.

[7]Hiroyasu, H., Shimizu, M., and Arai, M., "The Breakup of a High Speed Jet in a High Pressure Gaseous Environment," ICLASS-82, Univ. of Wisconsin, Madison, WI, 1982.

[8]Chehroudi, B., Onuma, Y., Chen, S.-H., and Bracco, F. V., "On the Intact Core of Full-Cone Sprays," SAE Paper 850126, 1985.

[9]Wu, K.-J., Su, C.-C., Steinberger, R. L., Santavicca, D. A., and Bracco, F. V., "Measurements of the Spray Angle of Atomizing Jets," *Journal of Fluids Engineering*, Vol. 105, Dec. 1983, pp. 406–415.

[10]Wu, K.-J., Coghe, A., Santavicca, D. A., and Bracco, F. V., "LDV Measurements of Drop Velocity in Diesel-Type Sprays," *AIAA Journal*, Vol. 22, No. 9, 1984, pp. 1263–1270.

[11]Mao, C.-P., Wakamatsu, Y., and Faeth, G. M., "A Simplified Model of High Pressure Spray Combustion," *Eighteenth Symposium (International) on Combustion*, The Combustion Institute, Pittsburgh, 1980, pp. 337–347.

[12]Bracco, F. V., "Structure of High-Speed Full-Cone Sprays," *Recent Advances in Gas Dynamics*, edited by C. Casci, Plenum Publishing Corp., New York, 1983.

[13]Ruff, G. A., "Structure and Mixing Properties of the Near-Injector Region of Nonevaporating Pressure-Atomized Sprays," Ph.D. Thesis, Univ. of Michigan, Ann Arbor, MI, 1990.

[14]Hinze, J. O., *Turbulence*, 2nd ed., McGraw-Hill, New York, 1975, pp. 427, 724–734.

[15]Schlichting, H., *Boundary Layer Theory*, 7th ed., McGraw-Hill, New York, 1979, p. 599.

[16]Modarress, D., Tan, H., and Elgobashi, S., "Two-Component LDA Measurements in a Two-Phase Turbulent Jet," *AIAA Journal*, Vol. 22, No. 5, 1984, pp. 624–630.

[17]Lockwood, F. C., and Naguib, A. S., "The Prediction of Fluctuations in the Properties of Free, Round-Jet Turbulent Diffusion Flames," *Combustion and Flame*, Vol. 24, Feb. 1975, pp. 109–124.

[18]Bilger, R. W., "Turbulent Jet Diffusion Flames," *Progress in Energy Combustion Science*, Vol. 1, 1976, pp. 87–109.

[19]Jeng, S.-M., and Faeth, G. M., "Species Concentrations and Turbulence Properties in Buoyant Methane Diffusion Flames," *Journal of Heat Transfer*, Vol. 106, Aug. 1985, pp. 721–727.

[20]Loth, E., and Faeth, G. M., "Structure of Underexpanded Round Air Jets Submerged in Water," *International Journal of Multiphase Flow*, Vol. 15, 1989, pp. 589–603.

[21]Solomon, A. S. P., Shuen, J.-S., Zhang, Q.-F., and Faeth, G. M., "Structure of Nonevaporating Sprays: I. Near-Injector Conditions and Mean Properties," *AIAA Journal*, Vol. 23, No. 10, 1985, pp. 1548–1555.

[22]Solomon, A. S. P., Shuen, J.-S., Zhang, Q.-F., and Faeth, G. M., "Structure of Nonevaporating Sprays: II. Drop and Turbulence Properties," *AIAA Journal*, Vol. 23, No. 11, 1985, pp. 1724–1730.

[23]Simmons, H. C., "The Correlation of Drop-Size Distributions in Fuel Nozzle Sprays," *Journal of Engineering for Power*, Vol. 99, July 1977, pp. 309–319.

[24]Levich, V. G., *Physiocochemical Hydrodynamics*, Prentice-Hall, Englewood Cliffs, NJ, 1962, pp. 639–646.

[25]Taylor, G. C., "Generation of Ripples by Wind Blowing Over a Viscous Liquid," *Collected Works of G. I. Taylor 3*, 1940, pp. 244–254.

[26]Lee, D. W., and Spencer, R. C., "Preliminary Photomicrographic Studies of Fuel Sprays," NACA Tech Note 424, 1932; ibid., "Photomicrographic Studies of Fuel Sprays," NACA Tech. Note 454, 1933.

[27]Reitz, R. D., "Atomization and Other Breakup Regimes of a Liquid Jet," Ph.D. Dissertation 1375-T, Princeton Univ., 1978.

[28]Reitz, R. D., and Bracco, F. V., "Mechanism of Atomization of

APPENDIX C: TSENG ET AL. (1992a)

AIAA JOURNAL
Vol. 30, No. 6, June 1992

Effects of Gas Density on the Structure of Liquid Jets in Still Gases

L.-K. Tseng,* G. A. Ruff,† and G. M. Faeth‡
University of Michigan, Ann Arbor, Michigan 48109

A theoretical and experimental study of the near jet-exit region of nonevaporating round liquid jets in still gases is described, emphasizing effects of ambient gas density in the atomization breakup regime where liquid breakup begins right at the jet exit. Mean liquid volume fraction distributions were measured for 9.5-mm-diam water jets in still air at pressures of 1–8 atm. Mixing was strongly affected by the gas/liquid density ratio and the degree of flow development at the jet exit, with the largest gas/liquid density ratio and fully developed turbulent pipe flow yielding the fastest mixing rates. Flow properties were predicted using the locally homogeneous flow approximation, where relative velocities between the phases are assumed to be small in comparison to mean flow velocities. Predictions were in good agreement with measurements, including representation of effects of gas/liquid density ratio and flow development at the jet exit, but only at relatively high mixture fractions. In contrast, separated flow effects caused predictions to overestimate rates of flow development at low mixture fractions.

Nomenclature

d = jet-exit diameter
f = mixture fraction
k = turbulence kinetic energy
L = injector passage length
Oh = Ohnesorge number, $\mu_f/(\rho_f d\sigma)^{1/2}$
p = pressure
r = radial distance
Re_f = jet Reynolds number, $\rho_f d u_{f,o}/\mu_f$
u = streamwise velocity
v = radial velocity
w = tangential velocity
$We_{i,o}$ = Weber number based on phase i and the jet diameter, $\rho_i d u_{i,o}^2/\sigma$
x = streamwise distance
α = volume fraction
ε = rate of dissipation of turbulence kinetic energy
μ = molecular viscosity
ρ = density
σ = surface tension
ϕ = generic property

Subscripts

c = centerline value
f = liquid-phase property
g = gas-phase property
o = jet-exit conditions
∞ = ambient conditions

Superscripts

$(\bar{\ }),(\bar{\ })'$ = time-averaged mean and rms fluctuating quantities
$(\tilde{\ }),(\tilde{\ })''$ = Favre-averaged mean and rms fluctuating quantities

Introduction

AN experimental and theoretical investigation of the near jet-exit region of nonevaporating round liquid jets in still gases is described. This flow is of interest for a variety of atomization and gas/liquid mixing processes; it also merits study as the multiphase counterpart of the single-phase turbulent jet. The objective of the research was to extend earlier studies of round water jets in still room air,[1-3] to consider effects of ambient gas density on the structure and mixing properties of the flow. Measurements of liquid volume fraction distributions were completed for water jets in still air at various ambient pressures. Tests were limited to atomization breakup, where liquid breakup into drops and the development of a multiphase mixing layer begins right at the jet exit, because this regime is most important for practical applications.[4,5] Jet-exit conditions included both fully developed turbulent pipe flow and low-turbulence intensity slug flow due to the known importance of the degree of flow development at the jet exit on flow properties.[1-3,6] The measurements were used to evaluate predictions of effects of gas/liquid density ratio on flow properties, found from an earlier model based on the locally homogeneous flow (LHF) approximation where relative velocities between the phases are assumed to be small in comparison to mean flow velocities.[1]

Only the main features of past work are considered, because reviews treating multiphase jets and dense sprays have appeared recently.[7,8] Past measurements have established the main features of the near injector region of liquid jets in still gases within the atomization breakup regime. The flow consists of a liquid core, much like the potential core of a single-phase jet, surrounded by a dispersed drop/gas mixing layer. Conductivity probes have been used to study the length of the liquid core at various ambient gas densities.[9,10] The liquid core tends to become shorter at high ambient gas densities due to increased entrainment rates. Nevertheless, the liquid core and its multiphase mixing layer are prominent features of the flow for typical gas/liquid density ratios, extending 200–400 jet-exit diameters for liquid jets in still gases at atmospheric pressure.[9]

Recent measurements of Ruff et al.[1-3] have yielded some information about the structure of the near jet-exit region of liquid jets in still gases. These experiments involved large (9.5- and 19.1-mm initial diameters) water jets injected in still air at atmospheric pressure. Measurements included liquid volume fraction distributions using gamma-ray absorption, drop

Received Jan. 26, 1991; revision received Aug. 14, 1991; accepted for publication Aug. 19, 1991.

*Graduate Assistant, Department of Aerospace Engineering.
†Graduate Assistant, Department of Aerospace Engineering; currently Assistant Professor, Department of Mechanical Engineering, Drexel University, Philadelphia, PA.
‡Professor, Department of Aerospace Engineering. Fellow AIAA.

sizes and velocities in the mixing layer using double-pulse holography, and air entrainment rates using laser velocimetry. The measurements of mean liquid volume fraction distributions showed that the rate of development of the flow was affected by both the breakup regime and the degree of flow-development at the jet exit: atomization breakup and fully developed turbulent pipe flow at the jet exit yielded the fastest mixing rates. Predictions based on the LHF approximation were effective for atomization breakup when mean liquid volume fractions were greater than 0.2; however, they progressively failed as the flow became dilute and as jet-exit conditions approached the wind-induced breakup regime. Difficulties with the LHF approach were identified by drop size and velocity measurements in the mixing layer, which showed significant effects of separated flow in regions where liquid volume fractions were low. Thus, the success of the LHF approximation at large liquid volume fractions was attributed to the small proportion of the momentum associated with the gas phase at these conditions due to the small gas/liquid density ratio of the flow. Similarly, entrainment rates are governed mainly by processes within the dilute portions of the mixing layer; therefore, LHF predictions generally overestimated entrainment rates due to separated-flow phenomena in the mixing layer. However, the findings suggested improved performance of LHF methods at large We_o with this limit approached more rapidly at large gas/liquid density ratios.

The objective of the present investigation was to explore effects of gas/liquid density ratio on the mixing properties of liquid jets in still gases and the adequacy of predictions of flow properties based on the LHF approximation. Experiments involved measurements of liquid volume fraction distributions within large-scale (9.5-mm initial jet diameter) water jets in still air at ambient pressures of 1–8 atm. The measurements were compared with predictions based on the earlier LHF approach,[1,2] to determine whether this methodology could treat effects of varying gas/liquid density ratios.

The paper begins with brief descriptions of experimental methods and the LHF computations. Results are then described, considering liquid volume and mass fraction distributions in turn.

Experimental Methods

Apparatus

Experimental methods were similar to Ruff et al.,[1] except that the flow was contained within a large pressure vessel so that the pressure of the ambient air could be changed. A sketch of the apparatus appears in Fig. 1. The arrangement involves a steady water jet injected vertically downward in still air within a large windowed pressure vessel (1.5-m diameter × 4.5-m long with two pairs of opposite windows having maximum opening diameters of 250 mm). Access to the interior of the pressure vessel was provided by a manhole at the top of the vessel. A second port at the top provided entry points to supply water to the jet and electrical cables needed to control the jet traversing system.

City water was fed to the injector using a centrifugal pump. The water was collected in the bottom of the tank with the liquid level maintained by outflow to a drain. A grate located above the liquid level reduced splash back into the test area. The rate of water flow was adjusted using a bypass system and was measured using a turbine flow meter that was calibrated by collecting water for timed intervals.

The water injectors had exit diameters of 9.5 mm and were the same as those used by Ruff et al.:[1] one yielding slug flow with low turbulence intensities, the other yielding fully developed turbulent pipe flow. The slug flow injector consisted of a honeycomb flow straightener (1.6-mm cells, 25-mm long) and two screens to calm the flow (16 × 16 square mesh, 0.18-mm-diam wire) followed by a 13.6:1 area contraction to the jet exit. The contraction was designed following Smith and Wang[11] to yield uniform velocities at the jet exit. The fully developed flow injector had the same flow straightener and contraction area ratio, but the contraction was followed by a constant area passage 41 jet-exit diameters long.

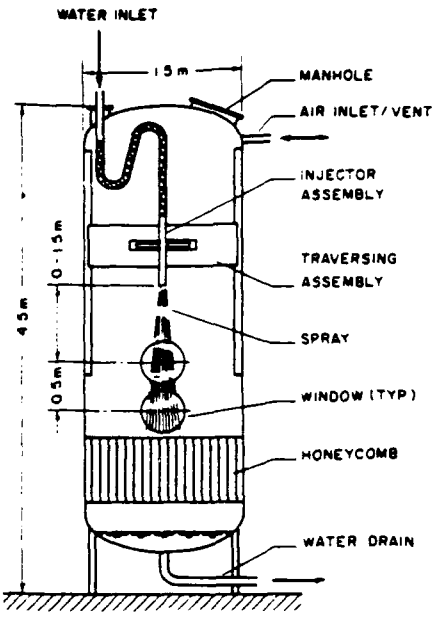

Fig. 1 Sketch of the variable gas density apparatus.

Instrumentation was mounted rigidly so that flow structure was measured by traversing the jet. Horizontal traverses were carried out using a stepping motor-driven linear positioner with a positioning accuracy of 5 μm. Vertical traverses involved moving the injector assembly along linear bearings with a manual positioner having a positioning accuracy of 0.5 mm.

Gamma-Ray Absorption Measurements

Distributions of mean liquid volume fractions were measured using gamma-ray absorption similar to Ruff et al.[1] An iodine-125 isotope source (5 mCi, emitting primarily at 27.20, 27.47 and 31.00 keV) provided a soft gamma-ray source with good absorption levels. The source was placed in a lead casket with an outlet aperture of 1.6-mm diameter and 13-mm long. Gamma rays passing through the flow were detected and counted with a Bicron X-ray probe (Model 1 × M.040/1.54) and a EG&G Ortec single-channel analyzer and counter timer (models 556, 590A, and 974). A lead aperture (1.5-mm diameter and 12-mm long) was placed in front of the detector to define the path observed through the flow. The energy window of the detector was set at 22–32 keV to minimize spurious counts due to background radiation and Compton scattering. The source and detector were placed in recessed mounts within opposing windows of the apparatus (not shown in Fig. 1) so that they were separated by a distance of 500 mm with the radiation path crossing horizontally through the chamber axis.

Absorption measurements (based on 20,000–25,000 counts) were made for 30–60 parallel paths through the flow and deconvoluted in the same manner as Santoro et al.[12] and Ruff et al.[1] The narrow absorption path minimized potential errors due to the orientation of liquid elements to less than 5%.[13] Experimental uncertainties were largely due to finite sampling times and background from the small drops dispersed within the pressure vessel. They are estimated (95% confidence) to be less than 30% for $\bar{\alpha}_l > 0.01$.

Test Conditions

Test conditions are summarized in Table 1. Operating conditions were selected to yield the same mean jet exit velocity for fully developed and slug flow at pressures of 1, 2, 4, and

Table 1 Summary of test conditions[a]

Jet-exit diameter (mm)	9.5
Ambient pressure (atm)	1, 2, 4, and 8
Jet flow rate (kg/s)	3.47
Injector pressure drop (kPa):	
Fully developed flow	2270
Slug flow	2110
Average jet exit velocity (m/s)	49.1
Re_d	462,000
We_d	312,000
We_{ad}	380, 760, 1520, 3040
Oh	0.00121

[a]Pressure-atomized water jet injected vertically downward in still air at various pressures and 298 ± 2K; in atomization breakup regime for both slug flow and fully developed turbulent pipe flow (L/d = 41) jet-exit conditions.

8 atm within the atomization breakup regime. Due to the limitations of the pump, this required a water flow rate roughly 13% lower than the atomization breakup condition used by Ruff et al.[1-3] for the 9.5-mm-diam injector. However, all test conditions are well into the atomization breakup regime defined by Ranz[4] and Miesse,[5] and exhibited initial liquid breakup right at the jet exit, which is characteristic of this breakup regime.

Flow properties at the jet exit were measured earlier using laser velocimetry.[1] For fully developed flow, mean streamwise velocity distributions were in good agreement with values in the literature for the same Reynolds number range.[14] However, rms streamwise and radial velocity fluctuations were more uniform across the central region, yielding streamwise and radial turbulence intensities of 7 and 4% near the axis, which are somewhat larger than literature values.[14] For slug flow, mean streamwise velocities were uniform over the central region of the flow and then declined near the wall (within 3–5% of the injector radius) due to boundary-layer growth in the nozzle passage. Streamwise and radial rms velocity fluctuations were roughly 1% of the mean streamwise velocity over the central region for slug flow.[1]

Theoretical Methods

Predictions of flow properties were limited to use of the LHF approximation similar to past work.[1,2,7] In addition to the LHF approximation, the major assumptions of the model are as follows: steady (in the mean) axisymmetric flow with no swirl, boundary-layer approximations apply, negligible kinetic energy and viscous dissipation of the mean flow, buoyancy only affects the mean flow, equal exchange coefficients of all species and phases, and negligible mass transport between the phases (no evaporation). These assumptions are either conditions of the experiments or are justified by past practice, except for the LHF approximation, which will be evaluated by the measurements. In particular, operation of well-atomized sprays within a closed container saturated the air with water vapor so that there was no potential for liquid evaporation.

Under these assumptions, the instantaneous mixture fraction (defined as the fraction of mass that originated from the injector) is either 0 (in the gas) or 1 (in the liquid). Then, time- and Favre-averages of any scalar property ϕ can be found in terms of the Favre-averaged mean mixture fraction, as follows:

$$\tilde{\phi} = \phi_g(1 - \tilde{f}) + \phi_l\tilde{f} \quad (1)$$

$$\bar{\phi} = (\phi_l\rho_l(1 - \tilde{f}) + \phi_g\rho_g\tilde{f})/(\rho_l(1 - \tilde{f}) + \rho_g\tilde{f}) \quad (2)$$

Given Eqs. (1) and (2), the flowfield can be found from a simplified version of the conserved-scalar formation of Lockwood and Naguib,[15] but using Favre averages following Bilger.[16] Governing equations are solved for conservation of mass, streamwise mean momentum, mean mixture fraction, turbulence kinetic energy, and the rate of dissipation of turbulence kinetic energy. The specific formulation, all empirical constants, and a discussion of calibration of the approach for a variety of constant and variable density single-phase jets, appears elsewhere.[7]

The specification of initial and boundary conditions, and the details of the numerical computations, can be found in Ruff et al.[1,2] For fully developed flow, initial profiles of $\tilde{u}$, k, and ε were taken from Schlichting[14] and Hinze[17] because they are good approximations of present measured jet-exit conditions and are readily available to others.[1] For slug flow, properties were assumed to be uniform except for bounding estimates of properties in the boundary layer along the wall for L/d = 0 and 5, with the latter conditions found assuming clean entry and no *vena contracta* along the nozzle passage from Schlichting.[14]

Results and Discussion

Mean Liquid Volume Fractions

Experimental Sensitivity

The mean liquid volume fraction distributions provide a quantitative indication of effects of gas/liquid density ratio and jet-exit conditions on flow properties. However, it is important to recognize the relationship between liquid volume fractions and mixing levels when interpreting these results. The present flows have large liquid/gas density ratios, which implies that liquid volume fractions vary rapidly with mixture fraction. This can be seen from the state relationship for liquid volume fraction:

$$\alpha_l = f/(f + (\rho_l/\rho_g)(1 - f)) \quad (3)$$

Using Eq. (2), an analagous expression can be obtained for time-averaged mixture fraction $\bar{\alpha}_l$ as a function of Favre-averaged mixture fraction $\tilde{f}$ as follows:

$$\bar{\alpha}_l = \tilde{f}/(\tilde{f} + (\rho_l/\rho_g)(1 - \tilde{f})) \quad (4)$$

Table 2 is a summary of f for α_l = 0.1 and 0.01 (or equivalently $\tilde{f}$ for the two values of $\bar{\alpha}_l$) over the present ambient pressure range. It is evident from the table that low levels of mixing cause large reductions in liquid volume fractions, even at the highest ambient pressures of the present test range. Thus, $\bar{\alpha}_l$ is an unusually sensitive indicator of mixing levels near the jet exit.

Axial Distributions

Measured and predicted time-averaged mean liquid volume fractions along the jet centerline are illustrated in Figs. 2 and 3 for fully developed and slug flow-jet exit conditions, respectively. Results are plotted as a function of distance from the injector, normalized by the injector diameter, with ambient pressure as a parameter. Predictions for slug flow jet-exit conditions are shown for L/d = 0 and 5, which bounds the potential degrees of flow development within the nozzle passage, as noted earlier. Measurements of Ruff et al.[1] at 1 atm for atomization breakup also are shown on the plots for both slug and fully developed flow; they agree very well with present results, although jet-exit velocities are slightly different. This is expected based upon the LHF predictions, which exhibit little variation of liquid volume fraction distributions with jet-exit velocity for the high Reynolds numbers of present flows.[1]

For fully developed flow, Fig. 2, the region near the jet exit (x/d < 3–8) exhibits mean liquid volume fractions near unity. Just beyond this region, however, mean liquid volume fractions decrease rapidly. The initial reduction of $\bar{\alpha}_l$ occurs at progressively smaller values of x/d as the pressure increases, with values of $\bar{\alpha}_l$ at a given value of x/d generally being lower

Table 2 f vs α_f for air/water mixtures[a]

	Pressure, atm			
α_f	1	2	4	8
0.10	0.990	0.979	0.960	0.923
0.01	0.897	0.813	0.684	0.520

[a]Air water mixtures at 300 K and various pressures.

at higher pressures as well. These trends indicate faster mixing rates at higher ambient gas densities, analogous to effects of flow density ratio for single-phase turbulent jets.[16] There is good agreement between measurements and predictions, indicating that the LHF approach correctly treats effects of the density ratio of the flow on mixing properties. However, conditions illustrated in Fig. 2 represent relatively low levels of mixing; for example, results in Table 2 suggest that Favre-averaged mixture fractions are generally greater than 0.85. For such low levels of mixing, predictions based on the LHF approximation have been reasonably good in the past,[1] because separated flow effects due to relative velocity differences between the gas and liquid are not very significant when the mass of the flow is predominantly liquid. Based on past evaluations of the methodology,[7] performance of the LHF approach is likely to be poorer as the dilute dispersed flow regime (where $f << 1$) is approached; behavior in this regime is considered later. Finally, although the variation of $\bar{\alpha}_{fc}$ suggests a relatively short liquid core, this is not the case when viewed in terms of mixture fraction. Favre-averaged mixture fractions are greater than 0.85 for all the results illustrated in Fig. 2, so that even low levels of flapping of the liquid core can explain the reductions of $\bar{\alpha}_{fc}$.

The slug flow results illustrated in Fig. 3 exhibit slower rates of mixing than the fully developed flows. First, $\bar{\alpha}_{fc}$ remains at unity until x/d is in the range 20–50. Similar to the results for fully developed flow, however, the value of x/d where $\bar{\alpha}_{fc}$ first begins to decrease from unity progressively decreases as the pressure increases, implying faster rates of mixing at higher ambient densities. The strong effect of the degree of flow development at the jet exit (cf. Figs. 2 and 3) is similar to earlier observations at atmospheric pressure.[1] This occurs because the liquid density is large in comparison to the gas; therefore, the fully developed flow carries significant levels of turbulence energy into the mixing layer, which enhances mixing rates. Predictions of properties for slug flow conditions are very sensitive to the degree of flow development at the jet exit. Thus, there are significant differences between predictions for pure slug flow ($L/d = 0$) and allowance for boundary-layer growth within the injector passage ($L/d = 5$). These conditions bound the range of possibilities for present tests, and it is encouraging that the two predictions tend to bound the measurements except at $x/d = 100$ and pressures of 4 and 8 atm. The discrepancies at $x/d = 100$ occur in a region where the streamwise variation of flow properties is rapid, and tends toward dilute conditions. Thus, because both predictions tend to overestimate the rate of development of the flow, separated flow effects are probably responsible for the difficulty.

Radial Distribution (Fully Developed Flow)

Predicted and measured radial profiles of mean liquid volume fractions for fully developed flow are illustrated in Figs. 4 and 5 for ambient pressures of 1 and 8 atm (results at 2 and 4 atm are similar). These results involve $\bar{\alpha}_f/\bar{\alpha}_{fc}$ plotted as a function of radial distance normalized by the injector radius, so that the actual width of the flow can be seen. Results are shown for various $x/d \leq 100$ because larger distances risked disturbances of the flow from the chamber walls. The measurements of Ruff et al.[1] at 1 atm are illustrated in Fig. 4 along with the present results. The two sets of experiments

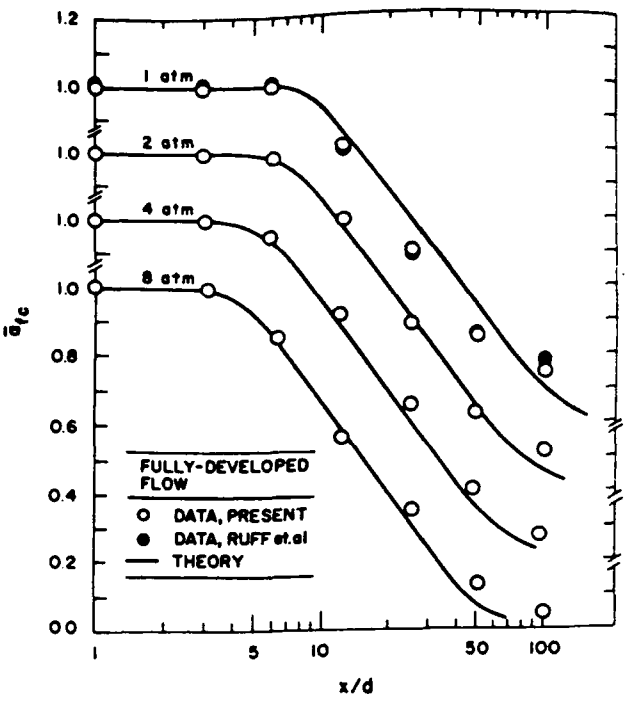

Fig. 2 Time-averaged liquid volume fractions along the axis at various ambient pressures for fully developed flow.

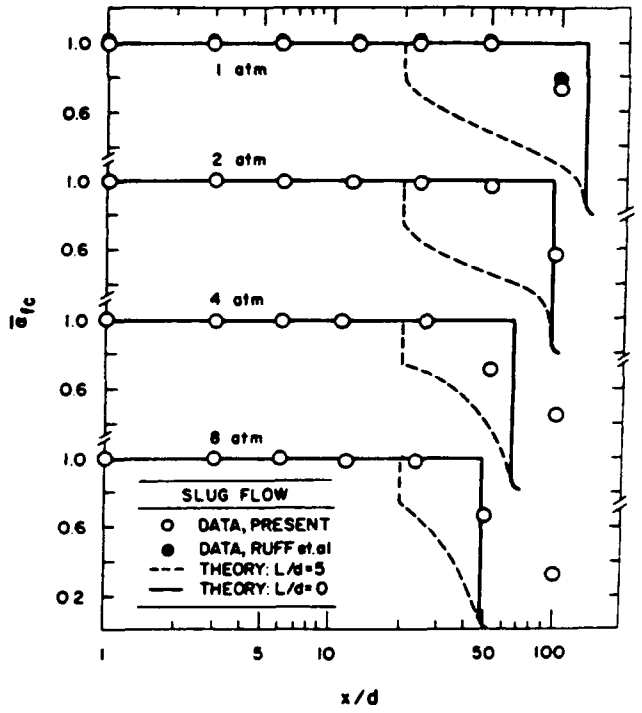

Fig. 3 Time-averaged liquid volume fractions along the axis at various pressures for slug flow.

agree within experimental uncertainties except at $x/d = 100$ where the confinement of the present jets may be responsible for somewhat reduced flow widths. As discussed earlier, predictions are essentially the same for the Reynolds number differences of the two tests. The measurements in Figs. 4 and 5 show a progressive increase of flow width with increasing distance from the jet exit, with flow widths increasing at a faster rate at the higher pressure. Apparent flow radii based on $\bar{\alpha}_f/\bar{\alpha}_{fc}$, however, are much smaller than for single-phase

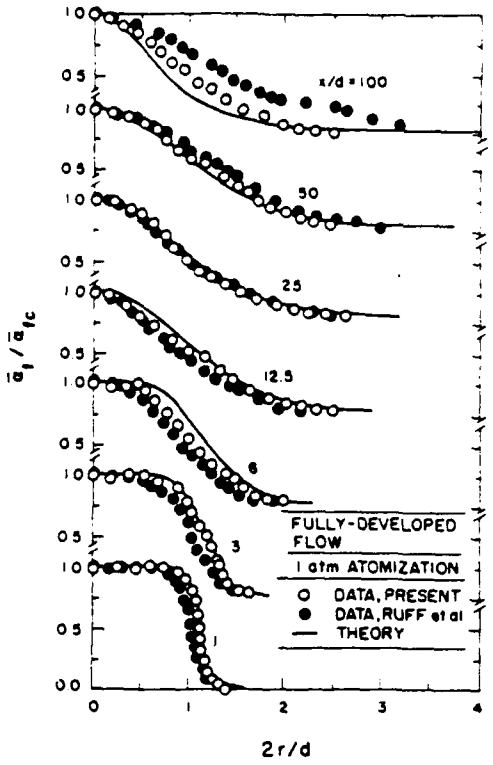

Fig. 4 Radial profiles of mean liquid volume fractions for fully developed flow at 1 atm.

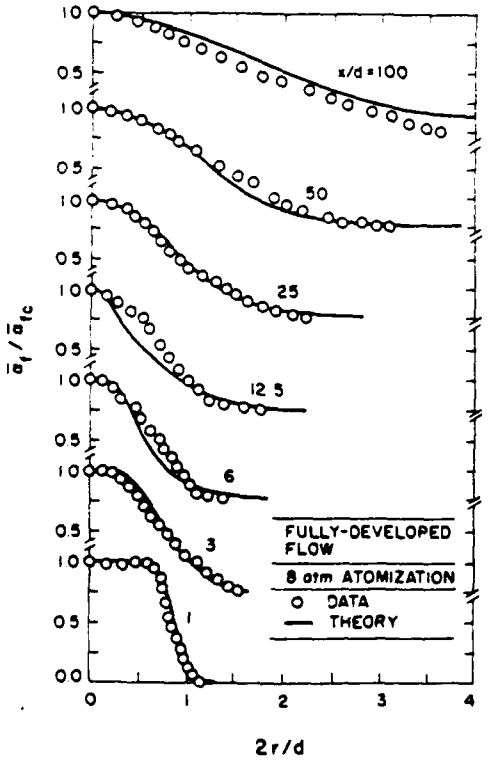

Fig. 5 Radial profiles of mean liquid volume fractions for fully developed flow at 2 atm.

jets because of the sensitivity of $\bar{\alpha}$ to the extent of mixing, discussed earlier. Notably, flow widths based on mean void fraction distributions for gas jets in liquids are unusually large for similar reasons.[19] For both turbulent liquid jets in gases and gas jets in liquids, however, predictions using the LHF approach indicate relatively normal flow widths far from the jet exit, in terms of $\bar{f}$; this is discussed more fully later.

The comparison between predicted and measured liquid volume fraction distributions in Figs. 4 and 5 is generally quite good, consistent with the good predictions of properties along the axis for fully developed flow observed in Fig. 2. The main exception is the farthest downstream position, $x/d = 100$, at 1 atm, where measurements exhibit a wider flow than predictions. Ruff et al.[1,2] show that this difficulty is largely due to effects of separated flow as the multiphase flow becomes more dilute. Predictions at $x/d = 100$ are improved at 8 atm, which is expected, because the larger gas density should yield smaller drops after secondary breakup, tending to reduce errors due to effects of separated flow.[2,3]

Radial Distributions (Slug Flow)

Predicted and measured radial profiles of mean liquid volume fractions for slug flow are illustrated in Figs. 6 and 7 for ambient pressures of 1 and 8 atm (results at 2 and 4 atm are similar). Measurements of Ruff et al.[1] at 1 atm for slug flow are illustrated in Fig. 6 along with the present measurements. In this case, both sets of measurements agree everywhere within experimental uncertainties, in accord with expectations from the predictions. Better agreement between the two sets of measurements for slug flow than fully developed flow at $x/d = 100$ is reasonable because the slug flow is narrower, which reduces effects of confinement for present measurements. Predictions for $L/d = 0$ and 5 are shown, similar to Fig. 3. Results illustrated in Figs. 6 and 7 exhibit a relatively sharp transition between the liquid core of the flow and the region where $\bar{\alpha}_l$ decreases, at least for $x/d \leq 50$. Additionally, the extent of radial spread of the slug flows is less than the fully developed flows. Both these observations are consistent with slower mixing rates for slug flow than fully developed flow. As before, however, flow widths at a particular x/d are significantly larger at 8 atm than 1 atm, suggesting faster mixing rates at higher pressures.

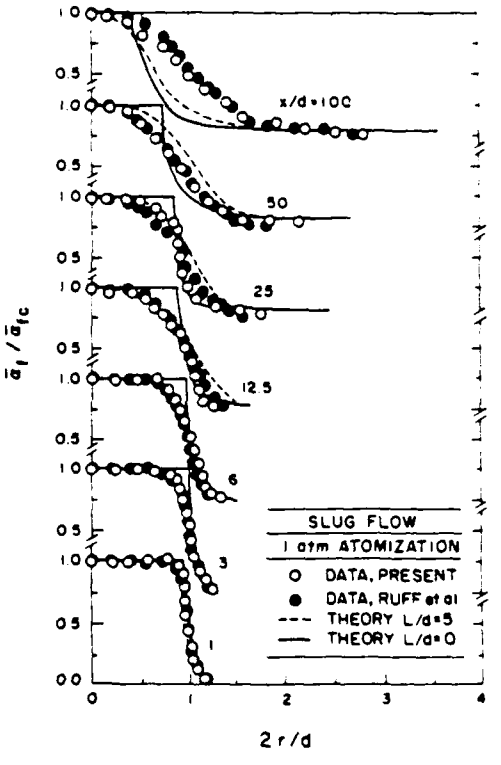

Fig. 6 Radial profiles of mean liquid volume fractions for slug flow at 1 atm.

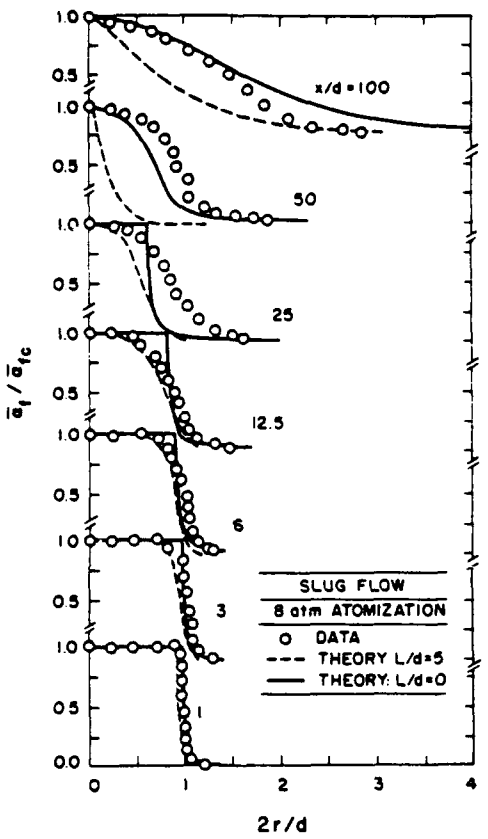

Fig. 7 Radial profiles of mean liquid volume fractions for slug flow at 2 atm.

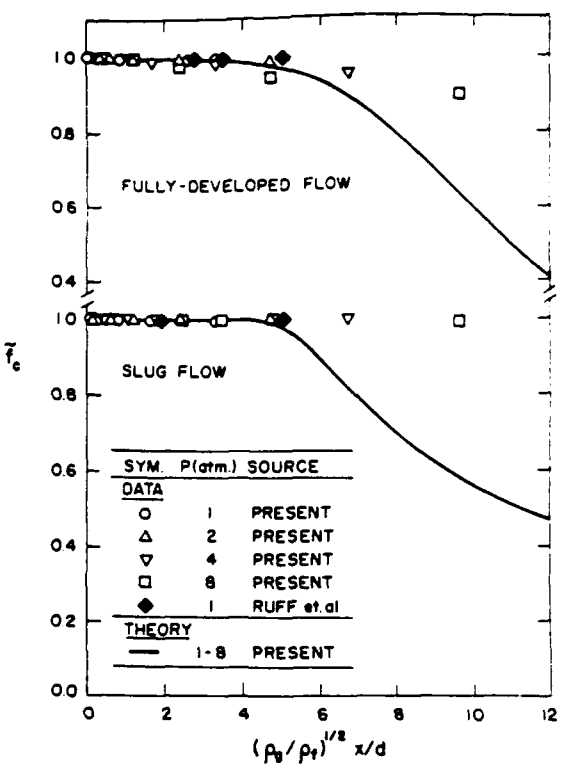

Fig. 8 Favre-averaged mixture fractions along the axis for fully developed and slug flow.

Predictions of slug flow properties in Figs. 6 and 7 are reasonably good for $x/d \leq 25$, within the bounds of the limiting estimates of the degree of flow development at the jet exit. Farther from the injector, however, predictions are less satisfactory. In particular, errors are large in the region where $\bar{\alpha}_{fc}$ first begins to decrease from unity (see Fig. 3). This behavior is caused by poor estimates of $\bar{\alpha}_{fc}$, due to uncertainties in the initial degree of flow development, because $\bar{\alpha}_{fc}$ is used to normalize both predictions and measurements in Figs. 6 and 7. Beyond this region, predictions are in better agreement with measurements but this is largely fortuitous because $\bar{\alpha}_{fc}$ is still not predicted very well by either limiting condition (see Fig. 3). These difficulties are probably due to the effects of separated flow in the rapidly developing region near the tip of the liquid core for slug flow, as discussed earlier.

Sensitivity Study

The sensitivity of present computations was examined similar to past work.[1,2] Predictions were very sensitive to initial mean velocity distributions, as can be seen from the results illustrated in Figs. 3, 6, and 7 for slug flow at the limits L/d = 0 and 5. Predictions were also sensitive to initial values of k and ε, with 10% changes in these properties causing 5–10% changes in $\bar{\alpha}_{fc}$ for x/d in the range 20–60. However, these properties were reasonably well known for the fully developed flows, whereas effects of low-turbulence levels in the case of the slug flow were not very significant. Thus, the uncertainties of the predictions were largely governed by difficulties in specifying the mean velocity distribution for slug flows, and the less quantifiable limitations of κ-ε turbulence models using the LHF approximation for multiphase boundary-layer flows.

Favre-averaged Mixture Fractions

Axial Distributions

Computations indicated that distributions of Favre-averaged mixture fractions were much less influenced by variations of ambient gas density than time-averaged liquid volume fractions; therefore, both present measurements and those of Ruff et al.[1-3] were examined in terms of this fundamental mixing property. This was done by computing $\tilde{f}$ from the measured values of $\bar{\alpha}$ using Eq. (4).

It is well known that properties along the axis of single-phase variable-density jets should scale in terms of a density-weighted streamwise distance, which becomes $(\rho_g/\rho_f)^{1/2}\, x/d$ for present measurements.[18] Chehroudi et al.[9] also find similar scaling for their correlation of the length of the liquid core. Thus, predicted and measured $\tilde{f}_c$ are plotted in terms of this variable for both fully developed and slug flows in Fig. 8. Measurements are identified by ambient pressure and source. When plotted in the manner of Fig. 8, predicted effects of ambient pressure, jet-exit Reynolds number, and L/d (for slug flow) were small; therefore, only single predicted lines are shown for fully developed and slug flow.

In contrast to $\bar{\alpha}_{fc}$, the sensitivity of present experiments to $\tilde{f}_c$ is relatively low due to the large density ratios of the flows. Thus, measured values of $\tilde{f}_c$ are generally greater than 0.85 as noted in connection with the plots of $\bar{\alpha}_{fc}$ (Figs. 2 and 3). Over this narrow range of $\tilde{f}_c$, however, the measurements at various ambient pressures correlated reasonably well in terms of density-weighted streamwise distance.

Predicted and measured $\tilde{f}_c$ shown in Fig. 8 are in reasonably good agreement for $(\rho_g/\rho_f)^{1/2}\, x/d < 5$. However, this observation is much less definitive than comparisons between predicted an measured values of $\bar{\alpha}_{fc}$ due to the reduced sensitivity of $\tilde{f}_c$. Similarly, the striking effect of jet-exit turbulence on the variation of $\bar{\alpha}_{fc}$ is much less evident for $\tilde{f}_c$. The measurements, however, yield larger values of $\tilde{f}_c$ than predicted at density-weighted distances greater than five, particularly for slug flow where predicted properties vary most rapidly in the streamwise direction. This implies slower rates of mixing along the axis than LHF predictions, suggesting significant effects of separated flow in the region just downstream of the end of the liquid core. This is plausible, because breakup of the end of the liquid core, the same as primary breakup along its

surface, should yield larger drops having significant relative velocities. Thus, the predicted universal behavior of $\tilde{f}_c$ was not approached for present test conditions as the flow become more dilute for density-weighted streamwise distances greater than five. This is much more evident from the plots of $\tilde{f}_c$ in Fig. 8 than those for $\bar{\alpha}_{f_c}$ in Figs. 2 and 3 due to effects of large density ratio on sensitivity to these properties.

Radial Distributions

Due to the length of the liquid core, present flows are transitional between a mixing layer and a jet when viewed in the radial direction. Thus, radial profiles of $\tilde{f}$ were limited to mixing layer conditions ($\tilde{f}_c \approx 1$) to avoid the complications of this transition. Within the mixing layer, predictions showed that $\tilde{f}/\tilde{f}_c$ was relatively independent of the density ratio when plotted in terms of $(r - r_{\tilde{f}=0.5})/x$ so that measurements will be considered in terms of these variables. In order to extend the range of $\tilde{f}$ that could be examined, the present gamma-ray absorption measurements were supplemented by holography measurements in the multiphase mixing layer from Ruff et al.[3]

Predicted and measured radial profiles of $\tilde{f}/\tilde{f}_c$ are plotted in Fig. 9 for both fully developed and slug flows. As mentioned earlier, predictions exhibit small changes with density ratio and position for present test conditions. The present gamma-ray absorption measurements are in reasonably good agreement with predictions when plotted in the manner of Fig. 9, however, they are limited to $\tilde{f}/\tilde{f}_c > 0.85$.

The agreement between predictions and the holography measurements illustrated in Fig. 9 is much less satisfactory. The holography measurements were obtained in the dispersed flow region where the liquid is present as irregular liquid elements and drops, which is typical of dilute dispersed flows. Thus, poorer performance of the LHF approximation is expected, based on observations in other dilute dispersed flows.[4]

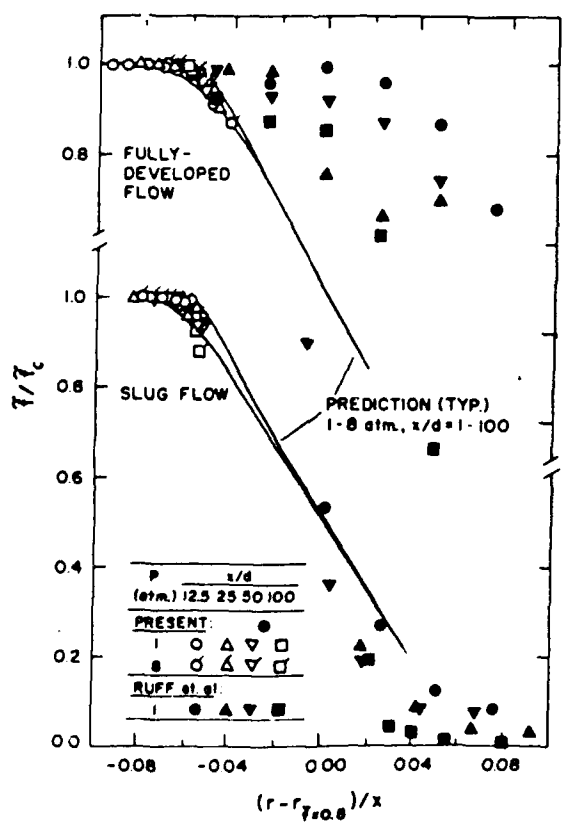

Fig. 9 Radial profiles of Favre-averaged mixture fractions in the multiphase mixing layer for fully developed and slug flow.

Nevertheless, the holographic measurements for slug flow conditions do approach predictions, with predicted overestimation of the mixing rates near the outer edge of the flow being attributable to separated flow effects. Discrepancies between predictions and measurements, however, are much larger for fully developed flow. Nevertheless, this behavior is reasonable because drop sizes after primary breakup were much larger for the fully developed flow than the slug flow (SMD of 1330 μm as opposed to 174 μm), which implies greater effects of separated flow.[3] Thus, improved atomization conditions might yield the universal results suggested by the predictions; however, additional measurements are needed to evaluate this possibility.

A final matter to be considered in connection with Fig. 9 is why the holography measurements show faster mixing than predicted for fully developed flow but slower mixing than predicted for slug flow. This behavior is caused by interactions between primary breakup and separated-flow phenomena.[3] Primary breakup of a turbulent liquid generates large liquid elements with radial velocities comparable to radial velocity fluctuations in the liquid. Thus, these large liquid elements are projected across the dispersed flow before they break up or relax to local flow velocities, which enhances mixing. In contrast, primary breakup of nonturbulent liquids yields small radial velocities, while large drops have poor response to turbulent dispersion due to their inertia, which retards mixing.

Conclusions

The structure and mixing properties of nonevaporating liquid jets in still gases were studied for various ambient gas densities at atomization breakup conditions, emphasizing the region near the jet exit. The major conclusions of the study are as follows:

1) Increasing gas/liquid density ratios reduces the length of the liquid core and increases the flow width, implying increased rates of mixing analogous to effects of density ratio for single-phase turbulent jets.

2) Turbulence levels and the degree of flow development at the jet exit have a strong effect on mixing rates, with turbulent flows mixing much faster than nonturbulent slug flows.

3) Use of the locally homogeneous flow approximation, in conjunction with a Favre-averaged turbulence model, yielded good estimates of effects of gas/liquid density ratio and initial liquid vorticity on time-averaged liquid volume fraction distributions and Favre-averaged mixture fraction distributions in the region near the liquid core where $\tilde{f} > 0.85$. The main reason for this is that separated flow effects, like small velocities of the gas and small drops, are not very important for these low degrees of mixing. Nevertheless, it is helpful that predictions provide reasonable estimates of the initial stages of mixing.

4) Distributions of $\tilde{f}$ were relatively independent of the density ratio of the flow in terms of $(\rho_g/\rho_l)^{1/2} x/d$ along the axis and $(r - r_{\tilde{f}=0.5})/x$ across the mixing layer for $\tilde{f} > 0.85$; therefore, many of the unusual mixing properties of these flows in terms of $\bar{\alpha}_f$ are due to the strong nonlinearities of the state relationship between α_f and f rather than unusual behavior of the fundamental mixing variable $\tilde{f}$ itself. Predictions suggest that this scaling of $\tilde{f}$ should extend to the full range of $\tilde{f}$ if effects of separated flow are small; however, this regime was not reached during the present experiments.

5) For $\tilde{f} < 0.85$, significant effects of separated flow were observed, causing poor performance of predictions using the locally homogeneous flow approximation and effects of the density ratio on the scaling of distributions of $\tilde{f}$. This agrees with other determinations of important effects of separated flow in dilute dispersed flows, however, quantitative estimates of conditions where separated-flow must be considered require more information on primary breakup properties than is currently available.

Present conclusions are based on large-scale sprays (9.5-mm injector diameter) that have much lower rates of deceleration than practical injectors, and regions of the flow having relatively high mixture fractions (generally greater than 0.9 along the axis) where the momentum of the gas does not have a strong influence on flow dynamics. These factors favor use of the locally homogeneous flow approximation, so that present observations are not necessarily in conflict with earlier work showing significant separated-flow effects within dense sprays for smaller injector diameters and mixture fractions.[1-3] Additional information concerning liquid breakup properties in dense sprays clearly is needed in order to provide a rational means of evaluating separated-flow effects and the adequacy of the locally homogeneous flow approximation for particular conditions.

Acknowledgments

This research was supported by ONR Grant N00014-89-J-1199 with G. D. Roy serving as Scientific Officer. Initial development of the variable ambient density test chamber was sponsored by the Air Force Office of Scientific Research, under Grant No. AFOSR-85-0244, with J. N. Tishkoff serving as Program Manager. The U.S. Government is authorized to reproduce and distribute copies of this paper for governmental purposes notwithstanding any copyright notation thereon.

References

[1]Ruff, G. A., Sagar, A. D., and Faeth, G. M., "Structure and Mixing Properties of Pressure-Atomized Sprays," *AIAA Journal*, Vol. 27, No. 7, 1989, pp. 901–908.

[2]Ruff, G. A., Bernal, L. P., and Faeth, G. M., "Structure of the Near-Injector Region of Non-Evaporating Pressure-Atomized Sprays," *Journal of Propulsion and Power*, Vol. 7, No. 2, 1991, pp. 221–230.

[3]Ruff, G. A., Wu, P.-K., Bernal, L. P., and Faeth, G. M., "Continuous- and Dispersed-Phase Structure of Dense Nonevaporating Pressure-Atomized Sprays," *Journal of Propulsion and Power*, in press.

[4]Ranz, W. E., "Some Experiments on Orifice Sprays," *Canadian Journal of Chemical Engineering*, Vol. 36, No. 8, 1958, pp. 175–181.

[5]Miesse, C. C., "Correlation of Experimental Data on the Disintegration of Liquid Jets," *Industrial Engineering Chemistry* Vol. 47, No. 9, 1955, pp. 1690–1697.

[6]Phinney, R. E., "The Breakup of a Turbulent Jet in a Gaseous Atmosphere," *Journal of Fluid Mechanics*, Vol. 6, Oct. 1973, pp. 689–701.

[7]Faeth, G. M., "Mixing, Transport and Combustion in Sprays," *Progress in Energy and Combustion Science*, Vol. 13, No. 4, 1987, pp. 293–345.

[8]Faeth, G. M., "Structure and Atomization Properties of Dense Turbulent Sprays," *Twenty-Third Symposium (International) on Combustion*, The Combustion Institute, Pittsburgh, PA, 1990, pp. 1345–1352.

[9]Chehroudi, B., Onuma, Y., Chen, S.-H., and Bracco, F. V., "On the Intact Core of Full Cone Sprays," Society of Automotive Engineers Paper 850126, 1985.

[10]Hiroyasu, H., Shimizu, M., and Arai, M., "The Breakup of a High speed Jet in a High Pressure Gaseous Environment," Univ. of Wisconsin, Madison, ICLASS-82, 1982.

[11]Smith, R. H., and Wang, C.-T., "Contracting Cones Giving Uniform Throat Speeds," *Journal of Aeronautical Science*, Vol. 11, No. 10, 1944, pp. 356–360.

[12]Santoro, R. J., Semerjian, J. H., Emmerman, P. J., and Goulard, R., "Optical Tomography for Flow Field Diagnostics," *International Journal of Heat and Mass Transfer*, Vol. 24, No. 7, 1981, pp. 1139–1150.

[13]Gomi, H., and Hasegawa, K. I., "Measurements of the Liquid Phase Mass in Gas-Liquid Sprays by X-ray Attenuation," *International Journal of Multiphase Flow*, Vol. 10, No. 4, 1984, pp. 653–662.

[14]Schlichting, H., *Boundary Layer Theory*, 7th ed., McGraw-Hill, New York, 1979, p. 599

[15]Lockwood, F. C., and Naguib, A. S., "The Prediction of Fluctuations in the Properties of Free, Round-Jet Turbulent Diffusion Flames," *Combustion and Flame*, Vol. 24, No. 1, 1975, pp. 109–124.

[16]Bilger, R. W., "Turbulent Jet Diffusion Flames," *Progress in Energy and Combustion Science*, Vol. 1, No. 1, 1976, pp. 87–109.

[17]Hinze, J. O., *Turbulence*, 2nd ed., McGraw-Hill, New York, 1975, p. 427 and pp. 724–734.

[18]Ricou, F. P., and Spalding, D. B., "Measurements of Entrainment by Axisymmetrical Turbulent Jets," *Journal of Fluid Mechanics*, Vol. 11, Jan. 1961, pp. 21–32.

[19]Loth, E., and Faeth, G. M., "Structure of Underexpanded Round Air Jets Submerged in Water, *International Journal of Multiphase Flow*, Vol. 15, No. 4, 1989, pp. 589–603.

APPENDIX D: TSENG ET AL. (1992b)

Dispersed-Phase Structure of Pressure-Atomized Sprays at Various Gas Densities

by

L.-K. Tseng,* P.-K. Wu* and G.M. Faeth*

Department of Aerospace Engineering

The University of Michigan

Ann Arbor, Michigan 48109-2140

ABSTRACT

The dispersed-phase structure of the dense-spray region of pressure-atomized sprays was studied for atomization breakup conditions, considering large-scale (9.5 mm initial diameter) water jets in still air at ambient pressures of 1, 2 and 4 atm., with both fully-developed turbulent pipe flow and nonturbulent slug flow at the jet exit. Drop sizes and velocities, and liquid volume fractions and fluxes, were measured using holography. Measurements were compared with predictions based on the locally-homogeneous flow (LHF) approximation as well as recent correlations of drop sizes after primary breakup of turbulent and nonturbulent liquids. The dispersed-flow region beyond the liquid surface was relatively dilute (liquid volume fractions less than 0.1%), with significant separated-flow effects throughout, and evidence of near-limit secondary breakup and drop deformation near the liquid surface. Turbulent primary breakup predictions were satisfactory at atmospheric pressure, where the correlation was developed, but failed to predict observed trends of decreasing drop sizes with increasing gas density due to aerodynamic effects; in contrast, the laminar primary breakup predictions successfully treated the relatively small effects of gas density for this breakup mechanism. Effects of liquid turbulence at the jet exit were qualitatively similar to single-phase flows, yielding faster mixing rates with increased turbulence levels even though drop sizes tended to increase as well. LHF predictions within the dispersed-flow region were only qualitatively correct due to significant separated-flow effects, but tended to improve as the ambient pressure and the distance from the jet exit increased.

* Graduate Assistant, Department of Aerospace Engineering, The University of Michigan, Ann Arbor, Michigan 48109-2140.

* Professor, Department of Aerospace Engineering, The University of Michigan, Ann Arbor, Michigan 48109-2140, Fellow AIAA.

Nomenclature

C_a	=	aerodynamic breakup constant, Eq.(7)
C_r	=	ligament residence-time constant, Eq. (6)
d	=	injector diameter
d_p	=	drop diameter
e_p	=	volume-averaged ellipticity
f	=	mixture fraction
FDF	=	fully-developed flow
g	=	liquid flux
L	=	injector passage length
MMD	=	mass median diameter
N	=	number of drops in sample

Oh_i = Ohnesorge number based on length scale i, $\mu_l/(\rho_l\sigma)^{1/2}$

r = radial distance

Re_d = jet Reynolds number, $U_o d/\nu_f$

SF = slug flow

SMD = Sauter mean diameter

u = streamwise velocity

u_p = streamwise drop velocity

v = radial velocity

V = sample volume

$We_{f\Lambda}$ = integral-scale Weber number, $\rho_f u_o^2 \Lambda/\sigma$

$\tilde{We}_g$ = spray Weber number, Eq. (2)

We_{id} = jet Weber number based on phase i, $\rho_i u_o^2 d/\sigma$

We_{gp} = drop Weber number, Eq. (3)

We^*_{gp} = critical drop Weber number for secondary breakup

We_{gSMD} = primary breakup Weber number, $\rho_g u_o^2 SMD/\sigma$

x = streamwise distance

α = liquid volume fraction

Λ = radial integral scale

μ = molecular viscosity

ν = kinematic viscosity

ρ = density

σ = surface tension

τ_b = ligament aerodynamic breakup time, Eq. (7)

τ_r = ligament residence time, Eq. (6)

Subscripts

f = liquid-phase property

fc = liquid core property

g = gas-phase property

o = injector exit condition

Superscripts

$(\bar{\ }), (\tilde{\ })$ = time- and Favre-averaged mean quantities

$(\bar{\ })'$ = time-averaged rms property

INTRODUCTION

The present study extends past work in this laboratory concerning the properties of the near-injector dense-spray region of pressure-atomized sprays.[1-6] The first phase of the investigation involved measurements of liquid volume fractions and dispersed-phase structure of large water jets (9.5 mm and 19.1 mm initial diameter) in still air at atmospheric pressure.[1-3] Tseng et al.[4] extended the liquid volume fraction measurements to treat effects of ambient air density at ambient pressures of 1-8 atm. Additionally, mechanisms of primary breakup of both nonturbulent and turbulent liquids have been studied in air at normal temperature and pressure considering various liquids and jet exit diameters and velocities.[5,6] The objective of the present investigation was to examine the effect of varying gas densities on the dispersed phase properties of dense sprays, emphasizing conditions within the multiphase mixing layer that begins right at the jet exit for atomization breakup conditions, for test conditions similar to Tseng et al.[4]

Past work on pressure-atomized dense sprays has been discussed in several recent reviews.[7-12] Early studies emphasized breakup regimes, identifying conditions for Rayleigh, wind-induced and atomization breakup—the latter having greatest practical importance because of its wide range of operating conditions and production of small drops needed for rapid mixing.[11-15] Subsequent work concentrated on visualization of the near-injector region of the flow and definition of the properties of the liquid core, which is much like the potential core of a single-phase jet.[15-20] More recently the properties of the multiphase mixing layer surrounding the liquid core have been studied, beginning with measurements within the dilute spray region near the outer edge of this flow.[21,22]

Past work in this laboratory has largely concentrated on the properties of the near-injector region during atomization breakup, using relatively large diameter liquid jets (3.5 - 19.1 mm) to provide known jet exit flow conditions and reasonable spatial resolution because the flow diameter is not thought to affect dense spray structure appreciably.[1-6]

This has included measurements of liquid volume fraction distributions using gamma-ray absorption for water jets in air at various ambient pressures.[1,4] These results showed that mixing rates were influenced by the breakup regime, turbulence properties at the jet exit and the ambient gas density. Predictions based on the locally-homogeneous flow (LHF) approximation, where relative velocities between the phases are neglected, were in good agreement with measurements for Favre-averaged mixture fractions greater than 0.85, but overestimated mixing rates at lower mixture fractions. The reasons for this behavior were explored by measuring the structure of the multiphase mixing layer at atmospheric pressure—drop sizes, phase velocities, entrainment rates, and liquid volume fractions and fluxes—using holography and phase-discriminating laser velocimetry.[2,3] The results showed significant effects of separated flow so that good performance of the LHF approximation only occurred at relatively large mixture fractions where the small velocities of the gas and small drops were not very important.

The most recent work in this laboratory has considered the properties of primary breakup, using holography to find drop sizes and velocities at atmospheric pressure.[5,1] Two modes of primary breakup were considered: turbulent breakup, due to distortion of the liquid surface by turbulence; and nonturbulent breakup, due to stripping of liquid from boundary layers formed on the windward side of waves along the liquid surface. Correlations of SMD after primary breakup were achieved for both modes of breakup for a variety of liquids and jet exit diameters and velocities, but only have been evaluated for liquid jets in air at atmospheric pressure.

The present investigation extends the earlier work in this laboratory,[1-6] addressing effects of ambient gas density on the properties of the dispersed phase during atomization breakup by observing water jets in still air at pressures of 1, 2 and 4 atm. with both turbulent and nonturbulent jet exit conditions. Holography was used to find drop sizes and velocities, and liquid volume fractions and fluxes, within the dispersed-flow region beyond the liquid surface. Following earlier work,[1-4] predictions of flow properties using the LHF

approximation were used to help assess separated-flow effects on the structure of the flow. The correlations for primary breakup properties also were evaluated for effects of varying ambient gas density. The present discussion is brief; additional details and a complete tabulation of data can be found in Tseng.[23]

Experimental Methods

Apparatus

The test apparatus involved a steady water jet injected vertically downward within a large windowed pressure vessel (1.5 m diameter × 4.5 m long).[4] The rate of water flow was adjusted with a bypass system and measured using a paddle-wheel flow meter. Two injectors having exit diameters of 9.5 mm were used: one yielding slug flow with low turbulence intensities, the other yielding fully developed turbulent pipe flow. The slug flow injector consisted of a honeycomb flow straightener, two screens to calm the flow and a 13.6:1 area contraction designed following Smith and Wang[24] to yield uniform velocities at the exit. The fully-developed flow injector had a similar configuration with the contraction followed by a constant area passage 41 jet exit diameters long to yield nearly fully-developed turbulent pipe flow at the exit. The injectors could be traversed to accommodate the rigidly mounted holocamera.

Holocamera

The holocamera and reconstruction systems were the same as Ruff et al.[2] Measurements were obtained over 6 × 6 × 4 mm^3 volumes, using at least three holograms per position. The data was spatially averaged over the width of the measuring volumes, or ± 1/2 the distance between adjacent radial positions, whichever was smaller. Drops and other nearly spherical objects were sized by finding the maximum and minimum diameters through the centroid of the image. Assuming that the object was ellipsoidal, its diameter was taken to be the diameter of a sphere having the same volume as the ellipsoid. This procedure was not appropriate for elongated liquid elements where the centroid was outside the boundaries of the image. Then, the projected area and perimeter of the image were

measured and the maximum and minimum diameters of the ellipsoid having the same crossectional area and perimeter were computed to find the effective sphere diameter as before. The ellipticity, defined as the ratio of the maximum and minimum ellipsoid diameters, also was computed for each object.

Drop velocity measurements were based on the motion of the centroid of the image and were correlated as a function of diameter using a least-squares fit. This allowed plots of drop velocities for fixed drop diameters across the width of the mixing layer while making maximum use of the data on the holograms at each position. Knowing the volume and velocities of liquid elements in the flow, liquid volume fractions and fluxes could be computed in a straightforward manner.

Measurements typically involved analysis of 150 objects at each position and pressure. Experimental uncertainties generally were dominated by sampling limitations rather than resolution of the reconstructed holograms. Experimental uncertainties (25 percent confidence) were as follows:[23] Sauter mean diameter (SMD) < 10%, volume-averaged ellipticity < 15%, liquid object velocities < 20%, liquid volume fractions < 15%, and liquid fluxes < 25%. All measurements were repeatable well within these limits.

Test Conditions

Mean flow conditions were the same for the slug and fully-developed flows, and were identical to Tseng et al.[4] This involved a water flow rate of 3.47 kg/s, an average jet exit velocity of 49.1 m/s, Re_d = 462,000, Oh_d = 0.00121, We_{fd} = 312,000, and We_{gd} = 380,760 and 1520 at pressures of 1, 2 and 4 atm. Due to limitations of the pump, this water flow rate was roughly 13% lower than the atomization breakup condition considered by Ruff et al.[1-3] for the same injectors. However, present flows were well within the atomization breakup regime defined in Refs. 13 and 14.

Ruff et al.[1] completed laser velocimeter measurements at the jet exit for the present injectors, spanning the present operating condition. For slug flow, mean streamwise velocities were uniform over the central region and declined near the wall (within 3-5% of

the injector radius), due to boundary layer growth in the nozzle passage, while rms velocity fluctuations were roughly 1% of the mean streamwise velocity over the central portion of the flow. For fully-developed flow, mean velocity distributions were in good agreement with literature values for the same Reynolds number range, while rms velocity fluctuations near the axis were somewhat larger than literature values.[25,26]

Theoretical Methods

Predictions of flow properties were limited to use of the LHF approximation similar to past work.[1-4] A detailed description of the approach is provided elsewhere.[7,23] In addition to the LHF approximation, the major assumptions of the model are as follows: steady (in the mean) axisymmetric flow with no swirl, boundary layer approximations apply, negligible kinetic energy and viscous dissipation of the mean flow, buoyancy only affects the mean flow, equal exchange coefficients of all species and phases, and negligible mass transport between the phases (no evaporation). The formulation followed the conserved-scalar formalism of Lockwood and Naguib[27] but used Favre averages following Bilger.[28] The specific formulation, all empirical constants, calibration of the approach for variable density single-phase flows, the numerical computations and specification of initial conditions are described in Refs. 1, 4 and 7.

Results and Discussion

Drop Properties

Similar to earlier findings,[3,5,6] present measurements of drop size distributions correlated quite well with Simmons' universal root normal distribution function.[29] The root normal distribution is defined by two moments: the SMD and the ratio of the mass median diameter (MMD) to the SMD. Typical of past observations,[3,5,6,29] MMD/SMD = 1.2 for present turbulent and nonturbulent flows so that the entire drop size distribution will be represented by the SMD in the following.

Typical distributions of drop properties across the mixing layer for fully-developed flow, illustrating flow properties for turbulent primary breakup, appear in Figs. 1-4. See

Tseng[23] for similar plots at all test conditions. Figures 1-3 illustrate flow properties at pressures of 1, 2 and 4 atm. at the fixed streamwise position of x/d = 6. Figures 3 and 4 illustrate effects of increasing x/d from 6 to 25 at a fixed pressure of 4 atm. The plots include volume-averaged ellipticity, e_p, SMD and drop velocities for d_p = 10, 50, 100 and 200 μm. The range of positions where the surface of the liquid core was observed and LHF predictions of flow velocities are also shown on the plots.

Many of the features of volume-averaged ellipticity and SMD seen in Figs. 1-4 are similar to earlier observations of Ruff et al.[2] at atmospheric pressure; however, significant effects of increasing ambient pressure are observed as well. Thus, at atmospheric pressure, the largest values of e_p and SMD generally are in the region of the liquid surface and with increased radial distance e_p approaches unity, and the SMD decreases, representing smaller round drops near the edge of the flow. This behavior supports the presence of primary breakup yielding large drops which subsequently undergo secondary breakup. With increasing pressure at x/d = 6, however, e_p remains near unity, and the SMD is relatively uniform across the flow. This reflects the increased propensity for secondary breakup, and shorter secondary breakup times, for particular drop sizes and relative velocities, as the gas density increases.[3] This altered behavior at increased gas densities also is evident from the substantial reduction of SMD near the surface as the ambient pressure increases. This suggests merging of primary and secondary breakup processes as the ambient pressure increases. Effects of streamwise distance on e_p and SMD seen at atmospheric pressure,[2,6] still are preserved at elevated pressures for present test conditions. Thus, comparing results at x/d = 6 (Fig. 3) and 25 (Fig. 4) shows increasing e_p and SMD with increasing distance from the jet exit that is characteristic of turbulent primary breakup.[6] Smaller relative velocities, caused by faster mixing rates at elevated pressures, also are probably a factor in this behavior.

Distributions of drop velocities in Figs. 1-4 have been normalized by the mass-averaged velocity at the exit of the jet. In general, there are substantial differences between

the velocities of drops of different size, with drop velocities generally overestimated near the liquid core and underestimated near the edge of the flow by the LHF predictions. This is clear evidence of significant separated flow effects. Drop velocities tend to decrease with increasing radial distance (reflecting effects of longer residence times in the flow for drops farther from the surface) and reduced drop diameters (reflecting smaller velocity relaxation times of smaller drops). Increasing pressure and x/d tend to decrease velocities for particular drop sizes near the edge of the flow. This is due to reduced velocity relaxation times with increased ambient pressures for the Reynolds numbers typical of drops in sprays. Drops near the surface are less affected by x/d increases, however, because they tend to be recently formed and have velocities representative of the liquid core which do not change significantly over the range of present observations.[4] A surprising feature of the velocity measurements is that the velocities of small drops, which provide a reasonable upper bound for gas velocities, remain low and relatively uniform across the flow—particularly at atmospheric pressure and small x/d, see Fig. 1. This implies that momentum exchange between the liquid and gas is not very effective. Such behavior is caused by the relatively large velocity relaxation times of large drops which contain most of the liquid momentum.

Mean Phase Velocities

The LHF predictions yielded mass-weighted (Favre)-averaged velocities; therefore, present measurements were used to compute these velocities, similar to Ruff et al.[4] To do this, mean gas velocities were taken to be equal to the mean velocities of 5-μm-diameter drops, which represents the smallest drop size that could be resolved during the holography measurements. Naturally, velocities of drops of this size only represent a potential upper bound for gas velocities because their velocity relaxation times are too large for them to be accurate seeding particles to find gas velocities. However, this effect is not very significant because the large drops contain most of the momentum of the flow. Favre-averaged

velocities were found by summing over the sample volume V, containing N drops, as follows:

$$\tilde{u} = \frac{\sum_{i=1}^{N} \rho_f d_{pi}^3 u_{pi} + (6V/\pi - \sum_{i=1}^{N} d_{pi}^3)\rho_g \bar{u}_g}{\sum_{i=1}^{N} \rho_f d_{pi}^3 + (6V/\pi - \sum_{i=1}^{N} d_{pi}^3)\rho_g} \qquad (1)$$

The evaluation of Eq. (1) only involved the dispersed-flow region where drops had separated from the liquid surface. This underestimates the true Favre-averaged velocity near the liquid surface because contributions from the liquid core and attached ligaments are ignored.

Mean phase velocities for fully-developed and slug flow jet exit conditions are illustrated in Figs. 5-8. Three mean velocities are shown: $\tilde{u}$, found from Eq. (1), $\bar{u}_g$ taken to be the mean time-averaged velocities of drops having a diameter of 5 μm, and the LHF predictions. Two predictions are illustrated for slug flow to indicate potential effects of the boundary layer forming along the walls of the injector passage: one for L/d = 0 where the presence of the boundary layer is ignored, and one allowing for boundary layer development for a length L/d = 5 following Schlichting,[25] see Refs. 1 and 4 for descriptions of the latter predictions. These conditions bound the range of possibilities for the present slug-flow injector.[1]

Except for two conditions which may not be representative (Fig. 6 at 4 atm. and Fig. 8 at 1 atm.) measured values of $\tilde{u}$ generally are significantly larger than $\bar{u}_g$ near the liquid surface with differences between these velocities tending to decrease with increasing radial distance, ambient pressure and x/d. Thus, the dense-spray region near the liquid surface is characterized by large relative velocities that help promote primary and secondary breakup.

The LHF predictions of $\tilde{u}$ are generally not very satisfactory in Figs. 5-8, because present measurements emphasize near-injector conditions where effects of separated flow remain important. Nevertheless, they tend to improve with increasing distance from the jet

exit and ambient pressure, in accord with earlier scaling arguments.[3] The tendency toward better agreement of LHF predictions comes about because large drops generally dominate the momentum content of the flow, similar to behavior at larger liquid volume fractions where the liquid core is present.[2,4] The small drops and the gas all have velocities that are generally much smaller than $\tilde{u}$. In fact, some of the apparent improvement of LHF predictions near the edge of the flow is due to the method of plotting Figs. 5-8 because all velocities become small so that differences between them are not very apparent. Similar to the findings of Ruff et al.[3] at atmospheric pressure, Favre-averaged separated flow factors, $(\tilde{u}_f-\tilde{u}_g)/\tilde{u}_f$, generally have values greater than 0.6 for the range of present measurements.[23] Finally, there is a tendency for LHF predictions to be better for slug than fully-developed flow, aside from the two untypical conditions noted earlier,because drops are generally smaller and have smaller velocity relaxation times for nonturbulent than turbulent primary breakup.[2,5,6]

The extent of the region where the liquid core is observed is another feature of interest seen in Figs. 5-8. In general, the width of this region does not vary appreciably at a fixed x/d as the ambient pressure varies. However, the effect of liquid turbulence on the liquid core is appreciable, with turbulent jet exit conditions causing the surface of the liquid to move over a wider range of radial positions and to penetrate farther from the flow axis at a given streamwise position. This behavior is due to distortion (flapping) of the liquid core by the large scale features of the turbulence, which tends to promote mixing, just like the smaller features of the turbulence tend to promote primary breakup. That these characteristics are dominated by jet exit conditions, rather than aerodynamic effects, is supported by the relatively small effect of ambient pressure on liquid surface properties.

Secondary Breakup

Similar to Ruff at al.,[3] the propensity for secondary breakup in the mixing layer was assessed by computing mass-averaged Weber numbers. Rather than summing over

the entire drop size distribution similar to Ref. 3, however, $\tilde{We}_g$ was found from the measured values of phase velocities and SMD, as follows:

$$\tilde{We}_g = \rho_g(\tilde{u}_f - \tilde{u}_g)^2 SMD/\sigma \qquad (2)$$

This definition has the advantage that maximum values of individual drop Weber numbers

$$We_{gp} = \rho_g d_p(u_p-\bar{u}_g)^2/\sigma \qquad (3)$$

are related quite simply to $\tilde{We}_g$. In particular, $\tilde{u}_f - \tilde{u}_g$ is characteristic of the relative velocities of the largest drops, while maximum drop diameters are 3-4 times larger than the SMD for the universal root normal size distribution function. Therefore, maximum We_{gp} are roughly 3-4 times larger than $\tilde{We}_g$, while more than 50% of the mass of the spray have We_{gp} larger than $\tilde{We}_g$.

Criteria for secondary breakup largely depend on drop Weber numbers for drops having low Ohnesorge numbers and large ρ_f/ρ_g, representative of present test conditions.[3,10] One criterion for water drops accelerated by shock waves is:[10,30,31]

$$We_{gp} > We_{gp}^* = 6.5 - 12 \qquad (4)$$

Slower disturbance rates for water drops falling in air also yield We_{gp}^* on the order of 10 for water drops in air.[3,32] Finally, We_{gp} on the order of unity indicates the onset of conditions where drops deform from a spherical shape after shock wave disturbances at low Ohnesorge numbers and large ρ_f/ρ_g.[31]

Distributions of $\tilde{We}_g$ are plotted as a function of r/x, with ambient pressure and jet exit conditions as parameters, in Figs. 9 and 10. Most of the drops at the liquid surface exceed the criterion for deformation but drops near the edge of the flow are well below this criterion. Direct observations of drop shapes from hologram reconstructions agree with behavior anticipated from the deformation criterion: deformed drops were quite prevalent near the liquid surface while drops near the edge of the flow were generally spherical. This behavior contributes to decreasing values of e_p with radial distance, approaching unity near the edge of the flow, although the presence of irregular ligament-like drops contributes to large values of e_p near the surface as well.

Results illustrated in Figs. 9 and 10 also show significant potential for near-limit secondary breakup near the liquid surface for some conditions. In particular, all conditions at atmospheric pressure, as well as all conditions at x/d = 25, involve significant fractions of drops that are unstable to secondary breakup near the liquid surface. However, drops near the edge of the flow generally have We_{gp} that are lower than the breakup criterion of Eq. (4). This supports the hypothesis that reduced SMD with increasing radial distance in Figs. 1-4 is caused by secondary breakup.

Effects of jet exit conditions also can be seen from the results illustrated in Figs. 9 and 10. Turbulent primary breakup generally yields larger drops than nonturbulent primary breakup, while the velocities of the largest drops near the liquid surface tend to approach liquid core velocities which are essentially the same in both cases, see Figs. 5-8. Thus We_g are largest near the liquid surface, with greatest propensity for secondary breakup for fully-developed jet exit conditions (aside from the untypical behavior at x/d = 25 and 4 atm., mentioned earlier). The tendency for processes of primary and secondary breakup to merge at elevated pressures for fully developed flow also is evident from the corresponding reduction of We_g at the liquid surface that is particularly noticeable for fully-developed flow. This effect will be discussed in greater detail in the next section.

Primary Breakup

Turbulent Primary Breakup. Recent studies have yielded correlations of drop sizes after turbulent and nonturbulent primary breakup.[5,6] These results were developed from measurements for a variety of liquids injected into air at atmospheric pressure; therefore, it is of interest to evaluate them for potential effects of varying ambient gas density using the present measurements. This will be done in the following, beginning with turbulent breakup.

Wu et al.[6] develop an expression for the SMD after turbulent primary breakup, ignoring aerodynamic effects. The correlation is based on the projection of liquid elements from the surface by radial velocity fluctuations, relating element size and velocity to the

turbulence spectrum within the inertial region. The size of elements leaving the surface is taken to be the largest turbulent scale that can complete its growth at a particular point, with the length of the element determined by Rayleigh breakup considerations. The maximum size produced by this mechanism is taken to be proportional to the integral scale. For second wind-induced and atomization breakup conditions and Oh < 0.006, the resulting expression for the SMD after primary breakup is:

$$SMD/\Lambda = 0.69(x/(\Lambda\, We_{f\Lambda}^{0.54}))^{0.57} \qquad (5)$$

where Λ is the crosstream integral scale of the flow. Notably, this expression only involves properties of the liquid phase because aerodynamic effects have been ignored.

Present measurements of SMD along the liquid surface for fully developed flow, along with the predictions of Eq. (5), are summarized in the upper part of Table 1. The agreement between predictions and measurements at atmospheric pressure, corresponding to the range of ρ_f/ρ_g used to develop Eq. (5), is excellent. However, the predictions do not anticipate the substantial reduction of drop sizes after primary breakup as the ambient pressure increases. The progressive reduction of SMD with increasing pressure clearly suggests the presence of aerodynamic effects that are not considered in the phenomenological theory used to develop Eq. (5).

A curious feature of the failure of Eq. (5) to correlate SMD after primary breakup at pressures of 2 and 4 atm. is that these expressions were developed over a wide range of We_{gd}, with resulting wide variations of aerodynamic forces; thus, the problem largely appears to be related to the variation of density ratio. Insight concerning this behavior can be obtained by considering the residence times of a typical ligament breaking away from the surface and secondary breakup times for liquid elements of comparable size, using the integral-scale limit to simplify the discussion. Taking the length of the ligament at the time it separates to be $e_p\Lambda$, and the velocity of liquid flow into the ligament to be $\bar{v}'_f$, the characteristic residence time of the ligament during its formation is

$$\tau_r = C_r e_p \Lambda/\bar{v}'_f \qquad (6)$$

where C_r is a constant on the order of unity. The mode of aerodynamic breakup of the ligaments is not known; fortunately, breakup times are relatively independent of mode.[33,34] Adopting the correlation of Ranger and Nicholls[34] for shear breakup, and taking the characteristic ligament dimension to be Λ, yields the characteristic aerodynamic breakup time of the ligament, as follows:

$$\tau_b = 5C_a\Lambda(\rho_f/\rho_g)^{1/2}/u_o \qquad (7)$$

where C_a is an empirical constant of order unity to allow for shape differences between drops and ligaments, and the relative velocity has been taken to be u_o, which is representative of velocity differences between ligaments extending from the surface and the local gas velocity. Solving for the ratio of Eqs. (7) and (6) then yields:

$$\tau_b/\tau_r = (5\,C_a/C_re_p)(\rho_f/\rho_g)^{1/2}(\bar{v}'_f/u_o) \qquad (8)$$

Noting that turbulence properties within the liquid do not change appreciably with position, $\bar{v}'_f/u_o$ is simply the intensity of radial velocity fluctuations at the jet exit which is a constant for the fully-developed turbulent pipe flow. Thus, Eq. (8) indicates that the relative importance of aerodynamic breakup effects only depends on the density ratio, in agreement with the present measurements and the observations of Ref. 6.

Equation (8) also suggests that the transition from turbulent breakup due to liquid turbulence alone, to conditions where aerodynamic effects also are important, occurs at pressures on the order of atmospheric pressure. For example, e_p generally is in the range 2-4 at the liquid surface for turbulent breakup, see Ref. 2 and Figs. 1-4; therefore, it is reasonable to take the first factor on the right hand side of Eq. (8) to be of order unity. The radial turbulence intensity, $\bar{v}'_f/u_o$, for fully-developed turbulent pipe flow generally is in the range 0.03-0.05.[25,26] Then, at ambient pressures of 1, 2 and 4 atm. for water and air: ρ_f/ρ_g = 846, 423 and 212, yielding τ_b/τ_r = 1.2, 0.8 and 0.6 (taking the radial turbulence intensity to be 0.04). These results suggest that aerodynamic effects begin to become important at ambient pressures on the order of 1 atm., and that this transition is largely a function of density ratio, which agrees with the SMD data of Table 1. More study is

needed to refine these order of magnitude considerations, however, present findings clearly show that use of Eq. (5) to find SMD for ρ_f/ρ_g less than the range considered in Ref. 6 is not appropriate.

Nonturbulent Primary Breakup. Wu et al.[5] have developed an expression giving the SMD after primary breakup for slug flow at the jet exit. This expression is based on aerodynamic stripping of boundary layers formed on the windward side of waves along the liquid surface. For liquid Reynolds numbers based on distance from the jet exit greater than 2×10^6, which corresponds to present conditions, a fully-developed breakup regime is entered where the SMD after primary breakup is relatively independent of distance from the jet exit. Within this regime, the correlation for SMD along the surface is

$$We_{g_{SMD}} = 16(We_{gd}/Re_d^{1/2})^{0.82} \qquad (9)$$

where the Weber and Reynolds numbers are based on mean jet exit velocity, assuming small variations of velocity within the liquid core and small gas velocities along the surface — the latter generally corresponding to present observations and those of Ref. 3.

Present measurements of SMD along the liquid surface for slug flow, along with the predictions of Eq. (9), are summarized in the lower part of Table 1. In this case, measured SMD are affected only slightly with increasing pressure and distance along the surface — trends that are consistent with the predictions of Eq. (9) as well as effects of distance within the fully-developed nonturbulent breakup regime observed in Ref. 5. However, the predictions overestimate the measured SMD by roughly a factor of two which is larger than the scatter of the data used to develop Eq. (9).[5] Specific reasons for this deficiency are not known, however, processes of nonturbulent breakup are notoriously sensitive to small disturbances within the injector so that differences in the injector passage design may be a factor. In any event, unlike turbulent primary breakup, present observations of the trends of nonturbulent primary breakup with variations of ρ_f/ρ_g appear to be consistent with the observations of Ref. 5. It should be noted, however, that parameters controlling secondary breakup (see Eqs. (4) and (7)) respond more rapidly to

increased gas densities than those controlling nonturbulent primary breakup (see Eq. (9)). Thus, higher pressures than considered here may involve merging of primary and secondary breakup, similar to present observations of turbulent primary breakup: this possibility should be explored.

Liquid Volume Fractions and Fluxes

Measured and predicted distributions of liquid volume fractions and fluxes are illustrated in Figs. 11 and 12 for both fully-developed and slug flow. Measurements of liquid volume fractions include both present findings, using holography, and those of Tseng et al.[4] using gamma-ray absorption for the same flows. LHF predictions for slug flow are shown at the limits L/d = 0 and 5 as before.

The measurements of liquid volume fractions by gamma-ray absorption are larger than those found by holography in the region where they overlap in Figs. 11 and 12. This region is associated with the presence of the liquid core; therefore, the main reason for the differences is that the holography measurements do not include the significant contributions of the liquid core and the attached ligaments protruding from its surface. Thus, the discrepancy largely reflects reduced liquid volume fractions anticipated when moving from a liquid region to a fully-dispersed multiphase flow region. Liquid volume fractions in the dispersed-flow region don't vary appreciably with increasing pressure and distance from the jet exit, with maximum values remaining at roughly 0.1% where effects of collisions are not very significant.[7] Distributions of liquid volume fractions generally are broader, with higher liquid volume fractions in the dispersed-flow region, for fully-developed than slug flow, reflecting the faster mixing rates of the turbulent breakup process at the liquid surface. The LHF predictions of liquid volume fractions are reasonably good up to the outer edge of the region where the liquid surface is present, which involves liquid volume fractions greater than 0.1. Thereafter, the LHF predictions only bear a crude resemblance to measured properties in the dispersed flow region: in part because the measurements

ignore the presence of the liquid surface and attached ligaments, as noted earlier; and in part, because of the significant effects of separated flow in the dispersed-flow region.

The liquid flux measurements and predictions illustrated in Figs. 11 and 12 are qualitatively similar to the liquid volume fractions. Fluxes for fully-developed flow generally are higher than for slug flow due to the faster rates of turbulent primary breakup (except for the untypical behavior for fully-developed flow at x/d = 25 and 4 atm., Fig. 12, noted earlier). Measurements of liquid fluxes do not account for contributions from the liquid core and its attached ligaments and underestimate fluxes in the region of the liquid surface as a result. Accounting for this, the LHF predictions are in qualitative agreement with the measurements, although consideration of separated-flow effects is needed to develop a quantitatively accurate methodology.

Conclusions

The near-injector region of pressure-atomized water sprays (9.5 mm initial diameter) was investigated at ambient air densities corresponding to ambient pressures of 1-4 atm, considering atomization breakup conditions for both fully-developed and slug flow at the jet exit. The main conclusions of the study are as follows:

1. Similar to earlier observations at atmospheric pressure,[2,3,5,6] drop sizes at each point satisfied Simmons' universal root-normal drop size distribution,[29] with an MMD/SMD ratio of 1.2. Thus, the entire drop size distribution can be characterized by a single moment, like the SMD.
2. Drop sizes after primary breakup generally were larger for fully-developed than for slug flow jet exit conditions, highlighting the importance of injector passage disturbances on spray properties. The correlation of Wu et al.[6] for SMD after turbulent primary breakup was in excellent agreement with present measurements at atmospheric pressure — the same ambient pressure used to develop the correlation. However, the correlation did not represent measured trends of reduced SMD after primary breakup as the ambient pressure increased. This suggests the presence of

aerodynamic effects, or merging of primary and secondary breakup, that were not considered when the correlation was developed. The difficulty is largely associated with an effect of density ratio; therefore, the correlation of Ref. 6 should only be used for $\rho_f/\rho_g > 580$, which was the range originally used to define it.

3. Measured trends of effects of ambient pressure and distance from the injector on SMD after nonturbulent primary breakup were in good agreement with the correlation developed by Wu et al.[5] which includes consideration of aerodynamic effects, although present values were 50% smaller than predicted. This implies relatively small effects of ambient pressure on drop sizes after nonturbulent primary breakup so that merging of primary and secondary breakup at higher pressures may still be a factor, due to the larger response of secondary breakup processes to changes in gas density. The size discrepancy and the potential merging effect require additional study before the correlation of Ref. 5 can be applied confidently to high-pressure sprays.

4. Spray Weber numbers after primary breakup imply that a significant fraction of the drops will undergo near-limit secondary breakup (particularly at low pressures and far from the injector) while most of the drops exceed conditions where they deform from a spherical shape even if they do not undergo secondary breakup. Drops near the edge of the flow, however, have Weber numbers well below values associated with secondary breakup and deformation.

5. Similar to earlie observations at atmospheric pressure,[2] liquid volume fractions in the dispersed-flow region beyond the liquid surface were relatively low, less than 0.1%. Thus, the flow in this region corresponds to a dilute spray, aside from added complications of secondary breakup and irregular or deformed drops.

6. Favre-averaged separated flow factors, $(\tilde{u}_f-\tilde{u}_g)/\tilde{u}_f$, were generally greater than 0.6 throughout the dispersed flow region, implying significant effects of separated flow and surprisingly low gas velocities even near the liquid surface. These effects

suggest that turbulence generation by drops,[7,8] is a major feature of the dispersed flow region.

7. Predictions based on the LHF approximation were only qualitatively useful due to significant separated-flow effects in the dispersed-flow region. Performance of the LHF approach, however, tended to improve with increasing liquid volume fractions, ambient pressure and distance from the injector. Pending resolution of existing uncertainties about the properties of primary and secondary breakup, the LHF approach offers a useful treatment of sprays in the atomization breakup regime at high ambient pressures where drop sizes are likely to be small. It should be recognized, however, that the LHF approach will overestimate the rate of development of the flow by a degree that cannot be quantified until uncertainties about breakup and other properties of the near-injector region are resolved.

Acknowledgements

This research was sponsored by the Office of Naval Research Grant No. N00014-89-J-1199 under the technical management of G. D. Roy; initial apparatus development was sponsored by the Air Force Office of Scientific Research, Grant No. 89-0516 with J. M. Tishkoff serving as technical manager. The U.S. Government is authorized to reproduce and distribute copies for governmental purposes notwithstanding any copyright notation thereon.

References

[1]Ruff, G.A., Sagar, A.D. and Faeth, G.M., "Structure of the Near-Injector Region of Pressure-Atomized Sprays," *AIAA Journal*, Vol. 27, No. 7, July 1989, pp. 901-908.

[2]Ruff, G.A., Bernal, L.P. and Faeth, G.M., "Structure of the Near-Injector Region of Non-Evaporating Pressure-Atomized Sprays," *Journal of Propulsion and Power*, Vol. 7, No. 2, March-April 1991, pp. 221-230.

[3]Ruff, G.A., Wu, P.-K., Bernal, L.P. and Faeth, G.M., "Continuous- and Dispersed-Phase Structure of Dense Nonevaporating Pressure-Atomized Sprays," *Journal of Propulsion and Power*, Vol. 8, No. 2, March-April 1992, pp. 280-289.

[4]Tseng, L.-K., Ruff, G.A. and Faeth, G.M., "Effects of Gas Density on the Structure of Liquid Jets in Still Gases," *AIAA Journal*, in press.

[5]Wu, P.-K., Ruff, G.A. and Faeth, G.M., "Primary Breakup in Liquid/Gas Mixing Layers," *Atomization and Sprays*, Vol. 1, No. 4, October-December 1991, pp. 421-440.

[6]Wu, P.-K., Tseng, L.-K., and Faeth, G.M., "Primary Breakup of Turbulent Liquids," AIAA Paper No. 92-0462, 1992.

[7]Faeth, G.M., "Mixing, Transport and Combustion in Sprays," *Progress in Energy and Combustion Science*, Vol.13, No. 3, 1987, pp. 293-345.

[8]Faeth, G.M., "Structure and Atomization Properties of Dense Turbulent Sprays," *Twenty-Third Symposium (International) on Combustion*, The Combustion Institute, Pittsburgh, 1990, pp. 1345-1352.

[9]Chigier, N.A., "The Physics at Atomization," *Proceedings of the Fifth International Conference on Liquid Atomization and Spray Systems*, NIST SP-813, National Institute of Standards and Technology, Washington, July 1991, pp. 1-15.

[10]Clift, R., Grace, J.R. and Weber, M.E., *Bubbles, Drops and Particles*, Academic Press, New York, 1978, p. 346.

[11]Reitz, R.D. and Bracco, F.V., "Mechanism of Atomization of a Liquid Jet," *The Physics of Fluids*, Vol. 25, No. 10, October 1982, pp. 1730-1742.

[12]Reitz, R.D., "Atomization and Other Breakup Regimes of a Liquid Jet," Ph.D. Dissertation No. 1375-T, Princeton University, Princeton, New Jersey, 1978.

[13]Miesse, C.C., "Correlation of Experimental Data on the Disintegration of Liquid Jets," *Industrial and Engineering Chemistry*, Vol. 47, No. 9, September 1955, pp. 1690-1697.

[14]Ranz, W.E., "Some Experiments on Orifice Sprays," *Canadian Journal of Chemical Engineering*, Vol. 36, August 1958, pp. 175-181.

[15]Phinney, R.E., "The Breakup of a Turbulent Jet in a Gaseous Atmosphere," *Journal of Fluid Mechanics*, Vol. 6, Part 4, October 1973, pp. 689-701.

[16]Hoyt, J.W. and Taylor, J.J., "Waves on Water Jets," *Journal of Fluid Mechanics*, Vol. 88, Part 1, November 1977, pp. 119-127.

[17]Hoyt, J.W. and Taylor, J.J., "Turbulence Structure in a Water Jet Discharging in Air," *The Physics of Fluids*, Vol. 20, No. 10, Part II, October 1977, pp. S253-S257.

[18]Hoyt, J.W. and Taylor, J.J., "Effect of Nozzle Boundary Layer on Water Jets Discharging in Air," *Jets and Cavities* (J.H. Kim, O. Furuya and B.R. Parkin, ed.) ASME-FED, Vol. 31, ASME, New York, 1985, pp. 93-100.

[19]Hiroyasu, H., Shimizu, M., and Arai, M., "The Breakup of a High Speed Jet in a High Pressure Gaseous Environment," Univ. Of Wisconsin, Madison, ICLASS-82, 1982.

[20]Chehroudi, B., Onuma, Y., Chen, S.-H. and Bracco, F. V., "On the Intact Core of Full Cone Sprays," SAE Paper No. 850126, 1985.

[21]Wu, K.-J., Su, C.-C., Steinberger, R.L., Santavicca, D.A. and Bracco, F.V., "Measurements of the Spray Angle of Atomizing Jets," *Journal of Fluids Engineering*, Vol 105, No. 4, December 1983, pp. 406-415.

[22]Wu, K.-J., Coghe, A., Santavicca, D.A. and Bracco, F.V., "LDV Measurements of Drop Velocity in Diesel-Type Sprays," *AIAA Journal*, Vol. 22, No. 9, September 1984, pp. 1263-1270.

[23]Tseng, L.-K., "Near-Injector Structure of Non-Evaporating Pressure-Atomized Sprays at Various Ambient Densities," Ph.D. Thesis, The University of Michigan, Ann Arbor, Michigan, 1991.

[24]Smith, R.H. and Wang, C.-T., "Contracting Cones Giving Uniform Throat Speeds," *Journal of Aerospace Sciences*, Vol. 11, October 1944, pp. 356-360.

[25]Schlichting, H., *Boundary Layer Theory*, 7th ed., McGraw-Hill, New York, 1979, p. 599.

[26]Hinze, J.O., *Turbulence*, 2nd ed., McGraw-Hill, New York, 1975, pp. 427 and 724-734.

[27]Lockwood, F.C. and Naguib, A.S., "The Prediction of Fluctuations in the Properties of Free, Round-Jet Turbulent Diffusion Flames," *Combustion and Flame*, Vol. 24, No. 1, February 1975, pp. 109-124.

[28]Bilger, R.W., "Turbulent Jet Diffusion Flames," *Progress in Energy and Combustion Science*, Vol. 1, No. 2, 1976, pp. 87-109.

[29]Simmons, H.C., "The Correlation of Drop Size Distributions in Fuel Nozzle Sprays," *Journal of Engineering for Power*, Vol. 99, No. 3, July 1977, pp. 309-319.

[30]Krzeczkowski, S.A., "Measurement of Liquid Droplet Disintegration Mechanisms," *International Journal of Multiphase Flow*, Vol. 6, No. 2, 1980, pp. 227-239.

[31]Hsiang, L.-P. and Faeth, G.M., "Secondary Drop Breakup in the Deformation Regime," AIAA Paper No. 92-0110, 1992.

[32]Pruppacker, H.R. and Klett, J.D., *Microphysics of Clouds and Precipitation*, D. Reidel Publishing Co., Boston, 1978, pp. 123-456.

[33]Borisov, A.A., Gel'fand, B.E., Natanzon, M.S. and Kossov, O.M., "Droplet Breakup Regimes and Criteria for Their Existence," *Inzhenerno-Fizicheskii Zhurnal*, Vol. 40, January 1981, pp. 64-70.

[34]Ranger, A.A. and Nicholls, J.A., "Aerodynamic Shattering of Liquid Drops," *AIAA Journal*, Vol 7, No. 2, February 1969, pp. 285-290.

Table 1 Measured and predicted SMD (μm) along liquid surface[a]

x/d	Pressure (atm.)	1		2		4	
		Meas.	Pred.	Meas.	Pred.	Meas.	Pred.
Fully-Developed Flow:[b]							
6		343	374	133	374	70	374
25		940	968	343	968	157	968
Slug Flow:[c]							
6		117	241	100	213	98	188
25		143[d]	215[d]	140	213	138	188

[a]Momentum averaged injection velocity (m/s) of 40[b], 48[c] and 56[d].

List of Figures

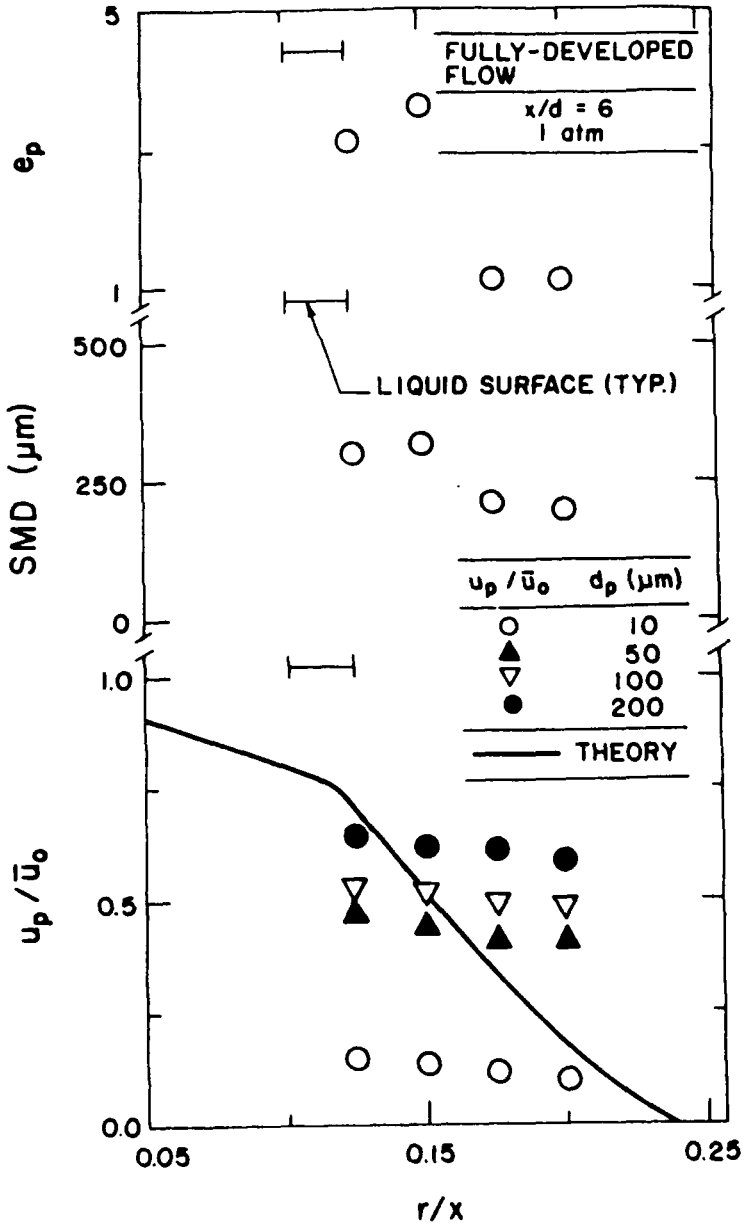
FULLY-DEVELOPED FLOW
x/d = 6
1 atm
LIQUID SURFACE (TYP.)
$u_p / \bar{u}_o$ d_p (μm)
10
50
100
200
THEORY
e_p
SMD (μm)
$u_p / \bar{u}_o$
r/x
5
1
500
250
0
1.0
0.5
0.0
0.05
0.15
0.25

FIG. 1

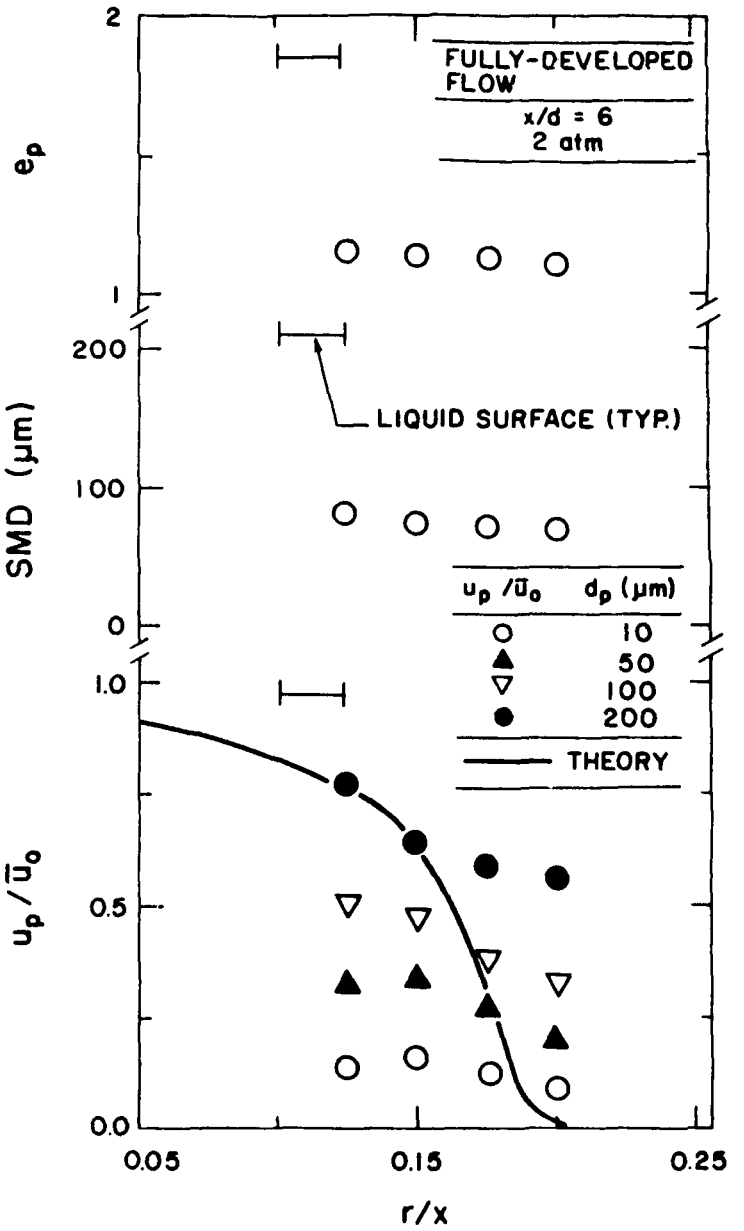
FULLY-DEVELOPED FLOW
x/d = 6
2 atm
LIQUID SURFACE (TYP.)
$u_p / \bar{u}_o$ d_p (μm)
10
50
100
200
THEORY
e_p
SMD (μm)
$u_p / \bar{u}_o$
r/x
2
1
200
100
0
1.0
0.5
0.0
0.05
0.15
0.25

FIG 2

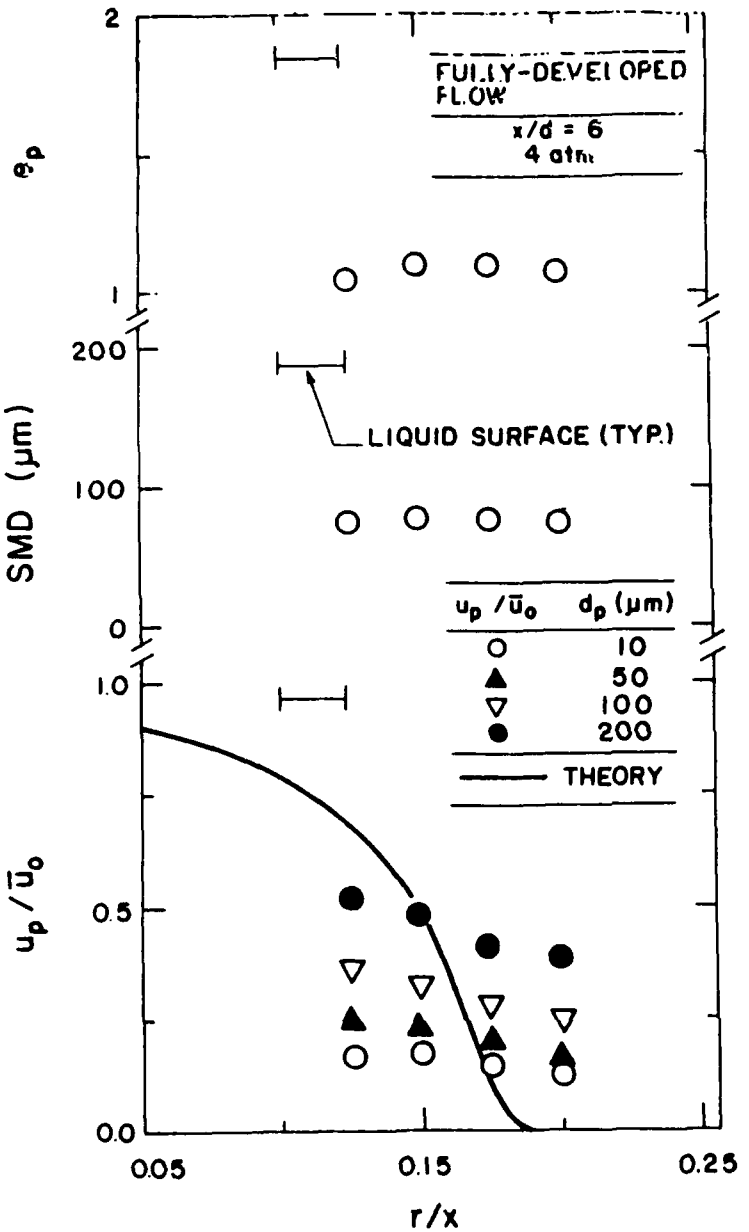
FULLY-DEVELOPED FLOW
x/d = 6
4 atm
LIQUID SURFACE (TYP.)
$u_p/\bar{u}_o$ d_p (μm)
10
50
100
200
THEORY
e_p
SMD (μm)
$u_p/\bar{u}_o$
r/x
2
1
200
100
0
1.0
0.5
0.0
0.05
0.15
0.25

FIG. 3

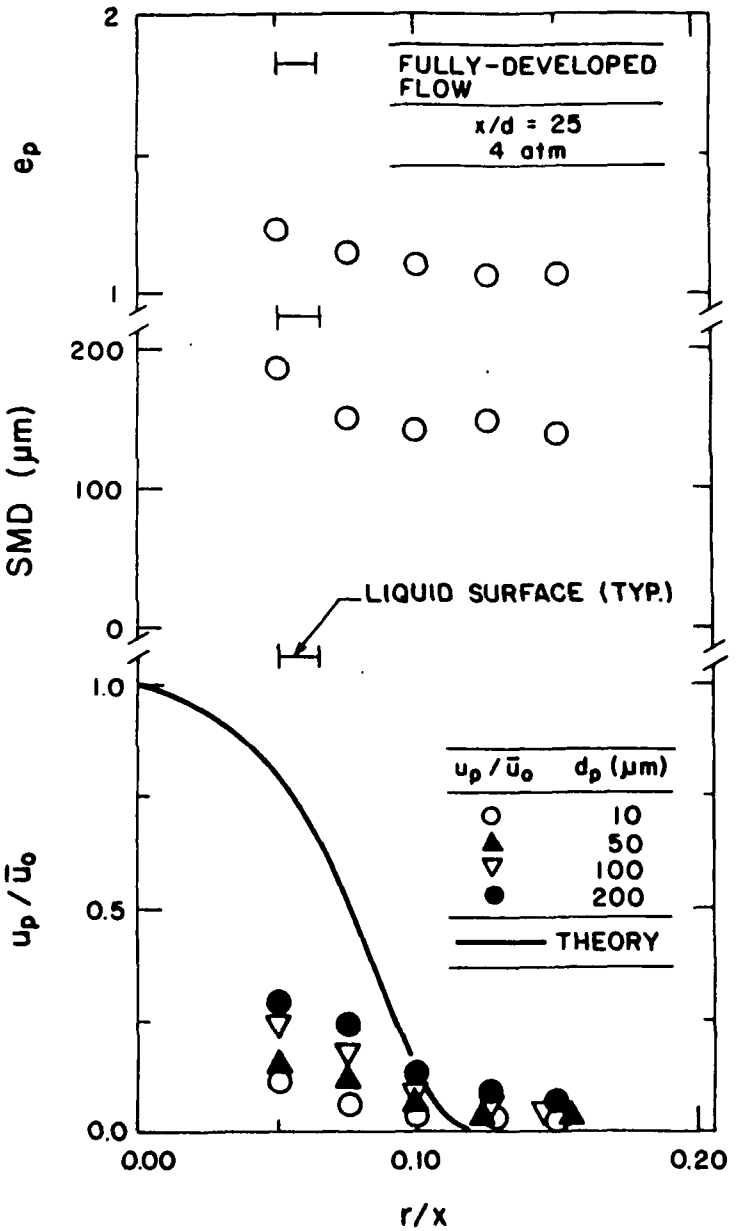
FULLY-DEVELOPED FLOW
x/d = 25
4 atm
LIQUID SURFACE (TYP.)
$u_p/\bar{u}_o$ d_p (μm)
10
50
100
200
THEORY
e_p
SMD (μm)
$u_p/\bar{u}_o$
r/x
2
1
200
100
0
1.0
0.5
0.0
0.00
0.10
0.20

FIG. 4

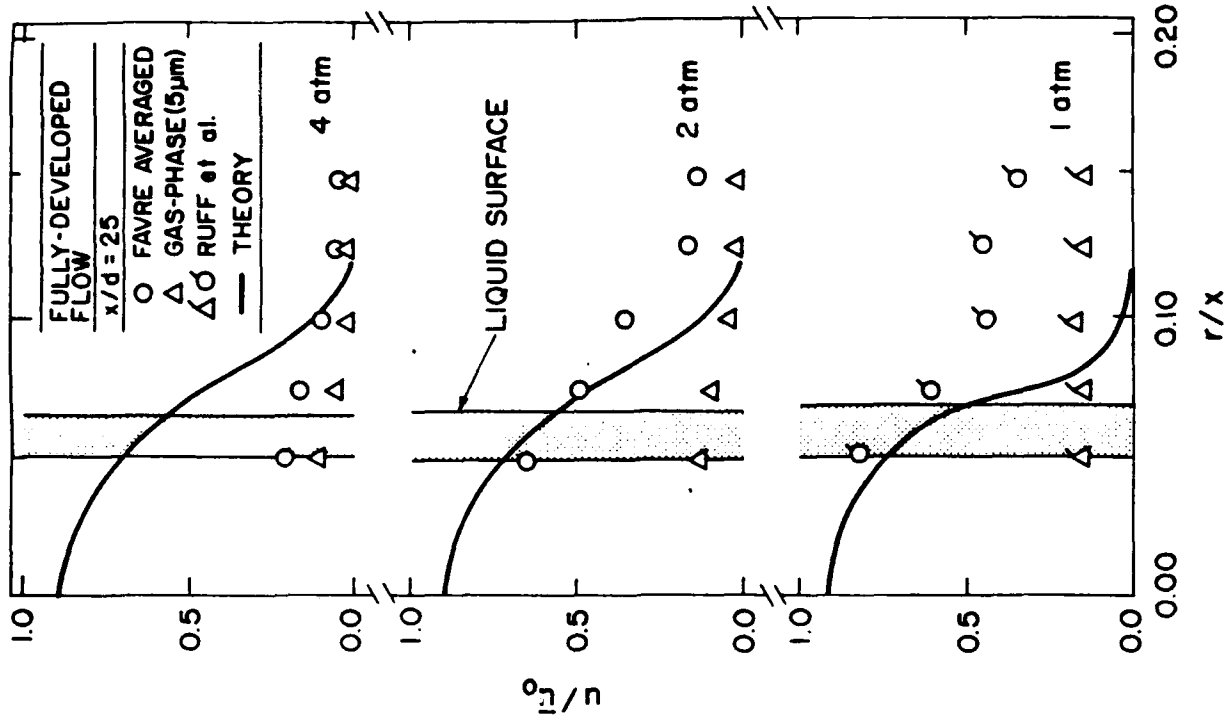
FULLY-DEVELOPED FLOW
x/d = 25
FAVRE AVERAGED
GAS-PHASE (5μm)
RUFF et al.
THEORY
4 atm
2 atm
1 atm
LIQUID SURFACE
u/ū₀
r/x
0.0
0.5
1.0
0.00
0.10
0.20

FIG. 6

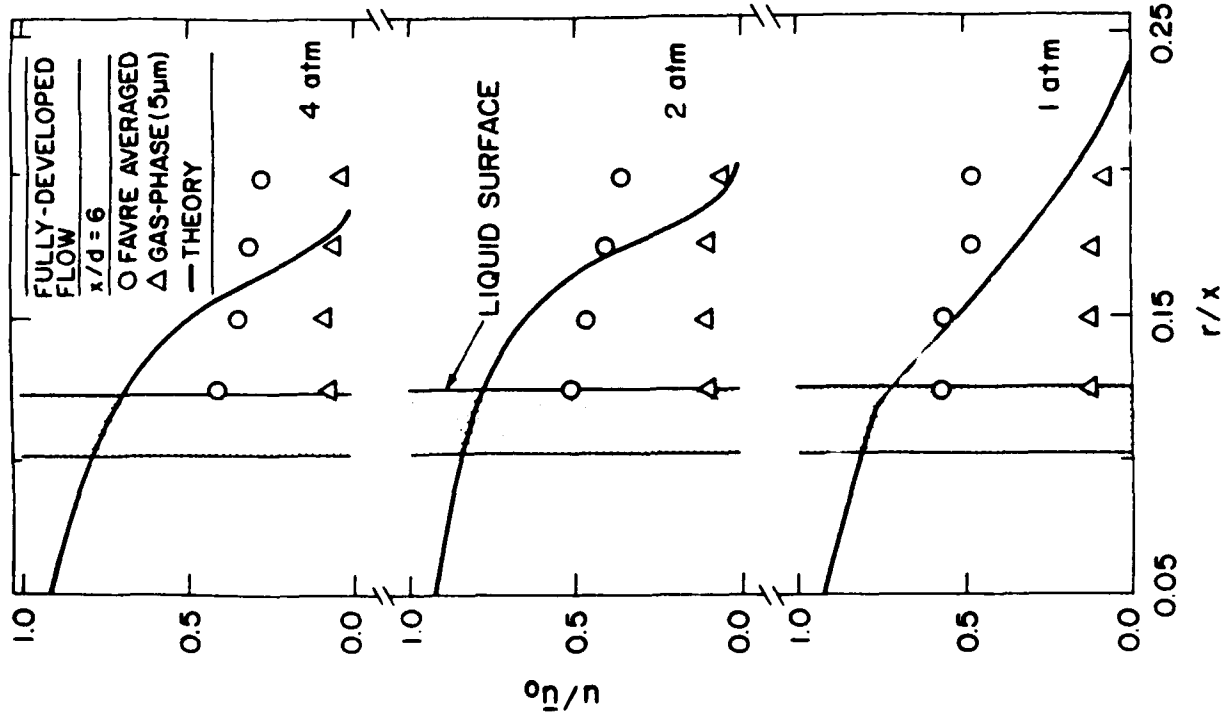
FULLY-DEVELOPED FLOW
x/d = 6
FAVRE AVERAGED
GAS-PHASE (5μm)
THEORY
4 atm
2 atm
1 atm
LIQUID SURFACE
u/ū₀
r/x
0.0
0.5
1.0
0.05
0.15
0.25

FIG. 5

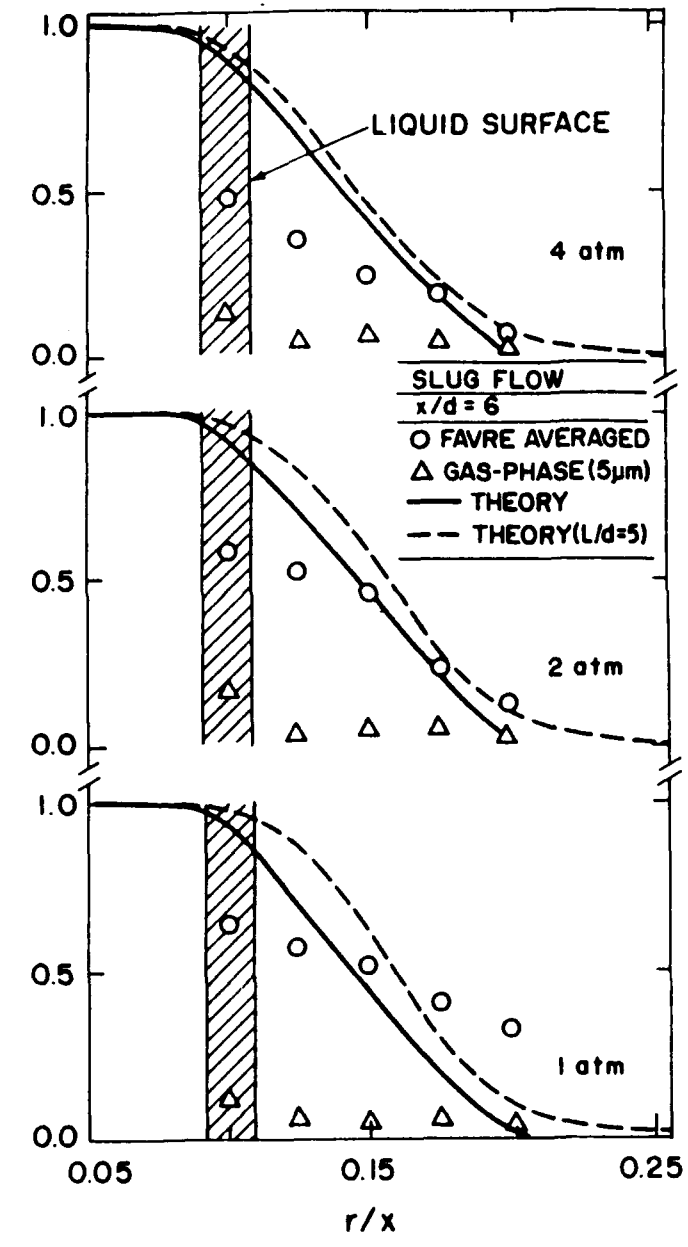
1.0
0.5
0.0
LIQUID SURFACE
4 atm
SLUG FLOW
x/d = 6
O FAVRE AVERAGED
Δ GAS-PHASE(5μm)
THEORY
THEORY(L/d=5)
2 atm
1 atm
u/ū₀
0.05
0.15
0.25
r/x

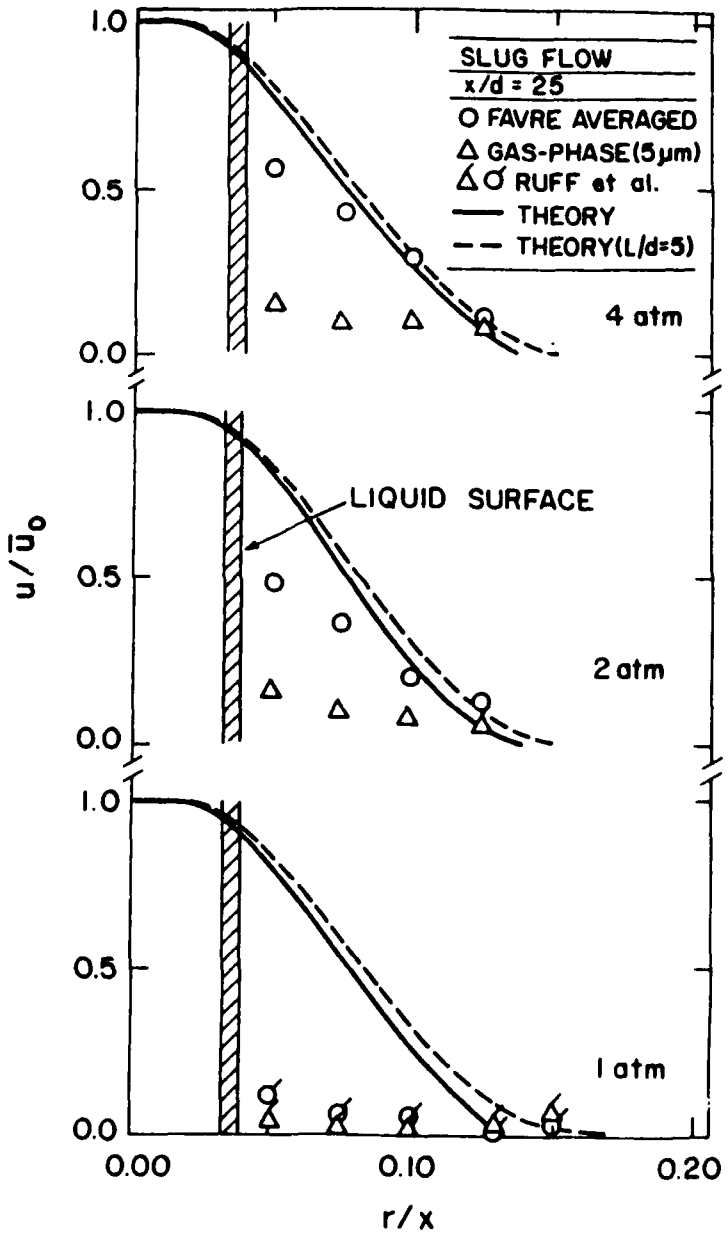
1.0
0.5
0.0
SLUG FLOW
x/d = 25
O FAVRE AVERAGED
Δ GAS-PHASE(5μm)
Δσ RUFF et al.
THEORY
THEORY(L/d=5)
4 atm
LIQUID SURFACE
2 atm
1 atm
u/ū₀
0.00
0.10
0.20
r/x

FIG. 7

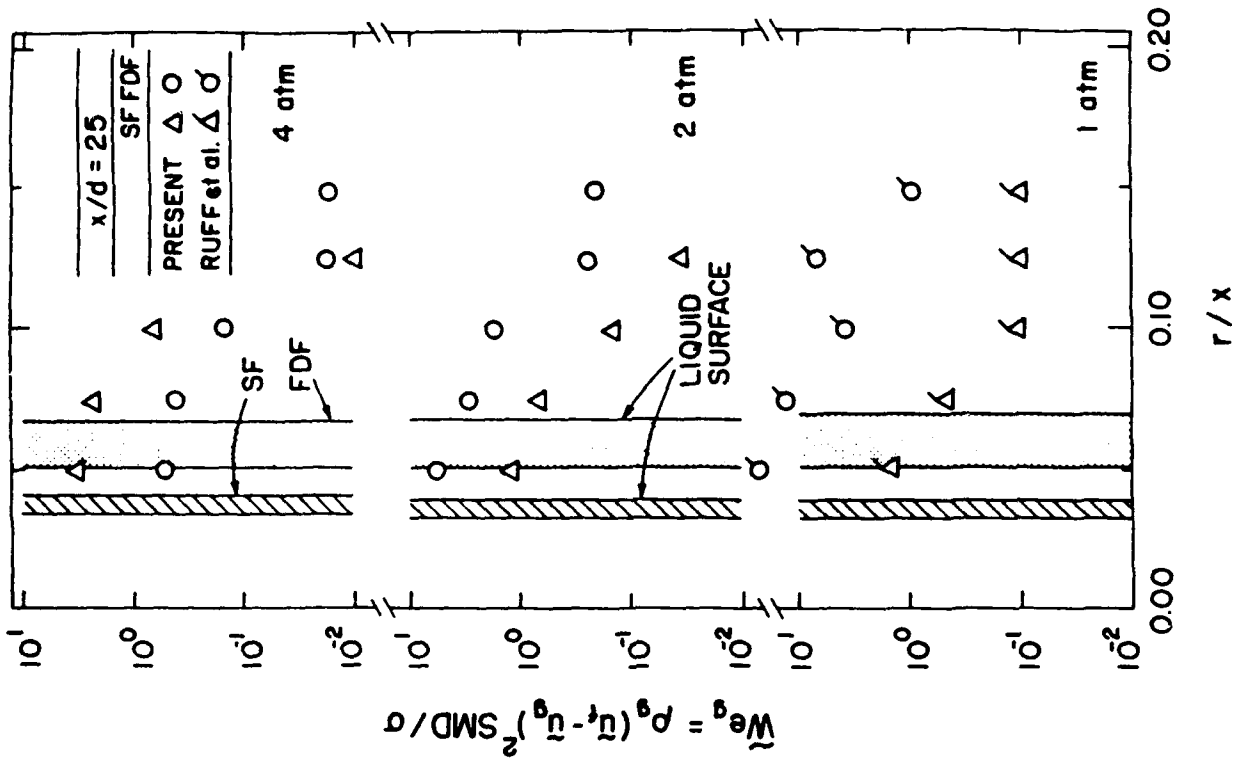
x/d = 25
SF FDF
PRESENT Δ O
RUFF et al. Δ σ
4 atm
2 atm
1 atm
SF
FDF
LIQUID SURFACE
0.20
0.10
0.00
r / x
10^{1}
10^{0}
10^{-1}
10^{-2}
$\tilde{We}_g = \rho_g(\tilde{u}_f - \tilde{u}_g)^2 SMD/\sigma$

FIG. 10

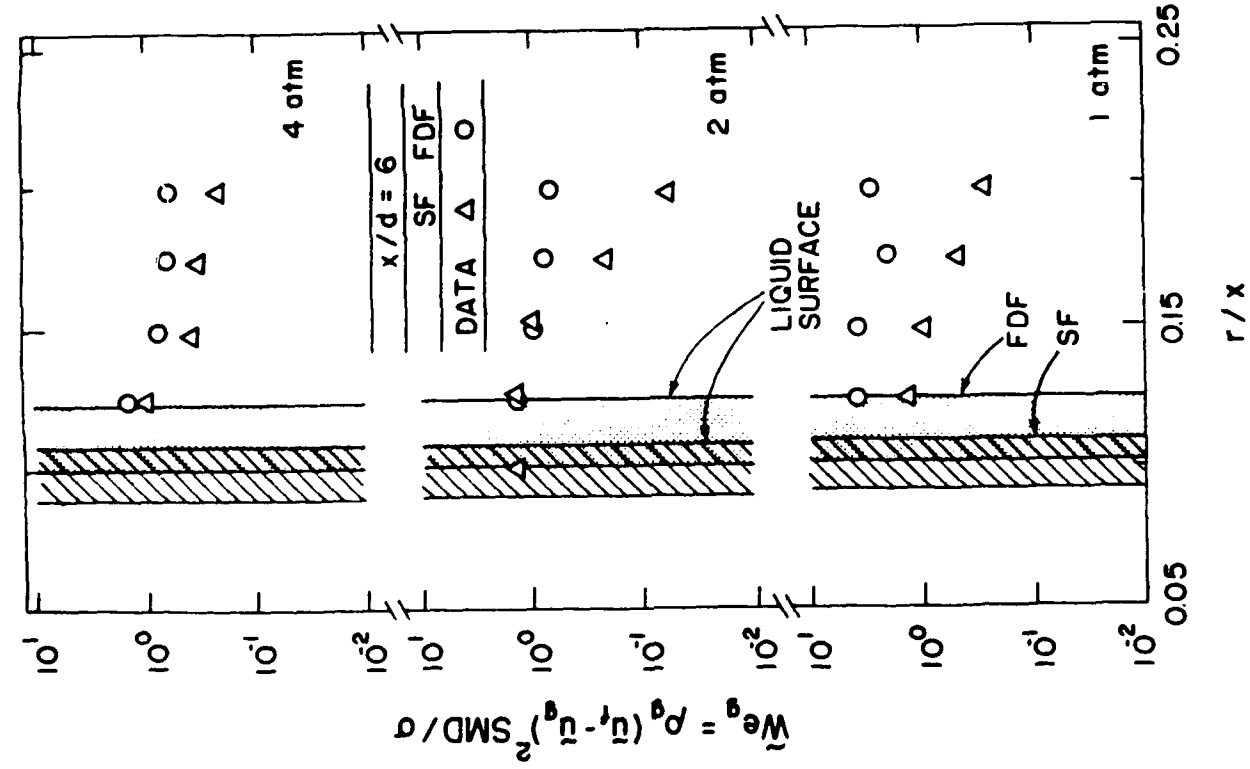
4 atm
2 atm
1 atm
x/d = 6
SF FDF
DATA Δ O
LIQUID SURFACE
FDF
SF
0.25
0.15
0.05
r / x
10^{1}
10^{0}
10^{-1}
10^{-2}
$\tilde{We}_g = \rho_g(\tilde{u}_f - \tilde{u}_g)^2 SMD/\sigma$

FIG. 9

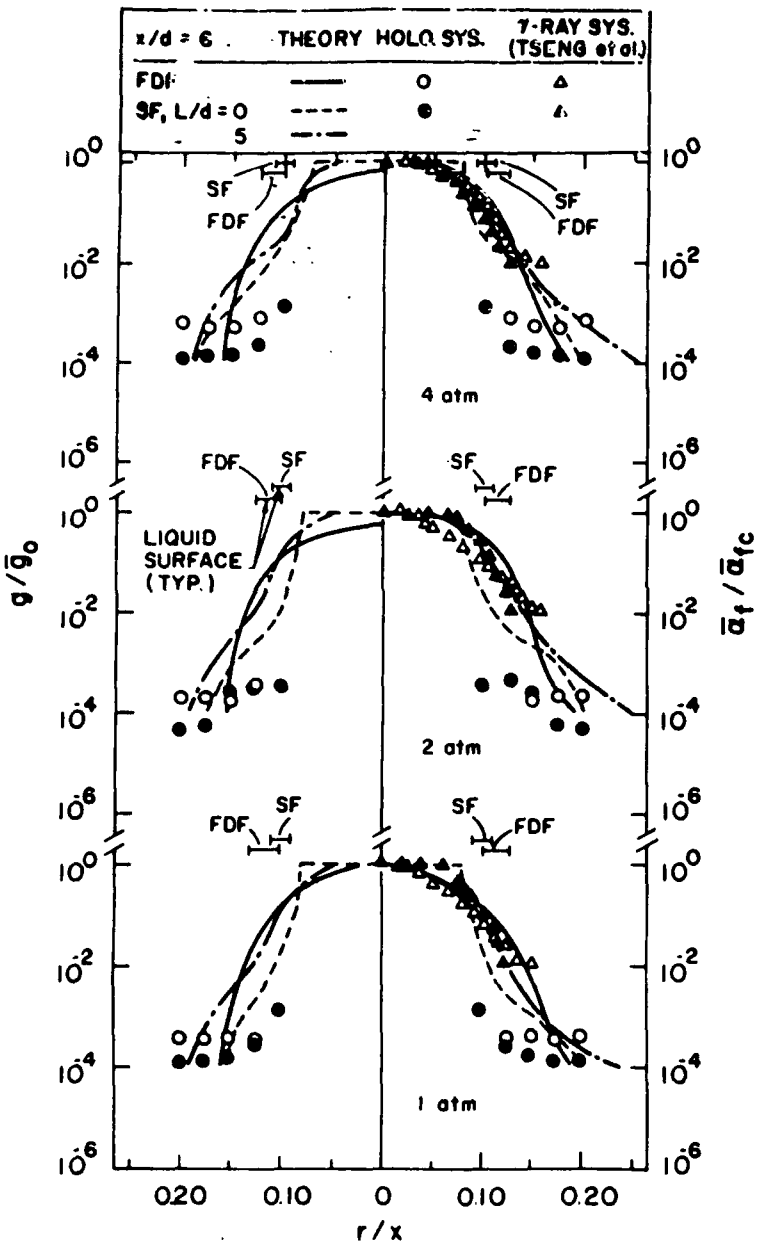
x/d = 6
THEORY HOLO SYS.
7-RAY SYS. (TSENG et al.)
FDF
SF, L/d = 0
5
SF
FDF
4 atm
2 atm
1 atm
LIQUID SURFACE (TYP.)
g/ḡo
ᾱf / ᾱfc
0.20
0.10
0
r/x

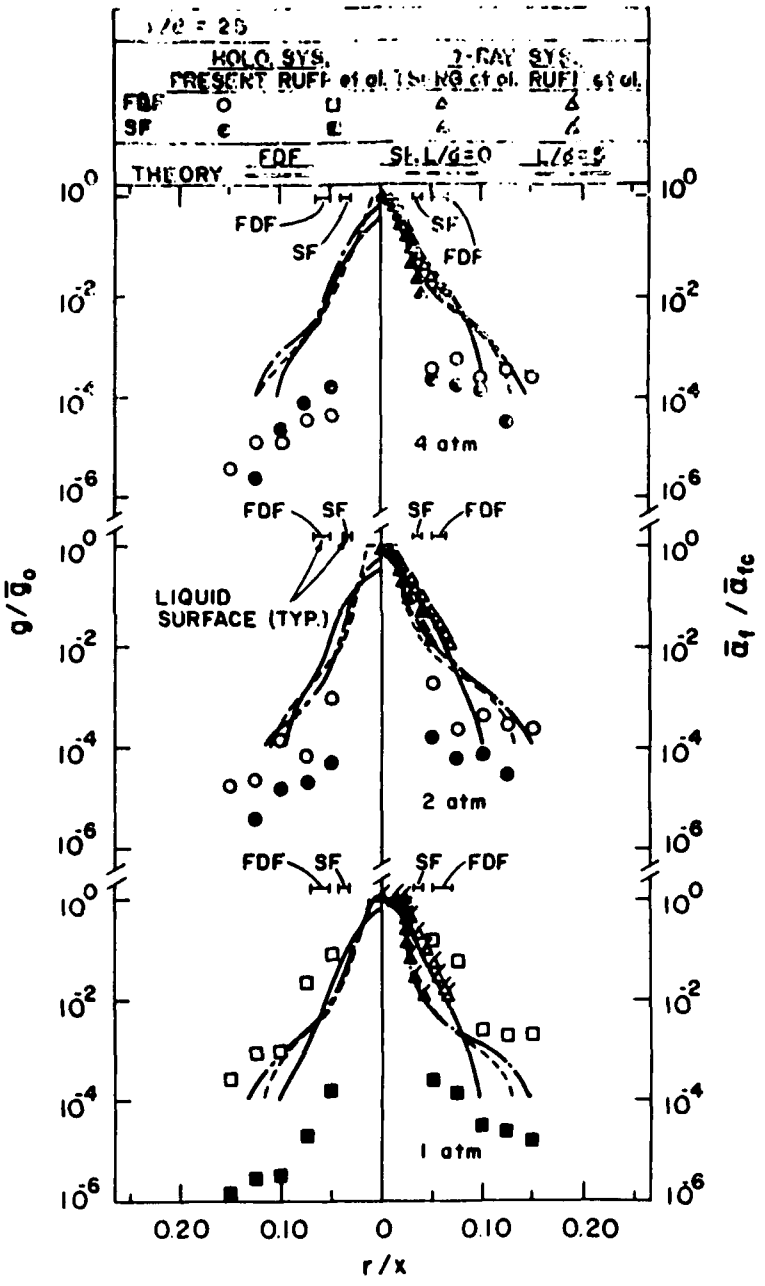
HOLO. SYS. PRESENT
7-RAY SYS. RUFF et al.
FDF
SF
THEORY
4 atm
2 atm
1 atm
LIQUID SURFACE (TYP.)
g/ḡo
ᾱf / ᾱfc
0.20
0.10
0
r/x

APPENDIX E: WU ET AL. (1991)

Atomization and Sprays, vol. 1, pp. 421–440, 1991

PRIMARY BREAKUP IN LIQUID-GAS MIXING LAYERS

P.-K. Wu, G. A. Ruff, and G. M. Faeth
Department of Aerospace Engineering, The University of Michigan, Ann Arbor, Michigan 48109-2140

An experimental study of primary breakup in the near-injector region of large-diameter (5.0 and 9.5 mm) liquid jets in still air is described. Holography was used to provide drop and liquid surface characteristics for initially nonturbulent liquids (water, n-heptane, and various glycerol mixtures) having various jet exit velocities. Drop sizes after primary breakup satisfied Simmons' universal root normal distribution and can be characterized solely by their Sauter mean diameter (SMD). The SMD increased with distance from the jet exit and then remained nearly constant within a fully developed primary breakup region. SMD measurements in the fully developed regime did not agree with existing expressions based on unstable surface wave growth. However, an expression based on stripping-type breakup due to boundary layer growth in the liquid along the windward side of surface waves yielded a reasonably good correlation of present SMD measurements. The nature of this primary breakup correlation implies that secondary breakup is a dominant feature of liquid-gas mixing layers.

INTRODUCTION

An experimental investigation of dispersed liquid generation along liquid surfaces within liquid-gas mixing layers (primary breakup) is described. The study was motivated by the importance of primary breakup within the near-injector region of pressure-atomized sprays as well as for gas jets in liquids. Drop size distributions after primary breakup were measured within multiphase mixing layers formed about the periphery of round liquid jets in still room air. Various liquids and relative velocities were considered for low turbulence intensity flows having nearly uniform velocity distributions (slug flows) at the jet exit. The measurements were used to evaluate existing and proposed theories and correlations of mean drop sizes after primary breakup. The objective was to extend work concerning the structure and mixing properties of the dense-spray region of pressure-atomized sprays [1–4] to focus on primary breakup because this process has a major influence on the rate of development and the importance of separated flow effects for these flows.

A number of reviews of liquid atomization and dense sprays have appeared [2-11]; therefore, only the main features of past work will be considered. The discussion also will be limited to the wind-induced and atomization breakup regimes, defined by Miesse

Address correspondence to G. M. Faeth.
G. A. Ruff is currently with the Department of Mechanical Engineering, Drexel University, Philadelphia, Pennsylvania.

NOMENCLATURE

C_B, C_R, C_{RT}	constants in primary breakup correlation	We_{g0}	jet exit Weber number ($= \rho_g d_0 u_0^2/\sigma$)
		We_{gg}	drop Weber number ($= \rho_g d_{ij} u_{ij}^2/\sigma$)
d	jet exit diameter	We_{gSMD}	spray Weber number ($= \rho_g SMD u_{ij}^2/\sigma$)
d_{max}, d_{min}	maximum and minimum image dimensions of drops	x	distance from jet exit
		Δp	stagnation pressure rise of liquid
d_{ij}	drop diameter	μ	molecular viscosity
e_{ij}	drop ellipticity	ρ	density
MMD	mass median diameter	σ	surface tension
Oh	jet exit Ohnesorge number ($= \mu_l/(\rho_l d_0 \sigma)^{1/2}$)	**Subscripts**	
Re_{l0}	jet exit Reynolds number ($= \rho_l d_0 u_0/\mu_l$)		
Re_{lx}	Reynolds number based on distance from the jet exit ($= \rho_l x u_0/\mu_l$)	l	liquid phase property
		FD	property in fully developed primary breakup regime
SMD	Sauter mean diameter		
Ta	Taylor number ($= (\rho_g/\rho_l)^{1/2} \mu_l u_0/\sigma$)	g	gas phase property
u_0	mean jet exit velocity		
We_{l0}	jet exit Weber number ($= \rho_l d_0 u_0^2/\sigma$)		

[12] and Ranz [13], because they are most important for practical applications, e.g., the other breakup regimes are limited to a small range of low jet velocities and yield large drops that are not very effective for dispersing and mixing the liquid. Within the wind-induced and atomization breakup regimes, primary breakup occurs along the liquid surface within a multiphase mixing layer adjacent to the surface. Both theories and measurements of primary breakup properties in this flow will be considered in the following.

Past theories seeking to provide correlations of drop sizes after primary breakup have been mainly limited to mean drop sizes for nonturbulent liquids. Two major approaches have been proposed: (1) aerodynamic breakup based on linear wave growth theory, which was initially proposed by Taylor [14], with subsequent development by Ranz [13] and Levich [15] and later application by Reitz and Bracco [16], among others; and (2) sheltered wave growth theory due to Mayer [17] and Adelberg [18], which rests on the surface wave growth model of Jeffreys [19]. Taylor's [14] aerodynamic breakup model involves assuming proportionality between the wavelength of the most rapidly growing waves on the liquid surface and the mean drop size (taken to be the Sauter mean diameter, SMD, in the following) from primary breakup. Wave growth properties are found from linear stability theory, allowing for effects of aerodynamic forces due to gas flowing across the waves as well as the stabilizing effects of surface tension and liquid viscosity. This yields a relatively complex relationship between the Weber number based on SMD from primary breakup, $We_{gSMD} = \rho_g SMD\, u_0^2/\sigma$, and what will be termed the Taylor number, $Ta = (\rho_g/\rho_l)^{1/2} \mu_l u_0/\sigma$. This form implies that the mean jet exit velocity, u_0, is the proper relative velocity near the surface, which is justified by the measurements of Ruff et al. [2, 3] for multiphase mixing layers near the jet exit ($x/d \leq 100$). Ranz [13] and Levich [15] propose formulas having a simpler limiting behavior at small Ta, where effects of liquid viscosity can be neglected, yielding

$$We_{gSMD} = C_B \tag{1}$$

where C'_B is a constant on the order of unity. Levich [15] also undertakes an approximate treatment of effects of liquid viscosity which suggests that We_{gSMD} should increase with increasing Ta, with primary breakup ceasing when Ta $\approx$ 1. Experimental confirmation of Eq. (1) and its large Ta behavior, however, has not been reported.

Mayer [17] developed an alternative primary breakup correlation that was also based on wave growth properties. However, he adopted the sheltered wave growth theory of Jeffreys [19] to find wave properties, because this approach had achieved some success in predicting the properties of wind-induced ripples on liquid surfaces. This yields

$$We_{gSMD} = C'_B Ta^{2/3} \tag{2}$$

where Mayer [17] recommends $C'_B = 21$ based on measurements by Weiss and Worsham [20]. This expression was adopted for the JANNAF liquid rocket performance code, although it became evident that C'_B had to be varied over an order of magnitude to achieve reasonable predictions for various injector systems [7]. Adelberg [18] developed a primary breakup expression along the same lines as Mayer [17] but suggests $C'_B = 45$, which represents one of many subsequent variations on C'_B to match limited ranges of particular data sets, as noted earlier. In particular, it is probable that the data used to fit Eq. (2) by both Mayer [17] and Adelberg [18] were influenced by secondary breakup (aerodynamic shattering of drops formed by primary breakup), because the measurements were made far from the injector within the dilute portions of sprays.

In contrast to the theories [14–18], which do not consider effects of liquid vorticity, most measurements of the near injector properties of dense sprays have exhibited strong effects of liquid flow characteristics at the jet exit [1–4, 8, 21–24]. In particular, Phinney [21] finds that transition between the wind induced and atomization breakup regimes is affected by the presence of liquid turbulence at the jet exit [8]. The degree of flow development at the jet exit was also found to influence initial mixing rates of liquid jets in gases, with fully developed turbulent pipe flow yielding much faster mixing than nonturbulent slug flows [1, 4]. This behavior must involve effects of liquid turbulence on primary breakup, because primary breakup controls the initial dispersion of liquid (no breakup, no mixing). Additionally, visualization of the flow by Hoyt and Taylor [22–24] indicated very little effect of relative velocities on the initial breakup for a fixed jet exit velocity, completely contradicting properties anticipated from the primary breakup theories. This implies that liquid vorticity within boundary layers developing in the nozzle passage dominates primary breakup very near the jet exit. Finally, measurements of drop size distributions from primary breakup for water jets in room air, at a single relative velocity, showed a much larger SMD for turbulent pipe flow than for nonturbulent slug flow [3]. Thus, experiments exhibit a variety of features that are not anticipated by existing models of primary breakup, however, the existing measurements are far too limited—water in room air at a single relative velocity [3]—to provide an adequate evaluation of predictions and needed direction for new development of theory.

The successful development of holography to provide observations of primary breakup properties within liquid gas mixing layers provides a means of addressing this gap in the literature [2, 3]. Thus, the objective of the present investigation was to observe primary breakup using pulsed holography, to exploit the results to evaluate existing theories [14–18], and to develop alternatives where necessary. The experiments

involved relatively large diameter nonevaporating liquid jets (5.0 and 9.5 mm) injected into still room air with nonturbulent slug flow at the jet exit. This provided a relatively long multiphase mixing layer (having a length, x/d, in excess of 200; see [10, 11]) so that jet exit disturbances could decay to reveal the fundamental evolution of primary breakup properties with position within the mixing layer. Various liquids (water, *n*-heptane, and glycerol solutions) and jet exit velocities were considered in order to examine the effect of a wide range of liquid damping and aerodynamic properties.

EXPERIMENTAL METHODS

Apparatus

The objective of the measurements was to resolve effects of liquid properties and relative velocities on primary breakup within multiphase mixing layers. Additionally, good optical access was a prime consideration. Thus, the test flows involved injection of modest amounts of liquid, to control costs, into still air at room conditions, to avoid optical distortion due to windows.

Figure 1 is a sketch of the injector system. The test liquid is placed within an accumulator having the jet nozzle passage at the bottom. Premature liquid outflow is

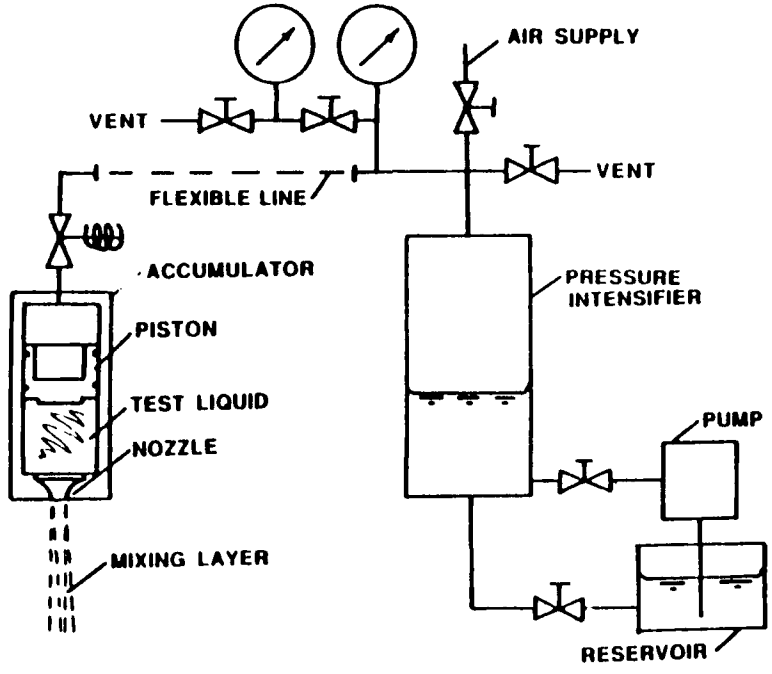

Fig. 1 Sketch of high speed multiphase mixing layer apparatus

prevented by placing a cork in the nozzle exit. The liquid is then forced through the nozzle, ejecting the cork at the start of the flow, by admitting high pressure air to the top of the accumulator through a solenoid actuated valve. A piston within the accumulator, sealed along its sides, prevents mixing between the air and the test liquid. The piston is hydraulically cushioned at the end of its travel in order to reduce shock and vibration of the apparatus. After venting air from the top of the piston, the piston is returned to the top of the accumulator so that the system can be refilled with liquid. The cork closure in the nozzle exit allowed the liquid to be filled from the bottom of the accumulator while venting trapped air from just below the piston face.

The high pressure air is supplied from a pressure intensifier that also serves as the air storage system for the accumulator. The laboratory air supply system can be used to charge the accumulator and no pressure intensification is needed for injection pressures up to 17 MPa. For higher pressure drops, air is first vented into the pressure intensifier to the maximum supply pressure with only a small quantity of oil in the bottom. Oil is then pumped into the bottom of the intensifier, reducing the gas volume and increasing the gas pressure to the desired level. The system is then sealed prior to execution of a test. At the end of operation, the oil is vented from the pressure intensifier and the filling process is repeated for the next test.

The piston has a diameter of 64 mm and a stroke of 200 mm, yielding a liquid sample size of roughly 500 ml. Testing was limited to 5.0 mm diameter slug flow at the jet exit. The contraction section of the nozzle was designed according to Smith and Wang [25] to provide a uniform velocity across the exit, aside from boundary layers along the walls of the passage. Detailed measurements of jet exit flow characteristics have not been made, but turbulence levels are expected to be low due to the relatively quiescent conditions at the start of contraction and the large nozzle contraction ratio (roughly 100:1) [26]. Injection is vertically downward with the liquid captured in a baffled tub and then discarded. Instrumentation is mounted rigidly, therefore, various positions in the flow are studied by moving the injector with positioning accuracies of 5 μm in the horizontal direction and 0.5 mm in the vertical direction.

Total times of injection were 230–1140 ms. These relatively short time periods were not problematic, however, because flow development times are short for the near injector region of the mixing layer, roughly 4–30 ms. Additionally, measurements are made using pulsed holography, which requires times less than 1.2 μs for triggering the data accumulation.

Instrumentation

Pressure Measurements. Apparatus performance was monitored by pressure measurements at the inlet of the accumulator using a piezoelectric transducer (Kistler Corp., Model 211B2) whose output was recorded with a digital oscilloscope (LeCroy, Model 9400A).

Injector performance for a given liquid and accumulator pressure was tested using an impact plate. This involved a rectangular plate (125 × 175 mm) whose center coincided with the injector axis, located 25 mm from the jet exit. A piezoelectric pressure transducer and oscilloscope, identical to the arrangement used to measure the accumulator pressure, were used to measure the impact pressure at the center of the plate. The

measured stagnation pressure difference then yielded the mean jet exit velocity as follows: $u_{ij} = (2\Delta p/\rho_l)^{1/2}$.

Holography. A single pulse holography system, similar to that used in earlier work [2, 3], was used to measure drop and liquid surface characteristics. An off-axis arrangement was used, based on the Spectron Development Laboratories Model HTRC-5000 system, with an angle of 28° between the object and reference beams. Adequate spatial resolution and sufficient light intensity to penetrate the spray were provided by reducing the diameter of the object beam through the spray and then expanding it (7–8:1) back to the same diameter (85 mm) as the reference beam when the two signals were optically mixed to form the hologram. The holograms were generated by a ruby laser that deposited 50 mJ in roughly 20 ns. This effectively stopped the flow so that objects as small as 5 μm in diameter could be measured. The holograms were obtained in a darkened room using AGFA 8E75HD NAH unbacked holographic film plates having a 100 × 125 mm format.

The holograms were reconstructed using a 15 mW HeNe laser beam that was expanded to a diameter of 50 mm to provide a real image of the spray in front of the hologram. The properties of the reconstructed spray were observed with an MTI Model 65 video camera with optics to provide a field of view of 1.4 × 1.6 mm. Computer-controlled x-y traversing the hologram (1 μm resolution) and z traversing of the video camera (5 μm resolution) allowed observation of the entire object field. The video image was analyzed using a Gould IDS5000 image display system. Reference pins of known size and location near the edge of the object field provided direct calibration of distances on the reconstructions.

Drops and other ellipsoidal objects were sized by measuring their maximum and minimum diameters through the centroid of the image. Assuming ellipsoidal shapes, the diameter of these objects was taken to be the diameter of an ellipsoid having the same volume, that is, $d_e^3 = d_{max}^2 d_{min}$. The shape of the object was also characterized by its ellipticity, defined as $e_e = d_{max}/d_{min}$. This approach was not feasible, however, for irregular liquid elements or in cases in which the centroid was not located within the boundaries of the image. Then the cross-sectional area and perimeter of the image were measured and the maximum and minimum diameters of an ellipsoid having the same cross sectional area and perimeter were computed. Given these parameters, the effective diameter and ellipticity were found in the same manner as for drops. The results at each condition were summed, considering 20–400 elements, to provide drop size distributions, mass median diameter (MMD), SMD, and the volume averaged ellipticity, e_e. The wavelength of disturbances of the liquid surface was also measured, considering roughly five holograms for each axial position and injector operating condition.

Experimental uncertainties were generally dominated by finite sampling limitations, because there are relatively few large drops after primary breakup of waves along the surface, rather than resolution of liquid element properties from reconstructed holograms (e.g., 20–400 elements for moments of the drop size distribution and roughly 10 waves for wave properties). Within the limitations of the definitions of liquid element sizes and ellipticities, which are difficult to quantify, estimates of experimental uncertainties (95% confidence) are less than 15% for MMD, SMD, and volume averaged ellipticity. Uncertainties of drop size distributions are best considered in the context of particular size distribution functions, therefore, these uncertainties will be taken up later. Surface wavelengths were difficult to measure because the waves were irregular and

their resolution was limited by line of sight effects; therefore, estimated experimental uncertainties (95% confidence) only were less than 40%.

Test Conditions

Test conditions are summarized in Table 1. A series of holograms for the region along the liquid surface were available from Ruff et al. [2, 3] and were used to provide results for an injector diameter of 9.5 mm. The remainder of the measurements were obtained with the present apparatus, which had a jet exit diameter of 5.0 mm. Both injectors involved nonturbulent slug flow at the jet exit with similar passage designs. The streamwise positions of the data involved x/d in the range 6.25–100.

Earlier work, reviewed in [10, 11], indicates that the length of the mixing layers (represented by the length of the all liquid core at the axis) was in excess of $x/d = 200$ for present test conditions. Thus, breakup of the liquid core as a whole was not a factor for present measurements.

Test liquids included water, *n* heptane, and various glycerin water mixtures (21, 42, and 63% glycerin, by mass). This provided the following ranges of fluid properties: liquid/gas density ratios of 575–975, liquid viscosities of 3.97–108.3 × 10^{-4} kg/ms, and surface tensions of 2.00–7.08 × 10^{-2} N/m. These fluid properties were verified by measuring liquid densities using a hydrometer (Fisher model 11-582, 0.1% accuracy), liquid viscosities with a Cannon/Fenske viscometer (Thomas model 9721, 3% accuracy), and surface tensions with a ring tensiometer (Fisher model 20, 1% accuracy).

Jet exit velocities were in the range 16.5–133.8 m/s, which was sufficient to resolve relative velocity effects without significant uncertainties due to temperature variations from compressibility effects. This yielded ranges of jet dynamic parameters as follows: Re_{fd} of 17,000–750,000, We_{gd} of 94–1520, and Oh of 0.00109–0.0181. All test conditions involved $We_{fd} \gg 8$ and $We_{gd} > 40.3$, so they were well into the atomization breakup regime [12, 13]. According to this classification, the multiphase mixing layer should begin right at the jet exit, however, transition to atomization breakup was also affected by the state of flow development at the jet exit, as observed earlier [1]. Thus, some test conditions were in the wind-induced breakup regime, as noted later, where breakup occurs in a multiphase mixing layer that begins at some distance from the jet exit. This delayed transition to atomization breakup was caused by the relatively low

Table 1 Summary of Test Conditions[a]

Liquid	ρ_f (kg/m^3)	$\mu_f \times 10^4$ (kg/ms)	$\sigma \times 10^2$ (N/m)	d (mm)	u_0 (m/s)	$Re_{fd} \times 10^{-4}$	We_{gd}	Oh × 10^3
Water[b]	997	8.94	7.08	9.5	56.4	60	499	1.09
Water	997	8.94	7.08	5.0	28.1–133.8	16.75	94–1480	1.50
n Heptane	683	3.97	2.00	5.0	16.5–72.1	14.62	80–1520	1.52
Glycerol 21%	1044	15.92	6.43	5.0	30.4–89.2	10.29	84–724	2.75
Glycerol 42%	1101	34.66	6.30	5.0	29.1–90.6	4.7–14	80–762	5.89
Glycerol 63%	1158	108.30	6.20	5.0	31.2–90.2	1.7–4.8	92–768	18.1

[a]Pressure atomized injection vertically downward in still air at 98.8 kPa and 298.1 ± 1 K with nonturbulent jet exit conditions.

[b]Results from the steady flow arrangement of Ruff et al. [2, 3].

levels of vorticity due to limited boundary layer growth in the injector passages and low turbulence levels at the jet exit due to the present slug flow injector design, so that initial disturbance levels of the flow were low, tending to retard the growth of disturbances leading to primary breakup.

RESULTS AND DISCUSSION

Drop Size Distributions

Ruff et al. [3] studied drop size distributions both along the liquid surface after primary breakup and across the mixing layer, presumably after secondary breakup. These measurements were carried out for both slug flow and fully developed turbulent pipe flow at the jet exit – the latter condition yielding a turbulent primary breakup mechanism whose characteristics were correlated with liquid turbulence properties rather than potential aerodynamic effects. Nevertheless, drop size distributions for all these conditions were represented reasonably well by the universal root normal distribution proposed by Simmons [27] based on extensive observations in the dilute region of a variety of sprays. Because this assessment was limited to a single jet exit diameter and relative velocity for water injection in air, however, it was of interest to extend the evaluation to the broader range of primary breakup conditions of the present tests.

Drop size distributions after primary breakup during the present tests are plotted in Fig. 2. Results are shown for all liquids and relative velocities used, plotted in terms of the universal root normal distribution of Simmons [27]. The results involve a variety of distances from the jet exit, but streamwise distance *did not effect* the nature of the distribution and is not indicated in order to reduce cluttering of the plots. The root normal distribution has two parameters, one of which can be taken to be the SMD and the other the MMD/SMD ratio. Simmons [27] recommends MMD/SMD = 1.2, therefore, root normal distributions in this range are also shown on the plot.

Similar to the findings of Ruff et al. [3], the root normal distribution with MMD/SMD = 1.2 yields an excellent correlation of the present measurements, except for a few outlying points. Firmly establishing drop size distributions requires sizing a large number of drops [5, 6], which is difficult for primary breakup because the drops are generally large and not very numerous. Thus, the outlying points seen at larger diameters in Fig. 2 are due primarily to insufficient numbers of drops in the distributions for some test conditions. Taking all the results as a whole, however, it was found that MMD/SMD = 1.18 with a 95% confidence interval of 1.14–1.22, so that Simmons' recommended value is within the range of the present measurements. This is very helpful because the entire drop size distribution can be related to the SMD in a simple manner. Thus, results concerning drop sizes after primary breakup will be discussed in terms of SMD in the following.

Development of Primary Breakup

It was found that drop characteristics tended to vary with increasing distance from the jet exit and then approached a regime where the rate of variation was relatively slow

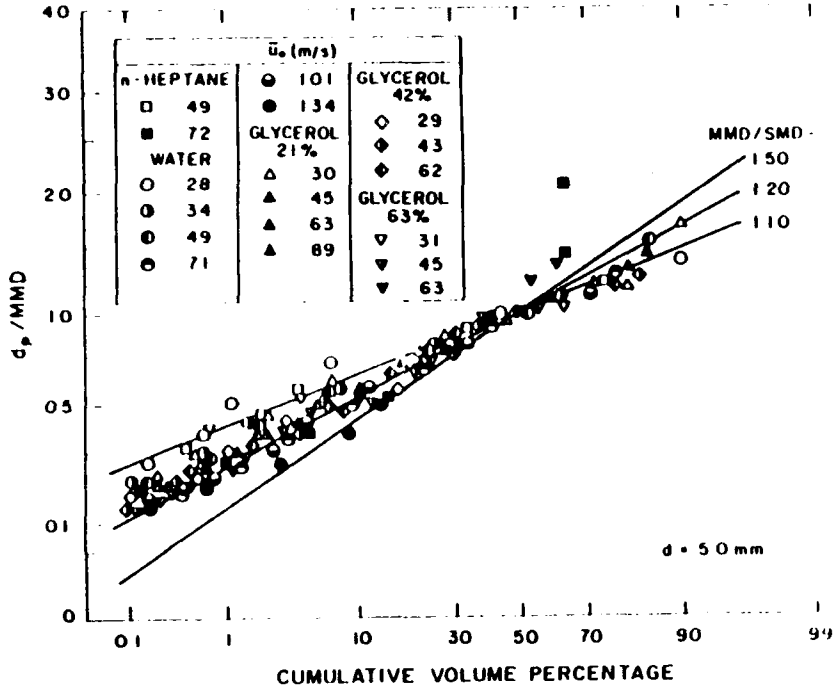

Fig. 2 Drop size distributions after primary breakup

This latter region will be termed the fully developed primary breakup regime in the following. Approach to fully developed conditions was slower for the more viscous liquids and tended to correlate as a function of the Reynolds number based on distance from the jet exit and liquid properties, Re_{l_x}.

Results illustrated in Fig. 3 show a progressive increase of SMD with Re_{l_x}. The data are relatively limited, however, fully developed primary breakup conditions are reached for Re_{l_x} on the order of 10^6. This corresponds to conditions where boundary layers typically undergo transition to turbulent flow [28]. However, the appropriate relative velocity and transition conditions for boundary layers along free surfaces and walls are not the same, so more study is needed to determine the relationship between the fully developed primary breakup regime and flow characteristics in the liquid. For low viscosity materials, like water and *n*-heptane, fully developed conditions are reached relatively close to the jet exit. However, for the most viscous glycerol solutions virtually the entire region where observations were made ($x/d \leq 50$ for this liquid) was in the development regime. This behavior suggests a close relationship between the

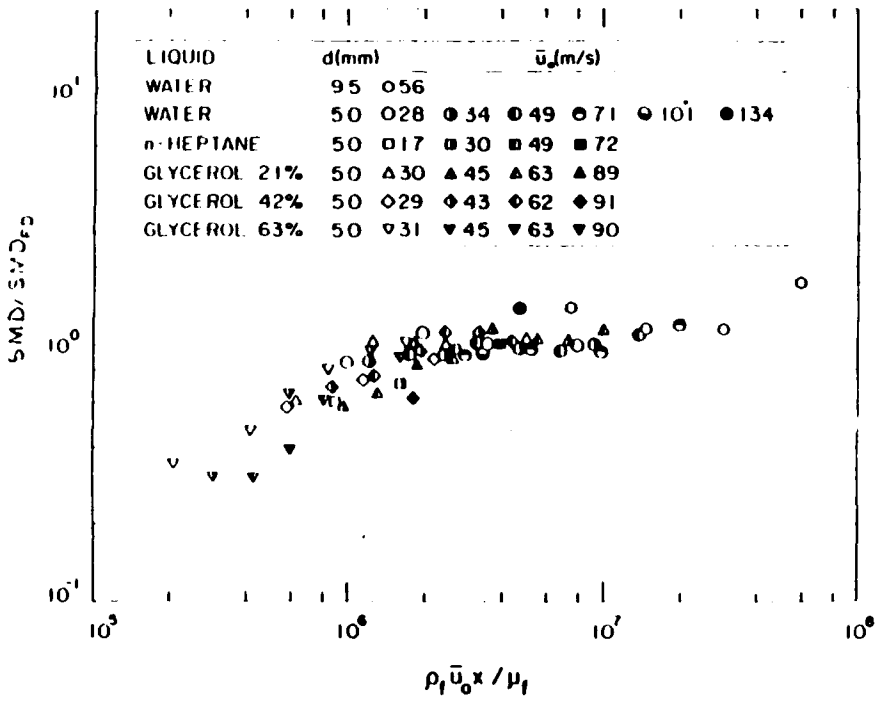

Fig. 3 Streamwise variation of SMD after primary breakup

development of vorticity in the liquid and processes leading to primary breakup, which is consistent with the strong effect of the degree of initial flow development on mixing rates [1, 4]. Certainly, a uniform liquid flow region is not expected to yield conditions required to eject liquid as ligaments from a liquid surface. Instead, a region of vorticity near the surface, having a thickness controlled by boundary layer growth rates, is a better setting for ligament formation, with the thickness of this layer tending to control ligament size. Thus, increases of SMD with increasing Re_{l_x} seem quite plausible.

A second feature observed in Fig. 3 is that SMD still varies somewhat in the fully developed primary breakup regime. Two effects could be responsible for this behavior: reduced relative velocities near the liquid surface and increased wavelengths of surface waves as distance from the jet exit increases. First of all, measurements of mean velocity distributions within the multiphase mixing layer show progressively increasing gas velocities along the liquid surface with increasing distance from the jet exit [2, 3]. Naturally, the resulting reduced relative velocities in the vicinity of the liquid surface would tend to increase drop sizes after primary breakup, if not eventually ending primary breakup by aerodynamic surface breakup mechanisms entirely. The second effect is related to the wavelengths of liquid surface disturbances, which were observed to increase with increasing distance (these results will be considered later). In this case,

longer wavelengths would be expected to yield larger drop sizes after primary breakup by any of the mechanisms advanced thus far [13-18].

The ellipticity of drops near the surface, after primary breakup, also was influenced by distance from the jet exit. Data showing this behavior are plotted in Fig. 4 as a function of Re_{t_0}. In general, e_p reaches a maximum for Re_{t_0} on the order of 10^6, which corresponds to conditions near the onset of the fully developed primary breakup regime seen in Fig. 3 for the SMD (note that there is one outlying point having an e_p of nearly 5 in this region, but most of the flows have maximum e_p in the range 1.5-2.5). Farther into the fully developed primary breakup regime, $e_p \approx 1.2$.

These results suggest that conditions within the fully developed primary breakup regime are relatively independent of distance from the jet exit, whereas conditions nearer the jet exit may be affected by vorticity generated by boundary layers in the injector passageway. Thus, further consideration of primary breakup will be limited to the fully developed regime to avoid uncertainties about effects of the degree of boundary layer development at the jet exit, which are likely to be apparatus dependent.

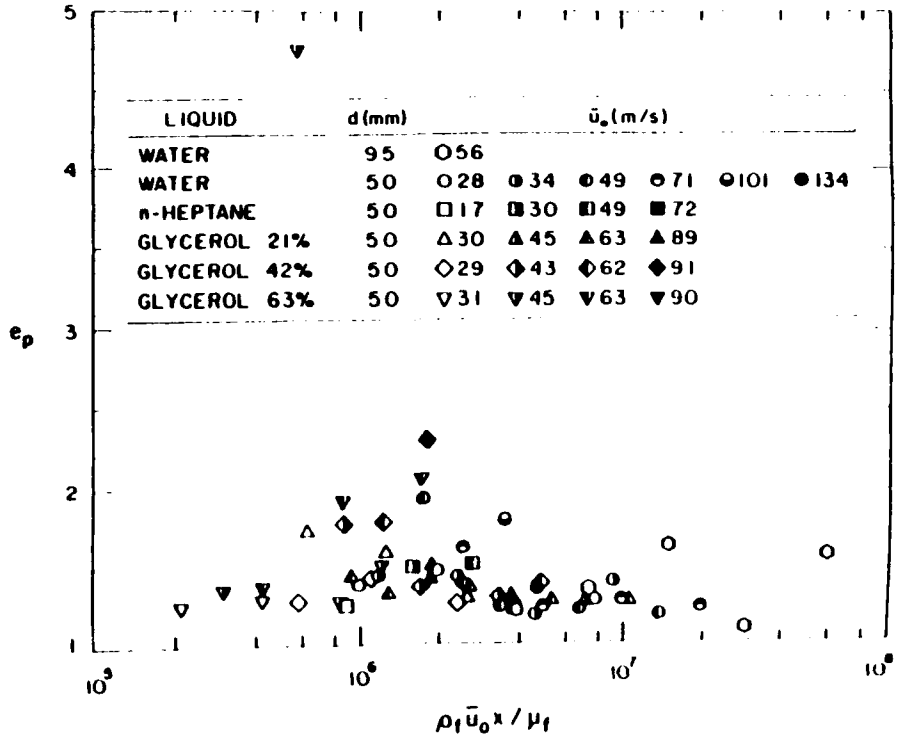

Fig. 4 Streamwise variation of e_p after primary breakup.

Fully Developed Primary Breakup

A correlation of SMD after primary breakup in the fully developed regime was sought based on the existing theoretical correlations of Taylor [14], Levich [15], Mayer [17], and Adelberg [18]. All these approaches yield We_{gSMD} as a function of Ta after primary breakup; therefore, a correlation of present measurements was sought as a function of these variables. The present measurements, those of Ruff et al. [2, 3], and the theoretical correlations are plotted in this manner in Fig. 5. The Taylor [14] and Levich [15] correlations are identical at small Ta, yielding Eq. (1), and have been fitted to the measurement by Ruff et al. [2, 3] in that regime for purposes of illustration. The limit of primary drop breakup proposed by Levich [15] has been illustrated at Ta = 1, although only this order of magnitude was proposed. The correlations of Mayer [17] and Adelberg [18] follow Eq. (2), with appropriate values of C_a. The measurements illustrated in Fig. 5 are limited to the fully developed primary breakup region.

Clearly, none of the theoretical expressions illustrated in Fig. 5 provide a successful correlation of the measurements. In particular, for a given liquid in air, Ta varies primarily with variations of u and the theoretical expressions do not yield the correct velocity dependence of SMD after primary breakup. For example, SMD $\sim u^{-2}$ and $u^{-1.5}$ for the aerodynamic and sheltered wave growth theories; whereas the measurements generally yield SMD $\sim u^{-0.8}$. This difference has serious ramifications concerning the relative importance of secondary breakup and collisions in dense sprays and multiphase mixing layers. For example, Reitz and Bracco [16] estimate very small drop sizes after primary breakup by applying the aerodynamic breakup theory of Taylor [14] to the test conditions used by Hiroyasu et al. [29]. The result implied that collisions within the dense spray region must be important in order to obtain drop sizes that were actually measured in the dilute portions of the spray. In contrast, the relatively low velocity dependence of the present measurements would imply significant effects of secondary breakup in the same flow. Other evidence to be discussed later suggests that this behavior is general, so the change in sensitivity of primary breakup to changes in velocity implies that dense sprays and multiphase mixing layers are more likely to be dominated by secondary breakup than collisions, the conventional view of liquid breakup [5], unless impinging liquid streams are considered.

Another difficulty with the correlations illustrated in Fig. 5 is that they do not accommodate effects of changing liquid properties. In particular, progressively increasing the liquid viscosity, by adding glycerin to water, causes nearly parallel shifts of the We_{gSMD} plots to higher values of Ta, but still with the same velocity dependence.

In an effort to diagnose the problem with existing models of primary breakup, wavelengths of disturbances of the liquid surface were measured. Present results, along with earlier measurements of Hoyt and Taylor [22, 23] for water and a polymer solution, are illustrated in Fig. 6. In view of the large uncertainties of present wavelength measurements, the present findings agree reasonably well with the results of Hoyt and Taylor [22, 23]. The wavelengths are comparable to the jet exit diameter over the region measured and increase roughly in proportion to distance from the jet exit. This behavior is representative of helical instability rather than sinuous modes of instability considered in the primary breakup correlations (the latter generally being observed only within a few diameters of the jet exit [22, 23]). Thus, the mechanism of primary breakup considered in [14-18] clearly is not relevant for the conditions of the present experiments.

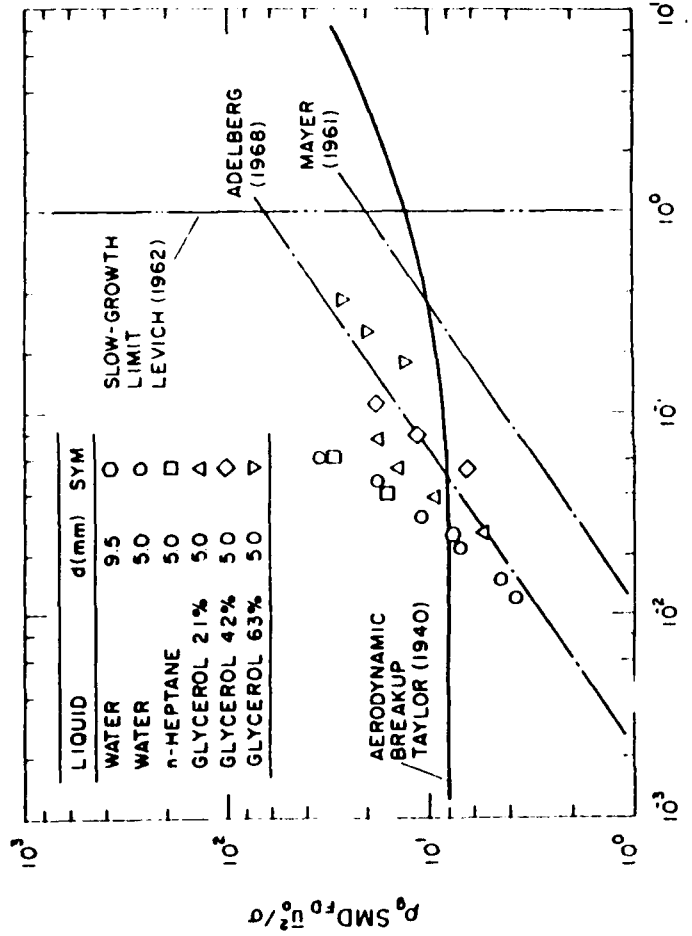

Fig. 5 Correlation of SMD after primary breakup in the fully developed region according to existing theories

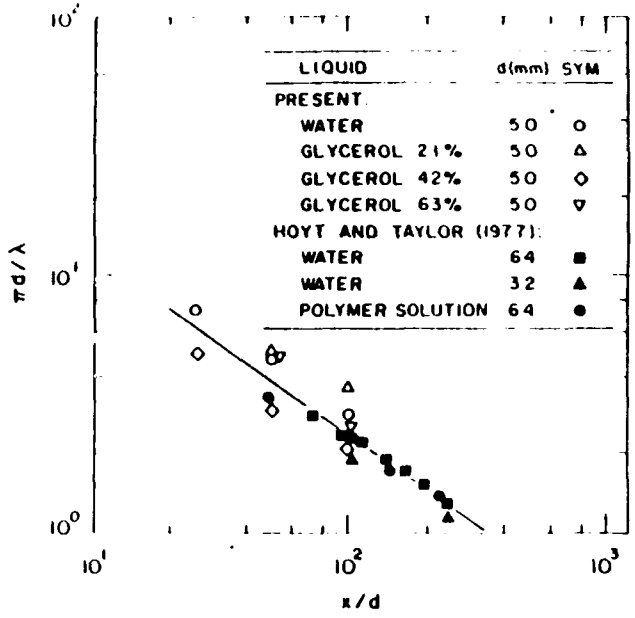

Fig. 6 Streamwise variation of liquid surface wavelength

An alternative view of primary breakup yielded a more successful correlation of present measurements. The general nature of the approach is illustrated in Fig. 7, where ligament formation from a surface wave is illustrated. The reference frame in the figure is with respect to the wave, assuming that the relative velocity of the liquid and the wave velocity are roughly the same. Then the relative motion causes a boundary layer to develop on the windward side of the wave and it is implied that drop sizes after primary breakup are comparable to the thickness of the boundary layer as it reaches the tip of the wave, i.e., that liquid is stripped from the tip of the wave, controlling its growth. This is plausible because the liquid in the bulk of the slug flow has no vorticity and cannot be deflected so that it leaves the liquid phase as a ligament. For present test conditions, wavelengths of disturbances along the surface in the fully developed primary breakup regime were comparable to the initial jet diameter and were probably helical waves as noted earlier. Then assuming that the SMD after primary breakup is proportional to the thickness of the surface boundary layer, that the distance the boundary layer grows is proportional to the jet exit diameter, that the relative velocity of the layer scales as u_0, and that the surface boundary layer is laminar, there results

$$\frac{\mathrm{SMD}}{d} = \frac{C_B''}{(\rho_l u_0 d/\mu_l)^{1/2}} \tag{3}$$

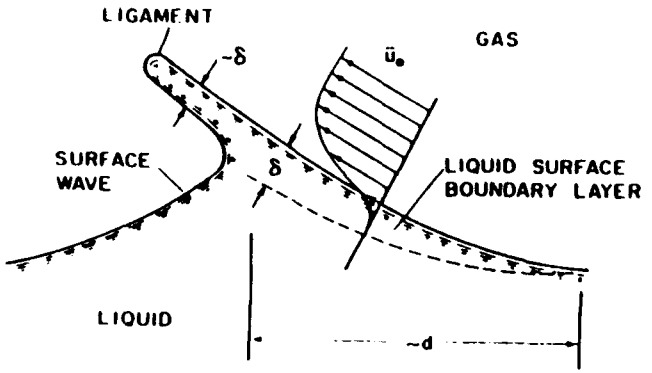

Fig. 7. Sketch of the shear type primary breakup mechanism

where C_B'' is an empirical constant involving the various proportionality factors. It is convenient to rearrange Eq. (3) so that We_{gSMD} is introduced because this simplifies comparison with the earlier theoretical correlations and the evaluation of secondary breakup effects. Completing this rearrangement yields

$$We_{gSMD} = \frac{C_B'' We_{gd}}{Re_{ld}^{1/2}} \tag{4}$$

Present measurements in the fully developed primary breakup regime are plotted in terms of the variables of Eq. (4) in Fig. 8. The correlation of the data for all liquids, the full range of velocities, and jet diameters of 5.0 and 9.5 mm is seen to be remarkably good. The power of the correlation in terms of $We_{gd}/Re_{ld}^{1/2}$ is not unity as suggested by Eq. (4), however, and can be represented better by the following empirical fit, which is shown on the plot:

$$We_{gSMD} = 16 \left(\frac{We_{gd}}{Re_{ld}^{1/2}} \right)^{0.82} \tag{5}$$

The standard deviations of the coefficient and power in Eq. (5) are 6 and 4%, respectively, with the correlation coefficient of the fit being 0.96. The reduction of the exponent of $We_{gd}/Re_{ld}^{1/2}$ from unity in Eq. (4) to 0.82 in Eq. (5) is statistically significant but is not large in view of the qualitative nature of the development of the correlation. Equation (5) implies that $SMD \sim u_0^{-0.11}$, which is roughly the velocity dependence observed for each liquid.

The reasonably good performance of Eqs. (4) and (5) suggests that wave growth properties determine the dimensions of surface waves but that boundary layer growth along the windward side of the wave controls drop dimensions from primary breakup. This picture is consistent with present observations that drop sizes from primary breakup are significantly smaller than surface wavelengths in the fully developed regime because

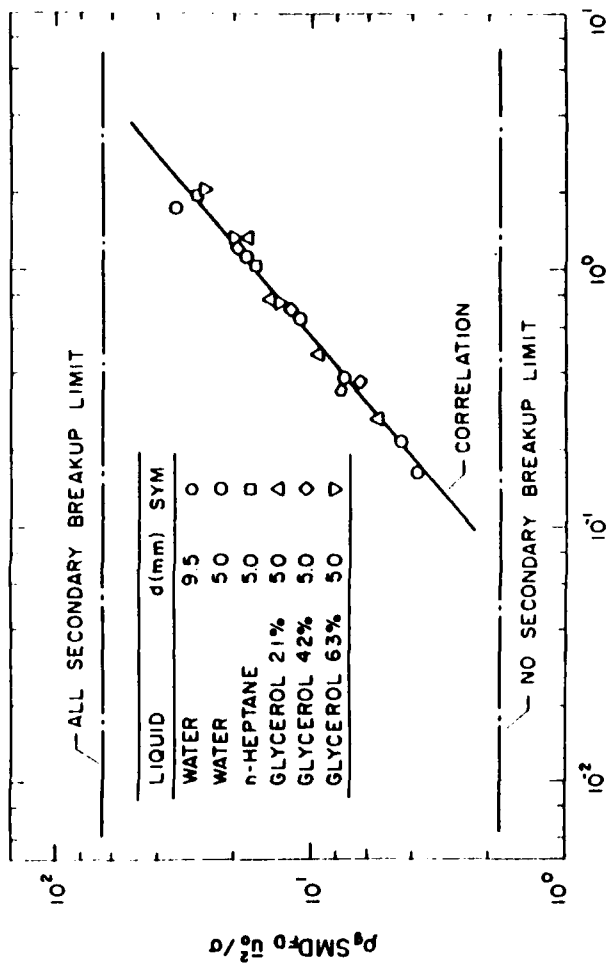

Fig. 8. Correlation of SMD after primary breakup in the fully developed region

101

boundary layer thicknesses are generally much smaller than their length of development. This behavior is analogous to stripping type secondary breakup of drops, where liquid boundary layers developed on the windward side of the drop, and ejecting into the gas phase at the drop periphery, have provided successful correlations of drop breakup times [30]. The importance of liquid vorticity in boundary layers near the surface for primary breakup is also consistent with differences observed in primary breakup near the jet exit and the fully developed region, as well as differences in primary breakup for nonturbulent slug flow and fully developed turbulent pipe flow at the jet exit, discussed earlier.

It is also of interest to consider the potential for secondary breakup based on the results of Fig. 8 and the universal root normal size distribution of Simmons [27]. First of all, it is generally agreed that drops are unstable to secondary breakup when their Weber number, We_{gp}, exceeds a critical value, as follows [3, 9]:

$$We_{gp} = \rho_g d_p u_0^2 / \sigma \geq 6.5 \tag{6}$$

Equation (6) has been written assuming that the relative velocity of large drops subject to secondary breakup is equal to the relative velocity of the mixing layer; this is reasonable based on the results of Ruff et al. [2, 3], where large drops near the liquid surface were observed to have velocities very near the mean injection velocity for conditions similar to present test conditions. Now the universal root normal distribution implies that drop sizes within 3 standard deviations of the MMD have the diameter range $0.098 \leq d_p/SMD \leq 3.5$ and contain 99.7% of the spray mass. This information, combined with Eq. (6), means that $We_{gSMD} = 1.8$ and 66 define limiting conditions where virtually no drops or all drops undergo secondary breakup.

The limits of secondary breakup are shown in Fig. 8 along with the primary breakup correlation. Noting that it is difficult to remain in the atomization breakup regime for values of $We_{g0}/Re_{l0}^{1/2}$ much lower than the present test range, it is evident that most sprays involve significant levels of secondary breakup. Additionally, as jet velocities increase, a progressively larger fraction of the drops undergo secondary breakup. Thus, at high relative velocities, approaching conditions where the locally homogeneous flow approximation is appropriate [3, 11], secondary breakup becomes a dominant mechanism within multiphase mixing layers.

Another effect of secondary breakup is that it tends to make We_{gSMD} more nearly constant as relative velocities change than is the case for primary breakup, correlated by Eq. (5). This helps explain the durability of primary breakup correlations like Eqs. (1) and (2) with their strong effect of relative velocity on the SMD; that is, any contamination of the measurements by secondary breakup helps support the trends of these relationships. Since past measurements of drop sizes were carried out after the sprays became dilute, it is probable that they involved significant levels of secondary breakup. Additionally, the results of secondary breakup do not depend on the jet diameter, which also helps explain the weak, or absent, jet diameter effects seen in early correlations of primary breakup [14–18]. Finally, present measurements in the fully developed primary breakup regime were obtained at some distance from the jet exit, x/d greater than 6.25, providing an opportunity to convect smaller drops from primary breakup near the jet exit, as well as drops having undergone secondary breakup, into the region of the measurements. This could explain the smaller power of $We_{g0}/Re_{l0}^{1/2}$ seen in the empirical correlation of the data, Eq. (5), than expected from Eq. (4).

CONCLUSIONS

Primary breakup within the multiphase mixing layer of the near injector region of large scale pressure atomized sprays was studied, considering nonturbulent slug flow at the jet exit. The major conclusions of the study are as follows:

1. Drop size distributions after primary breakup in the mixing layer approximate Simmons' universal root normal distribution with MMD/SMD = 1.2 and can be characterized by a single parameter, e.g., the SMD.
2. Drop properties after primary breakup tended to vary with increasing distance from the jet exit and then approach nearly constant values in a fully developed primary breakup regime for Re_{l0} greater than roughly 10^5. This transition process and drop properties near the injector, however, are probably apparatus dependent because liquid vorticity due to nonuniform velocities and wall boundary layers at the jet exit can influence primary breakup and these characteristics are affected by injector passage design.
3. Existing correlations of SMD after primary breakup based on unstable wave growth due to Taylor [14], Levich [15], Mayer [17], and Adelberg [18] were ineffective for correlating the present measurements. The main deficiencies were substantial overestimation of the rate of reduction of drop sizes with increasing relative velocities and inability to treat correctly effects of changes of liquid viscosity.
4. A reasonably good correlation of SMD in the fully developed primary breakup regime for various liquids, injector diameters, and relative velocities was achieved using Eq. (5). This expression was based on stripping type breakup due to boundary layer growth within the liquid along the windward side of surface waves, somewhat analogous to stripping type secondary breakup of drops.
5. The SMD and drop size distributions after primary breakup imply that most drops are subject to secondary breakup, more so as the parameter $We_{g0}/Re_{l0}^{1/2}$ increases. This means that secondary breakup, rather than collisions, is a major mechanism within multiphase mixing layer unless the flow involves impinging liquid jets. Additional evidence to support effects of secondary breakup in the multiphase mixing layer is reported in [2, 3].

Present results were limited to a small range of liquid/gas density ratios and particular slug flow injector designs; effects of density ratio and initial liquid vorticity conditions merit additional study as important variables affecting primary breakup properties. Furthermore, primary breakup near the end of the multiphase mixing layer should differ from present observations in the fully developed primary breakup regime because of the evolution of gas phase velocity distributions and instability (flapping) of the liquid core; therefore, primary breakup in this region deserves attention as well.

REFERENCES

1. G. A. Ruff, A. D. Sagar, and G. M. Faeth, Structure of the Near-Injector Region of Pressure-Atomized Sprays, *AIAA J.*, vol. 27, pp. 549–559, 1987.
2. G. A. Ruff, I. P. Bernal, and G. M. Faeth, Structure of the Near-Injector Region of Non-Evaporating Pressure-Atomized Sprays, *J. Prop. Power*, vol. 7, pp. 221–230, 1991.
3. G. A. Ruff, P.-K. Wu, I. P. Bernal, and G. M. Faeth, Continuous- and Dispersed-

Phase Structure of Dense Nonevaporating Pressure Atomized Sprays, *J. Prop. Power*, in press.
4 L. K. Tseng, G. A. Ruff, and G. M. Faeth, Effects of Ambient Gas Density on the Structure of Pressure Atomized Sprays, AIAA Paper No. 91-0690, 1991.
5 E. Giffen and A. Muraszew, *The Atomization of Liquid Fuels*, Wiley, New York, 1953.
6 A. H. Lefebvre, Airblast Atomization, *Prog. Energy Combust. Sci.*, vol. 6, pp. 233–216, 1980.
7 D. T. Harrje and F. H. Reardon, *Liquid Rocket Combustion Instability*, NASA SP-194, pp. 49–55, 1972.
8 M. J. McCarthy and N. A. Malloy, Review of Stability of Liquid Jets and the Influence of Nozzle Design, *Chem. Eng. J.*, vol. 7, pp. 1–20, 1974.
9 R. Clift, J. R. Grace, and M. E. Weber, *Bubbles, Drops and Particles*, Academic Press, New York, p. 346, 1978.
10 G. M. Faeth, Mixing, Transport and Combustion in Sprays, *Prog. Energ. Combust. Sci.*, vol. 13, pp. 298–345, 1987.
11 G. M. Faeth, Structure and Atomization Properties of Dense Turbulent Sprays, *Twenty-Third Symposium (International) on Combustion*, The Combustion Institute, Pittsburgh, pp. 1345–1352, 1990.
12 C. C. Miesse, Correlation of Experimental Data on Disintegration of Liquid Jets, *Ind. Eng. Chem.*, vol. 47, pp. 1690–1697, 1955.
13 W. E. Ranz, Some Experiments on Orifice Sprays, *Can. J. Chem. Eng.*, vol. 36, pp. 175–181, 1958.
14 G. I. Taylor, Generation of Ripples by Wind Blowing over a Viscous Liquid, *The Scientific Papers of Sir Geoffrey Ingram Taylor*, Vol. III, G. K. Batchelor, ed., Cambridge Univ. Press, Cambridge, England, pp. 244–254, 1963.
15 V. G. Levich, *Physicochemical Hydrodynamics*, Prentice Hall, Englewood Cliffs, N.J., pp. 639–646, 1962.
16 R. D. Reitz and F. V. Bracco, Mechanism of Atomization of a Liquid Jet, *Phys. Fluids*, vol. 25, pp. 1730–1742, 1982.
17 E. Mayer, Theory of Liquid Atomization in High Velocity Gas Streams, *ARS J.*, vol. 31, pp. 1783–1785, 1961.
18 M. Adelberg, Mean Drop Size Resulting From the Injection of a Liquid Jet into a High Speed Gas Stream, *AIAA J.*, vol. 6, pp. 1143–1147, 1968.
19. H. Jeffreys, On the Formation of Water Waves by Wind, *Proc. R. Soc. London Ser. A*, vol. A110, pp. 241–247, 1926.
20 M. A. Weiss and C. H. Worsham, Atomization in High Velocity Airstreams, *ARS J.*, vol. 29, pp. 252–258, 1959.
21. R. E. Phinney, The Breakup of a Turbulent Jet in a Gaseous Atmosphere, *J. Fluid Mech.*, vol. 6, pp. 689–701, 1973.
22. J. W. Hoyt and J. J. Taylor, Turbulence Structure in a Water Jet Discharging in Air, *Phys. Fluids*, vol. 20, pt. II, pp. S253–S257, 1977.
23 J. W. Hoyt and J. J. Taylor, Waves on Water Jets, *J. Fluid Mech.*, vol. 83, pp. 119–127, 1977.
24 J. W. Hoyt and J. J. Taylor, Effect of Nozzle Boundary Layer on Water Jets Discharging in Air, *Jets and Cavities*, J. H. Kim, O. Furuya, and B. R. Parkin, eds., ASME-FED, vol. 11, ASME, New York, pp. 93–100, 1985.
25 R. N. Smith and C. T. Wang, Contracting Cones Giving Uniform Throat Speeds, *J. Aerosp. Sci.*, vol. 11, pp. 356–360, 1944.
26 V. Rampee and A. K. M. F. Hussain, Influence of the Axisymmetric Contraction Ratio on Free Stream Turbulence, *J. Fluids Eng.*, vol. 108, pp. 506–515, 1976.
27 H. C. Simmons, The Correlation of Drop Size Distributions in Fuel Nozzle Sprays, *J. Eng. Power*, vol. 99, 309–319, 1977.

28 H. Schlichting, *Boundary Layer Theory*, 7th ed., McGraw-Hill, New York, p. 599, 1979.
29 H. Hiroyasu, M. Shimizu, and M. Arai, The Breakup of a High Speed Jet in a High Pressure Gaseous Environment, Univ. Of Wisconsin, Madison, ICLASS-82, 1982.
30 A. A. Ranger and J. A. Nicholls, Aerodynamic Shattering of Liquid Drops, *AIAA J.*, vol. 7, pp. 285–290, 1969.

APPENDIX F: WU ET AL. (1992)

PRIMARY BREAKUP IN GAS/LIQUID MIXING LAYERS FOR TURBULENT LIQUIDS

by

P.-K. Wu, L.-K. Tseng and G.M. Faeth†
Department of Aerospace Engineering
The University of Michigan, Ann Arbor, Michigan

Abstract

An experimental study of primary breakup of turbulent liquids in gas/liquid mixing layers is described. The experiments involved mixing layers along large round liquid jets (3.6, 6.4 and 9.5 mm dia.) injected at various velocities into still air and helium at atmospheric pressure with fully-developed turbulent pipe flow at the jet exit. Liquids studied included water, glycerol (42% glycerin by mass) and n-heptane. Pulsed shadowgraph photography and holography were used to find conditions where turbulent primary breakup was initiated as well as drop sizes and velocities after primary breakup. Drop sizes after primary breakup satisfied Simmons' universal root normal distribution with MMD/SMD = 1.2; therefore, they could be characterized solely by their SMD. Mass weighted mean streamwise and crosstream drop velocities after primary breakup were comparable to mean streamwise and crosstream rms fluctuating velocities in the liquid, respectively, with effects of mean velocity distributions in the jet passage reflected by somewhat lower streamwise drop velocities near the jet exit. Drop size properties after turbulent primary breakup were identical for tests in either air or helium and could be correlated reasonably well by phenomenological analyses considering effects of surface tension and liquid turbulence properties alone. However, limited data in the literature suggests that aerodynamic effects begin to influence drop sizes after primary breakup at ambient gas densities greater than those considered during the present experiments.

† Author to whom correspondence should be sent.

Introduction

Primary breakup to form drops near liquid surfaces is an important fundamental process with applications to liquid atomization, gas injection into liquids and multiphase flow in tubes, among others. Primary breakup is important because it determines the initial properties of the dispersed phase which affects mixing rates, secondary breakup, collisions and separated flow within the dispersed flow region. Motivated by these considerations, an experimental study of primary breakup of nonturbulent liquids in gas/liquid mixing layers recently was completed by Wu et al. [1]. The objective of the present investigation was to extend this work to consider primary breakup of turbulent liquids because this condition is encountered in practice as well. Similar to Ref. 1, measurements were carried out within the gas/liquid mixing layer at the periphery of round liquid jets in still gases. This region corresponds to the near-injector dense-spray region of a pressure-atomized spray for atomization breakup conditions.

Past studies of pressure-atomized sprays have established that spray properties are influenced by turbulence at the jet exit. First of all, the early studies of pressure atomization by De Juhasz et al.[2] and Lee and Spencer [3] showed that both atomization quality and mixing rates differed for laminar and turbulent flow at the jet exit. Next, Grant and Middleman [4] and Phinney [5] observed that jet stability and the onset of breakup were affected by turbulence at the jet exit as well. Finally, Hiroyasu et al.[6] and Chehroudi et al.[7] studied the length of the all-liquid core near the jet exit, which resembles the potential core region of single-phase jets. Their results suggest that the length of the liquid core is affected by turbulence at the jet exit, somewhat analogous to the effect of jet exit turbulence on the length of the potential core of single-phase jets.

The recent studies of Ruff et al.[8-10] and Tseng et al.[11,12] also have helped to quantify effects of turbulence at the jet exit on the mixing rates and structure of the

dispersed-phase region of pressure-atomized sprays. These experiments involved relatively large round water jets (9.5 and 19.1 mm dia.) in still air at ambient pressures of 1-8 atm, with both nonturbulent slug flow and fully-developed turbulent pipe flow at the jet exit. These experiments emphasized atomization breakup conditions, where drops begin to form right at the jet exit and the liquid core is completely surrounded by the dispersed-flow region. This was done because the atomization breakup regime dominates most practical applications due to the small range of liquid flow rates and poor atomization qualities of the other breakup regimes. [8]

The measurements of Ruff et al.[8-10] and Tseng et al.[11,12] involved mean liquid volume fraction distributions using gamma-ray absorption and dispersed-phase properties using pulsed holography. The measurements of liquid volume fraction distributions showed much faster mixing rates for fully-developed turbulent pipe flow than for nonturbulent slug flow at the jet exit [8,11]. Observed effects of jet exit turbulence on mean liquid volume fraction distributions were predicted reasonably well (for mean liquid volume fractions greater than 0.2) using the locally homogeneous flow (LHF) approximation, where interphase transport rates are assumed to be infinitely fast, i.e., relative velocities between the phases are ignored. This suggests significant effects of liquid turbulence on primary breakup because it represents the first stage of mixing. The pulsed holography measurements of drop sizes confirmed effects of liquid turbulence on primary breakup [9,10,12]. In general, drop sizes after primary breakup were larger for turbulent than nonturbulent liquids, approaching the dimensions of spatial integral scales in the liquid for turbulent primary breakup. Additionally, relative velocities between the phases were large near the liquid surface, implying significant effects of separated flow in the dispersed-flow region. It was inferred that liquid turbulence properties dominated the outcome of turbulent primary breakup at atmospheric pressure, with aerodynamic effects becoming more important at elevated pressures and causing drop sizes after primary

breakup to become smaller [9,10,12]. However, the mechanism of turbulent primary breakup was not pursued in any detail in these studies due to the relatively limited data base on drop properties near the liquid surface (water jets having only one jet exit velocity).

The previous review of the literature shows that past work has established significant differences between nonturbulent and turbulent primary breakup and has demonstrated that turbulent primary breakup enhances the mixing rates of pressure-atomized sprays. However, existing information about turbulent primary breakup is limited and the mechanism is not understood. In particular, no methods are available to estimate either the conditions for the onset or the subsequent outcome of turbulent primary breakup which impedes consideration of separated flow phenomena in the dispersed flow region.

In order to help fill this gap in the literature, the objectives of the present investigation were to observe the onset and outcome of turbulent primary breakup for a wide range of test conditions, and to use the measurements, as well as results available from Refs. 9 and 10, to develop approximate theories of these processes. Present experiments involved relatively large round liquid jets (3.6, and 6.4 mm dia.) in still gases at atmospheric pressure with fully-developed turbulent pipe flow at the jet exit. Effects of flow dynamics and liquid physical properties were studied by considering various jet exit velocities and liquids (water, 42% glycerol and n-heptane). Potential aerodynamic effects were studied by carrying out experiments in both air and helium at atmospheric pressure, providing roughly a 7:1 gas density variation while avoiding tests at low ambient pressures where problems of cavitation and enhanced drop vaporization can be encountered. Measurements included pulsed shadowgraph photography and holography to find conditions for the onset of turbulent primary breakup as well as drop sizes and velocities produced by this breakup mechanism.

The paper begins with a description of experimental methods. Results are then considered treating flow visualization, drop size distributions, drop velocities, onset of breakup and drop sizes and shapes, in turn. The paper concludes with discussion of potential aerodynamic effects on turbulent primary breakup, based on recent measurements in air at elevated ambient pressures due to Tseng et al.[12].

Experimental Methods

Apparatus

The following description of experimental methods will be brief because they are similar to the earlier study of nonturbulent primary breakup [1]. The apparatus consists of a pneumatically driven piston/cylinder arrangement containing the liquid to be injected with the liquid outlet centered on the axis of the piston. The piston has a diameter of 64 mm and a stroke of 200 mm, yielding a liquid sample size of roughly 600 ml. The outlet of the cylinder was rounded to prevent cavitation and was followed by a constant diameter passage having a length to diameter ratio ≥ 41, to yield nearly fully developed turbulent pipe flow at the jet exit, similar to Ruff et al.[8]. Jet passage diameters considered during the tests were 3.6 and 6.4 mm. Injection was vertically downward with the liquid collected in a baffled tub and then discarded. Tests in air were carried out by injecting directly into room air. Tests in helium were carried out within a windowed cylindrical chamber (300 mm diameter, 1300 mm long) that could be evacuated and backfilled with helium to atmospheric pressure. Instrumentation was mounted rigidly; therefore, various positions in the flow were studied by traversing the entire injector assembly.

The piston/cylinder arrangement was filled with the test liquid while venting trapped air or helium from just below the piston face. Operation was initiated by admitting high-pressure air to the upper side of the piston through a solenoid valve which forced the liquid through the jet passage. Total times of injection were 180-1400 ms due to the finite liquid

sample size. These relatively short time periods were not problematical, however, because flow development times are generally less than 1% of the flow time for the near-injector region where measurements were made while pulsed photography and holography only required times in the range 1-32 μs for triggering and data accumulation. Jet exit velocities at the time of the measurements were calibrated using an impact plate as described in Ref. 1.

Instrumentation

Photography. Pulsed shadowgraph photography was used to measure properties at the onset of turbulent breakup, where relatively low dispersed-phased concentrations makes this approach feasible and convenient. The holocamera was used for this purpose, operating in the single-pulse mode with the reference beam blocked to yield a shadowgraph rather than a hologram. The optics were arranged to give a primary magnification of 3-8:1 on the film. Drops were sized using an image analysis system in the same manner as the holography measurements to be discussed next. These photographs also were used to find the streamwise location of the onset of turbulent primary breakup. Experimental uncertainties (95% confidence) of this determination were generally less than 40%, the relatively large value being due to innate statistical variations of this event, i.e., whether drops completely detached from ligaments at the time the photograph was obtained.

Holography. The double-pulse holocamera and reconstruction systems were similar to the arrangements used by Ruff et al.[9,10]. Present optics provided a 5-6:1 magnification of the hologram image itself, coupled with reconstruction optics that allowed measurements of drop diameters as small as 5 μm. The ruby laser could be double pulsed with pulse separation times as short as 1 μs, to accommodate measurements of both large streamwise and small crosstream velocities of drops. The properties of the reconstructed sprays were analyzed using a Gould FD 5000 image display system with a field of view of

1.4 x 1.6 mm. Various locations in the hologram reconstructions could be observed by traversing the hologram in two directions and the video camera of the display system in the third direction.

Drops and other ellipsoidal objects were sized by measuring their maximum and minimum diameters through the centroid of the image. Assuming ellipsoidal shapes, the diameter of these objects was taken to be the diameter of a sphere having the same volume, $d_p^3 = d_{min}^2 d_{max}$. The shape of the object was described by its ellipticity, defined as $e_p = d_{max} / d_{min}$. More irregular objects were sized by finding the area and perimeter of their image, and computing the maximum and minimum diameters of an ellipsoid matching these properties: given these parameters, d_p and e_p were found as before. Results at each condition were summed, considering 20-400 elements, to provide drop size distributions, mass median diameter (MMD), Sauter mean diameter (SMD) and the volume averaged ellipticity, e_p. Experimental uncertainties generally were dominated by finite sampling limitations because there are relatively few drops after turbulent primary breakup due to relatively large drop sizes. Within the limitations of definitions of liquid element sizes and ellipticities, which are difficult to quantify, estimated experimental uncertainties (95% confidence) are estimated to be less than 38% for MMD and SMD and 39% for e_p.

Drop velocity measurements were based on the motion of the centroid of the image, allowing streamwise and crossstream velocities to be computed from the known intervals between laser pulses. Directional ambiguity was resolved by using different light intensities for the two laser pulses because the stronger pulse yielded a sharper image of the drops. Results at each condition were summed, considering 20-400 elements, to obtain mass-weighted (Favre) averaged drop velocities. Experimental uncertainties were dominated by finite sampling limitations, with the accuracy of finding the centroid of large irregular liquid elements also being a factor for the relatively small radial velocities that

were observed. The resulting experimental uncertainties (95% confidence) are estimated to be less than 19% for $\bar{u}_p$ and less than 60% for the much smaller values of $\bar{v}_p$.

Test Conditions

Test conditions are summarized in Table 1. A series of holograms for the region along the liquid surface were available from Ruff et al.[9,10], and were used to provide results for water in still air for a jet exit diameter of 9.5 mm at atmospheric pressure. The remainder of the measurements were obtained using the present apparatus with jet exit diameters of 3.6 and 6.4 mm. All injectors involved fully-developed turbulent pipe flow at the jet exit with passage length-to-diameter ratios of 41 for injection into air and 210 for injection into helium. In particular, Ruff et al.[8] measured flow properties at the exit of the 9.5 mm passage, finding distributions of mean and rms fluctuating velocities in agreement with results in the literature for the corresponding range of Reynolds numbers [13,14], within experimental uncertainties. In view of this, streamwise and radial integral length scales of the flow at the jet exit were taken to be 0.4d and d/8, respectively, based on measurements of Laufer for fully developed turbulent pipe flow cited in Hinze [14].

The streamwise positions of present measurements involved x/d in the range 0.2-100. Earlier work [4,6,7], indicates that the length of the liquid core was in excess of x/d = 200 for present test conditions. Thus, present measurements involve breakup at the surface of the liquid core rather than breakup of the entire liquid column itself

Test liquids included water, a glycerin/water mixture (42% glycerin, by mass) and n-heptane. All liquids were injected into still air, while water was injected into still helium as well, in order to assess potential aerodynamic effects as suggested by Tseng et al. [12]. This provided the following ranges of fluid properties: liquid/gas density ratios of 590-

6230, liquid viscosities of 3.94-34.66 × 10^{-4} kg/ms and surface tensions of 2.00-7.08 × 10^{-2} N/m^2. The liquid properties were verified as described in Ref. 1.

Jet exit velocities were in the range 16-109 m/s, yielding jet dynamic parameters as follows: Re_{fd} of 110,000-780,000, We_{gd} of 12-1240, We_{fd} of 230,000-1,090,000 and Oh_d of 0.0011-0.0052. Most test conditions involved $We_{fd} > 8$ and $We_{gd} > 40.3$ which places them in the atomization breakup regime where breakup should begin right at the jet exit according to jet breakup criteria for nonturbulent liquids due to Miesse [15] and Ranz [16]. A few test conditions for water were in the wind-induced breakup regime, where breakup begins along the sides of the liquid jet at some distance from the jet exit, according to the criteria of Refs. 15 and 16. Actually, the first appearance of drops from turbulent primary breakup is only crudely described by the criteria of Refs. 15 and 16 and always occurred at some distance from the jet exit: this will be discussed later in more detail.

Results and Discussion

Flow Visualization

Consideration of the results will begin with visualization of the flow in order to provide insight concerning the general nature of the turbulent primary breakup process. Shadowgraphs of the flow near the liquid surface at various distances from the jet exit are illustrated in Fig. 1. These results are for water injection into still air and d = 3.6 mm, with the relatively small injector diameter helping to minimize obscuration problems of the shadowgraph technique. The direction of motion of the liquid in the photographs is vertically downward, which corresponds to the orientation of the experiment. Three photographs are shown : one right at the jet exit (which can be seen at the top of this photograph) in the region of initiation of breakup, and the other two centered at x/d = 10 and 50, respectively. A 0.9 mm diameter pin is visible in the latter two photographs to provide a size and distance reference. The liquid core is to the left in all three photographs.

The photographs of Fig. 1 illustrate a number of general features of the liquid surface during turbulent primary breakup. First of all, even though the test condition is well within the atomization breakup regime defined by Refs. 15 and 16 (e.g., $We_{gd} = 72$), where breakup should begin right at the jet exit, the surface just becomes roughened or distorted very close to the jet exit while the first appearance of drops is deferred to x/d of roughly 0.3. A second feature of the liquid surface is that its mean position bulges outward within the first few diameters in the streamwise direction. Predictions based on the LHF approximation suggest that this is due to evolution of the mean velocity profile in the liquid from turbulent pipe flow conditions to a nearly flat profile consistent with the relatively low effects of drag on the liquid surface from the gas [8,11]. Another property of the liquid surface is that the scale of surface distortions progressively increases with increasing distance from the jet exit, in fact, small scale distortions are not even superimposed on the large wave-like structures seen at x/d = 50. Similar behavior was observed by Ruff et al. [8] for turbulent liquid jets in the first wind-induced breakup regime in the region prior to the onset of breakup; in particular, the liquid surface exhibited fine-grained roughness near the jet exit, with the surface becoming smoother and larger-scale irregularities appearing as the distance from the jet exit increased. This behavior can be attributed to two effects. First of all, small disturbances complete their growth more rapidly than large disturbances (as discussed later) so that they should appear first. The second effect involves reduced levels of turbulence production as mean velocities become more uniform in the liquid. This causes the turbulence to decay with increasing distance from the jet exit, with the small-scale high wave number range of the turbulence spectrum disappearing first, tending to reduce fine-grained distortion of the liquid surface accordingly. It seems likely that similar processes continue to act even in the presence of primary breakup yielding the properties of turbulent

distortion of the liquid surface seen in Fig. 1. Finally, the ligament-like structures protruding from the liquid surface exhibit little effect of drag from the gas phase — being randomly oriented from the liquid surface rather than predominantly deflected backward toward the jet exit due to drag from the more slowly moving gas [19]. In particular, tests in still air and helium yielded essentially the same results for comparable liquid jet conditions, in spite of a nearly order of magnitude change of We_{gd} and ρ_f/ρ_g, which normally control aerodynamic effects on primary breakup [1,2]. This suggests that the primary breakup process is dominated by the properties of the liquid turbulence rather than aerodynamic stripping for present test conditions. Such behavior is not surprising in view of the relatively large size of the ligaments and their relatively short residence times protruding into the flow: consideration of velocity relaxation times for drops of comparable size [9,10] indicates that the ligaments do not appreciably accommodate to local gas velocities in the period while they are attached to the surface.

Turning to drop properties seen in Fig. 1, it is evident that drop diameters near the liquid surface progressively increase with distance from the jet exit, similar to the scale of surface distortions. Additionally, examination of the surface distortion of individual ligaments, as well as drops apparently associated with some ligaments, suggests that separation of drops from attached ligaments occurs by a process analogous to Rayleigh breakup, i.e., the ligaments act somewhat like liquid jets in the Rayleigh breakup regime. Some of the larger ligament-like drops in the flow appear to be undergoing additional division by Rayleigh breakup as well. Other features of the flow are similar to earlier observations of the dispersed flow region for turbulent primary breakup conditions [9,10,12]: the region of the liquid surface has the largest and most irregular drops with smaller round drops near the edge of the flow, suggesting significant effects of secondary breakup; drop number densities increase with increasing distance from the jet exit but liquid volume fractions remain surprisingly low, tending to minimize potential effects of

collisions; and the width of the dispersed flow region progressively increases with increasing distance from the jet exit because drops have more residence time to move away from the surface due to their initial radial velocities after breakup and effects of turbulent dispersion.

Hologram reconstructions of the flow near the liquid surface for various liquid velocities at a fixed distance from the jet exit are illustrated in Fig. 2. These results are for water injection into still air at x/d = 10 with d = 6.4 mm. The direction of motion on the photographs is vertically downward and the 0.9 mm diameter reference pin is present as before, however, this time the liquid core is to the left of the photographs. Conditions at three liquid velocities are shown: 22, 40 and 81 m/s.

Significant effects of liquid velocity on the distortion of the liquid surface can be seen in the photographs of Fig. 2. First of all, while the size of the larger scale disturbances are similar for all three velocities (a property that was more evident by observing larger sections of the surface than shown in Fig. 2), the smallest scale disturbances become progressively smaller as the liquid velocity increases. This behavior also is similar to the distortion of the surface of turbulent liquid jets before primary breakup begins, where large scale features are not strongly affected by the jet Reynolds number but increasing Reynolds numbers increases the degree of fine-grained surface roughness [8]. This appears to be an effect of the power spectrum of the liquid turbulence, where the kinetic energy available to distort the surface at high wave numbers increases as the Reynolds number (which is proportional to the liquid velocity for the conditions of Fig. 2) increases. In a sense, this process is the inverse of the effect of distance from the jet exit seen in Fig. 1, where decay of the turbulence affects the high wave numbers first, tending to reduce the degree of fine-grained distortion of the surface with increasing distance from the jet exit. Finally, the direction of the ligaments protruding from the surface is not

particularly correlated with the relative velocity of the gas, even at the highest relative velocity. This suggests that the motion of the ligaments is largely the result of randomly directed liquid velocity fluctuations, with aerodynamic drag forces playing a secondary role for present test conditions (conditions where aerodynamic effects could be important will be discussed later).

Similar to Fig. 1, drop properties after primary breakup in Fig. 2 generally are related to the properties of the distortion of the liquid surface. Thus, [illegible]s tend to decrease, similar to the reduction of the size of surface disturbances or attached ligaments, as the liquid velocity increases. It also is seen that the number density of drops near the liquid surface increases as the relative velocity increases. This mainly is caused by the reduction of drop sizes with increasing relative velocities because liquid volume fractions in the dispersed phase are relatively independent of flow conditions for the high jet Reynolds numbers of present tests [8,9,11,12].

Drop Size Distributions

Drop size distributions after turbulent primary breakup were measured locally for all present test conditions. It was found that the size distribution functions agreed with Simmons' [17] universal root normal distribution function with the ratio MMD/SMD = 1.17 and the 95% confidence interval for this ratio being 1.11-1.23. This behavior agrees with earlier measurements of drop size distributions in sprays which find MMD/SMD = 1.20 with similar 95% confidence intervals: Ruff et al.[10] and Tseng et al.[12] for conditions along the liquid surface and throughout the dispersed flow region for pressure atomized sprays with both nonturbulent and turbulent jet exit conditions, Wu et al.[1] after primary breakup of nonturbulent liquids, and the original recommendation of Simmons [17] based on observations of industrial sprays. Since the root normal distribution only has two moments, the best estimate of MMD/SMD = 1.2 implies that the entire drop size distribution is known if the SMD is known. Thus, drop sizes will be described in terms of SMD alone in the following.

Drop Velocities

Drop velocities after primary breakup will be considered next, in order to help define the dynamic properties of primary breakup. Available measurements of volume (mass) averaged streamwise and crosstream drop velocities, both normalized by $\bar{u}_o$, are plotted as a function of x/d in Fig. 3. The measurements include all the test liquids and jet diameters at various jet exit velocities for injection into still air, drawing results for d = 9.5 mm from Ruff et al.[9].

The normalized drop velocities for all test conditions illustrated in Fig. 3 generally correlate as functions of x/d, with the larger scatter for $\bar{v}_p/\bar{u}_o$ being consistent with earlier estimates of the larger experimental uncertainties of this velocity component due to its relatively small magnitude. Very near the jet exit, $\bar{u}_p/\bar{u}_o$ has a value of roughly 0.6 which increases to reach a value near unity for x/d > 20. This behavior can be explained by assuming that streamwise drop velocities after primary breakup are roughly the same as streamwise velocities near the liquid surface. In particular, LHF computations of flow properties show that mean velocities in the liquid evolve from distributions appropriate for fully-developed pipe flow to a nearly flat profile having a velocity roughly 0.92 $\bar{u}_o$ in the region x/d < 20, relatively independent of specific flow conditions for the high Reynolds numbers used in these tests [9,11]. Thus, the lower streamwise drop velocities near the jet exit are due to the retarding effects of the jet passage walls on streamwise velocities near the liquid surface in this region.

In a similar manner, crosstream drop velocities appear to be comparable to crosstream velocity fluctuations in the liquid from the results illustrated in Fig. 3. In

particular, $\tilde{v}_p/\bar{u}_o \approx 0.07$ for $x/d < 20$ with a tendency to decrease at larger values of x/d although this trend is not very clear due to scatter of the data. These values of $\tilde{v}_p/\bar{u}_o$ are compatible with velocity fluctuations for fully developed turbulent pipe flow (for turbulent pipe flow, maximum values of $\bar{v}'/\bar{u}_o$ and $\bar{u}'/\bar{u}_o$ are 0.05 and 0.10 from Refs. 13 and 14) and the rapid adjustment of velocity fluctuations near the surface of the liquid to the absence of the passage wall found from LHF computations [9,11]. These same calculations indicate that turbulence levels in the liquid decay proportional to $(x/d)^{-1/2}$ for $x/d > 20$ which may account for the tendency for $\tilde{v}_p/\bar{u}_o$ to decrease in this region. Taken together, the velocities of drops after turbulent primary breakup are typical of velocities in the liquid. This is not surprising due to the relatively large velocity relaxation times of the large drops that dominate the properties of mass averaged drop velocities [10].

Onset of Breakup

The properties of the onset of turbulent primary breakup will be considered next because they provide valuable clues about the turbulent primary breakup mechanism. Properties of interest include conditions for turbulent primary breakup to occur at all, the drop sizes formed at the onset of breakup and the distance from the jet exit where breakup begins. The problem will be addressed by extending the preliminary considerations of Ruff et al. [10], where the onset of breakup was associated with conditions where the momentum of turbulent fluctuations in the liquid was sufficient to overcome surface tension forces so that drops could be formed.

Some of the properties of the onset of turbulent primary breakup are illustrated in Fig. 4. These results involve measurements for water injected into still air at atmospheric pressure with d = 6.4 mm, showing the variation of drop sizes and the distance from the jet exit where breakup begins, SMD_i and x_i, as a function of the mean jet exit velocity. Correlations of these properties found from Eqs. (5) and (11) for $\Lambda = d/8$ from Hinze [14],

are shown along with the measurements; the development of the correlations will be discussed later.

The behavior of the onset of turbulent primary breakup illustrated in Fig. 4 is qualitatively similar to behavior in the second wind-induced breakup regime of nonturbulent liquid jets [4,5,14,15]. This involves breakup along the sides of the liquid jet, rather than the liquid column as a whole, with the point where breakup begins moving toward the jet exit as the jet exit velocity increases. The same behavior can be seen in Fig. 4 for turbulent primary breakup, with breakup beginning very close to the jet exit (approximating the atomization breakup regime) at the highest velocities. Another feature of the results is that the SMD of the drops at the onset of turbulent primary breakup becomes smaller as the point of initial breakup moves toward the jet exit. Thus, the initiation of breakup is associated with conditions where the smallest drops can be formed. This trend also is supported by the photographs of Fig. 1, where drop sizes after primary breakup progressively increase with increasing distance from the jet exit. Finally, as noted earlier, varying the density of the gas by nearly an order of magnitude had little effect on drop sizes after turbulent primary breakup for present test conditions, suggesting negligible aerodynamic effects with breakup controlled by liquid properties alone.

Approximate analysis to find properties at the onset of turbulent primary breakup will be based on the configuration illustrated in Fig. 5. This involves the formation of a drop from a turbulent eddy having a characteristic size ℓ, and a characteristic crosstream velocity relative to the surrounding liquid v_ℓ. The eddy is shown with an elongated shape because length scales in the streamwise direction are larger than in the crosstream direction for fully-developed turbulent pipe flow [13,14]. The eddy is assumed to be convected in the streamwise direction by the local mean velocity, which is taken to be $\bar{u}_o$ based on the

results discussed in connection with Fig. 3. The drop formed by the eddy also is assumed to have a diameter comparable to ℓ.

Based on present measurements (e.g., Figs. 1 and 4), as well as time scale considerations to be considered subsequently, the drops at the onset of turbulent primary breakup are the smallest drops that can be formed by this mechanism. The smallest drop that can be formed is either comparable to the smallest scale of the turbulence, the Kolmogorov microscale, or the smallest eddy that has sufficient kinetic energy relative to its immediate surroundings to provide the surface energy needed to form a drop — whichever is larger. For fully-developed turbulent flow, the Kolmogorov length scale can be estimated as follows [18]:

$$\ell_k = 4\Lambda/(4\Lambda\, \bar{u}_o'/\nu_f)^{3/4} \qquad (1)$$

where the streamwise integral length scale has been taken to be 4Λ, based on Laufer's measurements for fully-developed turbulent pipe flow [14]. For present test conditions, ℓ_k is in the range 1-10 μm, which is much smaller than the smallest drop size estimated from energy considerations, or observed experimentally, thus, only the latter requirement is relevant for present test conditions.

The second criterion for the smallest drop that can be formed can be found by equating the kinetic energy of an eddy of characteristic size ℓ_i, relative to its surroundings, to the surface energy required to form a drop. This yields

$$\pi \rho_f \ell_i^3 v_{\ell i}^2/12 \sim \pi\, \ell_i^2 \sigma \qquad (2)$$

where only proportionality is implied to account for effects of ellipticity, nonuniform velocities within the eddy and the efficiency of conversion of kinetic energy into surface energy. In order for drops to be formed at all, ℓ_i must be less than the largest eddies present, which is comparable to Λ [10], while $\ell_k < \ell_i$ by definition for this primary

breakup mechanism. Thus, it is reasonable to assume that ℓ_i is within the inertial range of the turbulence spectrum where ℓ_i and $v_{\ell i}$ are related as follows [18]:

$$v_{\ell i} \sim \bar{v}_o'\,(\ell_i/\Lambda)^{1/3} \qquad (3)$$

where variations of turbulence properties within the liquid have been ignored. Combining Eqs. (2) and (3), setting $SMD_i \sim \ell_i$, and assuming that turbulence properties in the liquid can be approximated by jet exit turbulence properties, the following equation is obtained for the SMD at the onset of breakup:

$$SMD_i/\Lambda = C_{si}(\bar{u}_o/\bar{v}_o')^{6/5} We_{f\Lambda}^{-3/5} \qquad (4)$$

where C_{si} is an empirical constant involving the various proportionality constants. With fully-developed turbulent pipe flow at the jet exit, $\bar{v}_o'/\bar{u}_o$ also is essentially constant [13,14], so that SMD_i/Λ should only be a function of $We_{f\Lambda}$ for present test conditions.

Present measurements of SMD_i are plotted in terms of the variables of Eq. (4) in Fig. 6. The correlation of the data for all three liquids and jet diameters generally is within the scatter anticipated based on experimental uncertainties. The power of $We_{f\Lambda}$ for the correlation of the data is not -3/5 as suggested by Eq. (4), however, and can be represented better by the following empirical fit that is shown on the plot:

$$SMD_i/\Lambda = 133\, We_{f\Lambda}^{-0.74} \qquad (5)$$

The standard deviations of the coefficient and power in Eq. (5) are 10 and 7%, respectively, and correlation coefficient of the fit is 0.97. The reduction of the power of $We_{f\Lambda}$ from -3/5 in Eq. (4) to -0.74 in Eq. (5) is statistically significant but is not large in view of the approximations used to develop the correlating expression and experimental uncertainties. The coefficient of Eq. (5) is relatively large but this can be anticipated from Eq. (4) if C_{si} is on the order of unity because $(\bar{u}_o/\bar{v}_o')^{6/5}$ is large for fully-developed

turbulent pipe flow [14]. Finally, SMD_i estimates from Eq. (5) are seen to be in excellent agreement with the specific measurements for water illustrated in Fig. 4.

The next step is to develop an expression for the distance from the jet exit, x_i, where turbulent primary breakup is initiated. To find x_i, it is assumed that the drop-forming eddy convects along the liquid surface with a streamwise velocity $\bar{u}_o$, based on the results of Fig. 3. Then the location of the onset of turbulent primary breakup becomes:

$$x_i = \bar{u}_o \tau_i \tag{6}$$

where τ_i is the time required for an eddy having a characteristic size, ℓ_i, to form a drop. There are several characteristic times that can be associated with the time to form a drop. First of all, the protrusion of ligaments and their division into drops, seen in Figs. 1 and 2, suggests use of the characteristic time for Rayleigh breakup. A second possibility is the characteristic time of the eddy, $\tau_i \sim \ell_i/v_{\ell i}$, assuming that loss of the correlation of velocities near the surface causes the protruding ligament to become thin near its base and rapidly separate by Rayleigh breakup. A third possibility involves aerodynamic secondary breakup of the protruding ligament discussed by Tseng et al.[12]. Breakup times for this mechanism have not been established. However, secondary breakup times are relatively independent of the mode of breakup so that the correlation of Ranger and Nicholls [19] provides a reasonable estimate: this implies $\tau_i \sim \ell_i(\rho_f/\rho_g)^{1/2}/\bar{u}_o$ if the velocity of the gas near the liquid surface is assumed to be small. Breakup times of all three mechanisms are of the same order of magnitude for present test conditions; however, similar results for injection into air and helium in spite of significant potential changes of τ_i anticipated from the Ranger and Nicholls [19] correlation, suggests that the aerodynamic mechanism can be discarded. The remaining choice between Rayleigh breakup and eddy characteristic times is not obvious. However, the time for Rayleigh breakup clearly is shortest near the jet exit,

where onset of breakup occurs, and is supported by the appearance of the flow; therefore, this breakup time will be used in the following.

Considering Rayleigh breakup, ℓ_i is taken to be the diameter of a protruding ligament, having a jetting velocity of $v_{\ell i}$, from which the first drops are formed. Weber [20], found that the breakup length, L_i, of the liquid column for Rayleigh breakup can be expressed as follows:

$$L_i/\ell_i = (\rho_f \ell_i v_{\ell i}^2/\sigma)^{1/2} + 3\,\mu_f v_{\ell i}/\sigma \tag{7}$$

For present conditions, the second term in Eq. (7) is small and will be ignored in the following, although it could be a factor for very viscous liquids. Then assuming that τ_i is proportional to the time required for a ligament to grow to its breakup length, $L_i/v_{\ell i}$, τ_i becomes:

$$\tau_i \sim (\rho_f \ell_i^3/\sigma)^{1/2} \tag{8}$$

which is independent of $v_{\ell i}$. An expression for x_i is then found by substituting Eq. (8) into Eq. (6) and letting $SMD_i \sim \ell_i$ as before:

$$x_i/\Lambda \sim (SMD_i/\Lambda)^{3/2} We_{f\Lambda}^{1/2} \tag{9}$$

The results of Eq. (9) indicate that drop sizes increase with increasing distance from the jet exit, supporting the idea that the onset of turbulent primary breakup involves the smallest drops that can be formed. Finally, eliminating SMD_i from Eq. (9), using Eq. (4), the following correlating expression for x_i is obtained:

$$x_i/\Lambda = C_{xi}\,(\bar{u}_o/\bar{v}_o')^{9/5} We_{f\Lambda}^{-0.4} \tag{10}$$

where C_{xi} is a constant of proportionality and $(\bar{v}_o'/\bar{u}_o)$ is a constant for fully-developed turbulent pipe flow at the jet exit.

Present measurements of x_i are plotted in terms of the variables of Eq. (10) in Fig. 7. The correlation of the data for all three liquids and jet diameters is reasonably good in view of the relatively large experimental uncertainties of x_i, similar to the correlation of SMD_j in Fig. 6. As before, however, the power of $We_{f\Lambda}$ for the correlation of the data is not -0.4 as suggested by Eq. (10) but can be represented better by the following empirical fit which is shown on the plot:

$$x_j/\Lambda = 3980\, We_{f\Lambda}^{-0.67} \tag{11}$$

The standard deviations of the coefficient and power in Eq. (11) are 10 and 12%, respectively, and the correlation coefficient of the fit is 0.91. The large value of the coefficient of Eq. (11), even if C_{xi} is on the order of unity, can be anticipated from Eq. (10) because $(\bar{u}_o/\bar{v}_o')^{9/5}$ is quite large for turbulent pipe flow. Finally, x_i estimates from Eq. (11) are seen to be in excellent agreement with the measurements for water illustrated in Fig. 4.

A check of the internal consistency of the correlations for SMD_j and x_i is useful for developing an expression for the variation of SMD with distance from the injector. This can be done by combining the phenomenological expressions of Eqs. (4) and (10) to obtain an expression directly relating x_i and SMD_j, similar to Eq. (9), as follows:

$$x_j/\Lambda = (C_{xj}/C_{si}^{3/2})(SMD_j/\Lambda)^{3/2} We_{f\Lambda}^{1/2} \tag{12}$$

The coefficient of this expression is independent of $\bar{v}_o'/\bar{u}_o$ and is expected to have a value on the order of unity. Repeating the same exercise using the best fit correlations of Eqs. (5) and (11) yields:

$$x_j/\Lambda = 1.43[\,(SMD_j/\Lambda)^{3/2} We_{f\Lambda}^{1/2}]^{1.08} \tag{13}$$

Equation (13) is seen to be consistent with Eq. (12): the coefficient is on the order of unity and the power on the right-hand-side of Eq. (13) is not statistically different from unity in view of the standard deviations of the powers in Eqs. (5) and (11) — both as anticipated.

Drop Sizes and Shapes

Drop Sizes. The approach used to find an expression for the variation of SMD with distance from the jet exit was similar to the method used to find x_j. First of all, it is reasonable to assume that drops near the liquid surface have been formed recently due to primary breakup because they have relatively large radial velocities (see Fig. 3). Additionally, the SMD is dominated by the largest drops in the drop size distribution; therefore, it also is plausible that the SMD is proportional to the largest drop that can be formed at a particular position, i.e., in the time available for the flow along the liquid surface to reach the position in question. Then, adopting the Rayleigh breakup mechanism and letting SMD – ℓ, as before, a procedure similar to the derivation of Eq. (9) yields the following expression for the variation of SMD with distance from the jet exit:

$$SMD/\Lambda = C_{sx}\,[x/(\Lambda\, We_{f\Lambda}^{1/2})]^{2/3} \tag{14}$$

where C_{sx} is a constant of proportionality that should be on the order of unity.

Under present assumptions, the principles relating SMD to x are the same for both the onset of breakup and at larger distances from the jet exit. Thus, comparing Eqs. (13) and (14) suggests that SMD/Λ should be correlated as a function of $x/(\Lambda\, We_{f\Lambda}^{0.54})$ for consistency. Available measurements from the present study for injection into still air and helium at atmospheric pressure, including onset of breakup conditions, as well as from Refs. 9 and 10 for injection into still air at atmospheric pressure, are plotted in this manner in Fig. 8. Two correlations of the data are shown on the plot as well: the best fit of all the

data and Eq. (13) for onset of breakup conditions alone. The best fit correlation of all the data is:

$$SMD/\Lambda = 0.69[x/(\Lambda\, We_{f\Lambda}^{0.54})]^{0.57} \qquad (15)$$

The standard deviations of the coefficient and power of Eq. (15) are 14 and 3%, respectively, and the correlation coefficient of the fit is 0.98. Notably, results for injection into still air and helium at atmospheric pressure essentially are the same, suggesting negligible aerodynamic effects over the present test range, as discussed earlier.

Differences between the two correlations illustrated in Fig. 8 are small in comparison to experimental uncertainties so that drop formation both at the onset of breakup and at distances farther from the jet exit appears to be similar. The SMD of the smallest drops, formed at the onset of breakup, are in the range 10-20 μm which is roughly an order of magnitude larger than the Kolmogorov length scales for these test conditions. The characteristics of turbulent primary breakup should change when breakup involves Kolmogorov-sized drops which is an interesting issue for future study. The largest SMD observed in the data base illustrated in Fig. 8 approaches the order of magnitude of the radial integral scales of the turbulence. Somewhat larger scale drops are feasible because one-dimensional turbulence spectra still have significant energy at scales somewhat larger than the radial integral scale [18]. However, much larger SMD than those shown in Fig. 8 are unlikely for round liquid jets because of the finite length of the liquid core. This is indicated in Fig. 8 using the correlation for liquid core length (or jet breakup length) from Grant and Middleman [4]:

$$L_c/d = 8.51\, We_{fd}^{0.32} \qquad (16)$$

where the range of L_c/d shown in the figure results from the variation of We_{fd} over the present test range (note that $\Lambda = d/8$ has been used to plot Eq. (16) in Fig. 8, as before). A

more recent correlation of liquid core length for atomization breakup conditions, due to Chehroudi et al. [7], yields core length limitations similar to those pictured in Fig. 8 but the range of L_c/d is somewhat broader because it does not involve We_{fd} explicitly. The fact that the SMD approaches Λ near the end of the liquid core, and thus is comparable to the diameter of the liquid core itself, is consistent with the liquid column breaking up as a whole in this region.

Ellipticity. Measurements of volume averaged ellipticity are plotted as a function of x/d in Fig. 9. The data shown consists of present measurements, which includes onset of breakup conditions, as well as the measurements of Refs. 9 and 10. The measurements exhibit significant scatter, particularly at large x/d, and no correlation in terms of x/d should be implied by the plot. Nevertheless, the results help to complete the physical picture of the flow.

The measurements of e_p in Fig. 9 have values near unity at low x/d, which then increase toward a value of roughly 2 for x/d on the order of 100. This trend can be explained from the properties of both the turbulence spectrum and Rayleigh breakup, in connection with the observations of SMD/Λ illustrated in Fig. 8. For small values of x/d, SMD/Λ is quite small so the drops are formed from eddies at the high wave number end of the turbulence spectrum, approaching Kolmogorov length scales. Eddies in this region are nearly isotropic so that the drops formed by primary breakup are expected to be nearly round as well. In addition, conditions at small x/d appear to be dominated by Rayleigh breakup of ligaments protruding from the surface as discussed in connection with Fig. 1. Rayleigh breakup generally yields round drops rather quickly after breakup is completed when the diameter of the liquid column is small, which is typical of conditions near the jet exit [20].

In contrast to the near jet exit region, several factors suggest increasing e_p after primary breakup as x/d increases. First of all, drop sizes after primary breakup progressively increase with x/d so that the time required for a detached drop to evolve to a round drop from the elongated shape immediately upon Rayleigh breakup increases, which increases the probability of observing drops having large e_p. In particular, Rayleigh breakup theory implies a length-to-diameter of a drop at the instant of breakup of roughly 4:1 [20], which is comparable to the maximum values of e_p seen in Fig. 9. Another factor is that SMD/Λ approaches unity at large x/d so that drops are formed from eddies at the low wave number portion of the turbulence spectrum in this region. Integral-scale sized eddies exhibit anisotropy characteristic of the ratio of streamwise to crosstream spatial integral scales, which also is 4:1 for fully-developed pipe flow (assuming that liquid turbulence is similar to jet exit conditions) [14]. Thus, drops formed by primary breakup at large x/d might be expected to have e_p of similar magnitude which is consistent with the observations of Fig. 9, as well.

Discussion

The present results suggest that most features of turbulent primary breakup observed at atmospheric pressure — conditions at the onset of breakup and the variation of SMD and e_p with distance after breakup begins -- can be explained by interactions between liquid turbulence and Rayleigh breakup of ligaments protruding from the surface, ignoring aerodynamic effects. Observations during a companion study by Tseng et al.[12] of effects of ambient gas density on the properties of pressure-atomized sprays near the jet exit, however, show that aerodynamic effects also can be a factor in turbulent primary breakup. This involves a tendency for primary and secondary breakup to merge as the density of the ambient gas increases. It is argued in Ref. 12 that the onset of aerodynamic effects begins at ambient gas densities somewhat greater than air at atmospheric pressure conditions or

ρ_f/ρ_g somewhat less than 590. Present findings that variations of ρ_f/ρ_g over the range 590-6230 had little effect on turbulent primary breakup properties tend to support this conclusion. Thus, in view of these considerations, present correlations for SMD_i, x_i and SMD, Eqs. (5), (11) and (15), should not be used for $\rho_f/\rho_g < 590$. Future work should consider the properties of turbulent primary breakup in this low density ratio regime, due to its importance for high pressure spray combustion processes.

Conclusions

Primary breakup within the multiphase mixing layer of the near jet-exit region of large-scale pressure-atomized sprays was studied, considering liquid jets in still air and helium at atmospheric pressure with fully-developed turbulent pipe flow at the jet exit. The major conclusions of the study are as follows:

1. Drop size distributions after turbulent primary breakup approximate Simmons' universal root normal distribution with MMD/SMD = 1.2, similar to drops after nonturbulent primary breakup and at local conditions within the multiphase mixing layer of sprays [1,9,10,12]. Thus, given this ratio of MMD/SMD, the entire drop size distribution could be characterized by a single parameter like the SMD because this distribution function only has two moments.

2. Mass-averaged mean drop velocities after turbulent primary breakup approximate mean and rms velocity fluctuations of the liquid in the streamwise and crosstream directions, respectively (cf. Fig. 3).

3. Drop sizes at the onset of turbulent primary breakup could be explained by equating the surface tension energy required to form a drop to the kinetic energy of a corresponding liquid eddy relative to its surroundings within the inertial region of the turbulence spectrum,

yielding the correlation of Eq. (5). This indicates a close correspondence between liquid turbulence properties and turbulent primary breakup (cf. Fig. 6).

4. The onset of turbulent primary breakup always occurred at some distance from the jet exit but approaches the exit, approximating atomization breakup conditions, at large We_{fA}. The distance required for the onset of breakup could be explained considering the residence time needed to initiate Rayleigh breakup of ligaments protruding from the liquid surface, yielding the correlation of Eq. (11) (cf. Fig. 7).

5. Drop sizes from turbulent primary breakup increased with distance from the jet exit, with the SMD reaching values on the order of the radial spatial integral scale of the liquid turbulence as the end of the liquid core is approached. Additionally, the effect of streamwise distance on SMD was virtually the same at the onset of breakup and thereafter. This behavior could be explained by associating the SMD with the largest drops that had sufficient residence time in the flow to be formed at the point in question by Rayleigh breakup of protruding ligaments, yielding the correlation of Eq. (15) (cf. Fig. 8).

Present results are limited to liquids having moderate viscosities at conditions where the SMD at the onset of breakup is at least an order of magnitude greater than the Kolmogorov length scale of the liquid turbulence. Consideration of the Rayleigh breakup mechanism of ligaments protruding from the surface suggests potential effects of liquid viscosities on breakup times, and limitations of the breakup mechanism as Kolmogorov length scales are approached, that should be explored. Additionally, limited data on turbulent primary breakup at various ambient gas densities from Ref. 12 suggests potential aerodynamic effects due to merging of turbulent primary breakup and secondary breakup for $\rho_f/\rho_g < 590$. Until these effects are resolved, it is not recommended to apply the correlations reported here beyond the present test range.

Nomenclature

C_{si}	= empirical constant for SMD at onset of breakup
C_{sx}	= empirical constant for SMD variation with x
C_{xi}	= empirical constant for x at onset of breakup
d	= injector diameter
d_{max},d_{min}	= maximum and minimum image dimensions of drops
d_p	= drop diameter
e_p	= volume-averaged ellipticity
ℓ	= characteristic eddy size
ℓ_k	= Kolmogorov length scale
L_c	= liquid core length
L	= Rayleigh breakup length
MMD	= mass median diameter
Oh_d	= Ohnesorge number, $\mu_f / (\rho_f d\sigma)^{1/2}$
Re_{fd}	= jet Reynolds number, $\bar{u}_o d/\nu_f$
SMD	= Sauter mean diameter
u	= streamwise velocity
u_p	= streamwise drop velocity
v	= radial velocity
v_ℓ	= radial velocity associated with eddy of size ℓ
v_p	= radial drop velocity
We_{ij}	= Weber number based on phase i and length scale j, $\rho_i \bar{u}_o^2\, j/\sigma$
x	= streamwise distance
Λ	= radial integral length scale
μ	= molecular viscosity
ν	= kinematic viscosity

ρ = density

σ = surface tension

τ = characteristic drop formation time

Subscripts

f = liquid-phase property

g = gas-phase property

i = at point of breakup initiation

o = jet exit condition

Superscripts

$(\bar{\ })$ = time-averaged mean properties

$(\tilde{\ })$ = mass-averaged mean property

$(\bar{\ })'$ = time-averaged rms fluctuating property

Acknowledgements

This research was sponsored by the Office of Naval Research Grant No. N00014-89-J-1199 under the technical management of G. D. Roy. Initial development of instrumentation was sponsored by the Air Force Office of Scientific Research, Grant No. 89-0516 with J. M. Tishkoff serving as technical manager. The U.S. Government is authorized to reproduce and distribute copies for governmental purposes notwithstanding any copyright notation thereon.

References

1. Wu, P.-K., Ruff, G.A. and Faeth, G.M., Primary Breakup in Liquid/Gas Mixing Layers, *Atomization and Sprays*, vol. 1, pp. 421-440, 1991.

2. De Juhasz, K.J., Zahm, O.F., Jr. and Schweitzer, P.H., On the Formation and Dispersion of Oil Sprays, Bulletin No. 40, Engineering Experimental Station, Pennsylvania State University, University Park, PA, pp. 63-68, 1932.

3. Lee, D.W. and Spencer, R.C., Photomicrographic Studies of Fuel Sprays, NACA Report No. 454, 1933.

4. Grant, R.P. and Middleman, S., Newtonian Jet Stability, *AIChE J.*, vol. 12, pp. 669-678, 1966.

5. Phinney, R.E., The Breakup of a Turbulent Jet in a Gaseous Atmosphere, *J. Fluid Mech.*, vol. 88, pp. 119-127, 1966.

6. Hiroyasu, H., Shimizu, M., and Arai, M., The Breakup of a High Speed Jet in a High Pressure Gaseous Environment, Univ. of Wisconsin, Madison, ICLASS-82, 1982.

7. Chehroudi, B., Onuma, Y., Chen, S.-H. and Bracco, F. V., On the Intact Core of Full Cone Sprays, SAE Paper No. 850126, 1985.

8. Ruff, G.A., Sagar, A.D. and Faeth, G.M., Structure and Mixing Properties of Pressure-Atomized Sprays, *AIAA J.*, vol. 27, pp. 549-559, 1989.

9. Ruff, G.A., Bernal, L.P. and Faeth, G.M., Structure of the Near-Injector Region of Non-Evaporating Pressure-Atomized Sprays, *J. Prop. Power*, vol. 7, pp. 221-230, 1991.

10. Ruff, G.A., Wu, P.-K., Bernal, L.P., and Faeth, G.M., Continuous- and Dispersed-Phase Structure of Dense Nonevaporating Pressure-Atomized Sprays, *J. Prop. Power*, in press.

11. Tseng, L.-K., Ruff, G.A. and Faeth, G.M., Effects of Gas Density on the Structure of Liquid Jets in Still Gases, *AIAA J.*, in press.

12. Tseng, L.-K., Wu, P.-K. and Faeth, G.M., Dispersed-Phase Structure of Pressure-Atomized Sprays at Various Gas Densities, *J. Prop. Power*, in press.

13. Schlichting, H., *Boundary Layer Theory*, 7th ed., McGraw-Hill, New York, p. 599, 1979.

14. Hinze, J.O., *Turbulence*, 2nd ed., McGraw-Hill, New York, pp. 427 and 724-742, 1975.

15. Miesse, C.C., Correlation of Experimental Data on the Disintegration of Liquid Jets, *Ind. Engr. Chem.*, vol. 47, pp. 1690-1697, 1955.

16. Ranz, W.E., Some Experiments on Orifice Sprays, *Can. J. Chem. Engr.*, vol. 36, pp. 175-181, 1958.

17. Simmons, H.C., The Correlation of Drop-Size Distributions in Fuel Nozzle Sprays, *J. Engr. for Power*, vol. 99, pp. 309-319, 1977.

18. Tennekes, H. and Lumley, J.L., *A First Course in Turbulence*, M.I.T. Press, Cambridge, MA, pp. 248-286, 1972.

19. Ranger, A.A. and Nicholls, J.A., Aerodynamic Shattering of Liquid Drops, *AIAA J.*, vol. 7, pp. 285-290, 1969.

20. Weber, C., Zum Zerfall eines Flussigkeitsstrahles, *Z. Angew. Math. Mech.*, vol. 2, pp. 136-141, 1931.

Table 1 Summary of Test Conditions[a]

Liquid	Water[b]	Glycerol (42%)	n-Heptane
ρ_f (kg/m^3)	997	1101	683
ρ_f/ρ_g	870, 6230	960	590
$\mu_f \times 10^4$ (kg/ms)	8.94	34.66	3.94
$\sigma \times 10^2$ (N/m)	7.08	6.30	2.00
d (mm)	3.6, 6.4, 9.5	6.4	6.4
$\bar{u}_o$ (m/s)	16-109	32-99	20-45
$Re_{fd} \times 10^{-4}$	11-78	6-20	22-50
We_{gd}	12-1240	120-1150	150-750
$We_{fd} \times 10^{-4}$	2.3-106	11.4-109	8.7-44
$Oh_d \times 10^3$	1.09-1.77	5.23	1.10

[a]Pressure-atomized injection vertically downward in still air (ρ_g = 1.15 kg/m^3) or helium (ρ_g = 0.16 kg/m^3) at 98.8 kPa and 298 ± 3 K with fully-developed turbulent pipe flow at the jet exit (injector passage length/diameter ratio of 41 for injection into air and 210 for injection into helium).

[b]Data for water for d = 9.5 mm obtained from Ruff et al.[9,10].

List of Figures

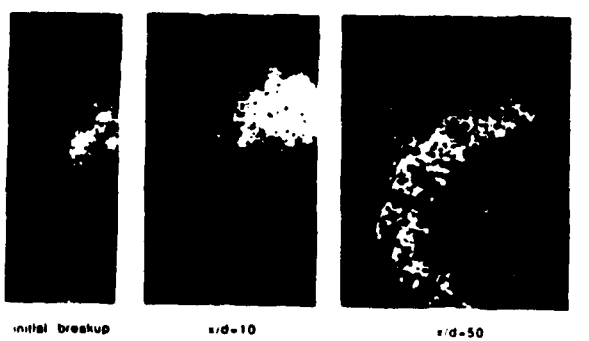

FIG. 1 Wu et al.

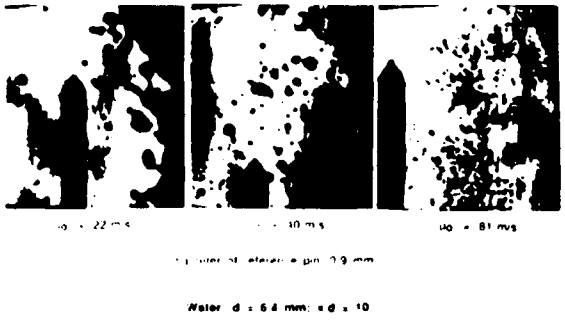

Water d = 6.4 mm; u_0 = 10

FIG. 2 Wu et al

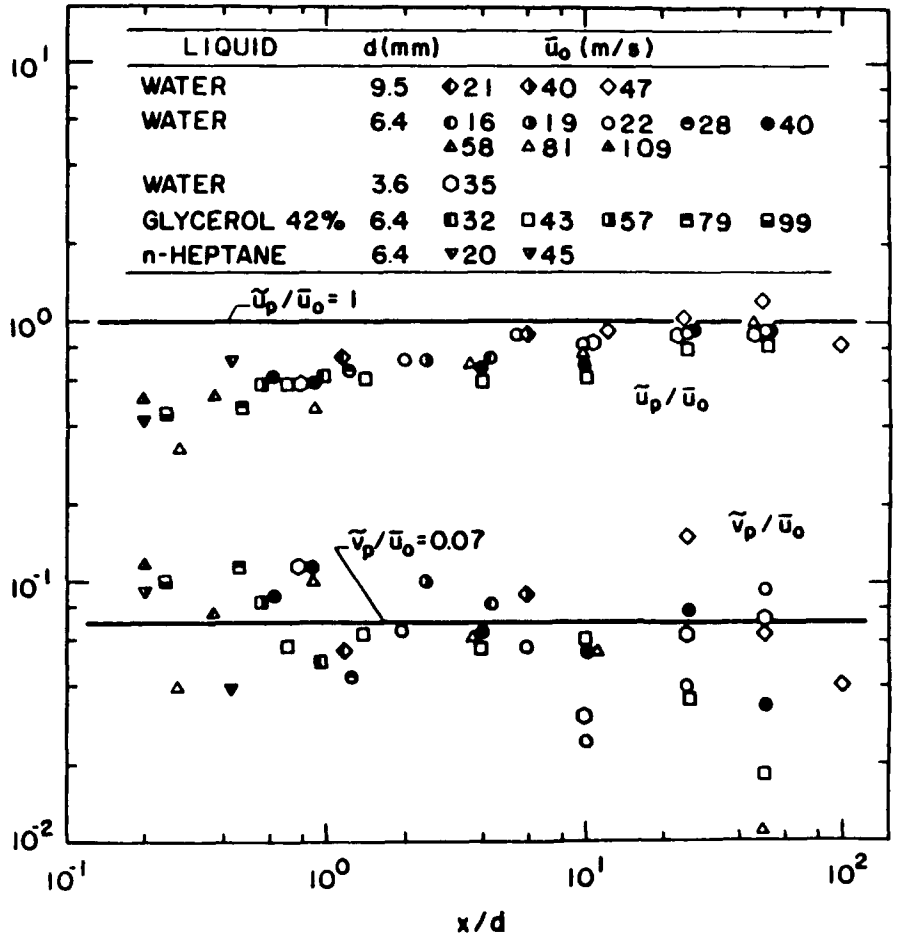

FIG 3

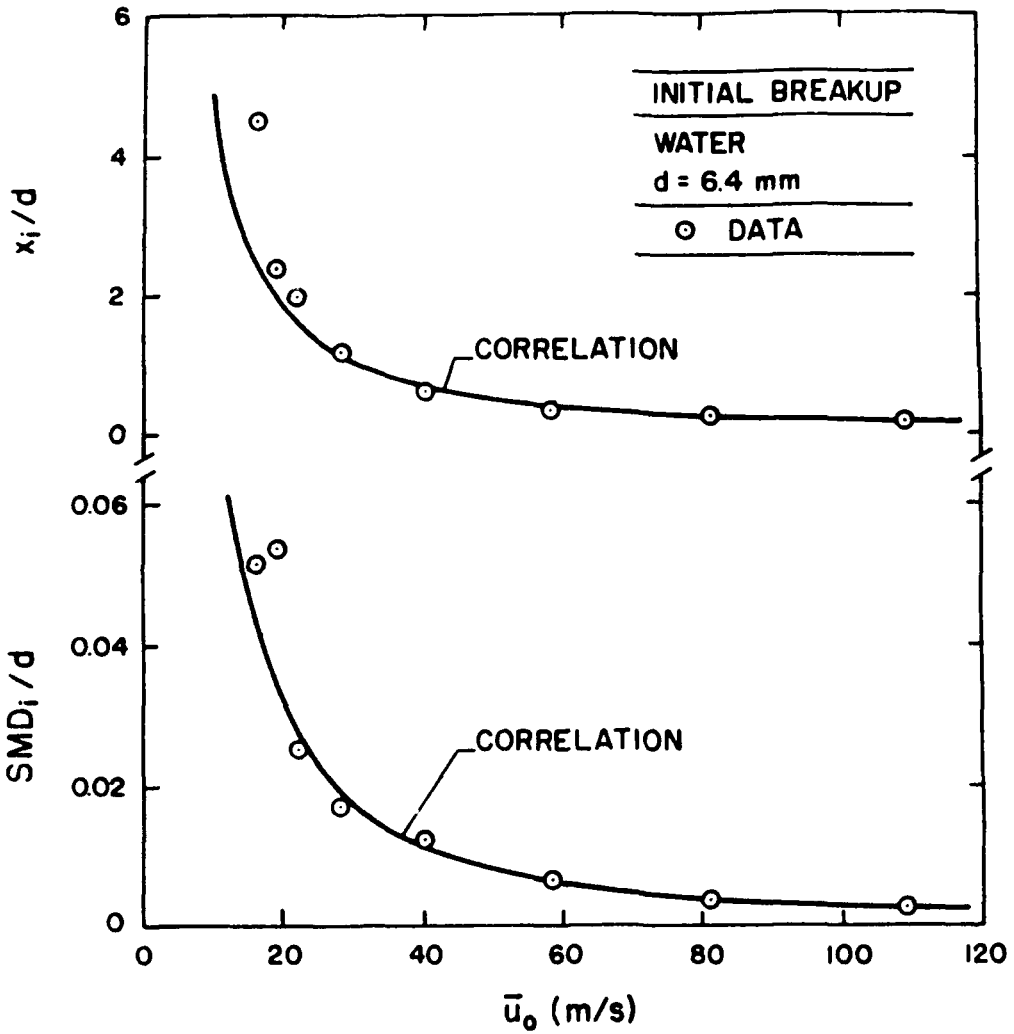

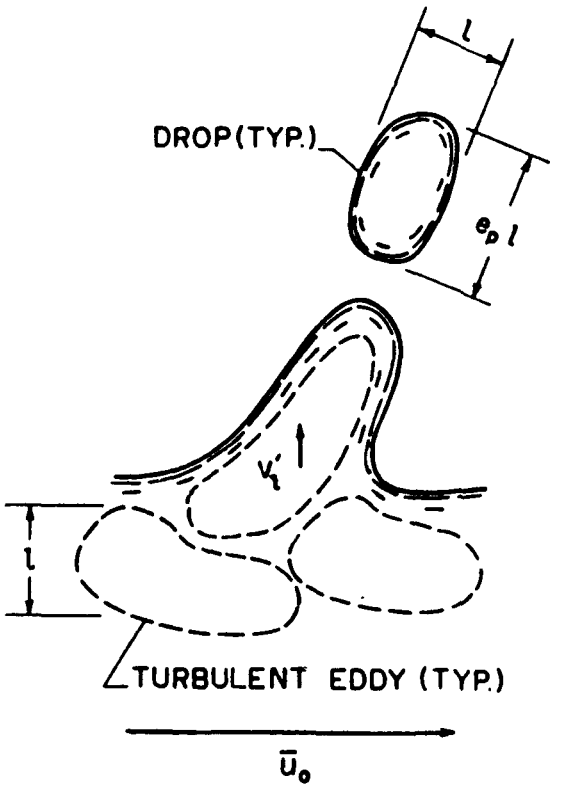

FIG. 4 Wu et al

FIG. 5 Wu et al.

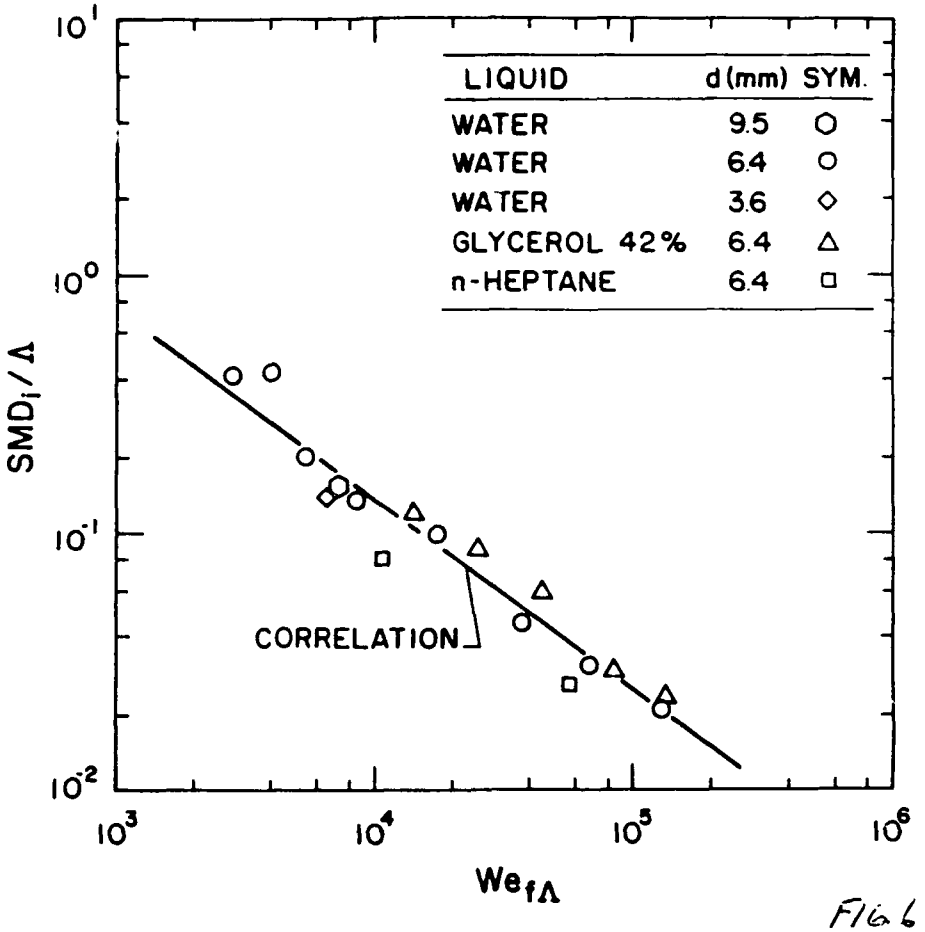
LIQUID d(mm) SYM.
WATER 9.5
WATER 6.4
WATER 3.6
GLYCEROL 42% 6.4
n-HEPTANE 6.4
CORRELATION
SMD$_i$ / Λ
We$_{fΛ}$

FIG 6

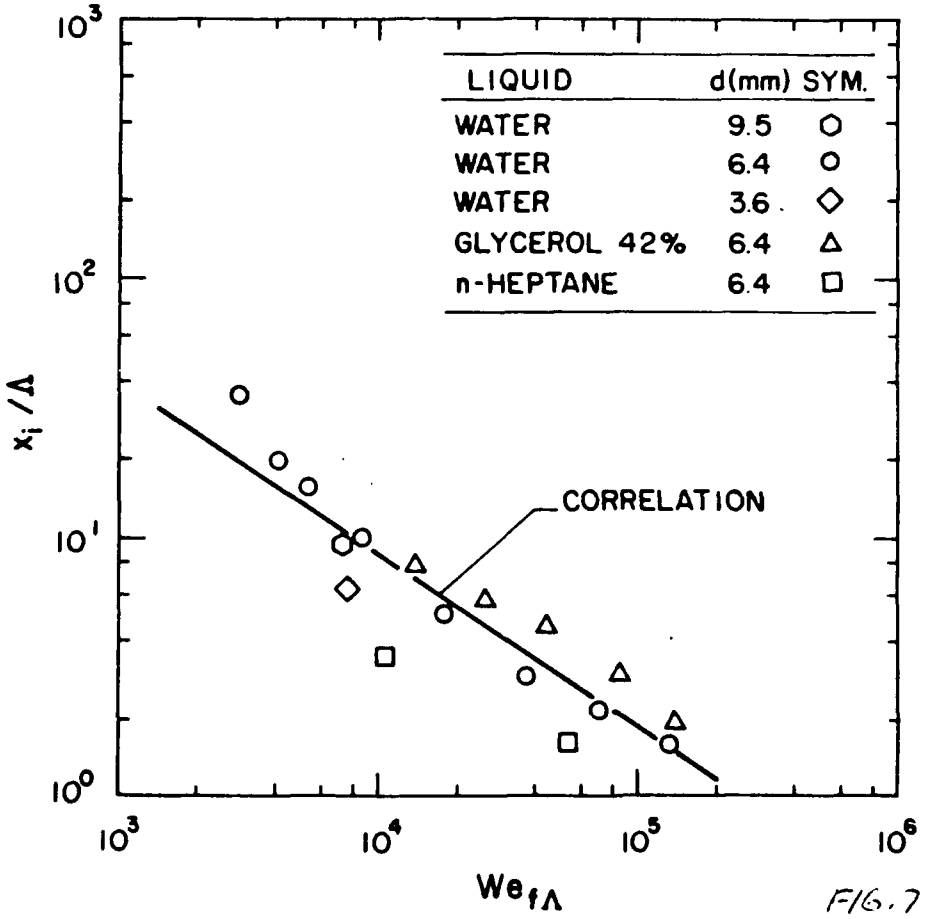
LIQUID d(mm) SYM.
WATER 9.5
WATER 6.4
WATER 3.6
GLYCEROL 42% 6.4
n-HEPTANE 6.4
CORRELATION
x_i / Λ
We$_{fΛ}$

FIG. 7

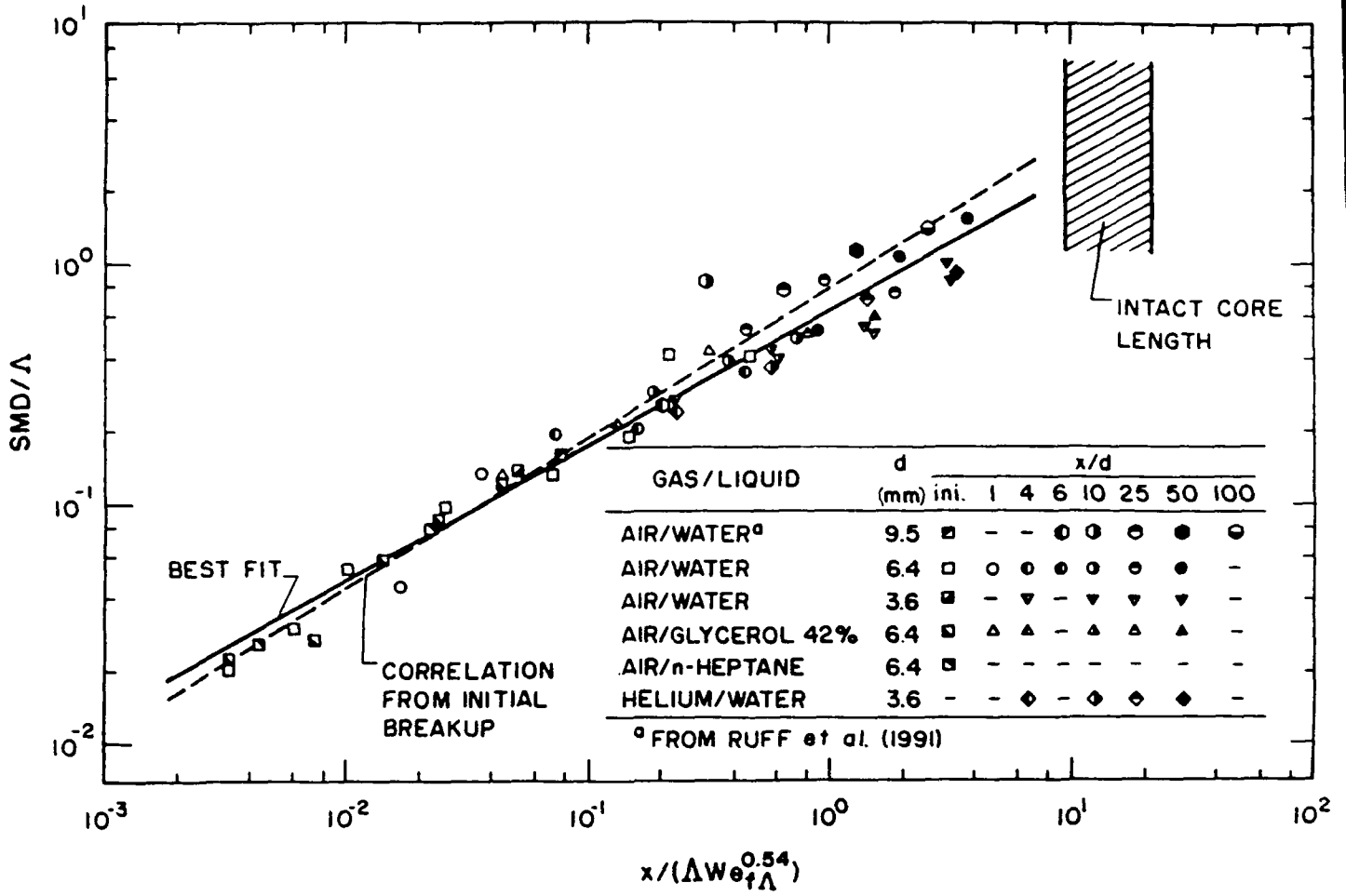
SMD/Λ
$x/(\Lambda We_{f\Lambda}^{0.54})$
INTACT CORE LENGTH
BEST FIT
CORRELATION FROM INITIAL BREAKUP
GAS/LIQUID
d (mm)
x/d
ini. 1 4 6 10 25 50 100
AIR/WATER[a] 9.5
AIR/WATER 6.4
AIR/WATER 3.6
AIR/GLYCEROL 42% 6.4
AIR/n-HEPTANE 6.4
HELIUM/WATER 3.6
[a] FROM RUFF et al. (1991)

FIG. 8

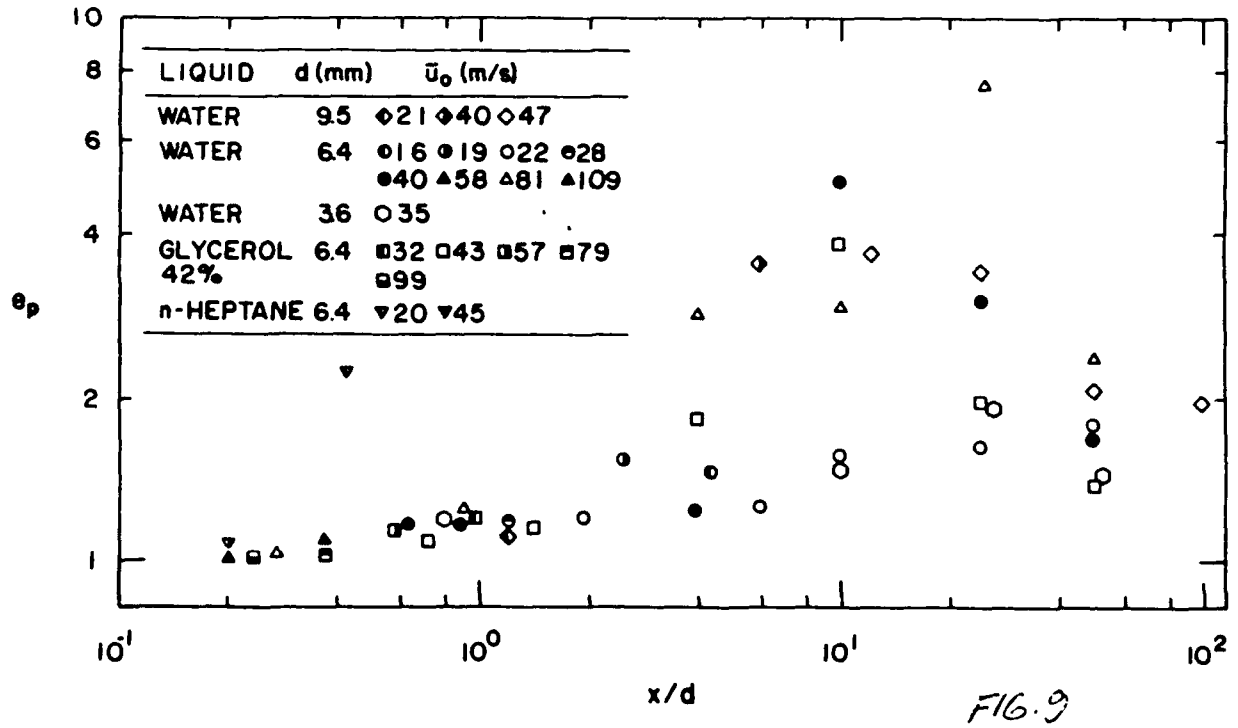
LIQUID d (mm) $\bar{u}_o$ (m/s)
WATER 9.5 ◆21 ◆40 ◇47
WATER 6.4 ●16 ●19 ○22 ●28 ●40 ▲58 △81 ▲109
WATER 3.6 ○35
GLYCEROL 42% 6.4 ■32 □43 ■57 □79 ■99
n-HEPTANE 6.4 ▼20 ▼45
θ_p
x/d

FIG. 9

APPENDIX G: WU AND FAETH (1992)

AERODYNAMIC EFFECTS ON PRIMARY BREAKUP OF TURBULENT LIQUIDS

by
P.-K. Wu and G. M. Faeth*
Department of Aerospace Engineering
The University of Michigan, Ann Arbor, Michigan

Abstract

An experimental study of primary breakup of turbulent liquids is described, emphasizing liquid/gas density ratios less than 500 where aerodynamics effects are important. The experiments involved multiphase mixing layers along round water jets (3.6 and 6.2 mm dia.) injected at various velocities into still helium, air and Freon 12 at pressures of 1 and 2 atm. with fully-developed turbulent pipe flow at the jet exit. Pulsed shadowgraph photography and holography were used to find conditions at the onset of breakup as well as drop properties as a function of distance from the jet exit. Two main aerodynamic effects were observed, as follows: (1) enhanced primary breakup near the onset of breakup, and (2) merged primary and secondary breakup when the Rayleigh breakup times of ligaments formed by turbulent fluctuations were longer than the secondary breakup times of similar sized drops. The predictions of phenomenological theories based on these ideas were in good agreement with the measurements.

INTRODUCTION

An experimental study of aerodynamic effects on the primary breakup of turbulent liquids is described, extending earlier work on the primary breakup of nonturbulent liquids [1] and on the primary breakup of turbulent liquids at conditions where aerodynamic effects were small [2]. The research is motivated by the importance of primary breakup to the

* Author to whom correspondence should be sent.

structure and mixing properties of sprays and other dispersed multiphase flows, in view of the potential for significant aerodynamic effects on primary breakup at the high pressures of many practical applications [3]. Similar to Ref. 2, the experiments involved conditions near the surface of round liquid jets in still gases, with fully-developed turbulent pipe flow at the jet exit. The measurements included properties at the location of the onset of turbulent primary breakup as well as drop sizes and velocities resulting from primary breakup as a function of distance from the jet exit. Additionally, phenomenological theories were developed to help interpret and correlate the measurements, extending the methods of Ref. 2 to include aerodynamic phenomena.

Many investigators have observed significant effects of liquid turbulence on the structure and mixing properties of pressure atomized sprays in still gases [4-14]. In general, liquid turbulence enhances mixing rates and yields larger drops after primary breakup at the liquid surface than nonturbulent liquid jets at comparable conditions. Wu et al. [1] studied the primary breakup of turbulent liquids at liquid/gas density ratios greater than 500, finding that turbulent primary breakup largely was controlled by liquid turbulence properties with negligible aerodynamic effects at these conditions. Thus, successful phenomenological theories (non-aerodynamic turbulent primary breakup theories) for both the onset and for drop properties after turbulent primary breakup were developed by treating interactions between surface tension and liquid turbulence properties alone [2]. Subsequent measurements at liquid/gas density ratios less than 500, however, yielded drop sizes that were significantly smaller than the non-aerodynamic turbulent primary breakup predictions and evidence that the appearance of aerodynamic effects was governed by the liquid/gas density ratio alone [4]. Nevertheless, only limited information about aerodynamic turbulent primary breakup was reported in Ref. 4, prompting the present more detailed study of the phenomenon.

The paper begins with a description of experimental methods. Results are then considered treating flow visualization, drop size distributions and velocities after primary breakup, the onset of primary breakup and the variation of drop sizes after primary breakup with distance from the jet exit, in turn. The paper concludes with a discussion of the regimes of non aerodynamic and aerodynamic turbulent primary breakup. Present considerations were limited to injection of water into various gases to obtain ρ_l/ρ_g in the range 104-6230, because effects of liquid type had been examined earlier [1].

EXPERIMENTAL METHODS

Apparatus

The apparatus involved liquid injection into still gases within a windowed chamber. A sketch of the test arrangement appears in Fig. 1. The injector was modified somewhat from earlier work [1, 2] to accommodate operation in the windowed test chamber. It consisted of a pneumatically driven piston/cylinder arrangement containing a roughly 600 ml water sample. The outlet of the cylinder was rounded to prevent cavitation and was followed by constant diameter passages having length-to-diameter ratios greater than 41, to yield nearly fully developed turbulent pipe flow at the jet exit [8]. Jet passage diameters of 3.6 and 6.2 mm were considered during the tests. Injection was vertically downward with the liquid collected in the bottom of the chamber and then discarded.

The windowed test chamber was cylindrical with a diameter of 300 mm and a length of 1370 mm. The chamber could be evacuated and refilled with various gases at pressures of 1 and 2 atm. to provide variations of the liquid/gas density ratio while avoiding problems of injector cavitation at low pressures. The instrumentation was mounted rigidly, therefore, various distances from the jet exit were considered by traversing the injector with respect to the chamber in the vertical direction while horizontal positions were varied by traversing the entire injector and chamber assembly.

The piston/cylinder arrangement was filled with water by venting the upper side of the cylinder and temporarily plugging the exit of the jet passage. Water was then admitted to the portion of the accumulator below the piston, forcing the piston upward and filling the sample volume. Once the chamber was full, the water flow was ended and the plug at the passage exit removed. Test operation was then initiated by admitting high-pressure air to the upper side of the piston through a solenoid valve which forced the liquid through the jet passage. Similar to earlier work [1, 2], total times of injection were short, 270-4000 ms, however, these times were sufficient due to short flow development and data acquisition times. Jet exit velocities at the time of the measurements were calibrated with an impact plate as described in Ref. 2.

Instrumentation

The instrumentation consisted of pulsed shadowgraph photography and pulsed holography. The following descriptions of these systems will be brief, see Refs. 1 and 2 for more details.

Photography. Pulsed shadowgraph photography was used to measure flow properties near the onset of breakup where dispersed-phase concentrations were relatively low so that this approach is feasible. This provided better resolution than pulsed holography to improve observations in the region where the smallest drops were observed. The holocamera was used for these photographs, operating in the single pulse mode with the reference beam blocked to yield a shadowgraph rather than a hologram. Image analysis to find drop sizes was the same as the holography measurements to be discussed next.

Pulsed shadowgraph photography also was used to find the streamwise location of the onset of turbulent primary breakup. The experimental uncertainties (95% confidence) of breakup locations were less than 40%, which is relatively large due to the angular variation of the direction of ligaments protruding from the surface and the randomness of drops separating from the tips of ligaments.

Holography. The double pulse holocamera and reconstruction systems were similar to past work [1, 2, 4, 6, 7]. The hologram image itself had a 5-6:1 primary magnification so that the reconstruction optics allowed drop diameters as small as 5 μm to be observed. The holocamera could be double pulsed with pulse separation times as small as 1 μs to allow drop velocities to be measured. The reconstructed images were analyzed with a Gould FD 5000 image display system having a field of view of 1.4 × 1.6 mm. Various locations in the reconstructed image could be observed by traversing the hologram to change the streamwise and radial position, and the video camera of the display system to change the tangential position.

For consistency, drop sizes and velocities were found in the same manner as past work [1, 2, 4, 6,7]. Small drops were sized by measuring their maximum and minimum diameters through the centroid of their image. Then, assuming an ellipsoidal shape, the drop diameter was defined as the diameter of a sphere having the same volume, i.e., $d_p^3 = d_{min}^2 d_{max}$. The shape of the drop was characterized by its ellipticity, i.e., $e_p = d_{max}/d_{min}$. More irregular objects, where the centroid was outside the projected image of the object, were sized by finding the area and perimeter of the image and proceeding as before for an ellipsoidal having the same area and perimeter. Measurements at each condition were summed over 40-200 objects to provide drop size distributions, the mass median diameter (MMD), the Sauter mean diameter (SMD) and the volume averaged ellipticity, e_p. Experimental uncertainties of these properties were dominated by finite sampling limitations

because primary breakup, particularly near the onset of breakup, yields relatively few drops. Within the limitations of the definitions of object sizes and ellipticities, experimental uncertainties (95% confidence) are estimated to be less than 40% for MMD, SMD and e_p.

Object velocities were based on the motion of the centroid of the image using holocamera pulses of different intensity to resolve directional ambiguity. Similar to object sizes, 40-200 objects were measured to find mass-weighted (Favre) averaged drop velocities. Experimental uncertainties (95% confidence) were dominated by finite sampling limitations, and are estimated to be less than 20% for u_p and less than 60% for the much smaller values of v_p.

Test Conditions

The overall data base included present measurements as well as those from Refs. 2, 4 and 7 for turbulent primary breakup. The operating conditions for these tests are summarized in Table 1. Using water as the injected liquid, with gas environments of helium, air and Freon 12 at pressures of 1 and 2 atm., liquid/gas density ratios in the range 104-6230 were obtained. Injector diameters of 3.6, 6.2 and 9.5 mm were studied in order to vary the integral scales of the turbulence; these arrangements had injector passage length-to-diameter ratios of 210, 121 and 41, respectively, all of which are sufficient to provide nearly fully-developed turbulent pipe flow at the jet exit [8, 15]. The streamwise and radial integral scales of the turbulence at the jet exit were taken to be 0.4 d and d/8, respectively, based on the measurements of Laufer for fully-developed turbulent pipe flow cited by Hinze [16].

The streamwise positions of the present measurements included x/d in the range 0.2-60. Earlier work [11, 13, 14] indicated that the length of the liquid core was in excess of x/d = 100 for present conditions which agrees with present observation of surfaces at all

test conditions. Thus, present experiments involve primary breakup at the liquid surface rather than conditions after breakup of the entire liquid volume itself.

Jet exit velocities were in the range 22-67 m/s, yielding the following ranges of jet and primary breakup dynamic parameters: Re_{fd} of 90,000-500,000, We_{gd} of 12-3790, We_{fd} of 60,000-390,000 and Oh_f of 0.0011-0.0018. All test conditions where aerodynamic effects were observed involved air and Freon 12 as the ambient gas, with $We_{fd} > 8$ and $We_{gd} > 40$. This places them in the atomization breakup regime for nonturbulent liquids defined by Miesse [17] and Ranz [18], where primary breakup should begin right at the jet exit. Actually, the onset of primary breakup always occurred at some distance from the jet exit as will be discussed later in more detail. The present low values of Oh_f imply that viscosity should not play a major role in the breakup of the flow as a whole [3], although it does affect the smallest scales of the turbulence [15, 16], and the properties of secondary breakup [19] that interact with primary breakup, as discussed later.

RESULTS AND DISCUSSION

Flow-Visualization

Consideration of the results will begin with visualization of the flow in order to provide an overview of the nature of aerodynamic effects on the turbulent primary breakup process. Similar visualizations, showing effects of varying the distance from the jet exit, and the velocity of the liquid, are presented in Refs. 2 and 8 for conditions where aerodynamic effects are not a factor. These results show that drop sizes after turbulent primary breakup roughly correspond to the sizes of ligaments and other protrusions from the liquid surface. Additionally, the sizes of surface protrusions, and corresponding drops, progressively increase with increasing distance from the jet exit for a given injection condition. This behavior was attributed to two effects [2]. First of all, small disturbances

complete their growth faster than large disturbances and should be observed sooner. Secondly, reduced levels of turbulence production as liquid velocities become uniform, once the retarding effect of the injector passage walls is removed, cause the liquid turbulence to decay with the small-scale high wave number range of the turbulence, and the corresponding distortion of the liquid surface, disappearing first. An observation supporting small aerodynamic effects for the conditions of Ref. 2 was that liquid protuberances were more-or-less randomly oriented with respect to the liquid surface, thus exhibiting little effect of drag forces from the gas. The main effect of velocity increases for these conditions was to reduce the size of the smallest scale disturbances while leaving the large scale disturbances relatively unchanged at a particular x/d. This behavior was attributed to the properties of the power spectrum of the turbulence, where for a particular flow configuration, increasing velocities (Reynolds numbers) do not modify integral scales appreciably but do increase the kinetic energy available to distort the liquid surface at high wave numbers [2, 8, 21]. These qualitative observations were supported by phenomenological theories based on these ideas that yielded reasonable agreement with measurements [2].

Some typical pulsed shadowgraph photographs for the present test conditions are illustrated in Fig. 2. These results all are for water injection with d = 3.6 mm, u_0 = 38 m/s and x/d = 10. The gas environments for these observations, however, were changed to highlight aerodynamic effects and consisted of still helium, air and Freon 12 at atmospheric pressure (from left to right), to provide ρ_f/ρ_g = 6230, 867 and 213, respectively. The direction of liquid motion in the photographs is vertically downward, which corresponds to the orientation of the experiment although effects of gravitational forces were negligible due to the high liquid velocity. The liquid core of the jet is toward the left of each photograph. Finally, a 900 μm diameter pin is visible in all three photographs in order to provide a size reference.

The photographs of Fig. 2 illustrate some of the main features of aerodynamic phenomena on turbulent primary breakup. First of all, it is evident from the left and center photographs that varying ρ_l/ρ_g from 6230 to 867 has virtually no effect on properties near the liquid surface, even though a density ratio change of this magnitude might be expected to influence aerodynamic forces on protrusions from the surface and drops near the surface. In particular, ligament properties and drop sizes and concentrations are essentially the same for these two conditions, while the orientation of ligaments protruding from the surface is random. This behavior is reasonable, however, because estimated velocity variations of ligament sized objects over the residence time of the ligaments is small at these density ratios [2]. Thus, primary breakup properties and the mass fluxes of liquid entering the dispersed phase depend on liquid turbulence properties rather than aerodynamic breakup and stripping at these conditions [2].

The lowest density ratio condition shown in Fig. 2, however, exhibits rather different behavior from the other two conditions. First of all, drop sizes are smaller and drop number densities are higher near the liquid surface for the low density ratio condition. This is a clear indication of the aerodynamic effects anticipated as ρ_l/ρ_g decreases, because all other properties of the flows are the same. The smaller drop sizes provide evidence of aerodynamic stripping of drops from ligaments which has been called merged primary and secondary breakup in Refs. 2 and 4. The larger number densities of drops are then reasonable due to the breakup of larger liquid elements. Rates of aerodynamic stripping of liquid from the surface are proportional to $(\rho_l/\rho_g)^{-1/2}$ which also should contribute to larger liquid volume fractions and thus more drops near the liquid surface [22-24]. In particular, decreasing liquid/gas density ratios below 500 has been observed to enhance the mixing rates of turbulent liquid jets in gases [5].

Other features of the photograph in Fig. 2 at the lowest liquid/gas density ratio support the presence of significant aerodynamic effects at this condition as well. For example, the ligaments generally are deflected toward the jet exit, as anticipated when drag forces are more significant, rather than the random orientations seen at the two higher density ratios. Furthermore, there is a tendency for the ligaments to be shorter at the lowest liquid/gas density ratio, which is consistent with effects of aerodynamic stripping of drops from their tips, i.e., merged primary and secondary breakup.

Another factor that suggested the appearance of aerodynamic effects for liquid/gas density ratios less than roughly 500, was the tendency for the onset of turbulent primary breakup to progressively move toward the jet exit as ρ_l/ρ_g was decreased in this regime. In contrast, the position of the onset of turbulent primary breakup was essentially independent of ρ_l/ρ_g when this ratio was greater than 500 [2]. This behavior of the onset of turbulent primary breakup will be taken up quantitatively, after the properties of drop size distributions and drop velocities after primary breakup have been considered.

Drop Size Distributions

Drop size distributions after turbulent primary breakup were measured for all the test conditions. It was found that the size distribution functions agreed with Simmons' [25] universal root normal distribution with the ratio MMD/SMD = 1.2 within experimental uncertainties. This behavior agrees with earlier measurements of drop size distributions after nonturbulent and turbulent primary breakup [1,2] as well as with drop size distributions near the surface and across the mixing layer in regions of dense sprays where the liquid core still is present [4, 6, 7], all of which yield MMD/SMD = 1.2 within similar experimental uncertainties. The root normal distribution only has two moments, therefore, taking the best estimate of MMD/SMD = 1.2 implies that the entire drop size distribution is

known if the SMD is known. Thus, drop sizes will be described in terms of the SMD alone in the following, similar to past work [1, 2, 4, 6, 7].

Drop Velocities

In order to help contrast the properties of non-aerodynamic and aerodynamic turbulent primary breakup, drop velocities after primary breakup will be considered next. Available measurements of volume (mass) averaged streamwise and crosstream drop velocities, both normalized by u_{lo}, are plotted as a function of x/d in Fig. 3. The measurements include all the test conditions summarized in Table 1. Results for $\rho_l/\rho_g <$ 500 are shown as darkened and half darkened symbols, while results for $\rho_l/\rho_g >$ 500 are shown as open symbols, in order to highlight the properties of the low liquid/gas density ratio regime where aerodynamic effects are thought to be important.

The normalized drop velocities illustrated in Fig. 3 provide crude correlations in terms of x/d but other factors probably are involved, as well. Near the jet exit, $\bar{u}_p/\bar{u}_o$ has a value of near 0.6 which increases to roughly 0.9 for x/d > 20. This behavior is consistent with drop velocities after turbulent primary breakup being roughly the same as streamwise liquid velocities near the liquid surface. The lower streamwise velocities are expected near the jet exit due to the retarding effect of the passage wall, evolving to higher values farther downstream where liquid velocities become more uniform [2]. Superimposed on this behavior, however, is a clear trend that measurements for $\rho_l/\rho_g <$ 500 have significantly lower mean streamwise velocities than the higher density ratio conditions — on the average roughly 20-40% lower. This can be attributed to aerodynamic drag if it is recalled that gas velocities near the liquid surface tend to be relatively low because the dispersed-phase region is very dilute (liquid volume fractions are less than 0.1%) so that momentum transfer to the gas phase is not very effective and separated-flow effects are large [4, 6, 7]. Then, recent measurements of mass averaged drop velocity changes during secondary

breakup of 20-40% [20] are consistent with similar reductions of streamwise drop velocities during present observations for conditions where aerodynamic effects are significant.

Similar trends with respect to density variations are much less clear for the crosstream velocity component, $\bar{v}_o'/\bar{u}_o$ in Fig. 3. In general, crosstream drop velocities are comparable to crosstream velocity fluctuations in the liquid similar to past observations [2]. In particular maximum values of $v_o'/\bar{u}_o$ = 0.058 for fully-developed turbulent pipe flow [15, 16] even in the region near the wall, which is comparable to the results seen in Fig. 3 in view of the large experimental uncertainties and scatter of this velocity component. An explanation of why the crosstream velocity component does not exhibit a reduction due to drag at low values of ρ_l/ρ_g, similar to the streamwise velocity component, is provided by an aerodynamic effect other than drag. In particular, the classical aerodynamic theories of primary drop breakup are based on the idea that flow velocities in the radial direction are increased for protuberances from the liquid surface due to acceleration of the gas over the tip of the protuberance [22, 24], see the sketch appearing in Fig. 4. This yields a radial pressure drop across the protuberance which should increase the radial velocities of drops near the surface when aerodynamic effects are significant. This mechanism would tend to compensate for drag effects in the radial direction during merged primary and secondary breakup. Thus, it is plausible that radial drop velocities are not significantly changed in the presence of aerodynamic effects within the rather large scatter of the measurements. Thus, the observations of Figs. 2 and 3 appear to be consistent with estimates of observable variations of the velocities of ligaments and large drops due to aerodynamic effects over the time period of primary breakup for ρ_l/ρ_g less than 500 [4].

Onset of Breakup

The properties of the onset of turbulent primary breakup will be considered next. The properties of interest include drop sizes formed at the onset of breakup and the distance from the jet exit where breakup begins. Conditions for turbulent primary breakup to occur at all can be inferred from these results, based on distances from the jet exit required for the onset of turbulent primary breakup that exceed estimates of the length of the liquid core itself. Estimates of liquid core lengths needed for this purpose can be found from past work in the literature [3,11-14] and will not be considered here. The onset problem will be addressed by extending the approach of Ref. 2, where the onset of breakup was associated with conditions where the momentum of turbulent fluctuations in the liquid was sufficient to overcome surface tension forces so that drops could form, to include aerodynamic contributions. Both the drop sizes at the onset of breakup, and the location where breakup begins, will be considered in the following.

Drop Sizes at Onset. Phenomenological analysis to find drop properties at the onset of breakup will be based on the configuration illustrated in Fig. 4. This implies that the onset of breakup for present test conditions did not involve merged primary and secondary breakup, which is plausible due to relatively long secondary breakup times at onset conditions [19], as discussed later. Thus, the onset mechanism is assumed to involve the formation of a drop from a turbulent eddy having a characteristic size, ℓ, and a characteristic crossstream velocity relative to the surrounding liquid, v_ℓ. The eddy is shown with an elongated shape because length scales in the streamwise direction are larger than in the crossstream direction for turbulent pipe flow [15,16]. The eddy is assumed to be convected in the streamwise direction at the local mean velocity, which is taken to be $\bar{u}_0$ based on the results discussed in connection with Fig. 3. The drop formed by the eddy also is assumed to have a diameter comparable to ℓ.

Drops formed at the onset of turbulent primary breakup are the smallest drops that can be formed by this mechanism [2]. The smallest drops that can be formed are either comparable to the smallest or Kolmogorov scales of turbulence, ℓ_K, or the smallest eddy that has sufficient mechanical energy to provide the surface energy needed to form a drop — whichever is larger. For present test conditions, ℓ_K was in the range 1-10 μm, which is much smaller than the smallest observed drop sizes; therefore, only the second criterion will be considered here, even though the first criterion may be relevant for some applications.

The second criterion for the smallest drop that can be formed can be found from energy considerations. The mechanical energy available to form a drop includes the kinetic energy of an eddy of characteristic size, ℓ_i, relative to its surroundings, plus the added mechanical energy due to the pressure drop caused by acceleration of the surrounding gas over the tip of the protuberance, as illustrated in Fig. 4. Equating these sources of mechanical energy to the surface energy required to form a drop then yields:

$$(\rho_f v_{\ell i}^2 + C_{sa} \rho_g \bar{u}_0^2) \ell_i^3 = C_{si} \sigma \ell_i^2 \qquad (1)$$

where various factors associated with surfaces, volumes, etc., have been absorbed in the empirical coefficients C_{sa} and C_{si}. These coefficients also include effects of ellipticity, nonuniform velocities within the eddy, nonuniform pressure variations over surfaces of the protuberance, and the efficiency of conversion of mechanical energy into surface energy. Equation (1) is similar to the expression used in Ref. 2, except for the addition of the second term on the left hand side of the equation which represents the aerodynamic enhancement of the mechanical energy available for the primary breakup process. In order for drops to be formed at all, ℓ_i must be less than the largest eddies present, which are comparable to Λ [16], while $\ell_K < \ell_i$ by definition for this primary breakup mechanism.

Then it is reasonable to assume that ℓ_1 is in the inertial range of the turbulence spectrum, which implies [21]:

$$v_{\ell_1} \sim \bar{v}_O' (\ell_1/\Lambda)^{1/3} \qquad (2)$$

where variations of turbulence properties in the liquid have been ignored, similar to Ref. 2. Combining Eqs. (1) and (2), setting $SMD_i \sim \ell_1$, and assuming that turbulence properties in the liquid can be approximated by jet exit turbulence properties, yields the following implicit equation for SMD_i:

$$\frac{SMD_i}{\Lambda}\left(1 + C_{sa}\left(\frac{\rho_g}{\rho_l}\right)\left(\frac{\bar{u}_O}{\bar{v}_O'}\right)^2\left(\frac{\Lambda}{SMD_i}\right)^{2/3}\right)^{3/5} = C_{si}\left(\frac{\bar{u}_O}{\bar{v}_O'}\right)^{6/5} We_{f\Lambda}^{-3/5} \qquad (3)$$

where the new proportionality constants have been absorbed into C_{sa} and C_{si} as before. With fully developed turbulent pipe flow at the jet exit, $\bar{v}_O'/\bar{u}_O$ is essentially a constant [15,16]. Thus, the effect of the aerodynamic enhancement term in Eq. (3) is largely controlled by the liquid/gas density ratio, yielding a non-aerodynamic regime at large ρ_l/ρ_g that was explored in Ref. 2, and an aerodynamic regime at small ρ_l/ρ_g where SMD_i depends on the liquid/gas density ratio. This helps support past observations that the onset of aerodynamic effects depend on the liquid/gas density ratio rather than dynamic properties related to the liquid velocity [2,4].

Present measurements of SMD_i are plotted in terms of the variables of Eq. (3) in Fig. 5. In doing this, C_{sa} was optimized to a value of 0.04, based on taking $\bar{v}_O'/\bar{u}_O$ = 0.058 for fully-developed turbulent pipe flow [16]. In addition to present results, measurements from Ref. 2 also are shown on the plot, which involve a variety of liquids for conditions where aerodynamic effects are not important. As before, test conditions for $\rho_l/\rho_g < 500$, where aerodynamic effects are observed, are denoted by darkened and half-darkened symbols, while tests at $\rho_l/\rho_g > 500$, where aerodynamic effects could not be

identified, are shown as open symbols. The correlation of the data for all conditions generally is within the scatter anticipated from experimental uncertainties. The power of $We_{f\Lambda}$ from the correlation of the data is not -3/5 as suggested by Eq. (3), however, and can be represented better by the following empirical fit that is shown on the plot:

$$\frac{SMD_i}{\Lambda}\left(1 + 0.04\left(\frac{\rho_g}{\rho_l}\right)\left(\frac{\bar{u}_O}{\bar{v}_O'}\right)^2\left(\frac{\Lambda}{SMD_i}\right)^{2/3}\right)^{3/5} = 76\, We_{f\Lambda}^{-0.69} \qquad (4)$$

The standard deviations of the coefficient and power in Eq. (4) are 9 and 6%, respectively, and the correlation coefficient of the fit is 0.97. Thus, the reduction of the power of $We_{f\Lambda}$ from -3/5 in Eq. (3) to -0.69 in Eq. (4) is not statistically significant within the uncertainties of the fit, and certainly in view of the approximations used to develop the correlation. Additionally, Eq. (4) agrees within 10% with the expression developed in Ref. 2 for the regime where $\rho_l/\rho_g > 500$. The coefficient of Eq. (4) is relatively large but this is anticipated from Eq. (3) because $(u_O/\bar{v}_O')^{6/5}$ is large for fully-developed pipe flow, e.g., $C_{si} = 2.5$ based on the $\bar{v}_O'/\bar{u}_O$ ratio used before, which is order unity as expected for a parameter of this type.

Location of Onset. Given SMD_i, the approach to find the location of the onset of turbulent primary breakup, x_i, is similar to Ref. 2. To find x_i, it is assumed that the drop-forming eddy convects along the liquid surface with a streamwise velocity, u_O, based on the results of Fig. 3. Then

$$x_i = \bar{u}_O \tau_i \qquad (5)$$

where τ_i is the time required for an eddy of characteristic size, ℓ_1, to form a drop. The aerodynamic enhancement effect will be ignored when finding τ_i, assuming that the aerodynamic pressure drop mainly allows primary breakup to occur for smaller characteristic eddy sizes, rather than modifying the breakup mechanism of protrusions or

ligaments. In addition, it is assumed that the onset of breakup is not due to merged primary and secondary breakup for present conditions, similar to considerations used to find SMD_i. Then, the time for growth of ligaments until their breakup into drops is taken to be the Rayleigh breakup time, which is the shortest characteristic breakup time for onset of primary breakup conditions, following Ref. 2.

Considering Rayleigh breakup for a protruding ligament of diameter ℓ_i and jetting velocity v_{ℓ_i}, the breakup length, L_i, of the liquid column, or ligament, is [26]:

$$L_i/\ell_i = (\rho_f \ell_i v_{\ell_i}^2/\sigma)^{1/2} + 3\mu_f v_{\ell_i}/\sigma \qquad (6)$$

For present conditions, the second term on the right hand side of Eq. (6) is small and will be ignored, although it could be a factor for very viscous liquids, i.e., for conditions where the Ohnesorge number based on ℓ_i is not small. Then assuming that τ_i is proportional to the time required for a ligament to grow to its breakup length, L_i/v_{ℓ_i}, τ_i becomes:

$$\tau_i = (\rho_f \ell_i^3/\sigma)^{1/2} \qquad (7)$$

Substituting Eq. (7) into Eq. (6), and letting $SMD_i \sim \ell_i$ as before, then yields:

$$x_i/\Lambda \sim (SMD_i/\Lambda)^{3/2} We_{f\Lambda}^{1/2} \qquad (8)$$

The results of Eq. (8) show that drop sizes increase with increasing distance from the jet exit for onset conditions, supporting the idea that onset involves the smallest drops that can be formed. Finally, substituting Eq. (3) for SMD_i into Eq. (8) and rearranging yields the following expression for x_i:

$$\frac{x_i}{\Lambda}\left(1 + C_{sa}\left(\frac{\rho_g}{\rho_f}\right)\left(\frac{\bar{u}_0}{\bar{v}_0'}\right)^2\left(\frac{\Lambda}{SMD_i}\right)^{2/3}\right)^{9/10} = C_{si}\left(\frac{\bar{u}_0}{\bar{v}_0'}\right)^{9/5} We_{f\Lambda}^{-4/10} \qquad (9)$$

where C_{si} is a constant of proportionality. Similar to Eq. (3), aerodynamic effects on x_i from Eq. (9) are controlled by the liquid/gas density ratio alone, in agreement with present and earlier [2,4] observations.

Both the present measurements of x_i, and those of Ref. 2, are plotted in terms of the variables of Eq. (9) in Fig. 6, adopting $C_{sa} = 0.04$ as before. Conditions where aerodynamic effects are significant are denoted by darkened and half-darkened symbols, similar to Figs. 3 and 5. The correlation of the data over the full range of aerodynamic effects is reasonably good in view of the relatively large experimental uncertainties of x_i. As before, however, the power of $We_{f\Lambda}$ for the correlation of the data is not 0.4 as suggested by the Eq. (9), but can be represented better by the following empirical expression which is shown on the plot:

$$\frac{x_i}{\Lambda}\left(1 + 0.04\left(\frac{\rho_g}{\rho_f}\right)\left(\frac{\bar{u}_0}{\bar{v}_0'}\right)^2\left(\frac{\Lambda}{SMD_i}\right)^{2/3}\right)^{9/10} = 2570\, We_{f\Lambda}^{0.61} \qquad (10)$$

The standard deviation of the coefficient and power on the right hand side of Eq. (10) are 8 and 10%, respectively, while the correlation coefficient of the fit is 0.89. Thus, the difference between the powers of $We_{f\Lambda}$ in Eqs. (9) and (10) is statistically significant but is not large in view of the approximations used to develop the correlating expression. The large value of the coefficient of Eq. (10) can be anticipated from Eq. (9) because $(\bar{u}_0/\bar{v}_0')^{9/5}$ is a large number for fully-developed turbulent pipe flow, e.g., taking $\bar{v}_0'/\bar{u}_0 = 0.058$ as before, yields $C_{si} = 12$.

A useful expression relating x_i and SMD_i can be obtained by combining the phenomenological results of Eqs. (3) and (9) to yield:

$$x_i/\Lambda = (C_{si}/C_{si}^{3/2})\,(SMD_i/\Lambda)^{3/2}\, We_{f\Lambda}^{1/2} \qquad (11)$$

Equation (11) is the same as the analogous result when aerodynamic effects are not important [2], because breakup times and distances were assumed to be uninfluenced by aerodynamic phenomena through Eqs. (5) and (7), i.e., aerodynamic effects only were assumed to allow smaller drops to form at the onset of turbulent primary breakup. Carrying out the same exercise for the best fit correlations of Eqs. (4) and (10) yields:

$$x_b/\Lambda = 3.88\,(SMD_b/\Lambda)^{3/2}\,We_{f\Lambda}^{0.41} \qquad (12)$$

Equation (12) is seen to be consistent with Eq. (11); namely, the coefficient is of order unity while the power of $We_{f\Lambda}$ is not statistically different than 1/2 based on the standard deviations of the powers of the empirical fits.

Drop Sizes

Aerodynamic secondary breakup times scale as $t_i \sim \ell_i\,(\rho_f/\rho_g)^{1/2}/\bar{u}_o$ for an object of size ℓ_i, if the velocity of the gas near the liquid surface is assumed to be small [19,27]. Thus, for conditions where aerodynamic effects are important, Rayleigh breakup times from Eq. (7) increase more rapidly than secondary breakup times as ℓ_i increases. This implies a tendency for secondary and primary breakup to merge as distance from the jet exit increases — a mechanism that dominated drop sizes near the liquid surface for present test conditions, except near the onset of turbulent primary breakup. The configuration considered during the present analysis is illustrated in Fig. 7, namely, that a drop of characteristic size ℓ forms by the turbulent primary breakup mechanism and immediately undergoes secondary breakup to yield a number of smaller drops.

Within the merged primary and secondary breakup regions, turbulent primary breakup properties will be found using the results of Ref. 2 while aerodynamic secondary breakup properties will be found using the results of Ref. 19. The variation of SMD with distance from the jet exit for turbulent primary breakup was found assuming that the SMD

was proportional to the largest drop that could be formed at a particular position with the time of breakup determined from the Rayleigh breakup time [2]. Thus, this approach was similar to the approach just described in connection with the onset of breakup. This yields the following expression for the variation of SMD with distance from the jet exit [2], analogous to Eq. (11):

$$SMD_p/\Lambda = C_{sx}[x/(\Lambda\,We_{f\Lambda}^{1/2})]^{2/3} \qquad (13)$$

The secondary breakup correlation of Ref. 19 was developed assuming that relative velocities at the time of breakup can be represented by the initial relative velocity and that drop sizes after breakup are proportional to the thickness of liquid boundary layers that form within the drop due to gas motion over its secondary surface. This yields the following expression for the SMD after aerodynamic secondary breakup of a drop of diameter d_p having a relative velocity $\bar{u}_o$ [19], assuming that the jet exit velocity is the appropriate relative velocity for merged primary and secondary breakup:

$$SMD/d_p = C_s\left(\rho_f/\rho_g\right)^{1/2}\left(\mu_f/\left(\rho_f d_p \bar{u}_o\right)\right)^{1/2} \qquad (14)$$

Then assuming that $d_p \sim SMD_p$, Eqs. (13) and (14) can be combined to yield the following expression for the SMD after merged primary and secondary breakup:

$$\rho_g\,SMD\,\bar{u}_o^2/\sigma = C_s\,C_{sx}^{1/2}\,(x/\Lambda)^{1/3}\,(\rho_g/\rho_f)^{3/4}\,We_{f\Lambda}^{5/6}\,Re_{f\Lambda}^{-1/2} \qquad (15)$$

where C_s in Eq. (15) is modified from Eq. (14) to account for a range of initial drop sizes rather than a single drop.

Present measurements of aerodynamic turbulent primary breakup, along with some results from Ref. 4, are plotted according to the variables of Eq. (15) in Fig. 8. The following best fit correlation of present measurements also is shown on the plot

$$\rho_g \, SMD \, u_{ij}^2/\sigma = 12.0 \left[(x/\Lambda)^{1/3} (\rho_g/\rho_f)^{3/4} \, We_{f\Lambda}^{5/6} \, Re_{f\Lambda}^{1/2} \right]^{1.17} \quad (16)$$

where the standard deviation of the coefficient and power on the right-hand-side of Eq (16) are 2 and 8%, respectively, with a correlation coefficient of 0.92 of the fit. Additionally, adopting the best fit values of C_s and C_{sx} in Eq. (15), the following theoretical prediction for SMD as a function of distance is obtained:

$$\rho_g \, SMD \, u_{ij}^2/\sigma = 12.9 \, (x/\Lambda)^{1/3} (\rho_g/\rho_f)^{3/2} \, We_{f\Lambda}^{5/6} \, Re_{f\Lambda}^{-1/2} \quad (17)$$

with the standard deviation of the constant of 21%. Thus, the differences between Eqs. (16) and (17) are not statistically significant, within experimental uncertainties. Present measurements also are in good agreement with the predictions. However, the measurements of Tseng et al. [4] definitely yield smaller drop sizes after merged primary and secondary breakup. An explanation of this behavior is that these flows involved the highest concentrations of drops after turbulent primary breakup of the data base, so that drop properties near the liquid surface could be influenced by small drops migrating from other parts of the multiphase mixing layer by turbulent dispersion.

The consistency of the merged primary and secondary breakup process also can be examined by inverting the process; namely, by computing the drop sizes that should have been observed after primary breakup in the absence of aerodynamic effects and comparing these results with other measurements at similar conditions. To do this, the non-aerodynamic turbulent primary breakup correlation was refitted to find C_{sx} in Eq. (13), based on present measurements in helium and air, along with initial breakup results for Freon 12. This yielded

$$SMD/\Lambda = 0.65 \left[x/(\Lambda \, We_{f\Lambda}^{1/2}) \right]^{2/3} \quad (18)$$

with the standard deviation of the coefficient of 34% and a 95% confidence interval of 0.60-0.71. This implies reasonably consistent measurements of turbulent primary breakup with respect to Ref. 2 where the constant of Eq. (18) was 0.64. Then from the fit of the measurements illustrated in Fig. 8, the relationship between SMD and SMD_p is given by:

$$SMD_p/\Lambda = 3.91 \times 10^{-3} (\rho_g/\rho_f)^{1/2} \, Re_{f\Lambda} \, (SMD/\Lambda)^2 \quad (19)$$

The results illustrated in Fig. 8, where primary and secondary breakup occurred, were inverted to get SMD_p using Eq. (19). These results are plotted in Fig. 9, along with previous results for turbulent primary breakup where aerodynamic effects are not important from Ref. 2. Aside from the few results of Ref. 4, mentioned earlier in connection with Fig. 8, the inverted aerodynamic turbulent primary breakup measurements are seen to be in good agreement with the other results, supporting the idea of merging of primary and secondary breakup. Other features of this figure, including the liquid core length of Grant and Middleman [11] shown on the plot, are discussed in Ref. 2.

Breakup Regimes

Present measurements suggested three regimes of turbulent primary breakup: (1) non-aerodynamic turbulent primary breakup; (2) aerodynamically-enhanced turbulent primary breakup, observed at onset conditions; and (3) aerodynamic turbulent primary breakup, which involves merging of turbulent primary and secondary breakup. The results also indicated that the liquid/gas density ratio, and the relative magnitudes of characteristic Rayleigh breakup times of ligaments and secondary breakup times of liquid objects, fixed the boundaries of these regimes. The breakup times used to define these regimes were based on the SMD after primary breakup, or after the primary breakup stage of merged primary and secondary breakup, for conditions beyond the onset of breakup for present data. Then by analogy to Eq. (7), the characteristic Rayleigh breakup time was taken to be

$\tau_R \sim (\rho_f\ SMD^3/\sigma)^{1/2}$. Similarly, by analogy to the results of Ref. 19 and 27, the characteristic secondary breakup time was taken to be, $\tau_R \sim (\rho_f/\rho_g)^{1/2}\ SMD/\bar{u}_0$. Then using Eq. (18) to eliminate SMD from the ratio, the characteristic time ratio was taken to be:

$$\tau_R/\tau_b = (\rho_g/\rho_f)^{1/2}(\pi\ We_{f\Lambda}/\Lambda)^{1/3} \tag{20}$$

The resulting turbulent primary breakup regimes based on present measurements, as well as those from Refs. 2, 4 and 7, are illustrated in terms of ρ_f/ρ_g and τ_R/τ_b in Fig. 10. The results yield the following criteria for transitions between regimes:

$$\rho_f/\rho_g = 500, \text{ non-aerodynamic/aerodynamic transition} \tag{21}$$

$$\tau_R/\tau_b = 4, \text{ merged/enhanced-aerodynamic transition} \tag{22}$$

In the non-aerodynamic breakup regime, the results of Ref. 2 can be used to find properties at the onset of turbulent primary breakup, and the subsequent variation of SMD with distance from the jet exit; or with similar accuracy, within experimental uncertainties, Eqs. (4) and (9) can be used to find onset properties and Eq. (18) to find the subsequent variation of SMD with x. Otherwise, onset conditions that fall in the enhanced-aerodynamic breakup regime are provided by Eqs. (4) and (9), while the subsequent variation of SMD with x in the merged aerodynamic breakup regime is given by Eq. (17).

DISCUSSION

The present results suggest that most of the features of turbulent primary breakup conditions at the onset of breakup and the variation of SMD with distance after breakup begins can be explained by interactions among liquid turbulence, Rayleigh breakup of ligaments and fast (merged) secondary breakup. Additionally, the classical aerodynamic effect that causes a reduced pressure over protuberances from the surface [21,23], appears

to play a role in reducing drop sizes near onset conditions of turbulent primary breakup when liquid/gas density ratios are less than 500. Furthermore, the rather close correspondence between effects of secondary breakup on the primary breakup process observed here, and secondary breakup of drops exposed to shock wave disturbances observed in Refs. 19 and 20, helps support the relevance of the latter measurements to practical spray processes. However, it still remains to be seen whether slower subsequent variations of drop properties, causing drops to again cross secondary breakup limits within a developing spray flow field, can also be handled successfully in the same manner.

It also should be noted that several features of turbulent primary breakup have not been addressed due to limitations of the available data base. This includes onset in the merged aerodynamic breakup regime, SMD variations with distance in the enhanced aerodynamic breakup regime, turbulent primary breakup limited by the Kolmogorov scales of the turbulence, liquid turbulence properties other than fully-developed turbulent pipe flow, and turbulent primary breakup involving significant effects of liquid viscosity (large Ohnesorge number effects), among others. Additionally, more work is needed to provide better definition of the breakup regime boundaries illustrated in Fig. 10, aside from potential effects due to the phenomena that just were enumerated. Finally, primary breakup near the tip of the liquid core still must be addressed along with the potential for merged primary and secondary breakup in this region. In view of the importance of primary breakup to the subsequent properties of sprays, these issues clearly merit additional study.

CONCLUSIONS

Aerodynamic effects on primary breakup within the multiphase mixing layer of the near jet-exit region of large-scale pressure-atomized sprays were studied, considering liquid jets in still gases with fully-developed turbulent pipe flow at the jet exit. The major conclusions of the study are as follows:

1 The presence of aerodynamic phenomena for turbulent primary breakup largely is controlled by the liquid/gas density ratio, and affect both conditions at the onset of breakup, and drop sizes and velocities (to a lesser extent) after breakup, when this ratio is less than 500. Within this region, regimes of enhanced aerodynamic breakup and merged primary and secondary breakup also were observed (cf. Fig. 10).

2 Aerodynamic enhancement of the onset of turbulent primary breakup was due to the aerodynamic pressure reduction over the tips of protruding liquid elements. This effect assists the kinetic energy of a corresponding liquid eddy relative to its surrounding to provide the surface tension energy needed to form a drop, thus allowing smaller drops to form. Phenomenological analysis based on these ideas yielded reasonable correlations of onset properties, Eqs. (4) and (9), for the enhanced aerodynamic breakup regime (cf. Figs. 5 and 6).

3 For conditions where secondary breakup times become small in comparison to Rayleigh breakup of turbulence-induced ligaments protruding from the surface, processes of turbulent primary and secondary breakup merge yielding smaller drops than when aerodynamic effects are absent. The reduction of drop sizes at these conditions correlated reasonably well with results for the secondary breakup of drops due to shock disturbances from Ref. 19, yielding the correlation of Eq. (17) (cf. Fig. 8).

4 Drop size distributions after aerodynamic turbulent primary breakup approximated Simmons' [25] universal root normal distribution with MMD/SMD = 1.2, similar to observations of other drop breakup processes as well as drops in the multiphase mixing layers of pressure-atomized sprays [1-8,19,20]. Additionally, mass-averaged drop velocities after aerodynamic turbulent primary breakup approximate mean and rms velocity fluctuations of the liquid in the streamwise and crossstream directions, respectively, although there was a tendency for streamwise velocities to be somewhat reduced by aerodynamic effects (cf. Fig. 3).

Present results are limited to liquids having moderate viscosities at conditions where the SMD at the onset of breakup is at least an order of magnitude greater than Kolmogorov length scales with fully-developed turbulent pipe flow at the jet exit. Effects of changes of these conditions, as well as other issues mentioned in the Discussion, merit further study due to the importance of primary breakup to the structure and dynamics of practical sprays.

NOMENCLATURE

C_s	= empirical constant for SMD after secondary breakup
C_{sa}	= empirical constant for enhanced breakup
C_{si}	= empirical constant for SMD at onset of breakup
C_{sx}	= empirical constant for SMD variation with x
C_{xi}	= empirical constant for x at onset of breakup
d	= injector diameter
d_{max}, d_{min}	= maximum and minimum image dimensions of drops
d_p	= drop diameter
e_p	= volume-averaged ellipticity
ℓ	= characteristic eddy size
ℓ_K	= Kolmogorov length scale
L_c	= liquid core length
L	= Rayleigh breakup length
MMD	= mass median drop diameter
Oh_d	= Ohnesorge number, $\mu_f/(\rho_f d\sigma)^{1/2}$

p = pressure

r = radial distance

Re_{ij} = Reynolds number base on phase i and length scale j, $\bar{u}_0 j/\nu_i$

SMD = Sauter mean diameter

SMD_p = SMD after primary breakup for a merged primary and secondary breakup

u = streamwise velocity

u_p = streamwise drop velocity

v = radial velocity

v_ℓ = radial velocity associated with eddy of size ℓ

v_p = radial drop velocity

We_{ij} = Weber number based on phase i and length scale j, $\rho_i \bar{u}_0^2 j/\sigma$

x = streamwise distance

Λ = radial integral length scale

μ = molecular viscosity

ν = kinematic viscosity

ρ = density

σ = surface tension

τ_b = characteristic secondary breakup time

τ_R = characteristic Rayleigh breakup time

Subscripts

f = liquid-phase property

g = gas-phase property

i = at point of breakup initiation

o = jet exit condition

Superscripts

$\bar{(\ )}$ = time-averaged mean property

$\tilde{(\ )}$ = mass-averaged mean property

$(\ )'$ = time-averaged r.m.s. fluctuating property

ACKNOWLEDGEMENTS

This research was sponsored by the Office of Naval Research Grant N00014-89-J-1199 under the Technical Management of G. D. Roy. Initial development of the instrumentation was sponsored by the Air Force Office of Scientific Research, Grant No. 89-0516 with J. M. Tishkoff serving as Technical Manager. The U.S. Government is authorized to reproduce and distribute copies for governmental purposes notwithstanding any copyright notation thereon.

REFERENCES

1. P.-K. Wu, G.A.Ruff, and G.M. Faeth, Primary Breakup in Liquid/Gas Mixing Layers, Atomization and Sprays, vol. 1, pp. 421-440, 1991.

2. P.-K. Wu, L.-K. Tseng, and G.M. Faeth, Primary Breakup in Gas/Liquid Mixing Layers for Turbulent Liquids, Atomization and Sprays, in press.

3. G.M. Faeth, Structure and Atomization Properties of Dense Turbulent Sprays, *Twenty-Third Symposium (International) on Combustion*, The Combustion Institute, Pittsburgh, pp. 1345-1352, 1990.

4. L.-K. Tseng, P.-K. Wu, and G.M. Faeth, Dispersed-Phase Structure of Pressure-Atomized Sprays at Various Gas Densities, J. Prop. Power, in press.

5. L.-K. Tseng, G.A. Ruff, and G.M. Faeth, Effects of Gas Density on the Structure of Liquid Jets in Still Gases, AIAA J., vol. 30, pp. 1537-1544, 1992.

6. G.A. Ruff, P.-K. Wu, L.P. Bernal, and G.M. Faeth, Continuous- and Dispersed-Phase Structure of Dense Nonevaporating Pressure-Atomized Sprays, J. Prop. Power, vol. 8, pp. 280-289, 1992.

7. G.A. Ruff, L.P. Bernal, and G.M. Faeth, Structure of the Near-Injector Region of Non-Evaporating Pressure-Atomized Sprays, J. Prop. Power, vol. 7, pp. 221-230, 1991.

8. G.A. Ruff, A.D. Sagar, and G.M. Faeth, Structure and Mixing Properties of Pressure-Atomized Sprays, AIAA J., vol. 27, pp. 901-908, 1989.

9. K. J. DeJuhasz, O. F. Zahm, Jr., and P.H. Schweitzer, On the Formation and Dispersion of Oil Sprays, Bulletin No. 40, Engineering Experiment Station, The Pennsylvania State University, University Park, PA, pp. 63-68, 1932.

10. D.W. Lee, and R.C. Spencer, Photomicrographic Studies of Fuel Sprays, NACA Report No. 454, 1933.

11. R.P. Grant, and S. Middleman, Newtonian Jet Stability, AIChE J., vol. 12, pp. 669-678, 1966.

12. R.E. Phinney, The Breakup of a Turbulent Jet in a Gaseous Atmosphere, J. Fluid Mech., vol. 88, pp. 119-127, 1966.

13. H. Hiroyasu, M. Shimizu, and M. Arai, The Breakup of a High Speed Jet in a High Pressure Gaseous Environment, University Of Wisconsin, Madison, WI, ICLASS-82, 1982.

14. B. Chehroudi, Y. Onuma, S.-H. Chen, and F. V. Bracco, On the Intact Core of Full Cone Sprays, SAE Paper No. 850126, 1985.

15. H. Schlichting, *Boundary Layer Theory*, 7th ed., McGraw-Hill, New York, p. 599, 1979.

16. J. O. Hinze, *Turbulence*, 2nd ed., McGraw-Hill, New York, pp. 427 and 724-742, 1975.

17. C.C. Miesse, Correlation of Experimental Data on the Disintegration of Liquid Jets, Ind. Engr. Chem., vol. 47, pp. 1690-1697, 1955.

18. W.E. Ranz, Some Experiments on Orifice Sprays, Can. J. Chem. Engr., vol. 36, pp. 175-181, 1958.

19. L.-P.Hsiang, and G.M. Faeth, Near-Limit Drop Deformation and Secondary Breakup, Int. J. Multiphase Flow, in press.

20. L.-P. Hsiang, and G. M. Faeth, Drop Size and Velocity Distributions Following Secondary Breakup, AIAA Paper No. 93-0000, 1993.

21. H. Tennekes, and J.L. Lumley, *A First Course in Turbulence*, M.I.T. Press, Cambridge, Massachusetts, pp. 248-286, 1972.

22. G.I. Taylor, Generation of Ripples by Wind Blowing over a Viscous Liquid, *The Scientific Papers of Sir Geoffrey Ingram Taylor*, Vol. III, G.K. Batchelor, ed., Cambridge Univ. Press, Cambridge, England, pp. 244-254, 1963.

23. V.G. Levich, *Physicochemical Hydrodynamics*, Prentice-Hall, Inc., Englewood Cliffs, NJ, pp. 639-646, 1962.

24. R.D. Reitz, and F.V. Bracco, Mechanism of Atomization of a Liquid Jet, Phys. Fluids, vol. 25, pp. 1730-1742, 1982.

25. H.C. Simmons, The Correlation of Drop-Size Distributions in Fuel Nozzle Sprays, J. Engr. for Power, vol. 99, pp. 309-319, 1977.

26. C. Weber, Zum Zerfall eines Flussigkeitsstrahles," Z. Angewesen. Math. Mech., vol. 2, pp. 136-141, 1931.

27. A.A. Ranger, and J.A. Nicholls, The Aerodynamic Shattering of Liquid Drops, AIAA J., vol. 7, pp. 285-290, 1969.

Table 1 Summary of Test Conditions[a]

Gas	Helium	Air	Air[b,c]	Air[c]	Freon 12
ρ_g (kg/m^3)	0.16	1.15	1.15	2.34,4.68	4.68,9.63
ρ_l/ρ_g	6230	867	867	213,426	104,213
d (mm)[c]	3.6,6.2	3.6,6.2	9.5	9.5	3.6,6.2
u_o (m/s)	30-67	30-47	21-47	40	22-67
$Re_{ld} \times 10^{-4}$	15-46	15-46	22-50	42	9-46
We_{gl}	12-63	84-452	70-350	502,1005	115-3790
$We_{ld} \times 10^{-4}$	7-39	7-39	6-30	21	7-39
$Oh_d \times 10^3$	1.4,1.8	1.4,1.8	1.1	1.1	1.4,1.8

[a]Pressure-atomized injection of water vertically downward in still gases at 298 ± 3 K with fully-developed turbulent pipe flow at the jet exit. Passage length-to-diameter ratios of 210, 121 and 41 for d = 3.6, 6.2 and 9.5 mm, respectively.
[b]From Ruff et al. [7].
[c]From Tseng et al. [4].

List of Figures

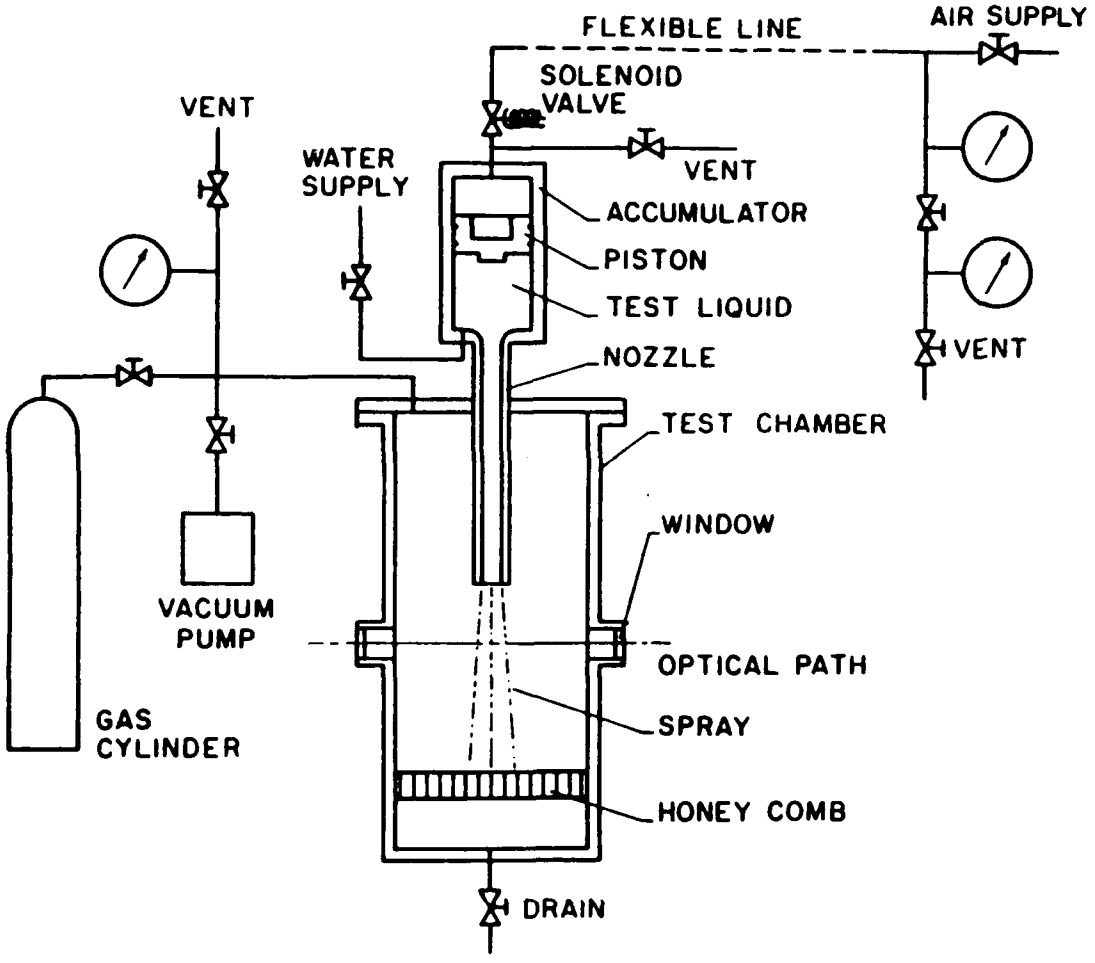

Fig 1

ρ_l/ρ_g = 6230 867 213

Diameter of reference pin: 0.9mm

WATER; $\bar{u}_o$ = 38 m/s; d = 3.6 mm; x/d = 10

Fig 2

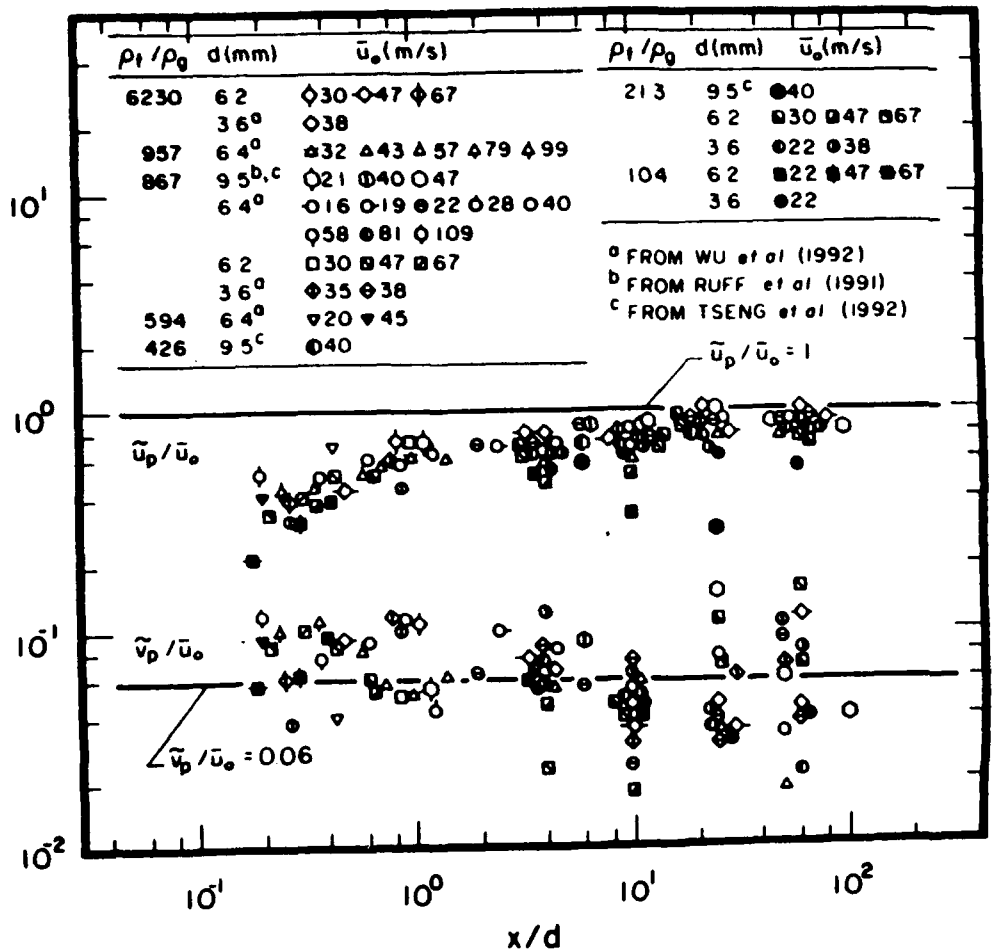
ρ_f/ρ_g d(mm) $\bar{u}_o$(m/s)
6230 6 2 ◇30 ◇47 ◆67
3 6[a] ◇38
957 6 4[a] ☆32 △43 △57 △79 △99
867 9 5[b,c] ◇21 ◐40 ○47
6 4[a] ○16 ○19 ●22 ◇28 ○40
◇58 ●81 ◇109
6 2 □30 ■47 ■67
3 6[a] ◆35 ◆38
594 6 4[a] ▽20 ▼45
426 9 5[c] ◐40
213 9 5[c] ●40
6 2 ■30 ■47 ■67
3 6 ●22 ●38
104 6 2 ■22 ◆47 ■67
3 6 ●22
[a] FROM WU et al (1992)
[b] FROM RUFF et al (1991)
[c] FROM TSENG et al (1992)
$\tilde{u}_p/\bar{u}_o = 1$
$\tilde{u}_p/\bar{u}_o$
$\tilde{v}_p/\bar{u}_o$
$\tilde{v}_p/\bar{u}_o = 0.06$
10^1
10^0
10^{-1}
10^{-2}
10^1
10^0
10^1
10^2
x/d

Fig 3

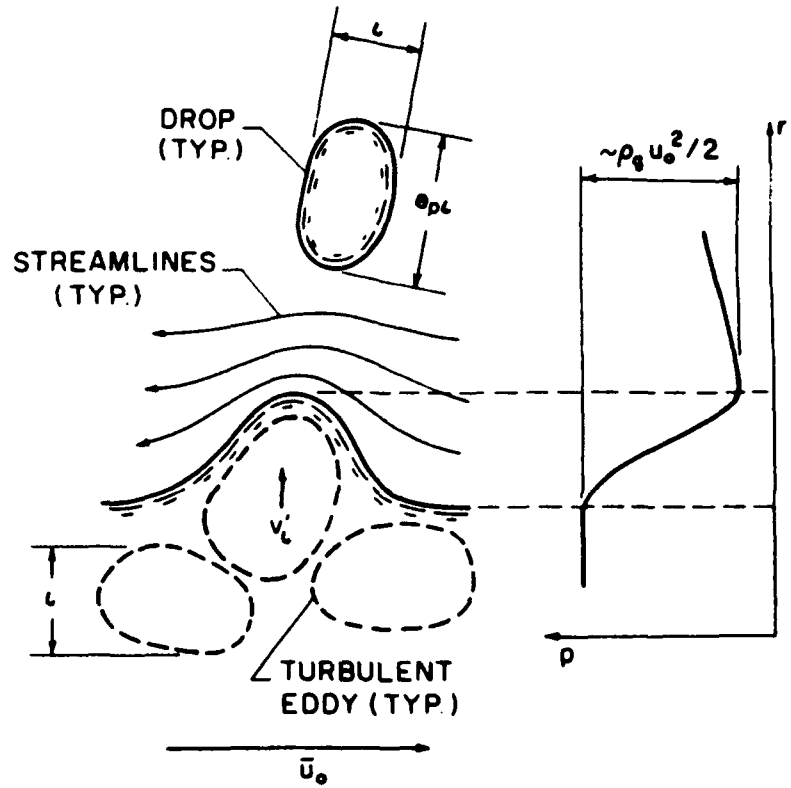
DROP (TYP.)
STREAMLINES (TYP.)
TURBULENT EDDY (TYP.)
$\bar{u}_o$
v_t'
$\sim\rho_g u_o^2/2$
r
p

Fig 4

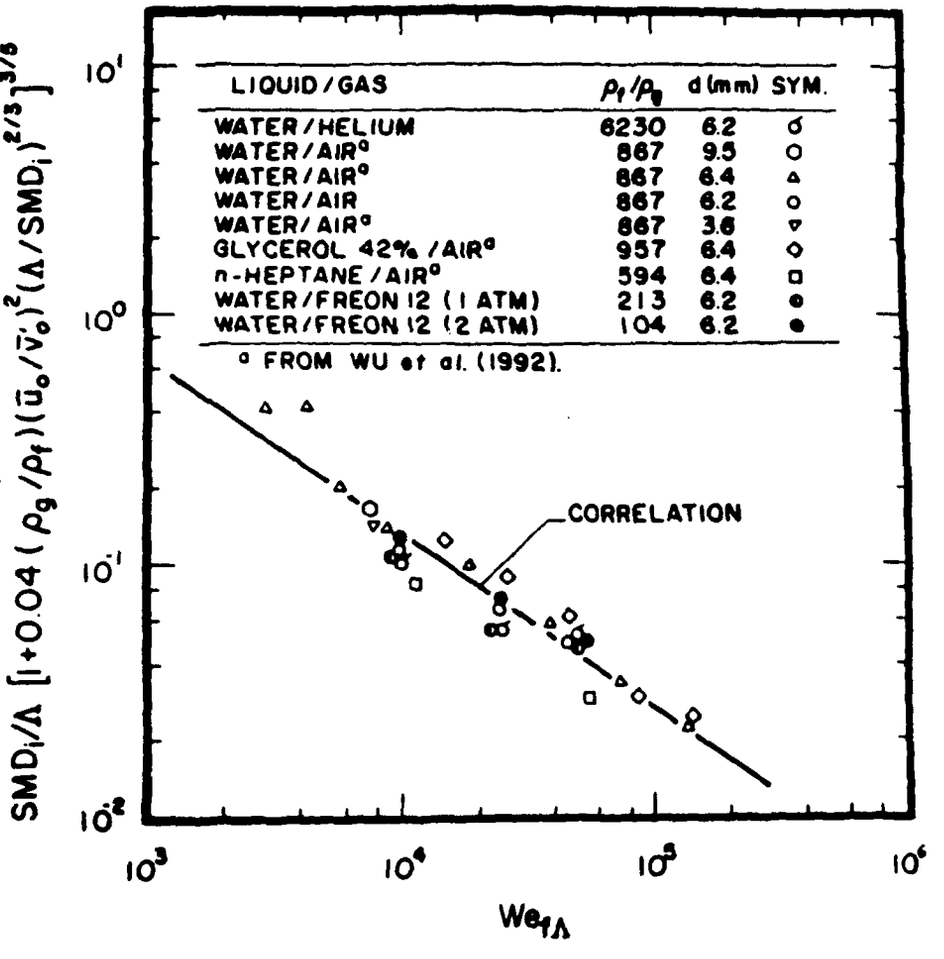
LIQUID / GAS | ρ_l/ρ_g | d (mm) | SYM.
WATER / HELIUM | 6230 | 6.2
WATER / AIR[a] | 867 | 9.5
WATER / AIR[a] | 867 | 6.4
WATER / AIR | 867 | 6.2
WATER / AIR[a] | 867 | 3.6
GLYCEROL 42% / AIR[a] | 957 | 6.4
n-HEPTANE / AIR[a] | 594 | 6.4
WATER / FREON 12 (1 ATM) | 213 | 6.2
WATER / FREON 12 (2 ATM) | 104 | 6.2
[a] FROM WU et al. (1992).
CORRELATION
$SMD_i/\Lambda \left[1+0.04\left(\rho_g/\rho_l\right)\left(\bar{u}_o/\bar{v}_o'\right)^2(\Lambda/SMD_i)^{2/3}\right]^{3/5}$
$We_{l\Lambda}$

FIG. 5

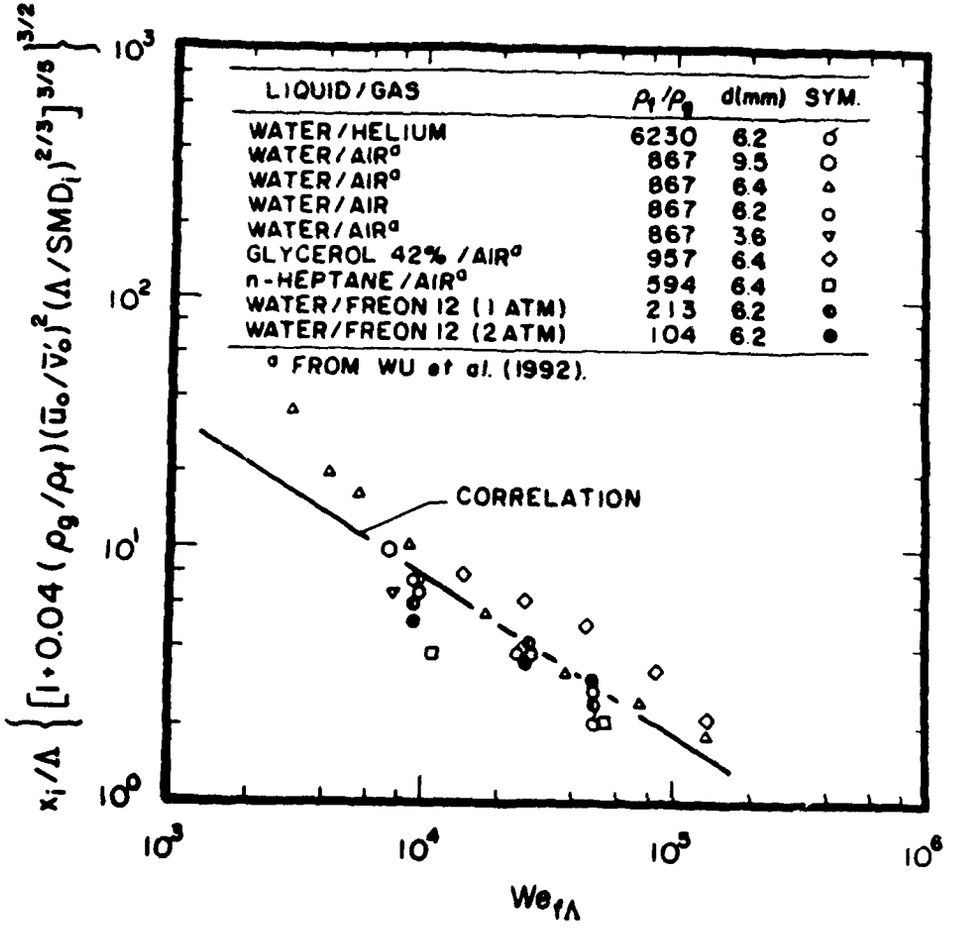
LIQUID / GAS | ρ_l/ρ_g | d(mm) | SYM.
WATER / HELIUM | 6230 | 6.2
WATER / AIR[a] | 867 | 9.5
WATER / AIR[a] | 867 | 6.4
WATER / AIR | 867 | 6.2
WATER / AIR[a] | 867 | 3.6
GLYCEROL 42% / AIR[a] | 957 | 6.4
n-HEPTANE / AIR[a] | 594 | 6.4
WATER / FREON 12 (1 ATM) | 213 | 6.2
WATER / FREON 12 (2 ATM) | 104 | 6.2
[a] FROM WU et al. (1992).
CORRELATION
$x_i/\Lambda \left\{\left[1+0.04\left(\rho_g/\rho_l\right)\left(\bar{u}_o/\bar{v}_o'\right)^2(\Lambda/SMD_i)^{2/3}\right]^{3/5}\right\}^{3/2}$
$We_{l\Lambda}$

FIG. 6

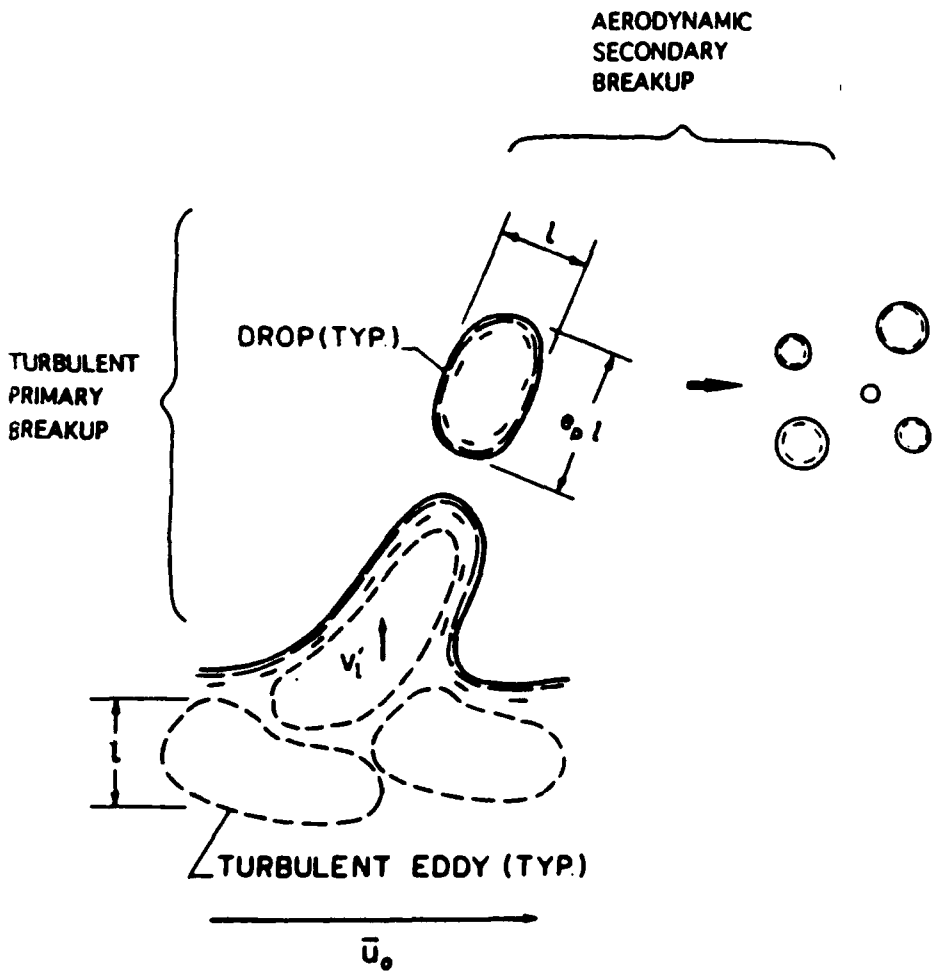
AERODYNAMIC
SECONDARY
BREAKUP
TURBULENT
PRIMARY
BREAKUP
DROP(TYP.)
l
$\delta_0 l$
v_i'
l
TURBULENT EDDY (TYP.)
$\bar{u}_0$

Fig 7

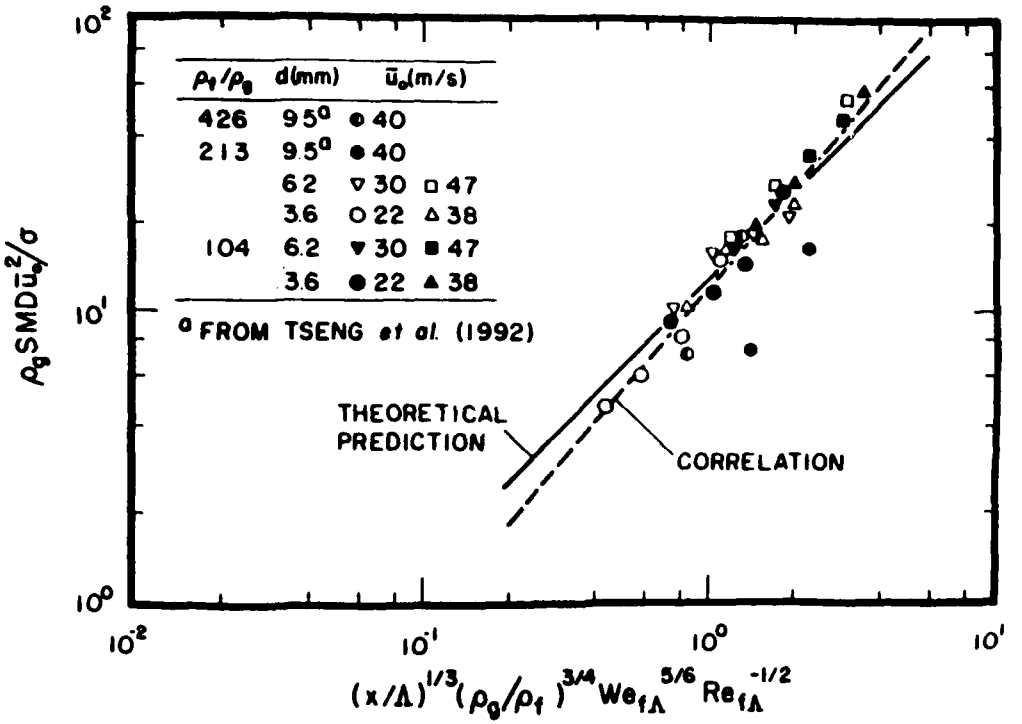
ρ_f/ρ_g d(mm) $\bar{u}_0$(m/s)
426 95[a] ● 40
213 95[a] ● 40
62 ▽ 30 □ 47
36 ○ 22 △ 38
104 62 ▼ 30 ■ 47
36 ● 22 ▲ 38
[a] FROM TSENG et al. (1992)
THEORETICAL PREDICTION
CORRELATION
$\rho_g SMD\bar{u}_0^2/\sigma$
10^2
10^1
10^0
10^{-2}
10^{-1}
10^0
10^1
$(x/\Lambda)^{1/3}(\rho_g/\rho_f)^{3/4} We_{f\Lambda}^{5/6} Re_{f\Lambda}^{-1/2}$

Fig 8

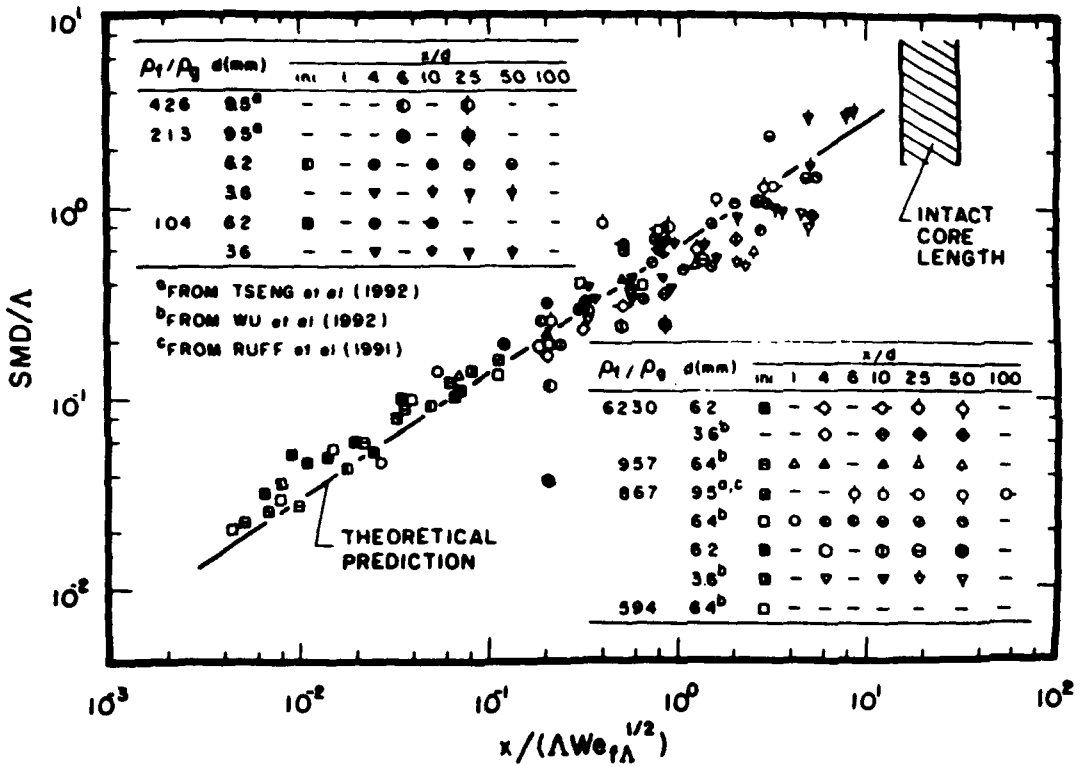
SMD/Λ
x/(ΛWe_fΛ^1/2)
INTACT CORE LENGTH
THEORETICAL PREDICTION
[a] FROM TSENG et al (1992)
[b] FROM WU et al (1992)
[c] FROM RUFF et al (1991)

Fig 9

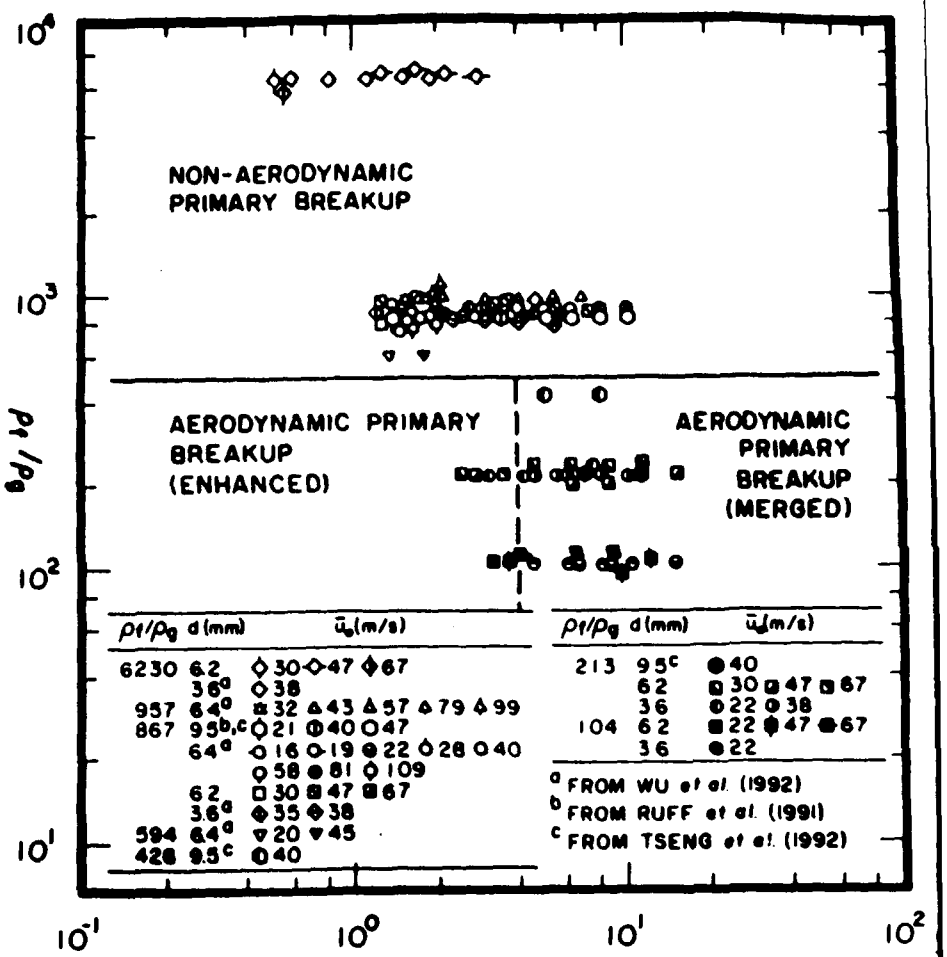
NON-AERODYNAMIC PRIMARY BREAKUP
AERODYNAMIC PRIMARY BREAKUP (ENHANCED)
AERODYNAMIC PRIMARY BREAKUP (MERGED)
τR/τb ~ (ρg/ρf)^1/2 (x/Λ)^1/3 We_fΛ^1/3

Fig 10